DOE / PC92544-18

VAPOR PRESSURES AND HEATS OF VAPORIZATION OF PRIMARY COAL TARS

FINAL REPORT

Grant Dates: August, 1992 - November, 1996

Principal Authors: Eric M. Suuberg (PI) and Vahur Oja

Report Submitted: April, 1997
Revised: July, 1997

Grant Number: DE-FG22-92PC92544

Report Submitted by:
ERIC M. SUUBERG
DIVISION OF ENGINEERING
BROWN UNIVERSITY
PROVIDENCE, RI 02912
TEL. (401) 863-1420

Prepared For:
U. S. DEPT. OF ENERGY
FEDERAL ENERGY TECHNOLOGY CENTER
P.O. BOX 10940
PITTSBURGH, PA 15236

DR. KAMALENDU DAS, FETC, MORGANTOWN , WV
TECHNICAL PROJECT OFFICER

United States Government Disclaimer

Executive Summary

This project had as its main focus the determination of vapor pressures of coal pyrolysis tars. It involved performing measurements of these vapor pressures and from them, developing vapor pressure correlations suitable for use in advanced pyrolysis models (those models which explicitly account for mass transport limitations).

This report is divided into five main chapters. Each chapter is a relatively "stand-alone" section. Chapter A reviews the general nature of coal tars and gives a summary of existing vapor pressure correlations for coal tars and model compounds. It is shown that the heterogeneous nature and the complexity of coal tars have made it unrealistic to apply detailed vapor pressure correlations which take into account the variation in the chemical structure of the tars.

Chapter B summarizes the main experimental approaches for coal tar preparation and characterization which have been used throughout the project. A significant aspect is the development of the new "non-isothermal" Knudsen effusion technique to measure the vapor pressures of complicated mixtures. The traditional isothermal Knudsen effusion technique has long been employed as an indirect method for determining the vapor pressures of pure low volatility materials. It is difficult to apply the method to complex mixtures of compounds, since the long time-scales required in the usual measurement may permit significant change in composition while waiting for pseudo-steady-state. For this reason, a modification was made to the traditional Knudsen method. The resulting non-isothermal method involves a straightforward modification of equipment and only a limited change in procedures. The technique has been applied to polycyclic aromatics and pyrolysis tars.

Chapter C is concerned with the selection of the model compounds for coal pyrolysis tars and reviews the data available to us on the vapor pressures of high boiling point aromatic compounds. This chapter also deals with the question of identifying factors that govern the vapor pressures of coal tar model materials and their mixtures. The measurements of vapor pressures for various large polycyclic aromatic hydrocarbons (PAH), including those containing heteroatoms, and some mixtures of these compounds are presented. We believe that our results might be among the first available on some of these materials.

Chapter D covers the vapor pressures and heats of vaporization of primary cellulose tars. Cellulose tar has a much narrower distribution of molecular weights than does coal tar, and is much more homogenous. Thus it was better to develop the methods to be used for coal tars on this simpler model system first. New vapor pressure data for sugar-compounds (levoglucosan, D-xylose, D-glucose and cellobiose) and for cellulose tar are presented. The volatility of the tar is similar to that of a widely accepted major component of the tar, levoglucosan. It is thus confirmed that levoglucosan can be a reasonable model for fresh cellulose tar.

This work has also resulted in a hypothesis regarding the role of tar evaporation in the global kinetics of cellulose pyrolysis. This study of the cellulose tar vapor pressure and heat of vaporization has been the first in the field of biomass pyrolysis. Therefore, future research could be directed at measuring the vapor pressures for the other biomass pyrolysis tars and at developing the pyrolysis models which take into account the heats of vaporization.

Chapter E discusses the results of the main focus of this study. Coal tars were prepared from various coal samples. Four coals from the Argonne Premium Coal set - the Illinois

No.6, the Pittsburgh No.8, the Pennsylvania Upper-Freeport and the Wyodak - were selected for this study. Also another Pittsburgh No.8 sample, Bruceton standard coal, was examined in preliminary work.

Characterization of tars was obtained via elemental analysis and gel permeation chromatography (GPC). This characterization shows the heteroatomic content of all tars to be comparable to the parent coal, and that tars likely contain a large amount of hydroxyl functionality. The coal tar separation by GPC, using a Phenogel column and pyridine as mobile phase, allows one to characterize tars in terms of compound classes, by drawing lines designating the region of elution for various classes of aromatics. This type of separation can be characterized only by an extensive calibration procedure. The actual assignment of classes is still tentative on the basis of the limited data at hand. However, we believe that this technique could serve as a good and simple basis for characterizing complex mixtures such as coal tars. This needs further verification by detailed chemical analysis.

The significant product of this study is a much improved understanding of the volatility and thermal behavior of coal tars. The volatility was studied by vacuum sublimation and Knudsen effusion experiments. The volatility behavior is considerably more complicated than had been earlier believed.

The tars evaporate in a "distillation-like" fashion. More volatile species are lost earlier in the process, leaving behind a progressively less volatile residue. The results suggest that there are three very different classes of compounds, and therefore, at least three different vapor pressure behaviors. The first corresponds to compounds of high molecular weight and significant alkyl character, the second to compounds with significant hydroxyl group content and medium molecular weight, and the third to medium molecular weight aromatic compounds without hydroxyl groups. Hydrogen bonding plays a major role in the determining the tar volatility.

There has been concern in pyrolysis modeling about how closely Raoult's law is followed in coal tar. It appears from our results that the assumption of ideal mixture behavior could be acceptable for rough models of pyrolysis despite the possibility of strong specific interactions between certain functional groups.

The results from the current work show that measuring the vapor pressures of complicated and thermally unstable mixtures is possible at low temperatures. There has also been some concern about condensation-type reactions influencing the results of vapor pressure measurements, even at modest temperatures, below 250°C. It was shown to be unlikely that such residue formation could affect the vapor pressure results very much, though the thermal instability of the tars was clearly demonstrated. The major reactions promote formation of some kinds of non-volatile residue. New vapor pressure correlations for Pittsburgh No.8 coal tar, Wyodak coal tar and Upper-Freeport coal tar have been developed for use in pyrolysis models.

In summary, this work provides improved understanding of the volatility of coal and cellulose pyrolysis tars. It has resulted in new experimentally verified vapor pressure correlations for use in pyrolysis models. Further research on this topic should aim at developing general vapor pressure correlations for all coal tars, based on their molecular weight together with certain specific chemical characteristics *i.e.* hydroxyl group content.

Contents

List of Figures:

List of Tables:

Chapter A. Introduction.

A.1. Overview.

As the world continues to deplete its petroleum reserves, heavy crude oil, coal liquids, and other heavy fossil fuels may be required to meet world energy needs. The thermodynamic and thermophysical properties of high molecular weight compounds are of increasing importance in the utilization of fossil fuels. Heavy fossil fuels contain molecules that are large and more aromatic and that contain more heteroatoms than those found in liquid crude oil.

There is also significant current interest in the general area of coal pyrolysis, particularly with respect to comprehensive models of this complicated phenomenon. This interest derives from the central role of pyrolysis in all thermally driven coal conversion processes - gasification, combustion, liquefaction, mild gasification, or thermal beneficiation. Earlier modeling work has shown that tars are key volatile products of coal pyrolysis, and their ability to evaporate from coal particles determines several key features of pyrolysis (tar yields, char yields, gas yields, tar molecular weight distribution, ability of the particles to soften). Regardless of how coal is thermally processed, development of a truly fundamental understanding of the process requires learning more about how the tars behave during pyrolysis. Since there is unquestionably a need to continue to improve coal utilization technologies, there is naturally a strong driving force for improving many aspects of understanding of the process. There remain several key data needs in these application areas. Among them is a need for more reliable correlations for prediction of vapor pressures of heavy, primary coal tars. Such information is important in design of all coal conversion processes, in which the volatility of tarry products is of major concern.

The experimental data to develop such correlations are not available. The vapor pressure correlations that exist at present for coal tars are very crude and they are not

considered reliable to even an order of magnitude. The tars obtained either by low-temperature or high-temperature carbonization of coal are complex mixtures of a myriad of aromatic compounds of widely ranging concentrations. Investigators have identified more than 100 condensed polynuclear aromatic hydrocarbon and heterocyclic compounds in coal tar, but it was estimated that as many as 5000 compounds may be present. Sophisticated general correlative approaches are slowly being developed, based upon group contribution methods, or based upon some key functional features of the molecules. These detailed group contribution methods, in which fairly precise structural information is needed, do not lend themselves well for application to very complex, poorly characterized coal tars. The methods based upon more global types of characterizations have on the other hand not yet dealt much with the question of oxygenated functional groups. In short, very few correlations exist, and these are not considered reliable to even an order of magnitude when applied to tars. Improving the ability to predict vapor pressures of coal tars is one of the remaining critical issues to be resolved in pyrolysis modeling. Detailed models of pyrolysis all include tar vaporization as a key element. Examples of codes that directly employ estimates of vapor pressure include FG/DVC (a product of AFR, Inc.), FLASHCHAIN (from Sandia/Stanford Univ./SRI, Inc.), and CPD. In some cases FG/DVC is incorporated in to the PCGC2 code also from Brigham Young University and ACERC.

A.2. General Nature of Coal Tars.

Tars are among the major products of pyrolysis of a great many organic solids. Tars are key volatile products of coal pyrolysis, and their ability to evaporate from coal particles determines several key features of pyrolysis. Knowledge of coal tar vapor pressures is important in predicting the pyrolysis behavior of coals, since most advanced models of coal pyrolysis utilize an evaporation step to describe the loss of tar from particles.

The definition of tar is arbitrary. Tars are generally operationally defined in any experiment. They are most often defined as any degradation products which have escaped the parent solid, and are condensable at room temperature. In this work we are interested in "primary tars" or tars that have not undergone secondary reactions.

Coal itself can be defined as a complex sedimentary rock, a heterogeneous mixture of higher-plant-derived organic materials which has undergone chemical changes related to depositional environment and diagenetic history. Since coal is not a homogenous substance, it is characterized by wide variations in its properties and compositions. The most common coal classification is by rank. The rank is a measure of the degree of coalification that organic plant sediment has reached in its metamorphosis from peat to near -graphite-like material. Some aspects of the characterizations of coals are given elsewhere [Smith et al., 1994]. Coal tars reflect the characteristics of parent coal.

Coal tars are very complex mixtures of individual components. Tars and their fractions are often represented in the terms of an "average molecule", based upon elemental composition, molecular weight, molecular weight distribution, functional group concentration and structural parameters such as the aliphatic and aromatic hydrogen-to-carbon ratio. A review of the techniques for characterizing coal tars is given by Solomon et al.[1992]. Some investigators [Orning and Greifer, 1956; Brown, 1958; Solomon et al., 1984] have reported that the chemical structural characteristics of primary tars are similar to

those present in the parent coal, although the chemical nature and composition of the tars vary substantially with rank characteristics of the parent coal and operating conditions [Solomon et al., 1981, 1992; Freihaut et al., 1989].

The rate of escape of tar from pyrolyzing coal particles depends strongly upon the vapor pressure of the tar, and this property depends to the greatest extent upon the molecular weight of the tar [Unger and Suuberg, 1984; Fletcher et al., 1992]. Thus, several investigators [Unger and Suuberg, 1984; Oh et al., 1989; Solomon et al., 1990] have studied the molecular weight distribution of coal tars released in rapid pyrolysis and noted its strong dependence on pyrolysis conditions (temperature, pressure, effect of different reactors and pyrolysis environment) and coal rank. There are relatively few data on the characterization of "primary" tars.

The reactor systems which most nearly approach conditions necessary for studies of primary tars are those in which the gas into which tars evolve remains cold. These reactors include the heated wire mesh type systems and flashlamp/laser heated systems. Even with these systems, gas phase secondary reactions sometimes take place. In any type of experimental device, secondary reactions may actually occur within the particles themselves, if transport limitations exist. Thus there is not an experimentally clean way to produce only "primary tars", and some reported differences in tars, from study-to-study, may have to do with how the tars were prepared.

A.2.1. Molecular Weight Characterization.

In earlier work, the molecular weight distribution determination techniques have been the subject of much concern. Two methods have been used for characterizations. Early attempts relied upon size-exclusion chromatography (SEC) or gel permeation

chromatography (GPC), and in later work field ionization mass spectrometry (FIMS) was used. The FIMS results generally suggest lower molecular weight tars than do the GPC results. There are, however, concerns about the reliabilty of both techniques.

Suuberg and co-workers [1984, 1985] determined molecular weights in the range 200-4000 daltons by GPC with THF as mobile phase, for high volatile bituminous coal primary tars. In fact, there is a concern that using THF as solvent results in a shift of the molecular weight to unrealistically high values. Oh et al. [1989] obtained a molecular weight distribution between 150 and 1500 daltons for a Pittsburgh bituminous tar using pyridine as the solvent. The difference was attributed to association of tar species in the THF, since pyridine is generally a stronger solvent for coal, and presumably, its tar.

Solomon et al. [1990] determined molecular weight distributions using FIMS for 8 Argonne premium coals pyrolysed to 450°C at 3°C/min in the FIMS apparatus. They showed that the intermediate rank coals, i.e., Pittsburgh No.8, Lewiston-Stockton, Utah Blind Canyon, and Illinois No.6 all have similar molecular weight distributions showing maxima in near 400 daltons. Upper-Freeport coal tar showed a maximum near 500 daltons. Low rank coals such as Wyodak and Zap showed that the majority of tars fall between 100 and 200 daltons. The maximum molecular weight extended to about 800 daltons for all tars.

Some other techniques have also been used to examine the molecular weights of vacuum pyrolysis tars and coal derived materials [Winas et al., 1991; Winas, 1991; Herod et al., 1993a, 1993b; Parker et al., 1993]. Winans et al. [1991] compared fast atom bombardment-mass spectroscopy (FAB-MS), laser desorption mass spectrometry (LDMS) and desorption chemical ionization DCI-MS of a vacuum pyrolysis tar. Very different upper limits were reported using the different methods. The tars were mostly found to be below 1000 daltons, with the exception of FAB. Using this technique, Winans [1991] observed the highest molecular weight values for vacuum pyrolysis tars to be on the order 1000 to 1200 daltons, with the peaks of the distributions centered at around 400 to 450

daltons. It is important in any mass spectrometric method to assure that the analysis of the whole sample is possible. Formation of a non-volatile residue in the inlet of the mass spectrometer warns that this may not be so. Such concerns have been voiced from time-to-time about the FIMS technique.

Existence in pyrolysis tars of high molecular mass materials between 1000 and 5000 daltons has also been recently observed by laser desorption mass spectrometry [Parker et al., 1993; Herod et al., 1993a, 1993b]. It is fair to say, in summary, that there remains some uncertainty as to the molecular weight distribution of the tars, with different methods of characterization suggesting different ranges. Still, there is general agreement that the materials of interest have molecular weights of several hundred up to thousands.

A.2.2. Functional Group Characterization.

It is known that vapor pressure is a property which depends on the interaction between molecules. Although the molecular size (number of atoms) is the most important factor in determining interactions, the specific interaction between particular structures may also play an important role. Thus it is important to identify chemical features which influence those interactions. The chemical analysis of the coal tars is, however, particularly difficult because of the high heteroatomicity and the wide range of the structures and functional groups present.

Individual chemical species in coal tars have been identified using glass capillary columns in gas chromatography (GC) [Borwitzky and Schomburg, 1979; Lee and Wright, 1980], gas chromatography -mass spectrometry (GC-MS) [Evans et al., 1985; Borwitzky and Schomburg, 1979] or high-performance liquid chromatography (HPLC). These techniques are always subject to questions about components that do not elute or vaporize, or that decompose during analysis. Molecular masses much greater than 300 to 350 daltons cannot readily be characterized by GC. Several 6-10 ring polycyclic aromatic hydrocarbons

have been identified in coal tars and coal tar pitches by HPLC [Fetzer and Kershaw, 1995], and this suggests how high the molecular weight can be, thought as the previous section suggests, the main problems might be encountered with a large amount of tar that falls between 300 and 1000 daltons.

Coal tar average structural and functional group characterization are most commonly based on elemental and spectroscopic analysis. Elemental analyses are used to determine the relative abundance of nitrogen, carbon, hydrogen and oxygen in coal tar samples (see Appendix A). Relatively little attention has been however paid to the variation of elemental composition of tar fractions with molecular weight. Freihaut [1989] showed that as the rank of the parent coal increases, the elemental composition of the primary tars becomes more like that of the parent coal at any given extent of tar evolution. The tar is generally richer in hydrogen than the parent coal. Three forms of hydrogen are typically distinguished: aromatic, aliphatic, and hydroxyl. Three forms of carbon are normally distinguished: aromatic, aliphatic and carbonyl, though more can be identified with sensitive methods. Four forms of oxygen are usually cited: carbonyl, carboxyl, hydroxyl and ether, though more can be identified by appropriate methods. The average functional group concentrations can in principle be determined by Nuclear Magnetic Resonance Spectroscopy (NMR) or by Fourier-Transform Infrared Spectroscopy. The question of the quantitative reliability and accuracy is still under discussion and often these methods are used for only relative characterization. ^{1}H NMR has been most commonly used to determine distribution of the various types of hydrogen in coal tars [Collin et al., 1980; Cerny, 1991; Evans et al., 1985; Fynes et al., 1984]. This technique enables the classification of hydrogen functional groups. ^{13}C NMR is used to identify carbon types and has been often used for the quantification of the structural parameters of average tar molecule [Calkins et al., 1984; Evans et al., 1985 ; Fletcher et al., 1990]. FTIR has been used mainly for the qualitative determination of functional groups in coal tars [Fynes et al., 1984; Solomon et al., 1990; Cerny, 1991; Evans et al., 1985], though it has also been

used quantitatively for several functional groups in coal and there is no reason why it cannot be used for the same purpose for tars.

Solomon and co-workers [Squire et al., 1986; Solomon et al., 1983; Solomon et al., 1984; Solomon and Colket, 1978,1979] suggested from the similarities in elemental composition, infrared spectra and NMR spectra that the primary tars are fragments of the parent coals, at least in bituminous coal. But it was also noted that the infrared spectrum for a lignite tar was significantly different from that of the parent coal, being richer in aliphatic groups and poorer in oxygen functional groups [Solomon, 1981; Solomon et al., 1984; Freihaut et al., 1989].

Lately UV-Fluorescence Spectroscopy (UV-F) has been applied to characterize the relative concentrations and sizes of fused aromatics ring systems in coal tars [Li et al., 1993, 1994]. Fluorescence spectroscopic properties of coal pyrolysis tars have been found to correlate with the rank of the original coals. With increasing rank, UVF emission from pyrolysis tars was increasingly observed to take place from progressively larger aromatic ring systems.

Calkins [1984], using GC-MS, FTIR, ^{1}H NMR and ^{13}C NMR techniques, noted that the concentration of polymethylene (series of n-olefin-paraffin pairs from C_{14} to C_{26} and higher) increased with decreasing rank from about 4% for high volatile bituminous coals to about 8% for lignites . The relative contribution of the polymethylenes to the tar therefore increases with decreasing rank. Some tars were observed to have even higher polymethylene contents, for example it was suggested by Calkins and Tyler [1984] that tar produced at 600°C from Millmeran coal contains long chain olefins and paraffins to an extent of 30 to 40%, and, from Texas lignite about 13% .

Fynes et al. [1984] noted for bituminous coal tars that their infra-red spectra showed prominent phenolic OH bands, and the high ratio of the absorbance due to aliphatic and aromatic C-H suggested aromatic ring multisubstitutions.

Coal nitrogen is almost entirely found in tightly bound rings such as pyridine and a large fraction of the fuel bound nitrogen in the bituminous coals is volatilized as a heteroatom in the tar component of the total volatiles [Solomon and Colket, 1981; Blair, 1976; Freihaut et al., 1989]. Sulfur appears in tars within rings as tightly bound ring sulfur and in chains as weakly bound sulfur [Solomon et al., 1981].

Freihaut et al. [1993] observed the following changes in tar characteristics with rank: the fuel nitrogen concentration of low rank primary coal tars is significantly lower than that observed in parent coals on a daf basis; the chemical nature of the primary tars varies systematically, for high vitrinite coals, from primarily polymethylene for low rank coals to primarily condensed aromatics for high rank coals; the thermophysical (softening temperatures) and volatility characteristics (transient vaporization temperatures and extent of revaporization) vary systematically with the rank of the parent coal, with lower rank coals producing primary tars having lower softening temperatures, lower vaporization temperatures and greater volatility in general.

The tar released from coal will undergo further secondary reactions if the surrounding gas temperature is high enough. These reactions can significantly change the tar composition. Knowing how the kinetics of secondary reactions depend upon temperature and time is important if the aim is to produce "primary" tars. The temperature at which such reactions become important has been shown to be below 700°C by several investigators using flash pyrolysis reactors.

Calkins et al. [1984] report that further pyrolysis, at 700 to 1100°C, of flash pyrolysis tars produced at low temperatures (600°C) produces the hydrocarbon products characteristic of those obtained during high temperature pyrolysis of coal itself. They also demonstrated that tar cracking would be a major source of light hydrocarbon gas at temperatures above 600°C in a fluidized bed reactor.

This is consistent with studies of Tyler [1979; 1980], and Nelson et al. [1988] which showed that the total C_1 to C_3 hydrocarbon gas yield increases strongly over the

temperature range from 600 to 800°C due to the secondary cracking reactions of tar vapors. As noted by Collin et al. [1980] marked changes occur in the composition of aliphatic components of flash pyrolysis tar (fluidized bed) above 600°C for Liddell tar, and 650 °C for Millmeran and Loy Yang tars .

Nelson et al. [1988], investigating Millmeran subbituminous coal and Yallourn brown coal tars, showed that at temperatures above 600°C, secondary reactions of tar occur and yields of simple aromatics increase as the polymethylene products disappear. The alkyl substituted aromatics and phenols decompose at temperatures above 700°C .

Freihaut [1993] showed that the gas phase, secondary reactions of primary tars which produce HCN from ring nitrogen compounds initiate at gas temperatures of approximately 700°C.

Thus the chemical nature of the "primary tars" is only crudely determined by the chemical characteristics of the parent coal. Many common "environmental" factors (e.g., tar residence time) are difficult to control, and can influence the tar characteristics.

A.3. Vapor Pressures of Coal Tars.

Tars are complicated mixtures of coal fragments and have widely variable chemical structure. As noted above, the chemical nature and composition of the tars vary substantially with rank of the parent coal and operating conditions. There is little hope of characterizing materials as complex as coal tars in very great detail. Therefore, there is strong incentive to keep the amount of data needed for prediction of vapor pressures of such mixtures to an absolute minimum.

Actual vapor pressure data on "primary" coal tar are unavailable. Pyrolysis modelers have turned to simple correlative techniques based upon extrapolation of known vapor pressure behavior of pure compounds or of coal liquid fractions, well beyond the conditions at which data are available. Historically there has been much use of correlations based upon molecular weight distributions alone, since molecular weight and temperature are the two most important variables in determining vapor pressures. These correlations have been of one particular form, obtained from the Clausius-Clapeyron equation, assuming that the heat of vaporization is a function of the molecular weight and not a function of temperature. The resulting form of correlation developed by Suuberg et al. [1979] is :

$$P = \alpha \exp\left(-\beta \frac{M^{\gamma}}{T}\right) \qquad \{A.1\}$$

This is the simplest expression which appears to be consistent with the known thermodynamics of the situation and is used because of the lack of detailed chemical structure and vapor pressure data on coal tar. It should also be noted, consistent with this approach, that it has been shown possible to correlate vapor pressure with molecular weight of coal liquids using only boiling point information, at least up to about 400 molecular weight [Tsonopoulos et al., 1986].

Several workers have employed a correlation such as {A.1}, and values of the constants they have obtained by fitting the data to literature data on various types of aromatic hydrocarbons are shown below:

Table A.1 Vapor pressure correlations for coal pyrolysis tar.

	α	β	γ
Suuberg et al.[1979]	1.23×10^5	236	0.654
Suuberg et al.[1985]	5765	255	0.586
Niksa [1988]	70.1	1.6	1.0
Niksa and Kerstein [1991]	3.0×10^5	200	0.6
Fletcher et al. [1992]	87060	299	0.59
Oh et al. [1989]	6.23×10^5	561	0.474

In this case, P is in atmospheres, T is in K, and M is in daltons. Comparisons of the predictions of several of these models have been offered elsewhere [Fletcher et al., 1992]. Wide variations were noted in the predictions, and there is a concern about adequacy of predictions of the vapor pressures under pyrolysis conditions. Nevertheless, it is clear that there is a general convergence of most of the values of α, β, and γ in the literature. A comparison of the predictions of boiling points with molecular weight is shown in Figure A.1, for various models. For reference, the measured properties of anthracene are indicated.

This type of correlation is used in network models of coal devolatilization to describe the tar evaporation process. A review of such models is given elsewhere [Solomon et al., 1992; Lee et al., 1994]. The models include the Functional Group - Depolymerization, Vaporization, and Cross-linking (FG-DVC) model [Serio et al., 1987; Solomon et al., 1988, 1990b, 1991], the FLASHCHAIN model [Niksa and Kerstein, 1987, 1991; Niksa, 1988, 1991a, 1991b], and the Chemical Percolation Devolatilization (CPD) model [Grant et al., 1989; Fletcher et al., 1990, 1992].

In the FG-DVC model, the tar is "formed" from a metaplast fraction via finite rate evaporation (controlled by the gas evolution rate), using the Unger-Suuberg correlation [1985] and assuming Raoult's law applies. In the FLASHCHAIN and CPD models, the tar evaporates assuming through an equilibrium flash distillation analogy and again the validity of Raoult's law is assumed and combined with a correlation such as {A.1}.

There are two questions that need to be examined at this time. The first one is how good are the predictions of the vapor pressures under pyrolysis conditions, the second is how closely Raoult's law is followed in tars. First, a survey of methods for correlating vapor pressures is presented. Then there is consideration of how well these techniques may apply to coal tars.

A.4. Pure Compound Vapor Pressure Estimation.

A.4.1. Pure Component Vapor Pressures - Survey.

Vapor pressures can vary as much as 11 orders of magnitude over the coexistence range, and generally no single technique is capable of measuring vapor pressure over the entire range. For this reason it is useful to define several somewhat arbitrary pressure ranges for purposes of discussion of different measurement techniques:

Table A.2. Vapor pressure ranges defind.

Pressure range	torr	kPa
High	$10^3 \ldots 10^5$	$10^2 \ldots 10^4$
Mid	$10^1 \ldots 10^3$	$10^0 \ldots 10^2$
Low	$10^{-3} \ldots 10^1$	$10^{-4} \ldots 10^0$
Very-low	$10^{-7} \ldots 10^{-3}$	$10^{-8} \ldots 10^{-4}$

Extensive experimental vapor pressure data have been accumulated and summarized in the literature [e.g., Stephenson and Malanowski, 1987; Reid et al., 1987]. In fact, most of the existing experimental data for high boiling organic compounds in the literature have been measured in the mid range, of order from 10 to 10^3 torr and for basic hydrocarbons in the low pressure range, of order 10^{-3} torr to 10 torr. The data on high molecular weight aromatic compounds are relatively scarce, which does not allow us to describe these data systematically. It is noteworthy that many of the published vapor pressure data appear to be questionable, especially for very low vapor pressure organic compounds. As a rule, as molecular weight increases, data become more scarce and vapor pressure data for hydrocarbons containing heteroatoms are often unavailable for even low molecular weight hydrocarbons.

Most of the experimental data in the literature on what might be considered model compounds for coal tars, have been measured in the very low to low pressure range from 10^{-5} to 10 torr. Measurements of vapor pressures of high molecular weight materials

require high temperatures to obtain conveniently measurable pressures, but high temperatures cannot be employed because of concerns about thermal decomposition during measurement. Yet it is the high temperature range that is of most practical interest for coal tars, since these materials are formed at high temperatures. A problem arises in extrapolating existing experimental data out of the temperature range in which they were obtained. The vapor pressure measurements are usually performed under sublimation conditions at low temperatures, where the heat of vaporization is a very weak function of temperature. Because the work is done at low and very low pressure conditions, the data are often inaccurate due to experimental difficulties. This makes the prediction of changes in vapor pressure with temperature in the high temperature range of interest very difficult. Not only is a correction required to correct for evaporation as opposed to sublimation (involving an enthalpy of fusion), but the enthalpy of evaporation itself is a decreasing function of temperature reaching zero at the critical point.

For the above reasons, many efforts have been directed at the development of improved correlative and predictive methods for extrapolating low pressure vapor pressures into the mid pressure ranges. Most standard vapor pressure curve-fitting/extrapolation techniques developed for the mid pressure range fail in the low pressure range and success can be seen only with correlations for aliphatic and monocyclic aromatic species.

A.4.2. Vapor Pressure Extrapolation and Estimation Methods.

Numerous expressions proposed in the literature represent actual experimental data with a high degree of accuracy, but they are often disappointing when used for extrapolation purposes. The solid and liquid vapor pressure curves with temperature (or even reciprocal of temperature) are highly nonlinear, and no method is currently available for calculating from theory alone the magnitude of vapor pressure and its dependence on temperature.

Several empirical and semi-empirical equations are based in some way on integration of the Clapeyron equation. These are used to fit experimental data and extrapolate out of the experimental region. They have the general form [Majer et al., 1989]:

$$\ln P = \sum_{i=k}^{m} A_i T^{i-1} + A_{\ln} \ln T + A_f f \qquad \{A.3\}$$

where the A_m are adjustable parameters and f is general function of the temperature (and pressure), which is used only in a limited number of cases. Different forms of this equation have been used for correlating vapor pressures, with the four- and five-parameter forms the most common. Modifications of these vapor pressure equations are often also given in the reduced form using critical properties as reducing parameters. Moreover, the number of adjustable parameters has been reduced by introducing the normal boiling temperature, melting temperature or the enthalpy of vaporization of interest. Due to the logarithmic nature of most vapor pressure correlations, correlating parameters must be known accurately to avoid large errors. The predictive ability of the equations based on the Clapeyron equation is generally poor. These methods will be reviewed further in the next subsection.

Many correlating and estimating equations, based on the classical theories of corresponding of states, have been proposed for calculating the vapor pressure of a given compound given a set of characteristic parameters. Vapor pressures for pure compounds have been correlated using methods in which the temperature or the vapor pressure of one compound is plotted against the corresponding function of a reference compound to obtain a relationship that is linear over a wide temperature range, especially for a homologous series; for example Cox's [1923] graphical correlation. The principle of corresponding states posits that all substances obey the same equation of state expressed in terms of the critical properties. In practice, another parameter, the acentric factor $\omega = f\ (T_b,\ T_c,\ P_c)$, was found to be required in order to accurately predict vapor pressures for a variety of substances. The problem of finding such information was noted in the last section.

Consequently, estimation procedures for critical properties and boiling point are also needed. In fact for many large aromatic species, these properties are not known accurately if at all. When data are available, results obtained are satisfactory in the high pressure range and usually are only roughly correct at medium and low pressures.

Comprehensive reviews of vapor pressure correlation/extrapolation/estimation methods are given by Reid et al. [1987], Majer et al. [1989] and Malanowski et al. [1992].

A.4.3. Integrated Forms of Clausius-Clapeyron Equation.

When the vapor phase of a pure fluid is in equilibrium with its liquid phase, then the chemical potential, temperature, and pressure in both phases are equal. The combined first-second law of thermodynamics provides the constraint on the vapor pressure (P) temperature (T) curve in the form of the differential Clapeyron equation. The differential equation determining the equilibrium in a two phase one component system can be written:

$$\frac{dP}{dT} = \frac{\Delta h}{T \Delta v} \qquad \{A.4\}$$

This equation relates the slope of the coexistence curves to the molar enthalpy of vaporization (Δh) and the molar volume change (Δv) on vaporization.Many vapor pressure correlations are based in some way on integration of the Clapeyron equation which indicates that the vapor pressure is an exponential function of temperature, with characteristic parameters for each individual compound. The basic approach involves the integration of the differential Clapeyron equation after making assumptions about Δh and Δv that make the integration possible. The integrated equations are empirically modified on the basis of actual vapor pressure data. Many empirical equations have been developed.

Only a small selection of equations has found universal acceptance. Here the most frequently used equations for correlation of vapor pressure data are reviewed .

At temperatures at which the vapor pressure is not very high equation {A.4} can be rearranged using the ideal gas law, or the actual compressibility of the vapor:

$$\frac{d\ln P}{dT} = \frac{\Delta h}{RT^2} \quad \text{, where} \quad \Delta v = \frac{RT}{P} \text{, or} \qquad \{A.5\}$$

$$\frac{d\ln P}{dT} = \frac{\Delta h}{RT^2 \Delta Z} \text{, where } \Delta v = \frac{RT\Delta Z}{P} \qquad \{A.6\}$$

In both cases the assumption was made that the molar volume of the condensed phase is negligible, in comparison with the molar vapor volume.

Equations {A.5} and {A.6} are referred to as the differential Clausius-Clapeyron equations. The simplest solution to {A.5} can be obtained based upon the assumption that Δh is independent of temperature and the result is sometimes called the Clausius-Clapeyron equation:

$$\ln P = -\frac{\Delta h}{RT} + C \qquad \{A.7\}$$

This integrated form of the Clausius-Clapeyron equation is widely used for low and very low vapor pressure data in the pressure region from 10^{-6} to 10^{-3} torr, where the assumption of constant Δh is fairly good. The assumption that Δh is constant implies that the vapor pressure curve in the ln P vs. 1/T plot is a straight line, and results in an over estimation of vapor pressure in middle pressure ranges. In the literature, this equation has quite often been rewritten in the equivalent form :

$$\ln P = -\frac{\Delta h}{RT} + \frac{\Delta s}{R} \qquad \{A.8\}$$

where Δh and Δs are enthalpy and entropy of sublimation (or vaporization), respectively.

A simple three parameter modification of the Clausius-Clapeyron equation was proposed by Antoine [1888], and is widely used to correlate vapor pressures accurately over the range from 1 to 200 kPa :

$$\ln P = A - \frac{B}{C + T} \qquad \{A.9\}$$

the third parameter C is introduced to take into account the variation of Δh with temperature and values of C are typically -20 to -50 K. Antoine constants are available in literature for over 5,000 compounds [Reid et al., 1987; Boublik et al., 1987; Ohe, 1976; Stephenson et al., 1987]. Although the extrapolation capabilities of the Antoine equation are limited [King and Al-Najjar, 1974; Scott and Osborn, 1979; Majer et al., 1989], this relationship appears to be routinely used in engineering calculations for extrapolating beyond the range of experimental data. Strictly speaking, the Antoine equation can only be used in the stated temperature limits. It is the most common, but not the best, three parameters correlating equation.

Generally speaking, the enthalpy of vaporization is a function of temperature. To take this into account several empirical and semi-empirical equations, based in some way on integration of the Clapeyron equation, are available to fit experimental data and extrapolate out of the experimental region.

The Rankine-Kirchhoff equation [Rankine, 1849; Kirchhoff, 1858] may be represented as:

$$\ln P = A - B / T - C \ln T \qquad \{A.10\}$$

The equation was derived on the assumption that ΔH is a linear function of temperature.

MacKay et al.[1982] developed a predictive equation in the form of the Rankine equation for low volatility liquid/solid hydrocarbons and halogenated hydrocarbons, that boil above 100°C. The constants of this equation were correlated for 72 hydrocarbons and halogenated hydrocarbons. Because the correlation was not extended to other species this

equation cannot be used for predicting the vapor pressures of O, N, and S containing compounds.

This equation was modified by Yalkowsky et al. [1991] applying it to the same data set developed by Mackay . These authors used recently proposed modifications of Walden's Rule and Trouton's Rule for ΔS_m and ΔS_b, respectively, to account for two molecular characteristics. One was the effect of high rotational symmetry (characterized by the rotational symmetry number) and the other conformational flexibility. All numerical coefficients were obtained from non vapor pressure data.

The Frost-Kalkwarf equation [1953] may be represented as:

$$\ln P = A + B / T + C \ln T + D P / T^2 \qquad \{A.11\}$$

This equation was derived on the assumption that Δh is a linear function of temperature and Δv can be estimated from the van der Waals equation of state. Parameters for many compounds are given in the book by Reid et al. [1987] and in the paper by Halacher and Brown [1975]. Rogalski et al. [1991] have reviewed several modified versions of this equation and proposed an extended Forst-Kalkwarf equation for extrapolating/predicting vapor pressures of over a very wide temperature range, using no adjustable parameters.

The Plank-Riedel equation [1948] is of a similar form:

$$\ln P = A + B / T + C / \ln T + D T^6 \qquad \{A.12\}$$

Lee and Kesler [1975] proposed a generalized form of this equation, where the parameters are established using the acentric factor and a universal relationship should be valid for all nonpolar compounds.

A.4.4. Other Empirical Correlations.

In what follows, there is a progressively less strong tie to the integration of the Clapeyron equation.

The Wagner equation [1973] is : $$\ln\left(\frac{P}{P_c}\right) = \frac{T_c}{T}\sum_{i=1}^{m} A_i \left(1 - \frac{T}{T_c}\right)^{\alpha_i} \qquad \{A.13\}$$

The exponents α_i have fixed values that were determined by the methods of statistical analysis [Wagner, 1973]. This equation has been considered efficient in the correlation of vapor pressures, and it is the only equation able to accurately describe the data with few constants at reduced temperatures between 0.5 and 1. The number of adjustable parameters is usually four, but five were used for correlations of very accurate data over a wide temperature range. The Wagner equations has become very popular for correlating vapor pressures up to the critical temperature [Ruzicka and Majer, 1996]. Several articles present parameters for certain groups of substances [McGarry, 1983; Reid et al., 1987; Ambrose and Walton, 1989].

The Lee and Kesler [1975] method is based on following relation (Pitzer expansion, 1955):

$$\ln P_r = f^0(T_r) + \omega f^1(T_r) \quad \text{and} \quad \omega = f(T_b; T_c; P_c) \qquad \{A.14\}$$

A fluid's properties are obtained by interpolating between the properties of a simple fluid (ω=0) and a reference fluid (octane with ω=0.3978). The equation is recommended for the prediction of vapor pressures at reduced temperatures of 0.8 and lower.

Gomez -Nito and Thodos [1977, 1978] proposed vapor pressure estimation techniques for three classes of compounds: nonpolar, polar and hydrogen-bonded. The equation is recommended for the prediction of vapor pressures at reduced temperatures between 0.5 and 1.

Ambrose and Patel [1984] proposed the use of two real fluids with well-correlated vapor pressures, this leads to:

$$\ln P_r = \ln P_{r1} + (\ln P_{r2} - \ln P_{r1})\frac{\omega - \omega_1}{\omega_2 - \omega_1} \qquad \{A.15\}$$

The equation is recommended for the prediction of vapor pressures at reduced temperatures between 0.5 and 1 is suitable for polar compounds.

Smith et al. [1976] correlated vapor pressure data of high boiling hydrocarbons in the region from 10 to 1950 torr. The SWAP (Smith-Winnik-Abrams-Prausnitz) correlation was based on the relation

$$\ln P_r = A + \frac{B}{T_r} + \frac{C}{T_r^2} \qquad \{A.16\}$$

and on the theory of polysegmented molecules [Prigogine, 1957]. This correlation is reliable to ±10% and can be extrapolated with good results to lower pressures. The only input data required are the boiling point at 10 mm Hg (vapor pressure) and approximate characterization of molecular structure: the fractional aromaticity, naphthenicity, branching, and heteroatomicity. Edwards et al. [1981] extended SWAP to include hydrocarbon derivatives containing either nitrogen or sulfur as heteroatoms.

A.4.5. Group-Contribution Methods.

A popular approach is to define a molecular property as consisting of the contributions of the various component groups of the molecule. When no vapor pressure data exist, but the molecular structure of a component is known, the group contribution methods can be used to provide an estimate.

Macknick and Prausnitz [1979] presented a group-contribution method for direct determination of two adjustable constants in the AMP equation [Moelwyn-Hughes, 1961; Abrams et al., 1974] to estimate vapor pressures (in the range 10 to 1500 torr) and enthalpies of vaporization for heavy hydrocarbons. Edwards and Prausnitz [1981] extended the group parameters to nitrogen and sulfur containing groups, Ruzicka [1983] to naphthenic 5-membered rings and a condensed naphthenic groups, and Burkhard [1985] to aromatic halogen groups.

Jensen et al. [1981] developed a group-contribution method, in part based on the UNIFAC model for vapor liquid equilibria [Fredenslund and Rasmussen, 1979; Fredenslund et al., 1975, 1977], for the prediction of pure-component vapor pressures in the range 10 to 2000 torr for polar and nonpolar compounds with molecular weights below 500. The model was applied to different hydrocarbons, alcohols, ketones, organic acids, and cloroalkanes. Yair and Fredenslund 1983 extended this correlation to include amines, pyridines, nitrites, ethers, esters, and ketones. Chandar and Singh [1985] extended it to include sulfur - and additional nitrogen-containing heavy hydrocarbons.

Skjold-Jørgensen [1984] developed a new group contribution equation of state, GC-EOS, especially designed to represent phase equilibria. Skjold-Jørgensen [1988] revised and extended the parameter tables for GC-EOS, so pure-component vapor pressures as well as critical temperatures and pressures are reliably predicted. The data base used to establish the parameter tables contains pure component vapor pressures in the pressure range 15 torr to the critical pressure.

Hoshino et al. [1985] developed a group-contribution method for prediction of vapor pressures for high molecular weight hydrocarbons based on substituted benzenes. In this work the three adjustable parameters in the Antoine equation were determined from boiling temperatures at three specified pressures (10, 760 and 1500 torr). The group-contribution method is used to calculate the boiling points of substituted benzenes at specific pressures. This method is suggested for use in the pressure range 10 to 1500 torr.

Tu [1994] developed a group-contribution method for predicting the vapor pressures of organic liquids based on the integrated Clausius-Clapeyron equation in the form

$$\ln P = A + \frac{P}{T} - C\ln T - DT \qquad \{A.17\}$$

The parameters for 42 organic groups were derived from 5359 experimental vapor pressure data on 342 organic compounds. This method may be used for both nonpolar and polar compounds and yields acceptable prediction up to a pressure of 60000 torr. The

model was applied to alkanes, alkenes, alkynes, cyclones, aromatics, alcohols, aldehydes, acids, ketones, esters, ethers, amines, nitrites, thiols and chlorides.

Although numerous vapor pressure curve-fitting/extrapolation/prediction techniques could be applicable to high molecular weight PAH, the correlations presented above were developed using data on low molecular weight aromatic and nonaromatic species with no strong polar groups present. They are thus often inaccurate for describing the entire vapor pressure curve even for monocyclic aromatic spieces.

A.5. Models of Vapor Pressure of Coal Liquids.

There have been some efforts made at characterizing vapor pressures of coal liquids, as opposed to coal tars [Tsonopoulos et al., 1986]. For the most part, that work was concerned with relatively lighter compounds than are interest in coal pyrolysis (typically, four fused aromatic rings or fewer, with molecular weights of about 300 or less). Primary coal tar exhibits molecular weights that can be well over 1000, though centered between 200 and 500 daltons. In addition, there is a tendency in liquefaction to reduce the heteroatom content of coal liquids, as compared to coal tars. The predictive methods seen to work reasonably well with hydrocarbon models of coal liquids were often noted to work more poorly in heteroatomic systems [Tsonopoulos et al., 1986]. The specific intermolecular interactions prevalent in coal derived liquids make these simple approaches inadequate.

Petroleum engineering computations require a simple and reliable correlation of vapor pressure/temperature relations whose parameters can be derived from minimum information on the oil fractions. These methods have been extended to coal liquids. Several methods for correlating vapor pressures of coal liquids have been summarized by Tsonopoulos et

al.[1986]. The methods assume that the cut is narrow, less than 50°F from initial to final boiling points. It has also been noted that the successful correlations used for many years in the petroleum industry tend to be difficult to apply to coal liquids because of their highly aromatic nature.

The parameter used as index of this nature is the Watson characterization factor, K_w

$$K_w = \frac{[T_b(°R)]^{1/3}}{S} \qquad \{A.2\}$$

where Tb is the normal boiling point in degrees Rankine and S the specific gravity at 60/60 °F. Heavy paraffins have K_w's in excess of 13, crude oil fractions have a value of about 12, coal liquids have fractions with K_w's less than 10 (e.g., tetralin has a K_w of 9.78, anthracene 9.21).

The vapor pressure of petroleum fractions have been reliably predicted with the Maxwell-Bonnell [1957] correlation, which only requires two input parameters, T_b and K_w. This correlation is principally designed for converting data on subatmospheric boiling points to normal boiling points, using n-hexane as a reference material. The Maxwell-Bonnell (MB) method is based on a formula, though it is also well known as a graphical procedure. This correlation can be used without correction when K_w =12. For hydrocarbons with K_w substantially different from 12.0 a correction is needed to the boiling point. The modified Maxwell-Bonnell correlation has been applied to coal liquids by Tsonopoulos et al. [1986], Zudkevitch et al. [1983], Wilson [1981], and there has been an attempt to apply it to tars by Zudkevitch et al. [1983].

Other methods, such as the Lee-Kesler correlation [Lee and Kesler 1980] or Reidel equation [Reidel, 1954] have been explored and discussed in the context of application to coal liquids [Tsonopoulos et al., 1986]. The Reidel equation can be used for fractions if their critical temperature (T_C), critical pressure (P_C) and acentric factor (ω) are known. T_C and P_C must be also known (or estimated) to use the modified Reidel equation, which is at its best between T_b and T_C. Application of other methods, such as a modified Benedict-

Webb-Rubin equation [Brule et al., 1982] also rely on having at least fraction boiling points and specific gravity as input parameters [Gray et al., 1985]. In their approach, Brule and co-workers [1982] replaced the acentric factor with a third corresponding state parameter.

The input information of these equations is not particularly useful for present applications to coal tars because data on K_w, subatmospheric boiling points, and critical properties are not yet readily available. The weakness of the modified MB and Lee-Kesler correlations comes in handling heteroatom-containing compounds [Tsonopoulos et al., 1986]. These equations are not applicable to coal tars without considerably more a priori knowledge of the properties of tars than exists now.

These problems are avoided by the use of techniques developed by Prausnitz and coworkers. The SWAP method incorporates limited information on molecular structure into a vapor pressure correlation [Edwards et al., 1981; Smith et al., 1976]. From information on the molecular weight, the aromaticity, and heteroatom content, it is possible to estimate the vapor pressure of nitrogen and sulfur containing hydrocarbons to within about 20%. The application of the SWAP method to coal tars is considerably more involved than were the earlier correlations presented, because of the need for molecular structure information.

In addition to the SWAP method, there have been developed simultaneously group contribution methods based on detailed knowledge of all functional groups in the molecules [Edwards and Prausnitz, 1981; Jensen et al., 1981]. In comparison to SWAP, these methods are less likely to be useful in application of coal tars, since the detailed structures of the coal tars are not likely to be easily determined. The group contribution methods have been applied to the estimation of vapor pressures of low molecular weight liquefaction products [Hartounian and Allen ,1989; Vajdi and Allen ,1989].

The above methods are being developed with an eye towards the important effect that strongly interacting groups, including especially hydroxyl groups can have. An approach based on another recent group contribution method [Slejold-Jorgenson, 1988] proved more

successful [Vajdi and Allen, 1989] , but again was tested only against coal liquids that are of considerably lower molecular weight than the tars that are of interest here. Still, the success of this attempt gives hope of applicability of similar methods to the higher molecular weight materials in the future.

It may, consequently, be concluded that at present there exist no reliable or at least demonstrated correlations for estimating vapor pressures of coal tar components. Apart from the rather simple correlation of the form developed by Suuberg et al. [1979] and extended by others, attempts to develop better correlations will generally be limited by a lack of detailed characterization information on these complicated mixtures. Lack of actual vapor pressure data on coal related materials at high temperatures has led to widespread use of correlations derived from data on low molecular weight species being extrapolated well beyond safe limits.

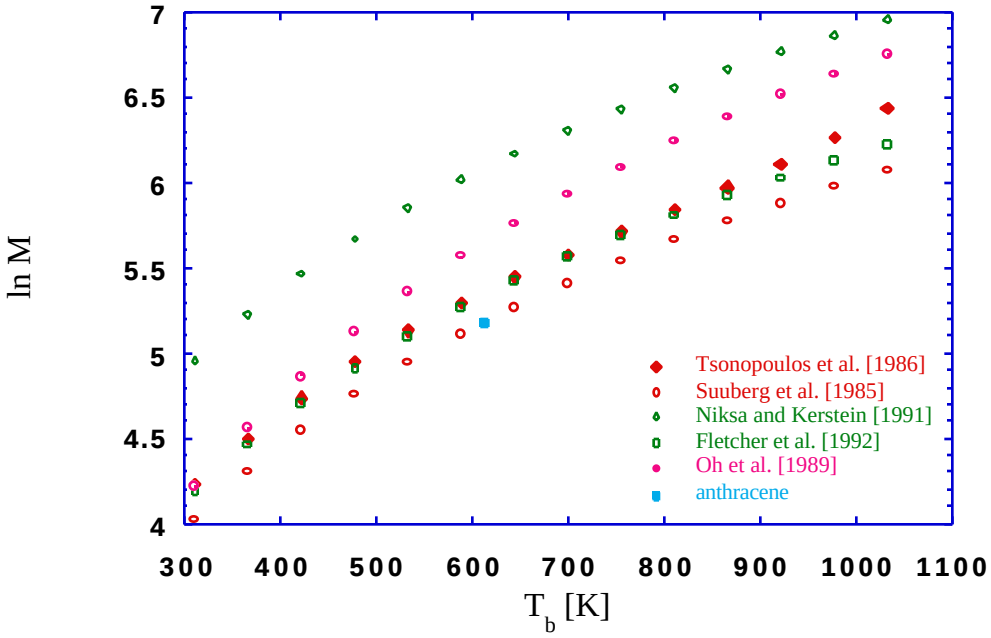

Figure A.1. Predicted variation of boiling point with molecular weight, for low molecular weight aromatics.

Chapter B. Experimental Techniques.

This chapter is divided into two parts. The first describes the preparation and characterization of coal tars. The second describes the methods by which vapor pressures of such materials can be measured.

B.1. General Experimental Procedure for Coal Tar Preparation and Characterization.

The coal tars were produced using rapid pyrolysis techniques (employing reactors and coals described below) and collected by washing the reactor with inhibitor-free THF. To prepare dry tars for testing, the solvent was evaporated from the collected tar solutions in a vacuum oven at 45°C. It is known that such vacuum drying will result in loss of some light material, especially that with a volatility greater than that of anthracene. So the starting tars can be defined, operationally, as a collection of room temperature condensables, with a molecular weight generally greater than 150 daltons. The overall approach for preparing and examining the tars is shown in Figure B.1.

The tars were, in some cases, first fractionated chromatographically, using a preparative scale gel-permeation chromatography (GPC) column. This fractionation crudely divides the tar into molecular weight intervals. Vapor pressure measurements have been made using the "non-isothermal" Knudsen effusion technique on these fractions, as well as on the whole, unfractionated tars.

Analyses of the different tar fractions were performed using vapor phase osmometry (VPO) and analytical mode gel-permeation chromatography. The latter provides the number average molecular weight of a fraction, and the former allows a crude characterization of chemical structure. An elemental analyzer was used to determine the

elemental compositions of the fractions. Differential Scanning Calorimetry (DSC) was used to examine the thermal behavior of the fractions.

B.2. Tar Preparation Techniques.

B.2.1. The Selection of the Solvent for Tar Collection, Fractionation and Analysis.

The selection of the solvent was based on a combination of three criteria: high solubility of the tars in the solvent, suitability for the liquid chromatographic and vapor phase osmometric work, and ability to evaporate it from coal tars. Pyridine and THF are on one basis approximately equally effective solvents for the coal tars; both are able to dissolve better than 97% by the mass of dry tar [Unger and Suuberg, 1984]. THF was employed instead of pyridine in the collection of tars in the preparative scale fractionation only because of the difficulty in disengaging pyridine from coal tars. Pyridine is, however, known to be a superior solvent for coal tars on the basis of GPC and VPO work, and would eliminate suspected association artifacts thought to occur in THF. These might give an incorrect impression of the molecular weight distribution [Oh et al., 1989; Solomon et al., 1992]. Thus pyridine was used in the analytical GPC and VPO characterization.

B.2.2. Tar Production Techniques.

As the project emphasizes study of primary tars (i.e., tars that have not been subject to extensive secondary reactions) the tar preparation systems have been selected to minimize the residence times of evolved volatiles in hot regions of the reactors and to avoid contact with oxidizing gases. It is difficult to produce large amounts of tar without creating the

possibility for secondary reactions of the tar [Solomon et al., 1992]. This is because the reactor systems must be chosen to provide a short residence time for the tars, and thus must be of limited dimensions. A review and the comprehensive description of a variety reactors which have been employed in pyrolysis experiments has been given elsewhere [Solomon et al., 1992]. Three systems have been used in this study: a wire mesh reactor, a fluidized bed reactor and a tubular reactor.

The wire mesh reactor (or heated grid reactor) is a rapid pyrolysis apparatus which has been described in detail elsewhere [Suuberg et al., 1978]. Typically, a pulverized coal sample was pyrolysed in an electrically heated wire mesh at a rate of 3000 °C/min to a temperature of 700°C, at which it was held for 3 seconds before cooling. The disadvantage of this method is a low tar productivity per run; producing large quantities of tar takes days because of the small coal loadings (100 mg) in each run. This method was used to prepare tar at high heating rate conditions, not readily achieved in the other devices. The other two systems could be used to pyrolyze larger masses of coal per run.

The fluidized bed technique involves pyrolysis of coal particles fluidized by an inert gas fed at the bottom of a 2 inch (5 cm) bed. The volatiles are carried away by this inert purge gas and tar is collected downstream of the hot zone. The temperature of the fluidized bed was maintained at 500°C. Collection and handling of the tars from this system are identical to the procedures followed after tar production in the heated wire mesh system. Disadvantages of this experimental method are that particle residence time and temperature history are unknown, particularly under conditions in which particles can be eluted from the bed. Also, there is the potential for significant secondary reactions of the tar, before it is eluted from the bed. The residence time of the gas in the bed may be estimated as 7 seconds. Another operational disadvantage of this technique is that this reactor needs millimeter size particles, which are not conveniently available when working with the well characterized Argonne Premium Coal samples (which come in <100 mesh and <20 mesh sizes).

Using the tubular reactor, it is possible to pyrolyze larger masses of coal than in the heated wire mesh reactor - several grams, as compared to one hundred mg per experiment. Also, particle size is not a major concern. The coal was contained in a wire mesh holder and then pushed suddenly into the heated zone of an oven. This was done to maximize the yield and to avoid secondary reactions, while at the same time allowing for moderate heating rates. The particle temperature was measured directly by a chromel-alumel thermocouple connected to the wire mesh holder. The volatiles, in this configuration, were swept away by an inert purge gas, and tar was collected on the cooled walls of a small tube, downstream of the hot zone.

The tube furnace was designed to keep secondary reactions to a minimum. An inert gas purge flow was 150 ml/min measured at 25°C, which corresponded to an average tar residence time of around 5 sec in the hot zone of the reactor. The reactor wall temperature was kept approximately at 700°C, leading to an ambient inert gas temperature of approximately 680 °C and a final particle temperature 670°C. The average particle heating rate from room temperature to 500°C was 15°C/sec and then the particle temperature reached 670°C in two minutes. The total reaction time was 3 minutes, after which the char was pulled out from heated zone. Again, handling procedures for the tars from this system were identical to those used in the other two cases.

B.2.3. Tar Fractionation Techniques.

Two different methods have been applied. The first one involved classical gel permeation chromatography (GPC), and the second, vacuum sublimation.

Gel permeation chromatography (GPC), also referred to as size exclusion chromatography (SEC) or gel filtration (GF), is a chromatographic technique in which molecules are separated on the basis of their ability to penetrate a porous gel. Larger molecules travel through the column at the same speed as the mobile phase, smaller

molecules are held back to an extent depending on their molecular size and the distribution of pore sizes within the gel [Evans et al., 1985].

The vacuum sublimation technique is based directly upon the difference in vapor pressures of tar components, leading to differences in ability to vaporize at different temperatures. Preliminary experiments showed that the separation by vacuum sublimation was less satisfactory and also the thermal decomposition of the tar was a concern when using this technique.

Thus, the tars were mainly fractionated using GPC in preparative mode, i.e., using large sample volumes. Two 25 cm columns were used in series, for this purpose. The first column was packed with μ-Styragel (styrene-divinylbenzene polymer) beads with a nominal pore size of 100 Å, and the pore size of the second column was 500 Å. The solvent was inhibitor free tetrahydrofuran (THF). The flowrate was typically 1 ml/min. The column operated at room temperature. Approximately 0.5 cc of solution containing around 500 mg/cc of tar was injected in each run.

The fractionations were based on an assumption that different molecular weight/size fractions elute at different elution times. Generally speaking, between 10 to 20 minutes were allowed for elution of each fraction. Six fractions were collected from the gel permeation chromatograph following UV detection at a wavelength of 283 nm. A typical preparative scale GPC chromatogram is shown in Figure B.2, along with the dividing lines between fractions. As may be noted, the earlier and later fractions are much more dilute than the middle fractions. Unger and Suuberg [1984] have verified the fact that all of the injected tar can elute from the μ-Styragel column when THF was used as solvent. Since around 30 mg of each fraction was needed for vapor pressure testing, three GPC runs were generally required to obtain enough material in each elution interval. After fractionation, the solvent was evaporated in a vacuum oven for approximately 24 hours, 12 hours at room temperature and room pressure, and then 12 hours at 50°C in vacuum.

B.3. Tar Characterization Techniques.

The characterization information of interest here is only that ultimately needed for the prediction of the vapor pressure and heat of vaporization. Thus very detailed chemical characterizations were not performed. Correlations based upon large amounts of characterization information may be fundamentally more appealing, but much more difficult to use.

B.3.1. Vapor Phase Osmometry.

A Knauer model 11 Vapor Phase Osmometer was used determine the number average molecular weights of tar fractions subjected to analytical GPC. All measurements were made at 90°C. Calibration was accomplished using pyrene (MW 202) as the standard and the accuracy of the VPO measurement was checked with 3-hydroxy-1H-phenalen-1-one (MW 196.21) and phenanthridine (MW 179) to ascertain the influence of heteroatoms on the calibration. Figure B.3 shows a comparison of the calibration curves based on the results for these three compounds. The slope of voltage vs. concentration appears to be slightly lower for compounds which are able to form stronger hydrogen bonds with pyridine. The results of phenanthridine were chosen to calibrate the VPO for work with a coal tar. Aspects of experimental procedure and construction of calibration curves are discussed elsewhere [Chung et al., 1979].

B.3.2. GPC in Analytical Mode.

Although not originally intended for this purpose, the analytical GPC allows to characterize tars in terms of compound classes. The analytical GPC characterization was performed using a Phenogel column of 300 mm length and 7.8 mm diameter, packed with

10 to 100 Å Phenogel. Pyridine was used as a solvent in this case. The change of solvent from THF to pyridine was dictated by the fact that pyridine is known to be a superior solvent for coal tars, and would eliminate suspected association artifacts in the THF. These might give an incorrect impression of the molecular weight distribution. Pyridine was not employed in the preparative scale fractionation only because of the difficulty in disengaging pyridine from coal tars (drying the tars prior to vapor pressure measurement is of course a key requirement for getting good vapor pressure data). The column was operated at 30 °C, and the solvent flowrate was 0.3 ml/min. Samples were prepared by dissolving a small amount of each tar fraction in pyridine. The sample injection volume was 20 µl of a 10 mg/ml solution. Detection of peaks was accomplished using a UV detector at a wavelength of 305 nm (UV cutoff was found to be slightly below 305 nm). The wavelength of 305 nm was selected to maximize the overall response factor, based upon measured signal strength as a function of wavelength. This is shown in Figure B.4. Figure B.4 shows that the ratios of different elution time fractions are not particularly sensitive to the choice of the wavelength, even though the absolute value of signal is quite sensitive.

B.3.3. Differential Scanning Calorimetry.

The Differential Scanning Calorimeter was used to study the thermal behavior of the coal tars in the temperature region of interest. The DSC would reveal where any thermally significant reaction events took place, so that the temperatures of vapor pressure measurement could be kept below such temperatures. The approximate values of the latent heat of fusion for model compounds have also been estimated using this technique.

The DSC device was a TA Instruments system 2910. The DSC system was calibrated with indium, zinc and water samples. Generally, between 5 and 10 mg of sample was used in each experiment. Heating rates were chosen between 0.5 °C/min and 60 °C/min, the

most common being 5 °C/min. Experiments were performed in the presence of a flowing inert purge gas, helium, at a flowrate of 50 ml/min through the sample cell.

B.3.4. Elemental Analysis.

Elemental analysis was used to determine the elemental composition of the tars and fractions. The elemental analyzer was the Perkin Elmer model 240B. The system was calibrated using $C_{25}H_{16}N_2O_5$ (benzophenone tetracarboxylic dianhydride 1,4 phenyl diisocyanate, elemental mass fractions C=0.7075, H=0.0377, N=0.0660 and O=0.1887) and checked by benz[gi]isoquinoline-5,10-dione, $C_{13}H_{14}NO_{2.}$ These measurements are based on complete conversion of the small quantity of sample (1 to 2 mg) by combustion to N_2, CO_2 and H_2O. The amounts of these gases formed were measured by a thermal conductivity detector which outputs corresponding signals for nitrogen, carbon, and hydrogen respectively following selective sorption of H_20 and CO_2 at different stages of analysis. Oxygen and sulfur were determined by the difference required to obtain mass closure.

B.4. Vapor Pressure Measurements.

Most ordinary devices cannot be applied to measure the vapor pressures of the primary tars because the temperatures at which they would have to be held in order to generate accurately measurable pressures are above the temperatures of decomposition of these materials. Thus, an acceptable instrument should be able to directly or indirectly determine the vapor pressures from experiments in which the samples are rapidly evaporated at low temperatures, so as to minimize thermal cracking or secondary reactions. The need to avoid pyrolytic reactions during the measurements has dictated that temperatures be kept below about 250 °C and the technique must be employed for only short times at temperatures close to 250°C. In fact, it appeared as though even lower temperatures might be called for in some cases. This will be discussed below.

B.4.1. Selection of the Technique.

The most accurate data reported in the mid pressure range were obtained by direct static techniques, where the equilibrium pressure exerted by liquid or solid at constant temperature is measured directly with a pressure gauge. This type of measurement of vapor pressures is usually used a over wide pressure ranges down to 1 torr. However, Sasse et al. [1988; 1989] have measured low vapor pressures of organic compounds down to 10^{-3} torr using this method. There are however no direct vapor pressure measurement techniques available below 10^{-3} torr.

Several techniques have been used to study low and very low vapor pressures of pure organic compounds. Reviews of low and very low vapor pressure measurementtechniques are given elsewhere [Nesmeyanov, 1963; Ambrose, 1975].

Of the different experimental techniques used to measure low vapor pressures, two have been considered here: transpiration and Knudsen effusion. These indirect dynamic

techniques have been widely used in the region from 10^{-1} to 10^{-6} torr. Both methods are standard methods, that are accepted by the Organization of Economic Cooperation and Development as pure compound vapor pressure measurement techniques.

B.4.1.1. The Transpiration Technique.

In the transpiration technique (also referred to as the gas saturation technique) a flow of insoluble and inert gas is passed in close proximity to the sample to be vaporized by either dispersing it through or passing it over the sample. The carrier gas can be passed through a volatile solid as well as a liquid. Vapor pressure is calculated from measured amount of material transported by a known amount of carrier gas by using the equation:

$$P_i^{sat} = \frac{P\ n_i}{(n_i + n_c)} \approx \frac{P\ n_i}{n_c}, \text{ as } n_C >> n_i \qquad \{B.1\}$$

where n_i is the molar flowrate of the vaporizing material, n_C is the molar flowrate of carrier gas, and P atmospheric pressure.

The concentration of organic material in the carrier flow has been determined by various methods including an infrared analyzer, UV spectroscopy, gas chromatography, liquid chromatography or by use of an electrobalance. The method adopted here involved measuring the flame ionization detector (FID) signal or response (in mV), and calculating concentrations from a ratio of this signal to a known calibration concentration signal. The flame ionization detector was selected for this purpose because of its high sensitivity to hydrocarbons and its linear concentration response over a very large range of concentrations. The calibration of the FID involved introducing a known amount of a calibration hydrocarbon into the detector system, and measuring the response. The equation for determining vapor pressure can be written in the convenient form:

$$P = \text{Constant}\ \frac{(\text{FID Response})\ (\text{experimental temperature})}{\text{Carrier Flowrate}} \qquad \{B.2\}$$

The temperature and the flowrate of the carrier gas are experimental variables, which can be controlled with high accuracy. The constant in this equation includes pressure and temperature corrections for the carrier gas flowrate, the molar volume, the barometric pressure, and the detector calibration in mV per mass or mole of carbon per time.

A problem arose in using this technique because the system had to achieve equilibrium with a small amount of material. The preparation of large quantities of *well-characterized* tar was difficult. The carrier gas can seldom be saturated with vapor in a simple pass-through cell. This is true even at low flow rates and with an extra-fine gas dispersion apparatus.

This was overcome by developing two different saturation devices. The first approach to achieving saturation is dictated by the fact that true saturation can most likely be assured if an initially partially saturated gas stream is forced to recondense. Thus an equilibrium concentration is established in a section of the saturation apparatus in which a somewhat reduced temperature zone is created, to force a partial condensation. When the vapor-gas mixture comes into contact with the cooled surface in this zone, condensation occurs, and an equilibrium is established between liquid on the surface and vapor. A temperature difference from 5 to 10 degrees between the initial saturator and the lower, constant temperature region which achieves true saturation, appears to be sufficient to provide an equilibrium saturation at the exit, based upon our own measurements. This technique is especially suitable for pure compounds. In the case of mixtures, however, changes of composition can occur during the condensation.

In the second saturation technique the carrier gas is passed through the sample, which is supported on a non-absorbent material such as a glass wool, inside a tube of 3 mm diameter and 10 cm length. The pressure drop was unimportant. This system gives good contact between the gas stream and the material, and ensures that the gas stream is almost completely saturated with vapor, while allowing a very small sample to be used. Preference

for this technique arises from a consideration of the method of separation of the coal tars. In this method, tars were already dissolved in THF. They could be easily coated in a fine layer onto a high surface area substrate (such as glass wool). The tar for which the vapor pressure is to be determined is first dissolved in a volatile solvent. It is then transferred into the saturator column after which the solvent is removed by evaporation in vacuum oven at room temperature.

The main problem occurred in analyzing actual tars. Consider an experiment in which 5 mg of any compound with molecular weight 300 is kept at a temperature at which the vapor pressure is 10^{-3} torr, under a 20 ml/min inert gas flow. For example, coronene (MW 300) generates such a vapor pressure at 200°C. To evaporate all this material under these conditions would take 10 days. Thus to analyze a full tar sample requires days, assuming that 5 to 10 mg of tar sample is necessary in order to reach saturation, and a two hour experiment is performed at each selected temperature. On the other hand, tars are complicated mixtures of thousands compounds with very different volatilities, and according to Raoult's law, the FID signal would be mainly determined by the more volatile compounds present at any time. To explore the full mixture requires patiently evaporating all of it, while at the same time worrying about loss of saturation when the mass of tar becomes low.

An additional disadvantage of this technique was the large uncertainty in calculating the vapor pressure and the mass loss from the FID signal. This is because of the highly heteroatomic nature of tars. Various features of the chemical structure (such as heteroatoms) influence the response of the FID, thus it is difficult to calibrate the FID for a coal tar, i.e., to find suitable calibration standard compound. Coal tar itself cannot be used, because of condensation type reactions and its low volatility. Moreover, it can be crudely estimated from the effusion results that only around 70% of HV bituminous tar would be GC volatile. Therefore the vapor pressure experiments of this study were carried out using the Knudsen effusion technique.

B.4.1.2. Knudsen Effusion Technique - Overview.

Effusion is the phenomenon in which molecules escape from a vessel through a small opening, without disturbing the equilibrium distribution within the vessel. Knudsen effusion involves measurement of the rate of loss of molecules of the evaporating substance, leaving the opening of the effusion cell under molecular flow conditions. The simplified equation for determining vapor pressure can be written as:

$$P = C\frac{d\omega}{dt} \qquad \{B.3\}$$

in which $d\omega/dt$ represent the mass loss per unit time from an orifice of an effusion cell under molecular flow conditions, and the constant C, among the other things, contains the orifice area, molecular weight, the temperature of effusing species and other correction factors. The principal application of this method has been for determining the vapor pressures of metals. It has, however, proven equally effective for obtaining the vapor pressures of organic crystals and compounds.

Reliable measurements using the Knudsen effusion method require particular attention to the problem of the measuring and controlling the temperature of the Knudsen cell within the vacuum enclosure. Most discrepancies between the results of various workers using this or related vacuum techniques are the result of insufficient attention to this problem. As the sample must receive heat purely by radiation (since the cell is operated in a high vacuum) isothermal steps as long as 5-10 hours duration are used for equilibration at any new temperature. The determination of a vapor pressure curve via the conventional "isothermal" mode of the Knudsen effusion technique requires days. During this time, there may be more than a 20% mass loss from the sample (up to 50%). This is an important consideration in work with mixtures, in which the condensed phase composition can be significantly changed by high extents of mass loss.

To address this problem we improved the traditional "isothermal" mode of the Knudsen effusion technique, so that the determination of the full vapor pressure curve requires from 5 to 10 hours. The most important advance was development of a new continuous non-isothermal technique. This new modification of the Knudsen effusion technique provides vapor pressure information while temperature is continuously varied and is faster than the "isothermal" mode. Thus the sample loss during an experiment may be kept quite low.

B.4.2. Knudsen Effusion Method - Basic Aspects.

In this study, the vapor pressures of primary coal tars have been examined using the Knudsen Effusion method, modified for application to mixtures containing components with a wide range of volatilities. The Knudsen effusion technique was selected because of the thermally labile nature of the primary tars (those that have not undergone secondary cracking). The technique permits measurements of vapor pressure at quite low temperatures.

B.4.2.1. The Theory of the Knudsen Effusion Method.

The basic theory of the effusion method has been often reviewed in the literature [Knudsen, 1909a; Knudsen 1909b; Hollahan, 1962; Dushman, 1962; Nesmeyanov, 1963]. The method is actually based upon the kinetic theory of gases. From these classical results, Knudsen derived an expression for the slow isothermal flow out of a cell with a small hole in it. According to Knudsen [1909a] the vapor pressure of a material in the cell can be calculated from:

$$P = \frac{\omega}{tA_o}\sqrt{\frac{2\pi RT}{M}} \qquad \{B.4\}$$

The above result is called the ideal Knudsen equation, in which P is the vapor pressure, ω is the weight loss during the effusion time interval, A_0 is the orifice area, M is the molecular weight in vapor phase, t is the effusion time , and T is the absolute temperature.

It is assumed when applying the basic effusion equation {B.4} to the effusion process that:

• Thermal equilibrium exists throughout the cell.

• Chemical equilibrium obtains with in the cell. This includes assuming a uniform composition in each phase, unit evaporation/condensation coefficients, and that the

equilibrium vapor pressure of the effusing species exists within the cell (This will generally be true if for r << A; r is the orifice radius and A is the effective evaporation area).

• The orifice walls do not intercept and return into the cell an appreciable fraction of molecular current entering the hole. This equation is strictly applicable only if the thickness of the wall, in which the orifice of area $A_0 = \pi r^2$ is located, is vanishingly small compared with the hole's radius r. This means that the orifice should be located in an infinitely thin wall or be cut such that the edge is exceedingly sharp (knife edge orifice).

• There is no back flux into the orifice exit from the surroundings - no molecules return once they have passed through the orifice.

• Free molecular flow exists in the vapor. This means that the number of intermolecular collisions in the vapor phase, occurring within the orifice, is negligible. This will be true if the molecular mean free path in the vapor is long compared to the orifice diameter. Knudsen's criterion [Dushman, 1962] is adopted to evaluate this, that is, molecular flow (collision free) occurs when $\lambda \geq D$, where λ is the mean free path of vapor molecules within the cell and D is the diameter of the orifice.

The equation (B.4) is the basic working equation for the technique. It has, however, been modified by a number of authors, for various experimental conditions, to obtain a true saturated vapor pressure from Knudsen effusion data. The corrections to the theory which have been studied have included the effects of the shape of the orifice and cell, nonunit evaporation coefficients, effects due to long mean free path (wall collisions more important than gas phase collisions), effects due to short mean free paths as the flow goes from free molecular to transition to hydrodynamical, and effects due effects to temperature gradients, to surface diffusion, and due to specular reflection.

B.4.2.2. Real Cells, Samples and Orifices.

B.4.2.2.1. Nonideal Orifice, the Clausing Factor for an Orifice.

Under ideal conditions, the saturated vapor in an enclosure effuses out through a perfect hole into a space in which the pressure of vapor is zero. In practice, the orifice is not located in an infinitely thin wall and it has the form a of channel of finite length. Thus the molecules may strike the orifice wall and be returned back to the cell. Therefore, the simplest and most widely used modification of equation (B.4) takes into account the resistance of the opening to the flow of vapor molecules, and has the following form:

$$P = \frac{\omega}{tA_o W_o}\sqrt{\frac{2\pi RT}{M}} \qquad \{B.5\}$$

The transmission probability W_0 (the Clausing factor) has values in the range zero to unity and may be physically understood as a probability that a molecule entering the orifice from the effusion chamber will reach the exterior of the orifice. It is assumed that molecules enter the orifice from an isotropic gas phase, from a random direction, according to the cosine law.

The determination of the Clausing probability factor W_0 for an orifice is one of the important requirements for performing reliable measurements by the Knudsen effusion technique. The Clausing factor has been shown to be a function of the ratio of the length to the radius of a cylindrical hole through which the molecules travel. There are two approaches used for determining W_0.

In the first approach, the cell can be fabricated so that the cell wall thickness and the hole diameter are accurately known, such that W_0 can be calculated using known empirical expressions, or the value can be found from Clausing tables. Values of W_0 for cylindrical and rectangular orifices are given by Clausing [1932], Dushman [1962], and Kennard [1938]. In order to calculate W_0 for molecular flow, the following empirical formula [Dushman, 1962] may be used:

$$W_0 = \frac{1}{1 + \frac{3l}{8r}} \qquad \{B.6\}$$

where l is the length and r the radius of the hole.

In the second approach, the effusion cell can be calibrated using reference materials for which pressures are accurately known and w_0 is back-calculated using equation {B.5}.

Even though the equation {B.5} is the most commonly used empirical equation, it has been modified by a number of authors to correct for other determinate errors and obtain more accurate equilibrium vapor pressures from Knudsen effusion data. These modified equations have been developed for a cylindrical cell by Clausing [1932], Mortzefeld [1955], Whitman [1952], and Balson [1961]. Carlson et al. [1963] have presented a mathematically rigorous description of the distribution of the gas within spherical and cylindrical cells.

B.4.2.2.2. Evaporation Coefficient, Cell Geometry.

At equilibrium the evaporative flux of molecules leaving the surface must be equal to the condensation flux of molecules striking the surface. It should be noted that the opening in the vessel disturbs the equilibrium between the condensed phase and vapor phase. Once an opening has been provided for molecules to effuse, there is no longer a closed system and the pressure over the sample is not the true equilibrium pressure P_{eq} but something less than this, a steady state pressure P_{ss}. This is clearly a different situation than presented above for an ideal equilibrium cell, and the real situation only approaches the ideal when the rate of effusion is quite small compared to the rate of both escape of molecules from the surface by evaporation and condensation onto the surface.

When this feature of the process is considered, equations for determination of the true vapor pressure, P_{eq}, must explicitly include consideration of the dynamic equilibrium at the surface of the vaporizing liquid. This requires inclusion of a term that recognizes that the

surface evaporation and condensation processes have a rate proportional to the surface area of the liquid, A_S.

Also, in a vaporization process which has attained equilibrium, the number of molecules which strike the surface of the condensed phase and remain with the condensed phase must equal the number of molecules which leave the surface. All of the molecules which strike the surface may not, however, "stick". Langmuir [1913] has shown that for metal atoms condensing on a surface the value of the condensation coefficient (sticking probability) may be assumed equal to 1 and Verhoek and Marshal [1939] showed that the same assumption is justified in high boiling point organic liquids. Accurate values of condensation coefficients are generally not available except for a very few materials. Plausible reasons for coefficients to be close to unity have been advanced for the types of materials of interest here. For the majority of cases they are probably between 0.7 to 1; only in the case of vaporization of species whose molecular structure is quite different in the gas than in solid or liquid (e.g. dimer liquids), are they thought to be very small, $0.001 < \alpha < 0.1$. Thus there is generally less than unity probability of condensation for every incoming molecule.

The geometry of the cell body and the location and area of the sample within it affect the total rate of flow from the pinhole. Several authors have introduced the transmission factor W_C, for a cell, which is the probability that a molecule leaving the bottom of the cell will reach the orifice.

In addition to the above processes, there may exist some others that can cloud interpretation of the results. Examples include interaction between cell walls and the effusing molecules, surface diffusion and sorption, specular reflection, and reaction at the walls.

The degree to which true equilibrium is maintained in an effusion cell depends upon the sticking probability being high enough such that effusion does not compete as a vapor

phase molecular loss process with condensation. Thus the corrected equation has the general form:

$$P_{eq} = P_{eq}(P_{SS}, \alpha, W_0, W_C, A_0, A_S) \qquad \{B.7\}$$

where A_S is the sample area from which evaporation occurs. This is usually taken to be the cross sectional area of the body of the cell (in the case of cylindrical cells).

For example, Whitman [1952] and Motzfeldt [1955] have shown that P_{eq} and P_{ss} are related in the case of cylindrical cells through the equation:

$$P_{eq} = P_{ss}\left[1 + \frac{W_0 A_0}{A_c}\left(\frac{1}{\alpha} + \frac{1}{W_c} - 2\right)\right] \qquad \{B.8\}$$

Ward and Fraser [1968] have simulated the real effusion process by Monte-Carlo calculations, and found that equation {B.8} has the correct form. For a cell of length equal to its diameter, which is also the case for our cells, W_C~0.5 and equation {B.8} becomes:

$$P_{eq} = P_{ss}\left(1 + \frac{W_0 A_0}{\alpha A_c}\right) \qquad \{B.9\}$$

The effect of cell geometry has been observed in the case of an ideal sample (α=1) and orifice (W_0=1) [Carter, 1970], and predicted values of P_{ss}/P_{eq} range from 0.97 to 1.0 for cells with the ratio of the orifice and cell radii (R_0/R_C) in the range from 0.1 to 0.2. Therefore one seldom finds any corrections made for the cell body geometry in the literature. By applying equation {B.9} for orifices of different areas at similar experimental conditions, it is possible to obtain the values of P_{eq} and the condensation coefficient α from a plot of P_{ss} versus $P_{ss}(W_0A_0/A_C)$ [Margrave, 1967].

Equations {B.8 and B.9} have been used to study the vapor pressures of low volatile organic compounds by several authors [De Silva and Monte, 1990; Pribilova and Pouchly, 1974; Boehncke et al., 1996]. However, Ribeiro Da Silva and Monte [1990] noted that in using three different orifices, accurate values of α and P_{eq} were not obtained.

The accuracy of different assumptions was checked here using materials of known vapor pressure, as described below. Again, it is not likely that α will be much different from unity, and $A_0 << A_C$, so $P_{eq}=P_{ss}$ will generally be assumed.

B.4.2.3. Implementation of the Method.

Equation {B5} has been successfully utilized to calculate equilibrium vapor pressures of organic compounds by many workers [Morecroft, 1964; Wiedemann, 1972; DePablo, 1976; DeKruif, 1980; Colomina et al., 1980; Colomina et al., 1982; Kelley and Rice, 1964; Murray and Pottie, 1974]. As was noted above, the steady state pressure P_{ss} may be expected to be slightly less than equilibrium pressure P_{eq}. On the other hand, the corrections for evaporation coefficient and cell body are difficult to perform and will not be significant in the case of coal tars. Thus more accurate values for P_{eq}, involving further corrections cannot normally be found in the literature [Ribeiro Da Silva and Monte, 1990]. Considering that the technique has been successfully applied to organic compounds without making these corrections, and that concern is with a class of materials for which the extra correction would not be expected to be important, it will be assumed that the corrections are not needed in this work.

The main working equation has the general form as suggested by equation {B.5} and the specific form:

$$P = 17.1463\frac{\omega}{tA_oW_o}\sqrt{\frac{T}{M}} \qquad \{B.10\}$$

where P is the vapor pressure in torr, ω is the weight loss in grams during the effusion time interval t in seconds, A is the area of the orifice in cm^2, M is the molecular weight of the effusing vapor in grams per mole, T is the absolute temperature in K, W_0 is a Clausing probability factor, obtained by interpolation from the table given by Dushman [1962].

As is evident from the above formula, it is necessary to know the molecular weight of the vapor, and hence, the chemical composition of the vapor, in order to determine vapor

pressure by the effusion method. This is by no means always possible, especially in the case of complicated mixtures such as coal tars.

If the vapor is composed of more than one gaseous species [Edwards and Franzen, 1995], then equation {B.10} must be written for each species, i:

$$P(i) = \frac{\omega(i)}{t \quad A \quad W_o} \sqrt{\frac{2 \quad \pi \quad R \quad T}{M(i)}} \qquad \{B.11\}$$

However, the equation {B.10} can be used even in the case of a vapor with N species, if the molecular weight is expressed as the appropriate value:

$$M_k = \left(\sum_{i=1}^{N} \frac{f(i)}{M(i)^{1/2}} \right)^{-2} \qquad \{B.12\}$$

where f(i) is the mass fraction of the species i in the vapor, $P = \sum P(i)$ and $\omega(i)=\omega \cdot f(i)$. The value of M_k is close to the average vapor molecular weight M* of the vapor phase, allowing {B.10} to be rewritten as follows:

$$P = \frac{\omega}{t \quad A \quad W_o} \sqrt{\frac{2 \quad \pi \quad R \quad T}{M^*}} \qquad \{B.13\}$$

B.4.3. Knudsen Effusion System.

B.4.3.1. Effusion System.

A high vacuum system must be used, and the vacuum outside the cell (10^{-6} to 10^{-7} torr) should be achieved quickly, so that the beginning of an experiment can be registered with sufficient temporal accuracy in work with mixtures. It is recommended that the pressure external to the cell be at least one order of magnitude below the vapor pressure to be determined [Ribeiro Da Silva and Monte, 1990].

The effusion system is represented schematically in Figure B.5. It consists of several main items of equipment. A mechanical vacuum pump is used both for pre-evacuating the system and for backing the oil diffusion pump. A 4 inch diffusion pump allows for drawing the necessary vacuum to ensure that the residual gas pressure is approximately ten times lower than the vapor pressure measured. It is connected to the microbalance chamber through a liquid nitrogen trap. An ionization gauge tube (3) connected to a Varian 840 Gauge Controller is used for measuring the vacuum maintained in the system throughout the effusion process. Two thermocouple gauges (1, 2) connected to Varian 801 TC Gauge Controllers are used for leak detection and for measuring the vacuum in the system during the pre-evacuation process. The needle valve (7) is used for filling the system with dry inert gas (to atmospheric pressure) at the end of an experiment. During the filling, the pressure in the system is measured using a pressure-vacuum gauge. The hardest vacuum reached in this system was 10^{-8} mm Hg, which is sufficient for the range of pressures that can reasonably be measured by this method.

B.4.3.2. TGA Apparatus.

The internal details of the effusion apparatus are schematically shown in Figure B.6. The effusion cell is suspended on the arm of a CAHN 2000 recording electrobalance that has a sensitivity 0.5 μg, capacity of 1.5 g and zero stability better than 10 μg. The suspension system, which is 40 cm. long, consists of tungsten wire with a diameter of 0.25 mm and a small hook made of 0.05 mm diameter tungsten wire. The cell (mass around 150 mg) itself actually hangs inside an aluminum capsule with a mass of 5 grams (painted black to increase the effectiveness of radiative transfer), which surrounds, but does not touch, the cell. This arrangement was found to be necessary in order to improve heat transfer to the cell, and to allow accurate measurement of temperature in the immediate vicinity of the cell. It has been used in performing both the traditional isothermal experiments, as well as the new continuous non-isothermal experiments. The capsule is intended to provide the cell with as close to an isothermal " black body" surrounding as possible. The long equilibration times for the isothermal experiments have more to do with how long it takes the capsule to come to a new thermal equilibrium than with how long it takes the cell to equilibrate.

The capsule temperature is measured by a chromel/alumel thermocouple in direct contact with the capsule, at a distance of no more than a few millimeters from the bottom of the cell. The thermocouple is calibrated against a Fisher brand mercury thermometer and its signal is recorded using an Omega DP85 digital indicator, with accuracy 0.1 K, interfaced to a chart recorder.

A cold trap near the orifice of the Knudsen cell has been recommended in the literature, in order to condense the vaporized compound and assist in keeping the back pressure low. Provision has not been made here for a cold trap near the cell, and reliance was placed upon a high pumping rate and a condenser slightly downstream of the cell, to give the necessary low pressures outside of the cell. The water cooler shown in Figure B.6 is designed for

this purpose. The troublesome effects of static charges on the vaporization tube could be eliminated by rinsing the outside of the tube with methanol or water.

Maintaining and measuring the cell temperature with a high accuracy is critical. It is noted by Wiedemann [1972] that a change of a few tenths of a degree Kelvin can alter the vaporization rate and lead to significantly erroneous values of vapor pressure, particularly if the temperatures are low. Temperature control and recording instrumentation are used that are capable of the required performance.

B.4.3.3. Heating System.

The heating system consists of an aluminum block oven surrounded by insulating material. This is a high mass heating system and offers temperature control comparable to an oil bath system. It does not have electromagnetic induction effects as would a resistance furnace. The heat source for the temperature control system consists of a 300 W heater for coarse regulation and 50 W heater for exact regulation. The latter is controlled by means of a RFL Industries, Inc. temperature controller, which is designed to regulate temperatures within a few tenths of a degree. The temperature in the block is measured using a chromel/alumel thermocouple and recorded using an Omega DP85 digital indicator.

B.4.3.4. Effusion Cell.

A Knudsen cell of new design was developed for this work with solid or tarry hydrocarbons. The design was limited by several special requirements: first it had to be very light, less than 1 gram (determined by the capacity of the microbalance); second, it had to allow using samples of a few tens of milligrams (large quantities of *well-characterized* tars were not available); and finally, it had to preferably be inexpensive enough so as to be disposable, to avoid concerns about cleaning. The result is a cylindrical sample container

with approximately 0.01 cm^3 internal-volume, stamped from 25 μ m thick brass foil or 25 μ m thick oxidation-resistant stainless steel foil, and closed hermetically by pressing the orifice plate to the cylinder with a hand press, thus ensuring no leak from the cell, except through the orifice. The cell is outgased under vacuum for several hours at a temperature of at least 300 C or cleaned by heating up to 1000 C using a propane flame. Unfortunately, the hermetic closure of the cells has proven to be a possible problem, as discussed below.

The effusion holes in the foil are made using fine drills. The orifice diameter is determined by use of an optical microscope. The determination is made at room temperature, but it is not felt that thermal expansion should alter the dimensions of the hole significantly. The Clausing factor is obtained by interpolation from the table given by Dushman [1962].

Orifice diameter selection was guided by published results, and examined parametrically. Morecroft has shown that the vapor pressure measurement is independent of hole size [Morecroft, 1964], within the guidelines suggested above. It is has been noted that it is necessary that the mean free path of the molecules be larger than the orifice diameter in order to employ the Knudsen formula; for practical purposes, this would normally be interpreted as a mean free path ten times large than the orifice diameter. Good results can, however, still be obtained when the diameter is about the same as the mean free path [Morecroft, 1964]. On the other hand, since the effusion rate is very small at low pressures, a large orifice (diameter 3 to 5 mm) is required to give reasonable rates [Wiedemann, 1972]. Very large holes can, however, yield erroneously low apparent values for vapor pressures, owing to self-cooling of the sample and failure to maintainequilibrium [Ribeiro Da Silva and Monte, 1990].

In addition to slow effusion rates, other problems also exist with small orifices. For example, the existence of small leaks in the cell can cause problems if the effusion hole has a small size. In this case, the effective effusion area is higher than believed, leading to a calculated vapor pressure that will be considerably higher than the true value, as a result of

using the “wrong” orifice area. It is also reported by Winterbottom and Hirt [1962] that the influence of surface diffusion increases as the radius of the hole decreases.

Holes with diameters from 0.6 to 1.1 mm were selected. Several replicate experiments were done to check on systematic errors and cell design. The vapor pressures were found to be independent of the hole size, and were reproducible.

B.4.4. Establishing the Performance of the Apparatus.

Analysis of the experimentally determined vapor pressure data was performed using the integrated form of the Clausius-Clapeyron equation {A.8} by plotting the natural logarithm of vapor pressure against the reciprocal of temperature. The latent heat of sublimation (ΔH), and the entropy of sublimation (ΔS) , can be calculatedusing this equation. The ΔH and ΔS values correspond to the average temperature of the measurement. The equivalent expression can be written in the form:

$$\ln P[\text{torr}] = -\frac{B}{T} + A = -\frac{\Delta H}{RT} + A \qquad \{B.14\}$$

where P is in torr, T is in K, $\Delta H = B*R$ in kJ/mol, $\Delta S = (A - 4.893)*R$ J/mol K, and R is ideal gas constant (R = 8.314 J/mol K).

B.4.4.1. Effusion Technique Using the Isothermal Method.

The isothermal step method was used to check the performance of this technique. Our results were compared with literature values. To verify that the procedures yielded accurate vapor pressures of low-volatile compounds , the vapor pressures of anthracene, naphtacene and phenanthrene were measured. Approximately 5% of each material was evaporated before actual measurements, to eliminate occasional artifacts due to volatile impurities.

Anthracene ($C_{14}H_{10}$, FW = 178.24, m.p.= 218°C , b.p.= 340°C)

Anthracene of 99+% purity was obtained from the Aldrich Chemical Company, Inc. This compound was tested because of the large number and generally good agreement of experimental data in the literature. It is also an appropriate standard for study of coal related compounds. Anthracene has been studied here at temperatures between 45 and 90°C and at pressures from $3.85*10^{-5}$ to $8.97*10^{-2}$ torr.

In order to ascertain that the pinhole diameter was not a critical variable in the cell design, experiments were performed with different size holes. The results are shown in Figure B.7, together with a curve based on the mean of the data from the literature. The mean curve was constructed by using each reference's recommended correlation applied to the maximum and minimum temperatures of that study. This procedure is admittedly somewhat arbitrary, but captures the essence of the data as the resulting correlation line in Figure B.7a shows. The vapor pressure appears to be independent of the hole size. Our results for anthracene lie near the average values of the literature data and give a heat of sublimation over the measured temperature range of 100.8 kJ/mol. This is in quite good agreement with the literature data.

The performance of the apparatus at higher temperatures was checked by measuring the vapor pressures of naphthacene and pentacene.

Naphthacene ($C_{18}H_{12}$, FW = 228.29, m.p.= 357C , b.p.= unknown)

Naphthacene of 98% purity was obtained from the Aldrich Chemical Company, Inc. This compound has been studied here at temperatures between 113 and 199°C and at pressures from $2.6*10^{-5}$ to $3.6*10^{-2}$ torr.

Figure B.8 shows the results obtained for naphthacene. Again, there is excellent agreement with the relatively few data in the literature. From these results, the latent heat of sublimation can be estimated to be 125.2 kJ/mol.

Pentacene ($C_{22}H_{14}$, FW = 278.35, m.p.= above 300 , b.p.= unknown)

Pentacene of 98% purity was obtained from the Aldrich Chemical Company, Inc. This compound has been studied here at temperatures between 170 and 210°C and at pressures from $1.2*10^{-5}$ to $1.3*10^{-4}$ torr. Figure B.9. shows the results obtained for pentacene. The values agree, within experimental error, with the literature values. The measured enthalpy of sublimation (154.4 kJ/mol) is in good agreement with the values from the literature data.

B.4.4.2. Non-Isothermal Technique.

The non-isothermal technique is identical to the isothermal technique, except that the system temperature is continuously varied, and the mass loss rate is continuously calculated.

Figure B.10. shows the results of measurements on anthracene performed using the non-isothermal Knudsen Effusion technique at heating and cooling rates of 5 °C/min. It is apparent that there is a significant deviation of the results from the isothermal technique data. The fact that the heating data underpredict and the cooling data overpredict the real vapor pressures might be anticipated. This performance suggests that the cell temperature is lagging the surrounding capsule temperature, and that the heat transfer limitation has shifted to the capsule-cell transport process. For this reason, it is logical to expect that by decreasing the rate at which the capsule is driven in temperature, this limitation can be minimized. This is borne out by the results obtained at 0.8 °C/min heating rate.

The new results for anthracene with a heating rate of 0.8 °C/min are seen in Figure B.11. There is in this case good agreement between the results obtained from the non-isothermal and isothermal techniques.

Figure B.12 and B.13 show the results of the non-isothermal technique applied to naphthacene, in "cooling" and "heating" modes, respectively. As seen in Figures B.12 and

B.13, there is again good agreement between the results of isothermal and non-isothermal heating and cooling runs. Thus the reliability of non-isothermal method appears to be established and this technique is suitable for the vapor pressure measurements with heating or cooling rates up to about 1 °C/min.

B.4.5. Conclusions.

Two different methods, effusion and transpiration, have been examined for measuring the vapor pressures of coal tars. The former has been chosen as the more suitable for work with mixtures. Two accurate effusion measurement methods, the isothermal and non-isothermal Knudsen effusion methods, have been developed. It can be seen that there is generally good agreement between the two techniques, and that both give results that agree well with published values.

An effusion apparatus suitable for measuring vapor pressures from 10^{-2} to 10^{-6} torr has been developed. The lower limit of measurable pressure is determined by the balance sensitivity, noise in the recording microbalance system and the design properties of the cell (thickness of the foil, diameter of the orifice). The upper limit is determined by the critical Knudsen number. The reliability of the measurements was carefully established using comparison of the results obtained here with literature values for well-studied materials.

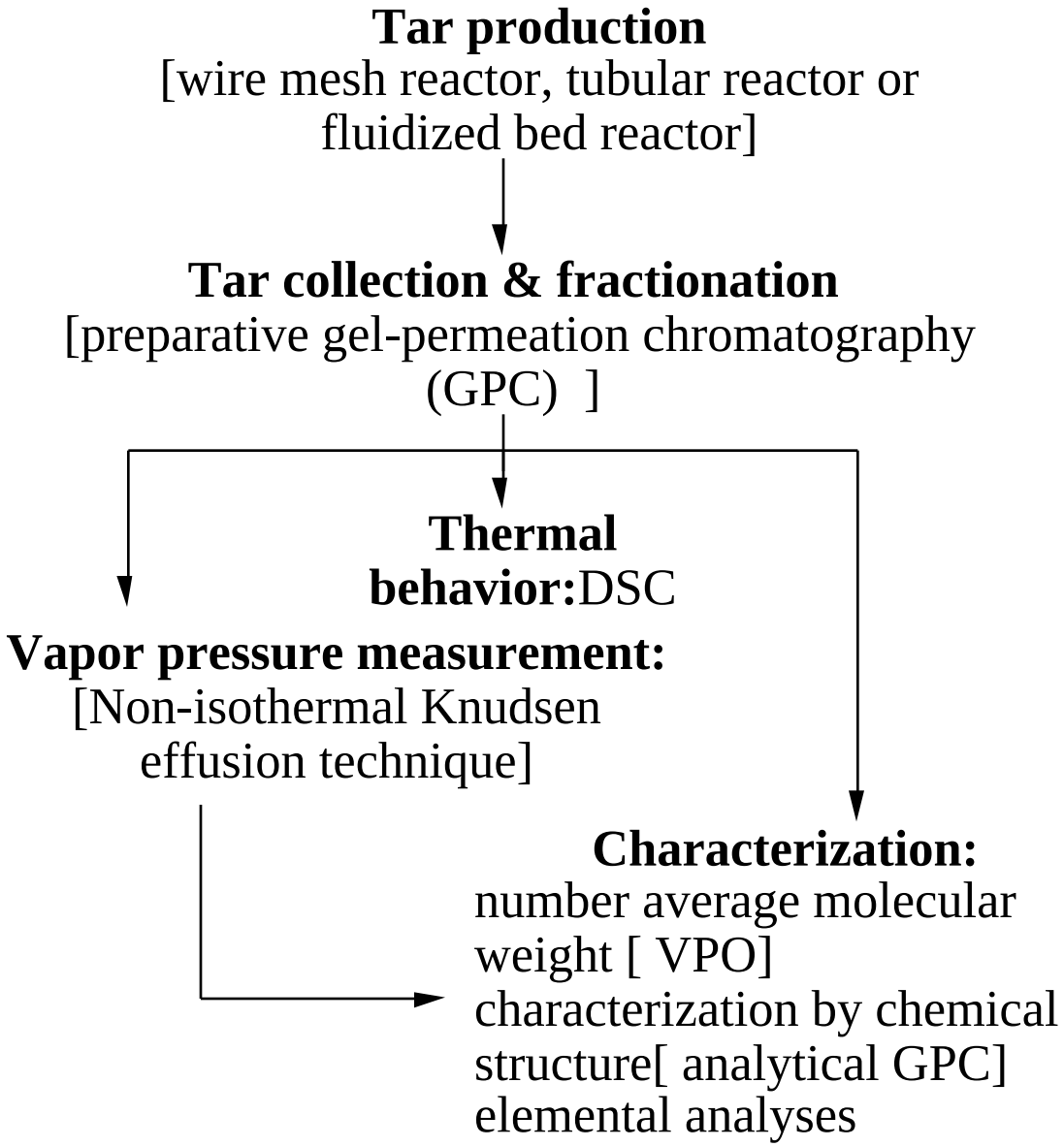

Figure B.1. General scheme for coal tar preparation and characterization.

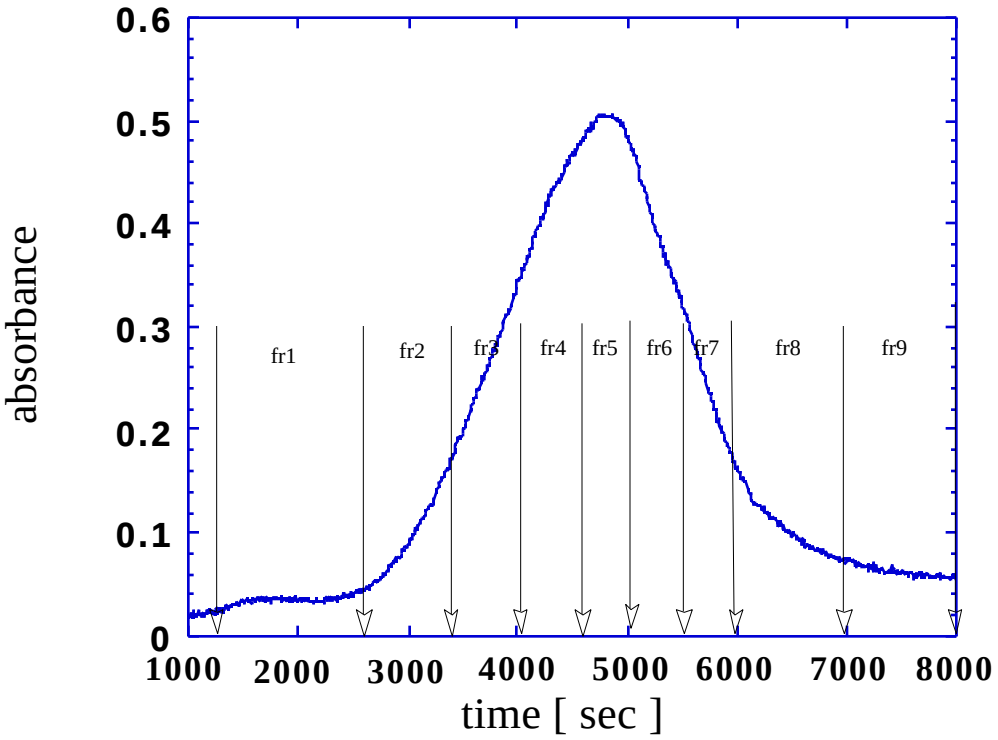

Figure B.2. Typical preparative GPC chromatogram, along with the dividing lines between fractions.

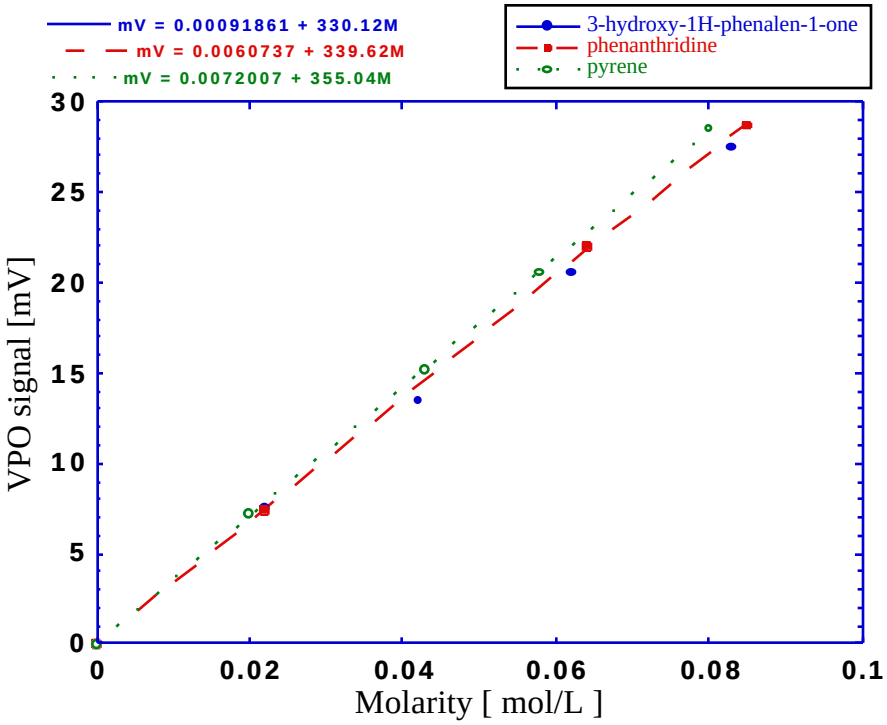

Figure B.3. VPO calibration constant determinations at 90°C using pyridine as the solvent.

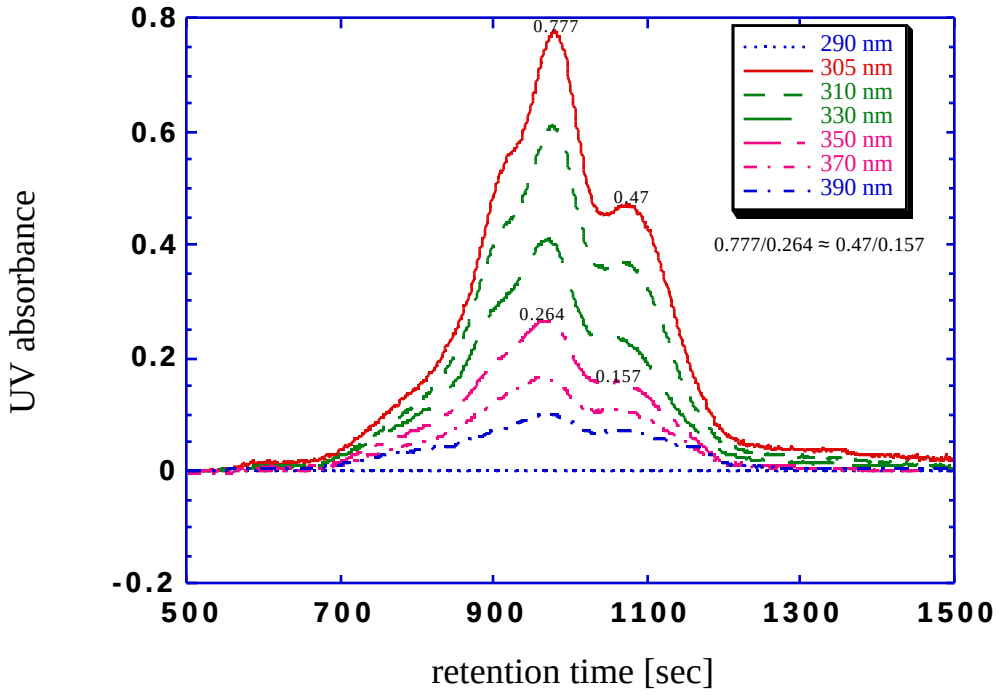

Figure B.4. Selection of wavelength to maximize the UV-detector response factor, using Bruceton coal tar. Uniform increase of absorbance is seen as the wavelength approaches 305 nm.

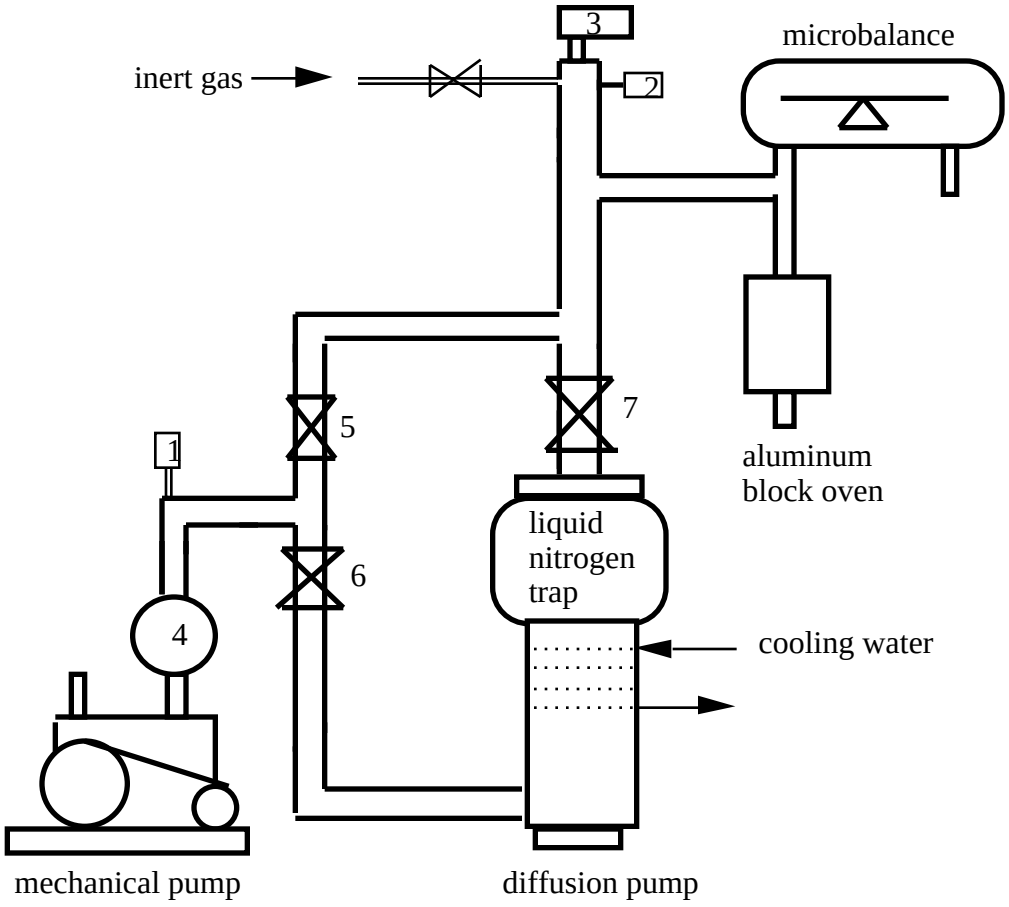

Figure B.5. General schematic of the effusion system; 1, 2 - thermocouple gauges 3- ionization gauge; 4 - molecular sieve trap; 5, 6 - valves; 7 - needle valve.

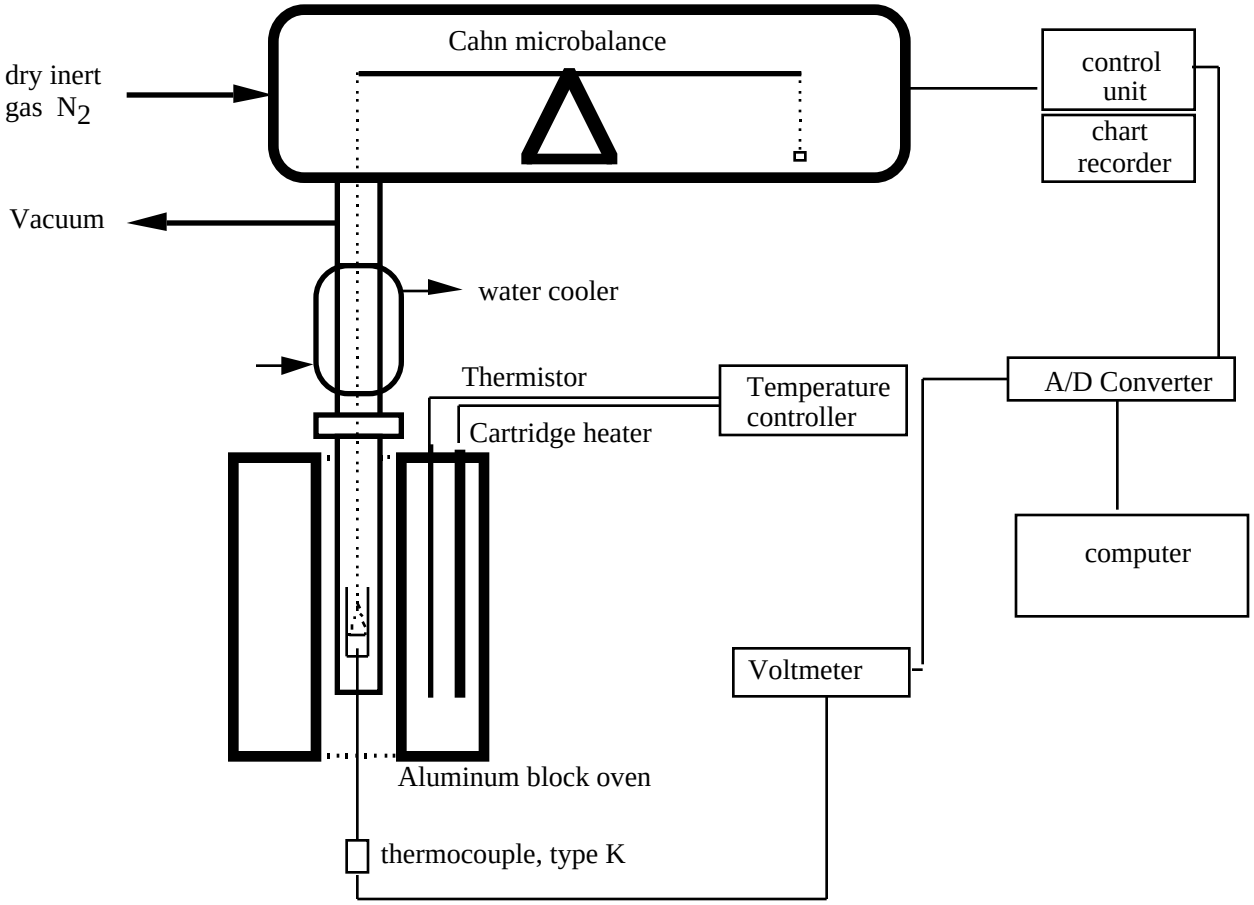

Figure B.6. Arrangment of an Effusion Apparatus with control and measurement system.

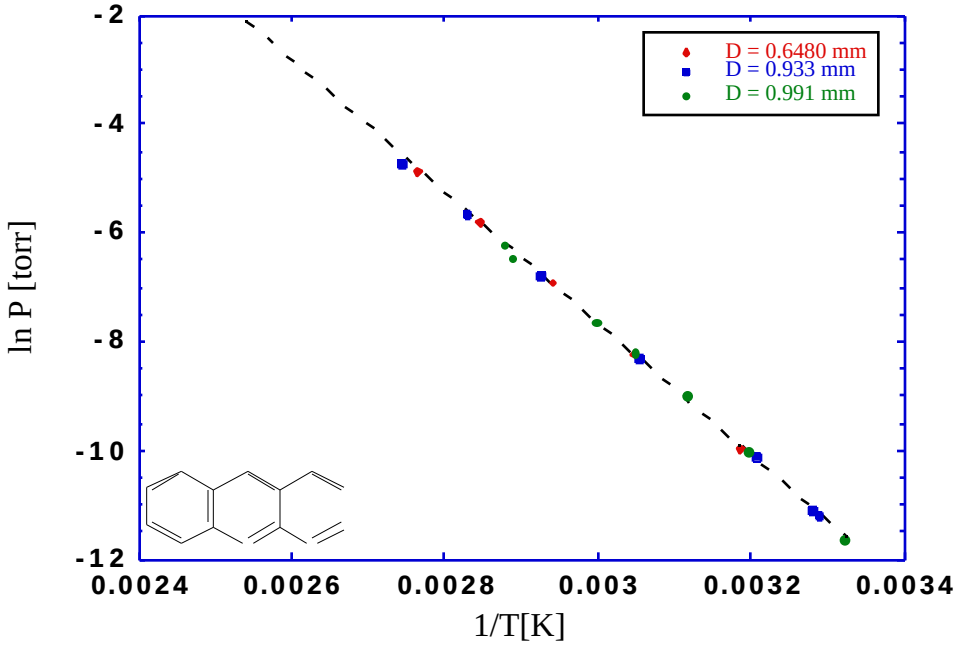

Figure B.7. The effusion method applied to anthracene, using different diameter effusion orifices. The dashed line is a mean of the data from the literature.

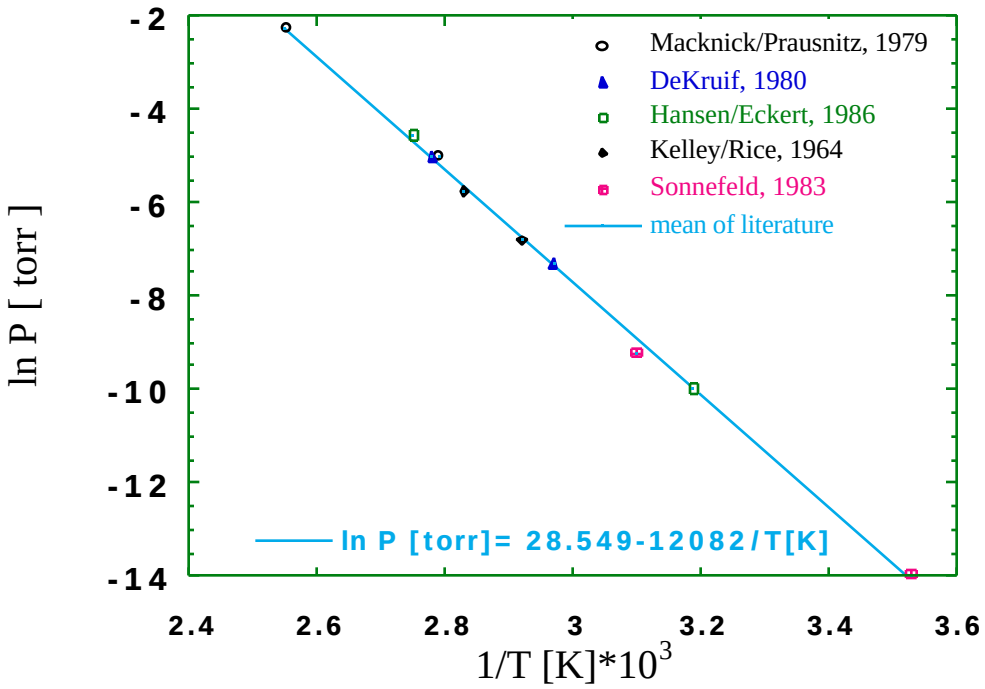

Figure B.7a. Mean of literature data for solid anthracene.

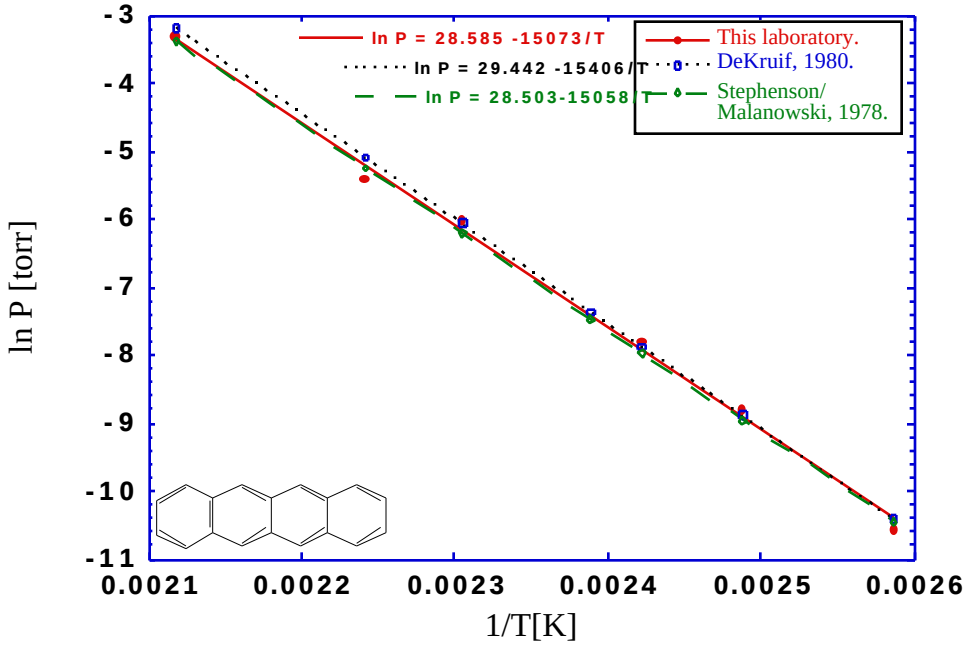

Figure B.8. Effusion method applied to solid naphthacene. The solid points are from this study, and the open points are calculated from references.

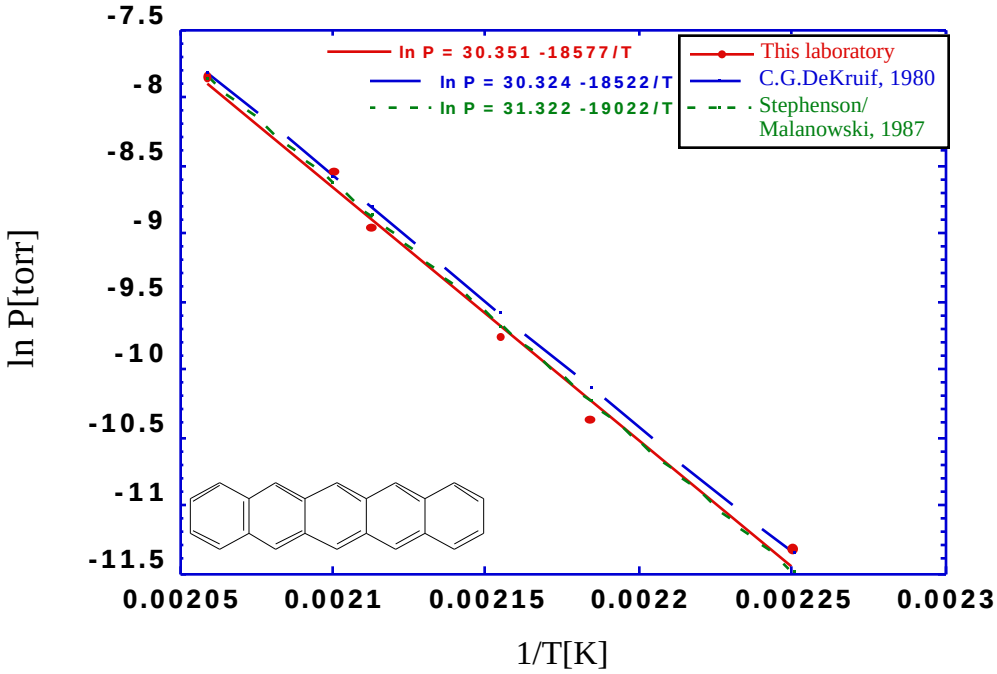

Figure B.9. Effusion method applied to solid pentacene.

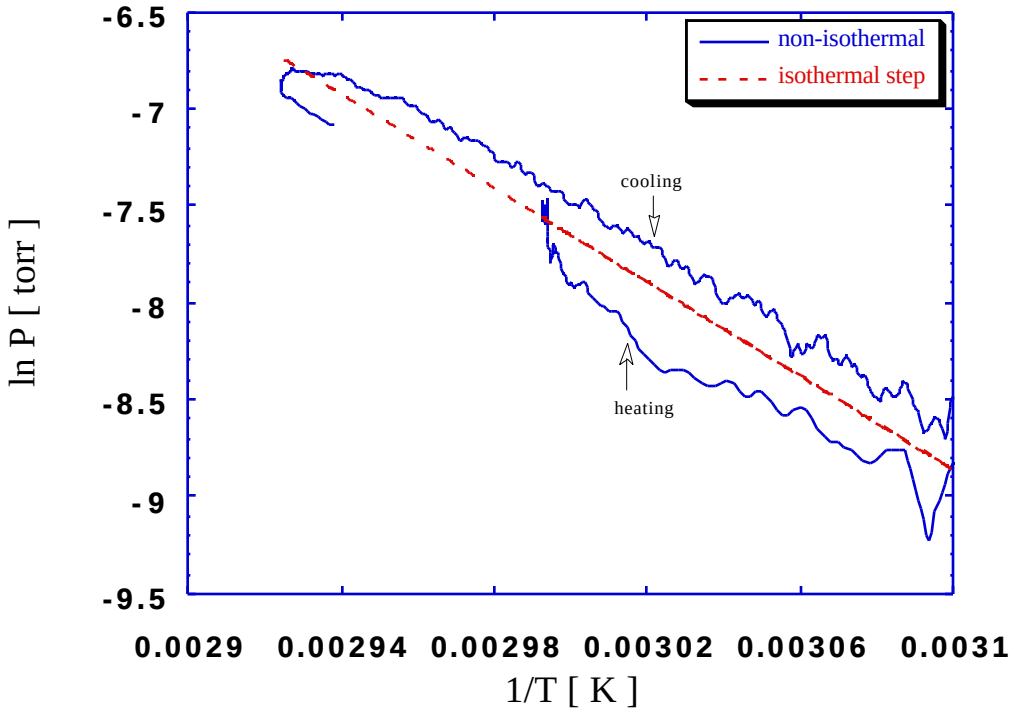

Figure B.10. Comparison of results obtained using the non-isothermal and isothermal effusion method on anthracene. Heating and cooling rates 5°C/min.

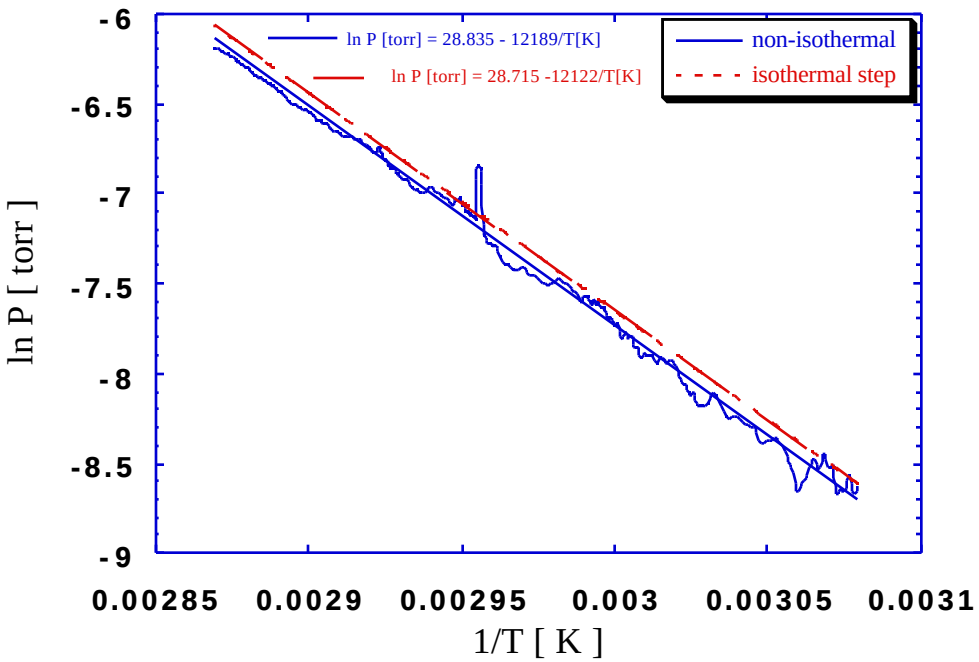

Figure B.11. The non-isothermal effusion method applied to solid anthracene. Heating rate 0.8 °C/min. The solid curve is obtained from the non-isothermal technique, and the solid line is a linear regression of these data. The broken curve is a fit to data obtained by the traditional isothermal method (reported earlier). The difference in the curves is within experimental error.

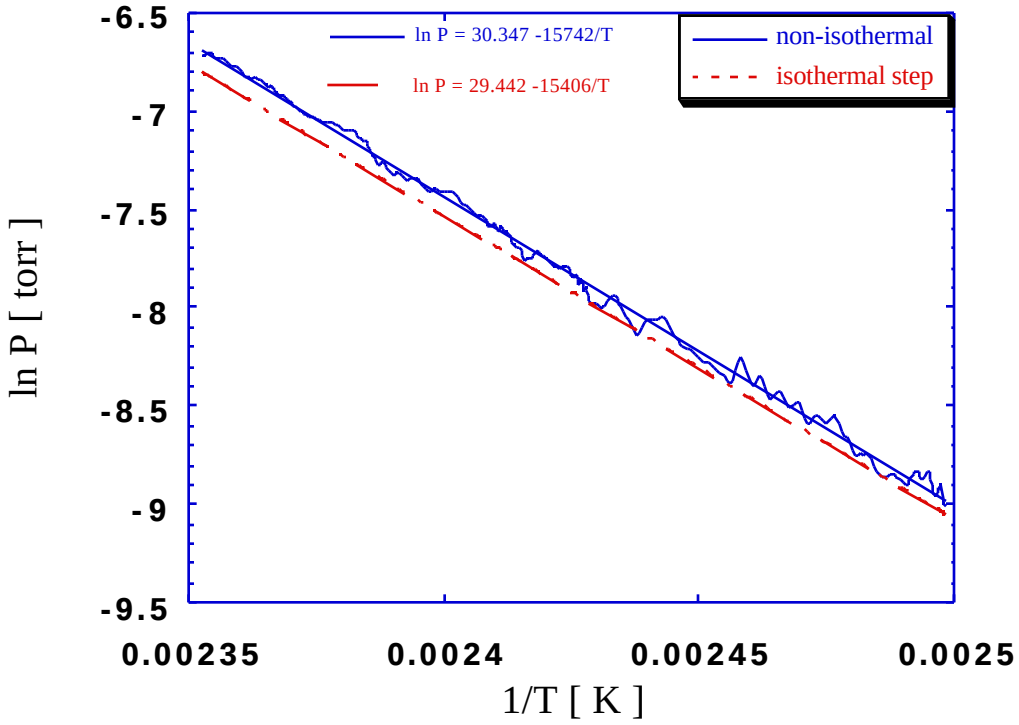

Figure B.12. Non-isothermal effusion method applied to naphthacene, with continuous decrease of sample temperature. Cooling rate 0.8°C/min.

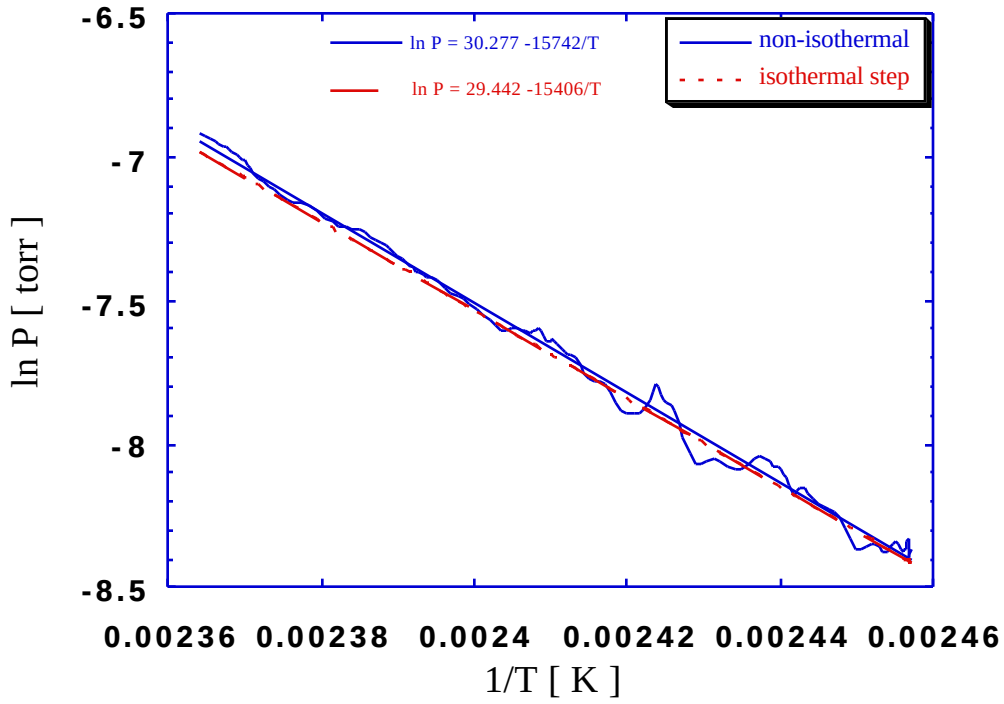

Figure B.13. Non-isothermal effusion method applied to naphthacene, with continuous increase in sample temperature. Heating rate 0.8 °C/ min.

Chapter C. Vapor Pressures of Polycyclic Aromatic Hydrocarbons and Model Mixtures.

This chapter reviews the data available to us on the vapor pressure of high boiling aromatic compounds. Also the measurements of vapor pressures for various large polycyclic aromatic hydrocarbons (PAH), including those containing heteroatoms, and some mixtures of these compounds are presented. The vapor pressures of pure compounds and model "tars", consisting of mixtures of the PAH, are measured using the Knudsen effusion technique in the ordinary isothermal step mode.

This part of the study was motivated by the lack of vapor pressure data on coal tar related compounds, which tend to have a highly aromatic nature and which also contain a significant number of heteroatoms.

C.1. Effects of Intermolecular Forces on Vapor Pressure - Overview.

There is a lack of information and understanding concerning the intermolecular forces present in coal-derived products and in coal itself. It is known that the thermodynamic properties of any pure substance are determined by intermolecular forces which operate between the molecules of that substance.

The physical forces between molecules play an important role in determining the properties of a solution. Properties which depend on interaction between molecules rather than on the characteristics of the molecules which are isolated are called configurational properties. For example, the energy of vaporization, vapor pressure and boiling point are configurational properties, but the specific heat at low pressure is not. To interpret and correlate thermodynamic properties of solutions, it is therefore necessary to have some understanding of the nature of intermolecular forces. The case of a mixture is necessarily more complicated, because consideration must be given not only to the interaction between

molecules belonging to the same component, but also to interactions between dissimilar molecules. When a molecule is in the proximity of another, forces of attraction and repulsion strongly influence its behavior.

The significance of the effect can be seen by considering the saturation vapor pressure of some important classes of organic compounds. These will be categorized by general structural features and actual measured vapor pressures from the literature will be used. It is worth noting that only relatively small molecules, with molecular mass between 100 and 300 daltons, are considered. Distinctions are drawn between several classes of aromatic compounds (aromatics are, of course, of considerable interest in this project). There are the cata-condensed (linear) aromatics such as naphthalene, anthracene, naphthacene. There are the other "non-linear" aromatics, including pericondensed. None of these have any substitutents. A third class of aromatics are those with phenyl substitutents, such as rubrene or hexaphenylbenzene. A fourth class of compounds is aromatics with alkyl substitutents. A fifth class is aromatic ring hydrocarbons with heteroatoms (such as N, S and O), and the sixth is those with hydroxyl groups (-OH) or hydroxyl/carboxyl substitutents such as 6,11-dihydroxynaphthacene dione or 1-hydroxy-anthraquinone. The vapor pressures of these classes of organic compounds at 75 °C are presented on Figure C.1. As can be seen, vapor pressures can differ by many order of magnitude for the same molecular weight. These compound-to-compound variations arise from differences in molecule- molecule interactions.

It is important to keep this general result in mind, as data are presented for various aromatics. The importance of the details of chemical structure will be alluded to often in what follows.

C.2. Vapor Pressure Measurements for PAH .

The vapor pressures of thirteen hydrocarbons with molecular weights in the range of 178 to 300 g/mol were measured by the standard Knudsen Effusion Technique. Literature data on heteroatom-containing aromatic hydrocarbons are extremely scarce. We believe that our results might be among the first available on some of these materials.

All the chemicals were used as supplied. Only their thermal behavior was investigated and melting point determined, using differential scanning calorimetry, to verify the purity. The method has been described in the previous chapter. It should only be added that in all cases at least 5% of the weight of each hydrocarbon sample was vaporized before measurement. This was to assure that small amounts of volatile impurity would not influence results. For each material, experimental results were obtained in two independent series of experiments.

C.2.1. Polycyclic Aromatic Hydrocarbons.

The previous section gave some results on the vapor pressures of PAH (anthracene, naphtacene and pentacene). Here, the results on several other PAH are considered.

Phenanthrene ($C_{14}H_{10}$, FW = 178.24, m.p. = 101 °C, b.p.= 338 °C)

Phenanthrene of 99% purity was obtained from Kodak, Inc. This compound has been studied here at temperatures between 30 and 60 °C and at pressures between $2.78*10^{-4}$ and $7.5*10^{-3}$ torr. The results are given in Figure C.2. Reasonable agreement is noted with the other values reported in the literature.

Pyrene ; ($C_{16}H_{10}$, FW = 202.3, m.p. = 156°C , b.p.= 393 °C)

Pyrene of 99% purity was obtained from the Sigma Chemical Company, Inc. This compound has been studied here at temperatures between 35 and 125 °C and at pressures between $1*10^{-4}$ and $6.7*10^{-3}$torr. The results are shown in Figure C.3 together with some literature values. Our data exhibits satisfactory agreement with the literature data.

Coronene; ($C_{24}H_{12}$, FW = 300.36, m.p. = 438 °C , b.p.= 525 °C)

Coronene of 97% purity was obtained from the Pfaltz & Bauer, Inc. This compound has been studied here at temperatures between 421 and 504 K and at pressures between $1.4*10^{-5}$ and $7*10^{-3}$ torr. There are many fewer data to be found in the literature on this compound than on the previous two and the data are widely scattered. Comparison between our results and those in the literature is shown in Figure C.4. It can be seen that we show good comparison with one of those sets, but the results differ sharply from data obtained by the other two investigators calculated to our temperatures. We are not discouraged by this, because the other two sets appear to be of lower reliability; those given by Stephenson and Malanowski [1987] are from a correlation without attribution or description of technique. Those determined by Wakayama et al. [1967] are from a series of measurements on many compounds, which consistently showed significant discrepancies from other published studies. They cannot therefore be regarded as reliable.

Perylene ($C_{20}H_{12}$, FW = 252.3, m.p.= 278°C , b.p.= unknown)

Perylene of 99+% purity was obtained from the Aldrich Chemical Company, Inc. This compound has been studied here at temperatures between 118 and 151°C and at pressures between $3.9*10^{-5}$ and $9*10^{-4}$ torr. The results are shown in Figure C.5 together with values calculated from literature data. Additionally we present our

experimental data for perylene of 95% purity, obtained from Pfaltz & Bauer, Inc. The data from our studies differ considerably from the results of two preceding studies, obtained from a handbook [Stephenson and Malanowski 1987]. These literature data, as described earlier in the case of coronene, could be of questionable reliability.

2,3-Benzofluorene ($C_{17}H_{12}$, FW= 216.28, m.p.= 209°C , b.p.= 402°C)

2,3-benzofluorene of 98% purity was obtained from the Aldrich Chemical Company, Inc. This compound has been studied here at temperatures between 71 and 124.5 °C and at pressures between $3.4*10^{-5}$ and $9.2*10^{-3}$ torr. There were no experimental data for the vapor pressure of 2,3-benzofluorene in the literature. Results are shown in Figure C.6.

C.2.2. Polycyclic Aromatic Hydrocarbons Containing Heteroatoms.

The following polycyclic aromatic hydrocarbons containing heteroatoms have also been examined:

Phenanthridine ; ($C_{13}H_9N$, FW = 179.22, m.p. = 108°C , b.p.= 349°C)

Phenanthridine of 99% purity was obtained from the Aldrich Chemical Company, Inc. This compound has been studied here at temperatures between 36 and 163.5 °C and at pressures between $1.1*10^{-4}$ and $3*10^{-3}$ torr. The results are shown in Figure C.7 together with the only available literature data. The earlier study [McEachern et al. 1975] involved use of a restricted molecular flow apparatus [McEachern, 1973]. As only these two data sets exist, it is difficult to comment on the reliability of one against the other.

1,2-Benzodiphenylene sulfide; ($C_{16}H_{12}S$, FW= 234.32, m.p.= 188-190°C , b.p.= unknown)

1,2-benzodiphenylene sulfide of 99% purity was obtained from Aldrich Chemical Company, Inc. The data were obtained for the temperature range from 51.5 to 100 °C and the pressure range from 7 $*10^{-6}$ and 1.3$*10^{-3}$ torr. Literature references were not found for this compound. The results are shown in Figure C.8.

1-Hydroxypyrene; ($C_{16}H_{10}O$, FW =218.26, m.p. = 179...182°C, b.p.= unknown)

1-Hydroxypyrene of 99% purity was obtained from the Aldrich Chemical Company, Inc. This compound has been studied here at temperatures between 96 and 121 °C and at pressures between 1.1$*10^{-4}$ and 1.6$*10^{-3}$ torr. Literature references were not found for this compound. The results are shown in Figure C.9, together with those for pyrene itself. These two compounds have very similar molecular weights, but that containing the hydroxyl group displays the expected lower vapor pressure and slightly higher enthalpy of vaporization.

Perinaphthenone ; ($C_{13}H_8O$, FW = 180.21, m.p. = 153...156 °C , b.p.= unknown)

Perinaphthenone of 99% purity was obtained from the Aldrich Chemical Company, Inc. This compound has been studied here at temperatures between 53 and 75 °C and at pressures between 1.8$*10^{-4}$ and 1.8$*10^{-3}$ torr. Literature references were not found for this compound. The results are shown in Figure C.10, together with those for 3-hydroxy-*1H* -phenalen-1-one.

3-hydroxy-*1H* -phenalen-1-one; ($C_{13}H_8O_2$, FW = 196.21 m.p. = 264°C , b.p.= unknown)

3-hydroxy-*1H* -phenalen-1-one of 98% purity was obtained from the Adrich Chemical Company, Inc. This compound has been studied here at temperatures between 129 and 159°C and at pressures between $5.4*10^{-5}$ and $1.3*10^{-3}$ torr. Literature references were not found for this compound. Comparison with perinaphthenone shows the enormous influence of the hydroxyl substitutent.

6,11-Dihydroxy-5,12-naphthacenedione; ($C_{18}H_{10}O_4$, FW= 290.28 m.p.= 350°C, b.p.= unknown)

6,11-Dihydroxy-5,12-naphthacenedione of 98% purity was obtained from the Adrich Chemical Company, Inc. This compound has been studied here at temperatures between 153 and 173°C and at pressures between $1.1*10^{-4}$ and $7*10^{-4}$ torr. Literature references were not found for this compound. The results are shown in Figure C.11, together with the data for naphthacene.

Benz[g]isoquinoline-5,10-dione; ($C_{13}H_7O_2N$, FW=209.21, m.p.=178...180°C, b.p.= unknown)

Benz[g]isoquinoline-5,10-dione of 99% purity was obtained from the Adrich Chemical Company, Inc. This compound has been studied here at temperatures between 61 and 108 °C and at pressures between $6.4*10^{-5}$ and $8.2*10^{-3}$ torr. Literature references were not found for this compound. The results are shown in Figure C.12, together with the literature data for anthraquinone [Bardi et al., 1973]. The substitution of a nitrogen atom for carbon is seen to have only a modest effect on vapor pressure, because no new hydrogen bonding interactions are introduced.

Aspirin or salicylic acid acetate; ($C_9H_8O_4$, FW = 138.1)

The main ingredient of aspirin, salicylic acid acetate, accounts for approximately 80% of the typical aspirin formulation. The remaining 20% is unknown in this case. "Aspirin" was anticipated to have a relatively low vapor pressure despite the low molecular weight of its main component, because its carboxylic functionalities. This is shown in Figure C.13. The vapor pressure of pure salicylic acid acetate has never been investigated.

Figures C.2 to C.13 verify that the widely used assumption, concerning constant enthalpy of sublimation, is reasonable below the melting point, where most of our experiments were performed. The other feature which is clear from some of these figures is the spread of the data in the literature. This is indicative of the difficulty in performing such measurements.

C.3. Model Compounds for Coal Tars - Some Considerations.

It is known that the thermodynamic properties of any pure substance are determined by intermolecular forces which operate between the molecules of that substance. The comparison of structurally related compounds is one way to determine the different energetic contributions and this has been done to a limited extent above. The heat of vaporization can be considered as a measure of the energy required to transfer molecules from the condensed state into the gaseous state, and therefore provides information on intermolecular interaction energy. Further discussion of this point is found below.

C.3.1. Van der Waals Forces.

All compounds in a condensed phase are subject to van der Waals forces. Van der Waals forces are defined as attractive forces between neutral or nonpolar molecules that are caused by orientation (dipole-dipole), induction (dipole-induced dipole), and dispersion (induced dipole-induced dipole) interaction. They are considered to be one of the primary forces responsible for holding molecules together in the condensed state and they play the dominant role in nonpolar systems regardless of molecular size. Except in small molecules with large dipole moments, dispersion forces tend to dominate the other intermolecular forces. Larger molecules generally exhibit lower vapor pressure since the summation of van der Waals attractions is directly related to their size.

The ease with which an organic compound escapes to the vapor phase from a condensed phase is controlled by the magnitude of ΔH_{vap}. This ΔH_{vap} gives the temperature dependence of vapor pressure. Relationships have been sought between ΔH_{vap} and the molecular weight. Here, most of the data obtained were actually ΔH_{sub} opposed to ΔH_{vap}. This makes analysis somewhat easier, since the temperature dependence of ΔH_{sub}, is often not significant. There have been several attempts to correlate ΔH_{sub} with the number of

carbon atoms in condensed aromatic hydrocarbons. Inokuchi et al.[1952] attempted to establish a simple linear relationship, where each carbon was assigned an inner heat of vaporization of 1.5 kcal/mol or 6.29 kJ/mol. De Kruif et al. [1980], assuming a linear relationship, showed that the increase in ΔH_{sub} (25°C) has constant value 8.33 kJ/mol per carbon atom, which is about 17% higher than the value derived by Inokuchi. Morawetz [1972] has attempted to establish a better correlation by classifying the C-C bonds in aromatic compounds according to eight different types.

The heat of sublimation for twenty PAH are plotted against their carbon numbers in Figure C.14 and against their molecular weights in Figure C.14b. The enthalpies of sublimation were calculated from the vapor pressure data found in the literature or measured by us. The data shows such a correlation to be poor for accurate work. A distinction needs to be drawn between linear and peri-condensed aromatic hydrocarbons. From Figure C.14 we suggest 7 kJ/mol for linear aromatics and 5 kJ/mol for pericondensed aromatics.

To emphasize this point further, it may be shown that there exist significant differences between the vapor pressures of similar molecular weight aromatic hydrocarbons containing exactly the same functional groups, or very similar structures. Figure C.15 shows graphically results on aromatic compounds of identical molecular weight. It should be noted that these are not compounds of vastly different structures. It is apparent from the general similarity of the slopes of the curves in Figure C.15 that at least for this family of condensed aromatics, the assumption of a similar latent heat of vaporization is not bad. The vapor pressures at any temperature are however different by orders of magnitude.

It can be noted from appendix A.1 that the H/C atomic ratio for coal tars is around 1. PAH have an H/C ratio around 0.5. This suggests that significant amounts of alkyl groups are present in the coal tars. For example, the H/C ratio for trimethyl-anthracene ($C_{17}H_{16}$) is 0.94. The influence of alkyl and phenyl groups on the heats of sublimation of PAH is shown in Figure C.16. The effect is small, but clear.

Figure C.17 shows the comparison of the solid vapor pressures for anthracene, 9,10-dimethyl anthracene, and 5-butylanthracene. Clearly, alkyl substitutents do not necessarily increase the vapor pressure of given aromatics just because they increase molecular weight. Addition of the bulky t-butyl group, and all its mass, had surprisingly little effect on vapor pressure. For a given molecular weight, they do generally lower the boiling point slightly, as can be seen from Figure C.18. Many PAH thermally decompose before they reach their atmospheric boiling points [Smith et al., 1980]. Figure C.18 and some other figures presented earlier cannot therefore be extended to much higher molecular weight.

C.3.2. Polar Attraction.

As a result of the differing electron-attracting properties or electronegativities of the various types of atoms included in organic compounds, specific intermolecular interactions are possible. In coal tars, the main heteroatoms are O, S, N, which can contribute polar interaction possibilities. Polar characteristics affect interactions in two ways. The first involves permanent dipoles. A dipole will align itself with other dipoles resulting in dipole:dipole attraction between molecules. Second, if a polar group is positioned near an evenly charged structural region of an adjacent molecule, electrons in the neighboring molecule will be displaced in response to the approaching polar unit, and an induced dipole attraction will result.

The contribution of heteroatoms to the heat of sublimation of aromatic compounds of various molecular weights is shown in Figure C.19. Generally, it can be seen that the presence of heteroatoms does not have a consistent effect on the heat of sublimation though clearly the earlier presented results (Figure C.9 and C.10) indicate that hydrogen bonding substitutents can have a significant influence on both vapor pressure and ΔH_{sub} in particular cases. The heteroatomic compounds of Figure C.19 generally do not have a

hydrogen-bonding character. The effect of heteroatoms in the aromatic ring is small unless they can participate in polar (hydrogen bonding) interactions.

The influence of heteroatoms on the vapor pressure of structurally similar compounds is shown in Figure C.20, and for some other structurally similar compounds in Figures C.12 and C.21. A significant influence of the heteroatoms is seen on the vapor pressure in some cases, but not in others. Again, it is clear that there is no easily generalized effect of the heteroatoms. Large vapor pressure differences can occur. Once again, however, the latent heat is relatively comparable for all the compounds. Thus depending upon subtle details of the structure, large variations in vapor pressure can be seen, even when these features do not show themselves in the latent heat. The latent heat depends most upon the number of atoms, and thus crudely, upon molecular weight. This is why correlations such as {A.1} work to some level of approximation. The correlation does not account for potentially large variations in ΔS_{sub}.

The above results (in Figures C.20 and C.21) are generally striking in the terms of the similarity of enthalpies of sublimation, but in none of these cases is hydrogen bonding significant. This suggests that to a good approximation, structurally similar PAH molecules have very similar sublimation enthalpies, if hydrogen bonding is not involved. Predicting ΔS_{sub} appears difficult. The key to correctly predicting vapor pressures for this class of compounds is thus in the prediction of the entropy.

C.3.3. The Entropy of Sublimation.

The entropy of sublimation is associated with a change in the "ordering" of the molecules in the system during vaporization and is a function of the molecular structure. In the vapor phase molecules interact minimally, and the molecules are in a state of disorder. Thus, the differences in ΔS_{vap} can be interpreted in terms of differences in the internal order in the condensed phase. This degree of order depends on the geometric and chemical

character of molecules. The values of the entropy of sublimation for some aromatic compounds are plotted against their molecular weights in Figure C.22. Figure C.22 a shows a weak correlation with the carbon number. The plot shows large a scattering in the data, and the entropy per mole generally increases as molecular weight increases. Nonpolar substances with spherical molecules are generally in a state of greater disorder than a system containing asymmetric and polar molecules. A high degree of order is especially pronounced for systems with hydrogen bonds. Increased ordering leads to high values of ΔS_{vap}.

C.3.4. The Contribution of Hydrogen Bonding.

Hydrogen bonding interaction are a special, important subset of polar interactions. The formation of hydrogen bonds in fluids modifies their physical and chemical properties in many ways. In particular, hydrogen bonding substantially changes solubilities of various substances, dielectric properties and electrical conductivity, freezing and boiling points, density, vapor pressure and heat of vaporization. In a hydrogen bond, a hydrogen atom is effectively shared by an other atom. The atom to which hydrogen is more tightly linked is called the hydrogen bond donor, whereas the other atom is the hydrogen bond acceptor. The latter carries a partial negative charge. Since the two atoms connected by the hydrogen atom are highly electronegative, the hydrogen bond is a result of electrostatic interaction between the nearly bare proton and the electron-rich atom.

Hydrogen bonds are stronger than van der Waals bonds but much weaker than covalent bonds (10 to 20 times weaker) [Stryer, 1981], i.e., bond energies in the range 10 to 50 kJ/mol are associated with hydrogen bond formation. An important feature of hydrogen bonds is that they are directional: in the strongest hydrogen bond, the donor, the hydrogen, and the acceptor atoms are collinear. The bond becomes weaker with increasing the acceptor atom angle to the line joining the donor and hydrogen atoms. Letcher et al. [1996]

has calculated the hydrogen bond interaction energies from partial molar enthalpies at infinite dilution for liquids and show the order of hydrogen bond strengths OH...N > OH...O > OH...S or SH....S > SH...O > SH...N or NH...S > NH...O > NH...N.

It will be shown in Chapter D that the contribution of the hydroxyl group to the heat of sublimation of the sugar-like compounds is around 30 kJ/mol. The influence of hydroxyl groups on the heat of sublimation of aromatic compounds is more complex. Comparison of the literature values of some heats of sublimation [Stephenson and Malanowski, 1987] is given in Table C.1.

Table C.1. The heats of sublimation for benzene, phenol and benzenediols.

compound	benzene	phenol	1,3-benzenediol	1,4-benzenediol
average T[°C]	-10	-5	90	90
ΔH_{sub}[kJ/mol]	69.8	93.3	92.7	101.7
OH contribution [kJ/mol]		23.5	11.3	16

Literature data [Stephenson and Malanowski, 1987] on the vapor pressures of naphthalene, 1-naphthol and 2-naphthol are shown in Figure C.23. The hydroxyl group contributions may be crudely estimated to be 25.1 and 19.6 kJ/mol for 1- and 2-naphthol respectively. Our results for hydroxypyrene and pyrene in Figure C.9 suggest that the hydroxyl group contribution to the heat of sublimation is around 28 kJ/mol.

A hydrogen bond may exist between two different molecules or within the same molecule. Not all hydrogen bonding interactions need involve the same functional group. For example, groups such as carbonyl (C=O) and tightly bound nitrogen (N:) display a tendency to form hydrogen bonds with hydroxyl group. Comparison of the heats of sublimation of perinaphthenone and 3-hydroxy-1H-phenalen-1-one in Figure C.10 show the hydroxyl group contribution to be about 54 kJ/mol. Here, the carbonyl may be acting as the H-bond acceptor. The hydroxyl group contribution in hydroxy anthraquinones and

dihydroxy anthraquinones can estimated to be between 7.5 and 45 kJ/mol [Stephenson and Malanowski, 1987].

The formation of each hydrogen bond involves a significant decrease of free energy and it is, therefore, obvious that systems will display a tendency to form all possible hydrogen bonds to minimize free energy. Geometric or steric restrictions may preclude hydrogen bond formation, if there is a large free energy penalty of some other kind involved. Experimental evidence indicates that, as a rule, nature succeeds in building up the unit cell of a crystal so that the hydrogen bonds would affect but slightly the molecular packing density (for example water). The geometries of saturated hydrogen bonds may be quite different depending on the arrangement of the donor and acceptor groups in the molecule.

In summary, it is clear that structural elements of organic compounds are attracted to each other in a manner that reflects several electronic forces operating simultaneously. These attractions cause molecules to be "bound" to a condensed phase, and the stronger the sum of the attractions, the lower the vapor pressure or the higher the boiling temperature of the compounds will be.

C.4. Vapor Pressure of Coal-Tar Model Mixtures.

Coal tars are very complicated mixtures containing many hundred or thousands of components. It is quite unclear what mixture models can be used to describe solid-vapor and liquid-vapor equilibrium for tars. In practice ideal solution behavior has generally been assumed for tars (or metaplast), but this is certainly suspect. Here, attention is focused upon the special problem of mixtures of compounds containing significant amounts of heteroatoms, as primary coal tars (and cellulose tars) would tend to have.

The mixtures for preliminary studies were prepared by the so called "quenching" method. This involved transferring weighed amounts of two components into a stainless steel capsule under an inert gas environment. After closing the capsule, the contents were melted and homogenized by shaking. "Instant" cooling was achieved by dropping the capsule into liquid nitrogen. The compositions of the mixtures were calculated from the amounts of components added to the capsule, assuming perfect mixing. This was assumed appropriate because no macroscopic phase separation was observed in any of the samples reported on here.

Close to ideal mixture behavior was seen in the vapor pressures for aromatic hydrocarbon mixtures, but care must be exercised in drawing conclusions concerning mixture ideality. Examples of the data obtained are shown in Figures C.24 through C.26 The results reveal no major deviations from ideal mixture-like behavior, but as a result of the choice of mixtures, a rigorous test of ideality is not possible.

Figure C.24 shows results for a mixture of anthracene and perylene, which should form a nearly ideal binary *liquid* mixture (both are pure polycyclic aromatic hydrocarbons). Results for the actual solid mixture are seen to be near the Raoult's law prediction, which in this case is dominated by the vapor pressure of the more volatile component. Strictly speaking, we cannot assure formation of a truly single phase system upon quenching - phase separation might have occurred on a scale smaller than visual observation can reveal.

If the mixture were entirely phase separated, then behavior quite similar to what was observed would also be expected, and the vapor pressure would be dominated by the vapor pressure of the more volatile component. Bouwstra et al. [1985] compared "quenching" and zone-leveling [Kolkert, 1975] techniques and showed that the preparation of mixed organic crystals by quenching a liquid mixture often leads to inhomogenities in the solid mixture. This is also supported by DeKruif et al. [1981b]. They showed that the vapor pressures of the quenched samples are 10% higher than the vapor pressures of the zone-leveled samples for p-dichlorobenzene/p-dibromobenzene mixtures. Thus, the present results are of little value in distinguishing the nature of the mixture. Better agreement with Raoult's law behavior might be anticipated if we performed our measurements with the mixture in a liquid phase.

Figure C.25 shows the results for a mixture of 75% anthracene and 25% benzofluorene. Again, this should be expected to be a nearly "ideal" system, given its primarily PAH character. The predictions from Raoult's law are, however, again somewhat low. Once more, phase separation must be suspected. In this case, the mixture vapor pressure is actually quite close to the sum of the vapor pressures of the individual components. This is precisely the behavior expected from a phase-separated mixture.

Figure C.26 shows results for a mixture of 25% anthracene and 75% benzofluorene. Again, Raoult's law under-predicts the vapor pressure of the mixture. It should be remembered that an under-prediction of one unit on the logarithmic scale corresponds to a factor of 2.3 in actual vapor pressure. The curvature away from a straight line at higher temperatures could be the result of the loss of the more volatile component during heating, since this could influence the subsequent measurements of vapor pressure of the mixture. There may be another explanation for the convergence with the Raoult's law results at high temperatures as well. It is possible that the mixtures approach ideal liquid phase behavior as the melting temperature of the mixture is approached.

It is noteworthy that the two different mixtures of the same pair of components gave different mixture vapor pressures in Figures C.25 and C.26. This would argue against purely phase-separated systems, since in that case slightly more than the vapor pressure of pure anthracene would be obtained regardless of mixing ratio.

Coal tars are not pure polycyclic aromatic hydrocarbons, but may contain significant numbers of heteroatoms. The mixture phenanthridine/1-hydroxypyrene gives vapor pressure behavior as illustrated in Figure C.27. Clearly the mixture behaves highly non-ideally, and the deviation from Raoult's law was substantial (about an order of magnitude). The fact that the mixture shows a much lower vapor pressure was not surprising. It is known that the hydroxyl functional group has a significant effect on the vapor pressure. The mixture chosen for study here was selected to exhibit a very strong interaction between a nitrogen base and the hydroxyl (OH) group. There is little doubt that these sorts of interactions may exist in coal tars, since these materials contain both pyridinic and hydroxyl functionalities. Finally, it should be noted that the mixture was deliberately selected to exhibit a very strong, specific electron donor-acceptor interaction. It is likely that in the real tar mixtures, the number of such interactions per unit volume will not be as great.

These experiments were extended to study other heteroatom-containing mixtures that would not exhibit such strong interactions. Results are shown in Figures C.28, C.29 and C.30. Figure C.28 shows results for the same strong nitrogen base in mixture with a PAH compound. The behavior is similar to what was observed in the absence of heteroatoms. Again, it is impossible to say whether the result is simply near Raoult's law or that phase separation has occurred. Once again, there is a tendency to approach the Raoult's law behavior at higher temperatures.

Figures C.29 and C.30 show the results for a mixture of a cyclic sulfide and a nitrogen base (at two different mixture compositions). Once again, aromatic mixtures containing only sulfur and nitrogen heteroatoms exhibited vapor pressures quite close to those

"predicted" from Raoult's law. However, once again, phase separation is strongly suspected because of the apparent lack of composition dependence of the mixture vapor pressures; the results of both Figures C.29 and C.30 follow the pure phenanthridine results quite closely, deviating only at higher temperatures. It was noted above in some systems that the Raoult's law prediction was approached at high temperatures. The tendency to approach Raoult's law as temperature is raised is of interest. This might suggest that ideal liquid phase behavior is more closely approached as the liquid melting temperature of the mixture is approached.

Additionally we have applied the non-isothermal effusion technique to study a mixture of 55% 1-hydroxypyrene and 45% perinaphtenone. This time the mixture was prepared by dissolving these two components in HPLC grade ethyl alcohol. The solvent was evaporated in a vacuum oven at room temperature. To avoid artifacts due to impurities and solvent residue, 5% of the sample placed into the effusion cell was evaporated before beginning actual data collection. During the actual run only 0.2% of sample was evaporated and mixture composition was determined chromatographically after the run. Results are shown in Figure C.31. The prediction from Raoult's law is in good agreement with experimental results, considering experimental uncertainty.

The need to study the vapor pressure behavior of the mixtures of hydrocarbons is apparent, given the approach that has been defined for studying coal tars. The tars may contain any combination of molecules of different structure and heteroatomic content. Both of these factors have been illustrated above to influence the measured vapor pressure significantly.

C.5. Variation of Vapor Pressure with Temperature-Summary.

The latent heat of vaporization decreases with temperature and reaches zero at the critical point. The problem of correlation and prediction of enthalpies of vaporization between the triple point (T_{tr}) and the critical point (T_c) has not been fully solved [Svoboda and Basarova, 1994]. The problem of extrapolating ΔH_{vap} to T_c arises because of a need to describe two entirely different temperature dependencies. Above the normal boiling point to about 2/3 of the distance to T_c, the decrease of ΔH_{vap} with temperature is quit slow. In the last third there follows a steep decrease towards T_c [Svoboda and Smolova, 1994]. This is a clear indication of the danger in blindly extrapolating vapor pressure data over a wide range of temperatures. To illustrate the problem, consider some literature data presented in Table C.2.

Table C.2. Literature data for some aromatic compounds

compound	MW [g/mol]	ΔH_{vap},tp [kJ/mol]	ΔH_{vap},bp [kJ/mol]	T_b [C] exper.	T_b[C] est	P error % at bp
naphthalene	128	50.9	43.18	218	208.5	25%
fluorene	166	62.3	58.15	294	287	35%
anthracene	178	59.9	52.35	341.5	336	25%
phenanthrene	178	69.1	52.72	338	313	50%
pyrene	202	72.9	65.81	393	378	30%
fluoranthene	202	78.8	66.52	383	374	40%
crysene	228	77.5	69.54	448	420	35%

The normal boiling points are used for comparison because of the lack of other experimental values in the literature [White, 1986]. The experimental normal boiling points and heats of vaporization at the boiling points are obtained from White [1986]. The heats of vaporization at the triple point (ΔH_{vap},tp), estimated boiling points, and the vapor pressure estimation error at the boiling point are shown. These estimates were calculated using available vapor pressure data at the triple point. The errors in estimated boiling points using the ΔH_{vap} values at the triple point suggest that the assumption of a constant heat of vaporization is not so bad. If it is necessary to assume constant ΔH_{vap} in order to extrapolate measured vapor pressure up to the boiling point for coal tars, these results give us confidence in doing so. Figure C.32 graphically supports this assumption. In this case,

a constant ΔH_{vap} was assumed between the boiling and melting points. Thus, equation {A.7} could be used for the purpose of correlating tar vapor pressures.

Experimental determination of the critical temperatures (T_c) for high molecular weight substances has proven difficult and subject to high uncertainty because of thermal decomposition and other reactions which occur near the critical point. Experimental values are available only for benzene, naphthalene, anthracene and phenanthrene. There are multiple ways of estimating T_b and T_c of large PAH, but unfortunately these show a lack of agreement. For example, the critical temperatures for PAH with molecular weight 300 daltons can be estimated to be between 750 and 1100 °C, for 400 daltons to be between 900 and 1200, and for 600 daltons to be between 1100 and 1700 °C using the methods of Forman and Thodos [Homann, 1984], Somayajulu [1989] and Joback [Löffler and Homann, 1990] combined with several boiling point estimation techniques (Homann, 1984; Frenklach et al., 1984; Kroto and Mckay, 1988). Estimates of critical temperatures and normal boiling points for some PAH, obtained from Wang and Frenklach [1994], are listed in Table C.3.

Table C.3. Normal boiling points and estimated critical temperatures for some PAH.

compound	MW	T_b[C]	T_c[C]
anthracene	178.2	340	628
phenanthrene	178.2	340	628
pyrene	202.3	393	695
1,2-benzofluorene	216.3	413	714
1,2-benzanthracene	228.3	435	723
chrysene	228.3	448	756
triphenylene	228.3	425	723
perylene	252.3	350...400	608...679
acenaphthanthracene	254.3	193.... 194	377...379
picene	278.3	518...520	827...829
coronene	300.4	525	838

The critical temperatures were estimated by the group contribution technique [Somayajulu, 1989]

The coal pyrolysis experiments of interest here occur in the temperature region between 500 and 1000°C. Thus pure compounds with molecular weights up to 300 daltons may not even exist as a liquid at these temperatures, nor is it likely that mixtures very rich in these compounds can either. Tars, however, are complicated mixtures of thousands compounds exhibiting molecular weights that are well over 1000, centered in the range of 200 to 600 daltons and extending much higher in the "metaplast" phase of the coal. Thus, it is evident that there cannot be a single critical point for a coal tar, but rather a continuous change of critical conditions with different compositions, temperatures and pressures as the pyrolysis process occurs. All that may be concluded is that the pyrolysis experiments are generally far away from the gas-liquid critical region, and that the enthalpies of sublimation/vaporization determined here have relevance.

C.6. Vapor Pressure Correlation for Aromatic Compounds.

As emphasized previously, the primary motivation of this work was to develop a vapor pressure correlation for coal tars based upon actual measurements on the tars.

As a first step, a new vapor pressure correlation has been developed based on the sublimation vapor pressure data for 34 model compounds, obtained either from our measurements or from the literature. The purpose behind developing this correlation is to provide a way of estimating vapor pressure over a broad range of pressure with the only inputs being the temperature and molecular weight. This is similar to the empirical correlation of vapor pressures proposed by Suuberg et al.[1979], where it is now assumed that the heat of sublimation and the entropy of sublimation are functions of molecular weight only, and that all compounds with the same molecular weight generate similar vapor pressures. In this approach we use the integrated form of the Clausius-Clapeyron equation, where the constants A and B are functions of the molecular weight, estimated from the raw experimental values shown in Figures C.15, C.19 and C.22. Therefore, under sublimation conditions for aromatic compounds:

$$P = 6.954 \cdot 10^{8} \exp(0.039M) \exp\left(-\frac{63M}{T}\right) \qquad \{C.1\}$$

In this expression, P is in torr, T is in K, and M is in daltons.

Under pyrolysis conditions, vaporization has been assumed to occur from the liquid phase. The heat of vaporization ΔH_{vap} of the hypothetical liquid at any temperature below the melting point may be considered as the difference between the heat of sublimation (ΔH_{sub}) at this temperature and the heat of fusion ΔH_{fus} (which is usually less than a fourth of ΔH_{sub}). The calculation of the entropy of vaporization could be based on the common identity that, at any temperature $\Delta S = \Delta H/T$. The hypothetical subcooled liquid can be considered as an imaginary liquid that is cooled below its melting point without allowing it to crystallize.

The enthalpy of fusion is very difficult to correlate with any other properties. The variation of ΔH_{fus} and the entropy of fusion ($\Delta H_{fus}/T_m$) is as great as that of the melting points [Reid et al., 1987]. Data on heats of fusion are extremely scarce in the literature, as are predictive methods to estimate these values. It is fair to say that the enthalpy of fusion has been largely ignored. These data are difficult to obtain, because the various solid-solid, solid-liquid-crystalline, and other mesomorphic transitions may occur before the compound actually melts. Convenient reference sources for ΔH_{fus} have not been found for the materials of interest. Some data have been collected in the literature [Weast et al.(CRC), 1985; Acree, 1991]. Based on available experimental data we suggest that the heat of fusion could be estimated as 20% of the heat of sublimation and the entropy of fusion to be 25% of the entropy of sublimation for aromatic hydrocarbons. Figures C.33 and C.34 show graphically the validity of this assumption. The equation {C.1} can then be rewritten in the following form for vaporization from the liquid phase:

$$P = 1.465 \cdot 10^{7} \exp(0.03M) \exp\left(-\frac{50.5M}{T}\right) \qquad \{C.2\}$$

In the developing this equation, no account has been taken of hydrogen bonding. Comparison of equation {C.2} with the pure compound normal boiling point data (shown earlier in Figure C.18) is given in Figure C.35. The same data are also compared with the old correlation {A.1}.

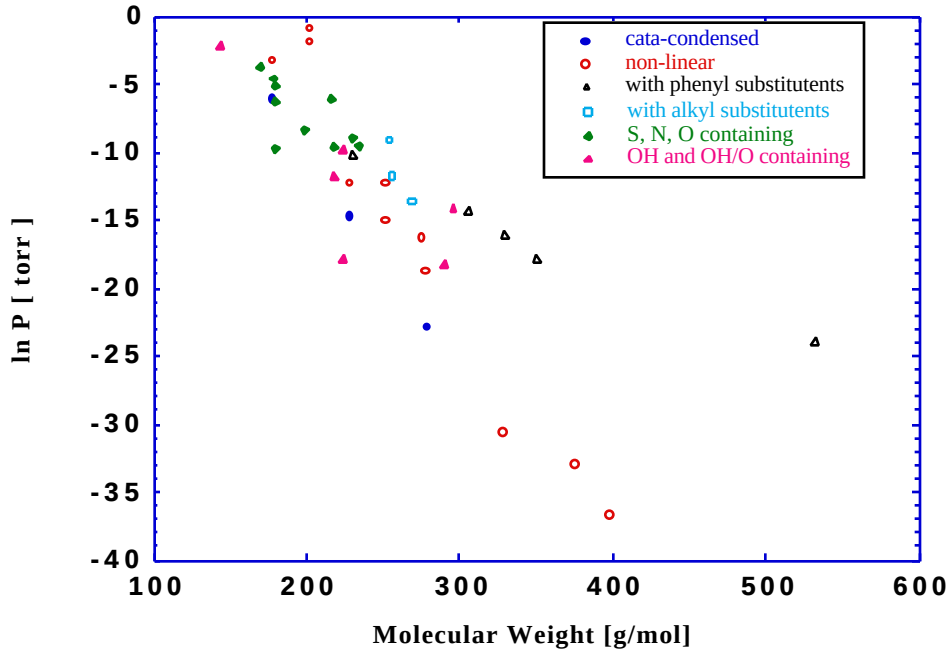

Figure C.1. Vapor pressure data for aromatic compounds at 75°C.

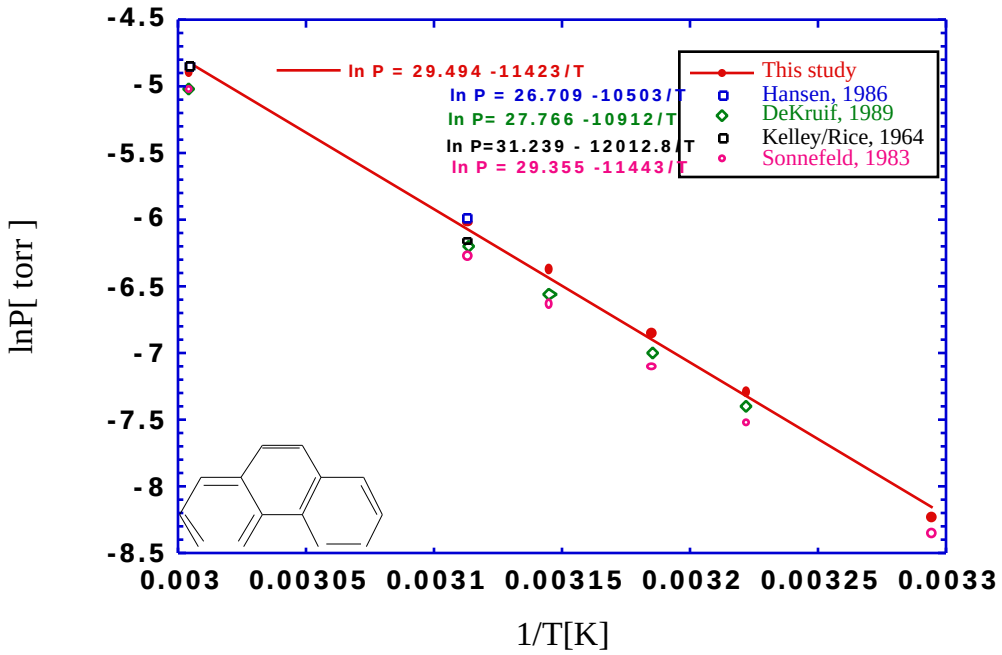

Figure C.2. Effusion method applied to solid phenanthrene.
Solid points are from this study, open points are calculated from references shown.

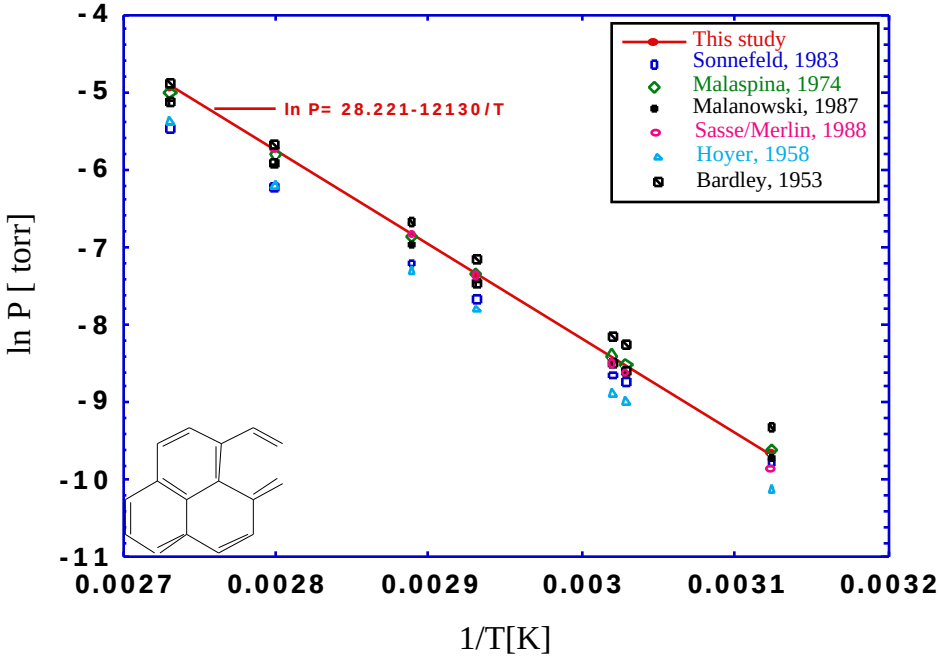

Figure C.3. Effusion method applied to solid pyrene.
Solid points are from this study, open are calculated from references.

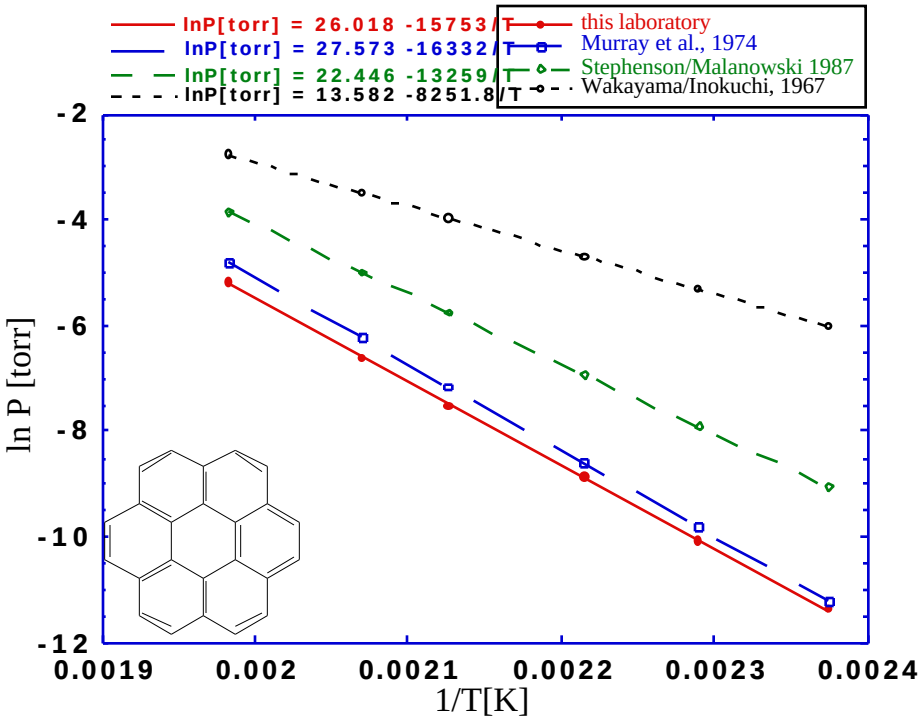

Figure C.4. Effusion method applied to solid coronene.
The effusion method was used by J.J. Murray and N. Wakayama.

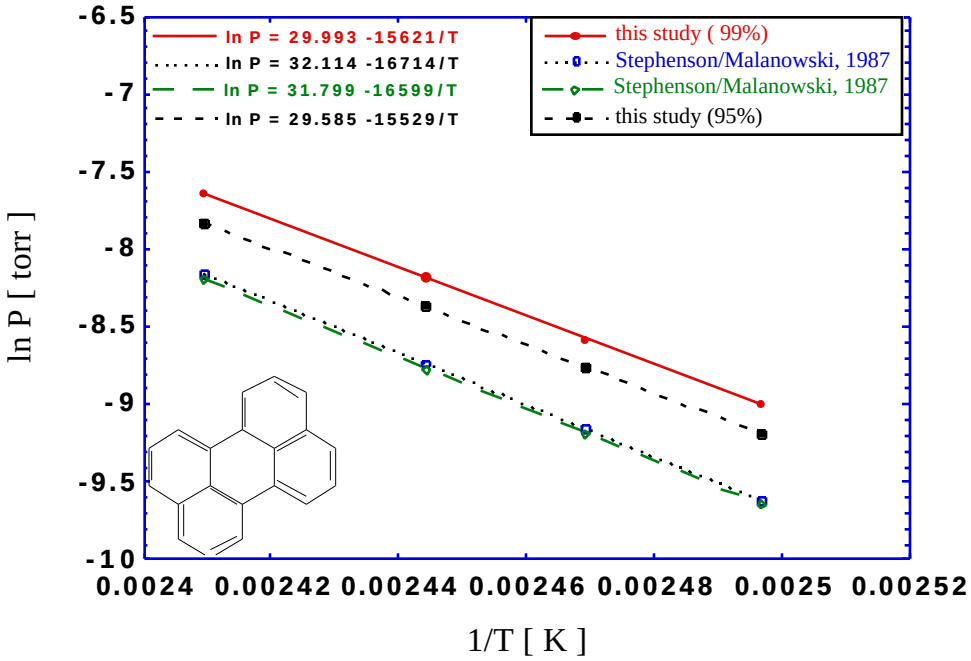

Figure C.5. Knudsen effusion method applied to solid perylene.
Solid points are from this study, open are calculated from references.

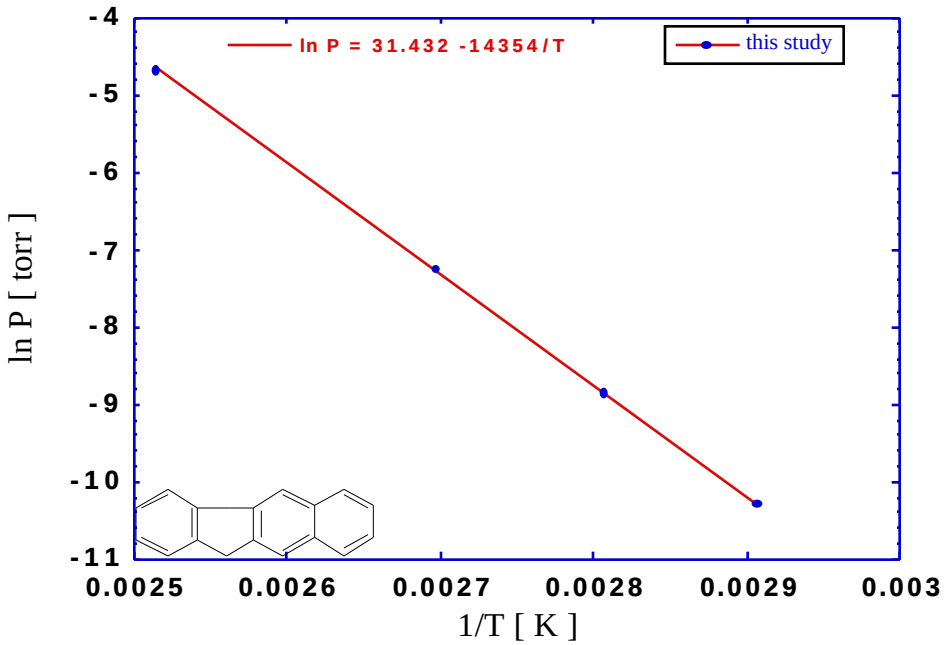

Figure C.6. Effusion method applied to solid 2,3-benzofluorene.

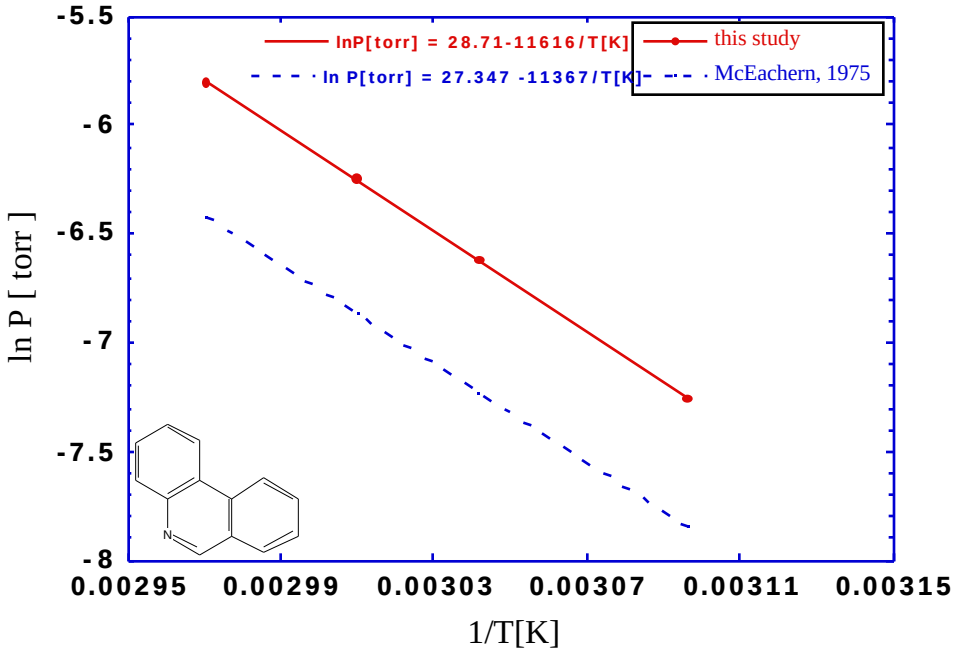

Figure C.7. Effusion technique applied to solid phenanthridine.

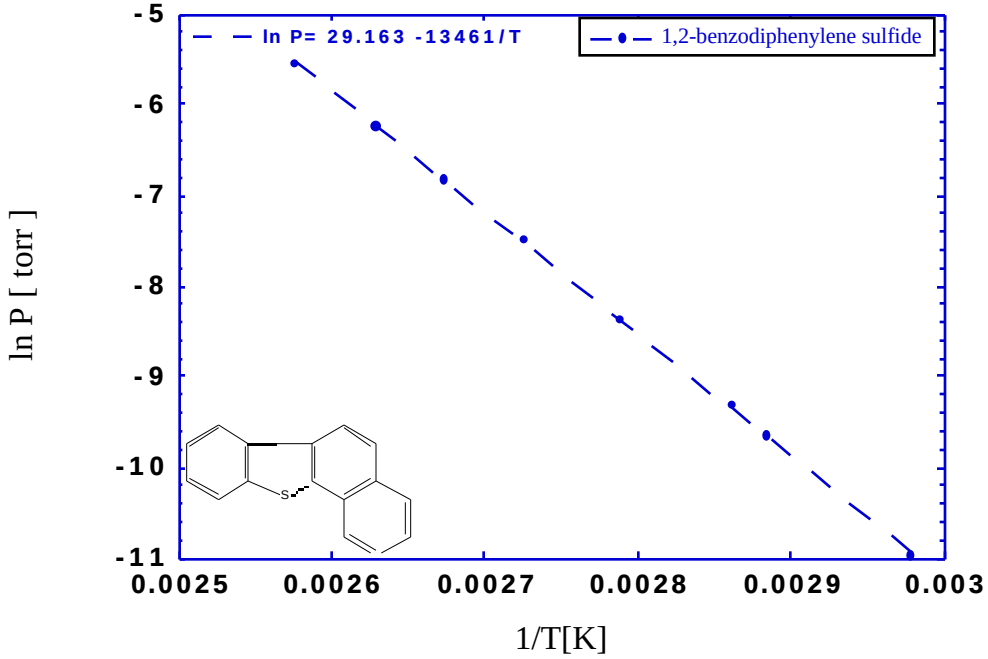

Figure C.8. Effusion method applied to solid 1,2-benzodiphenylene sulfide.

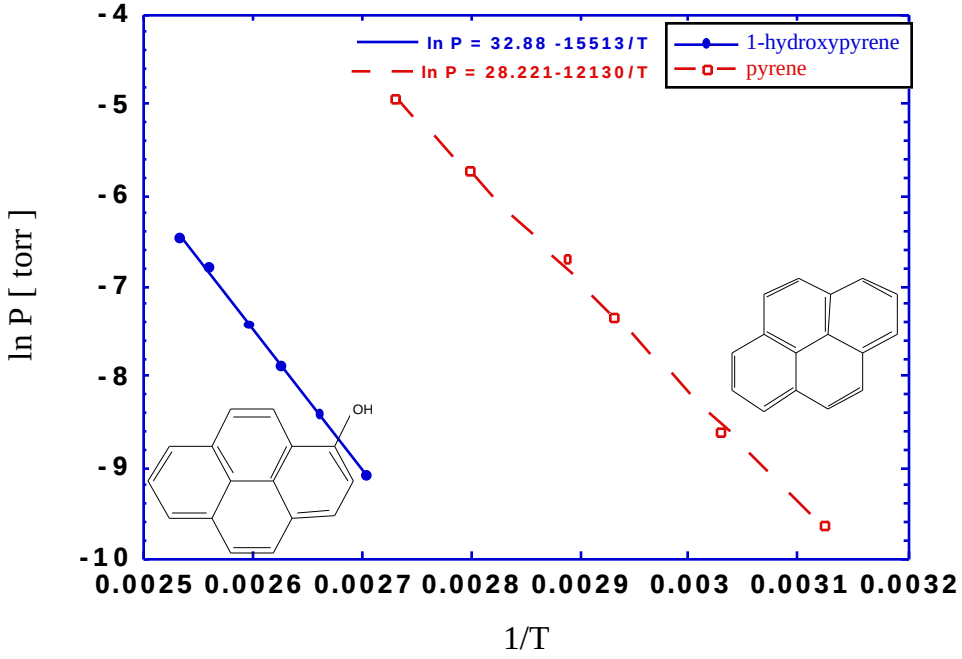

Figure C.9. Effusion method applied to solid 1-hydroxypyrene. Data for pyrene are shown for comparison.

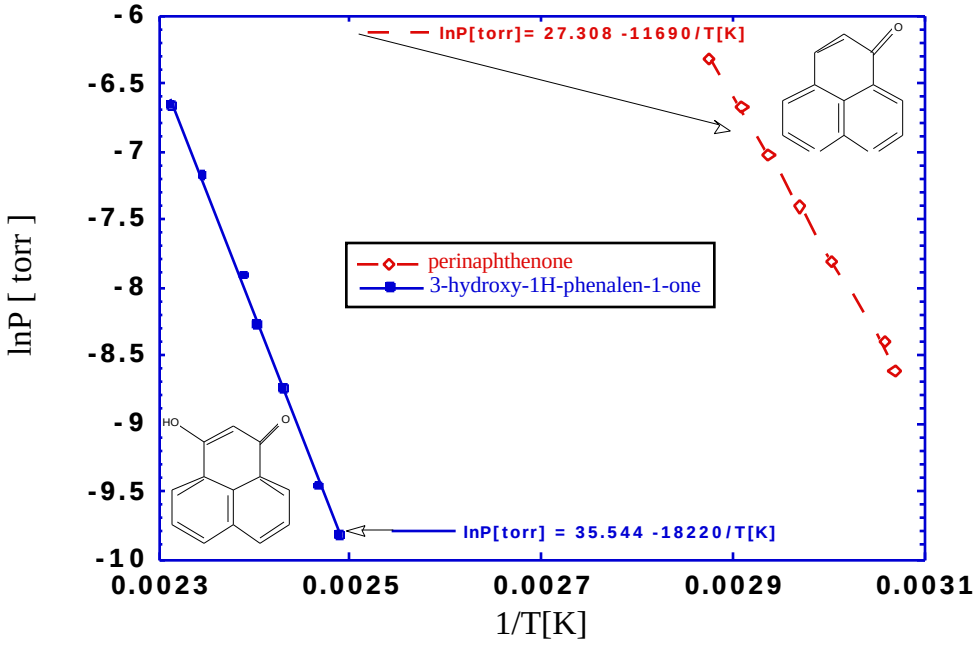

Figure C.10. Effusion method applied to solid perinaphthenone and 3-hydroxy-1H-phenalen-1-one.

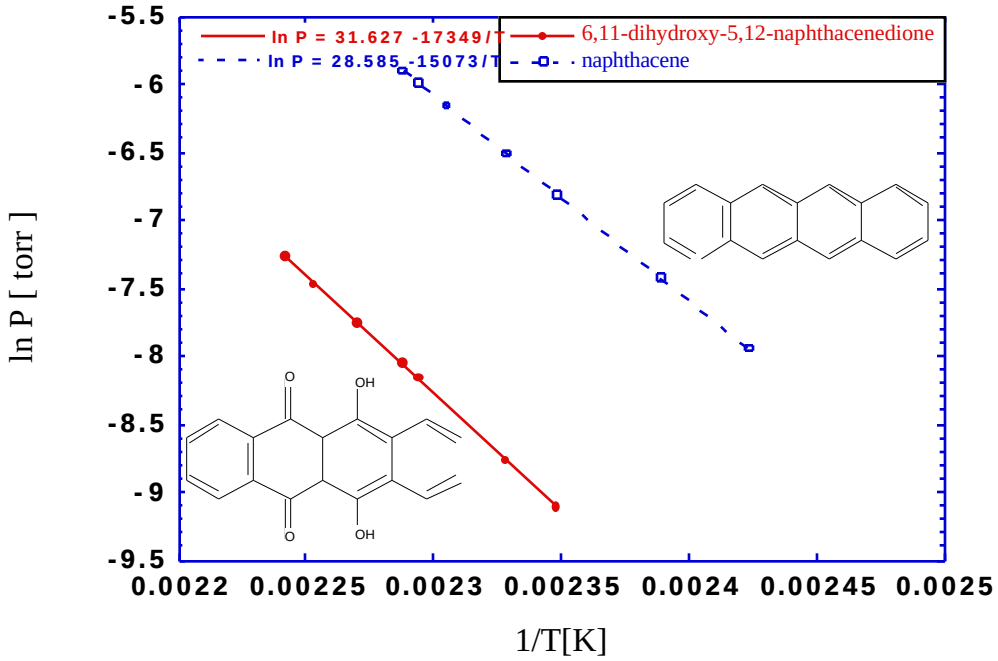

Figure C.11. Effusion method applied to solid 6,11-dihydroxy-5,12-naphthacene dione. Data for naphthacene are shown for comparison.

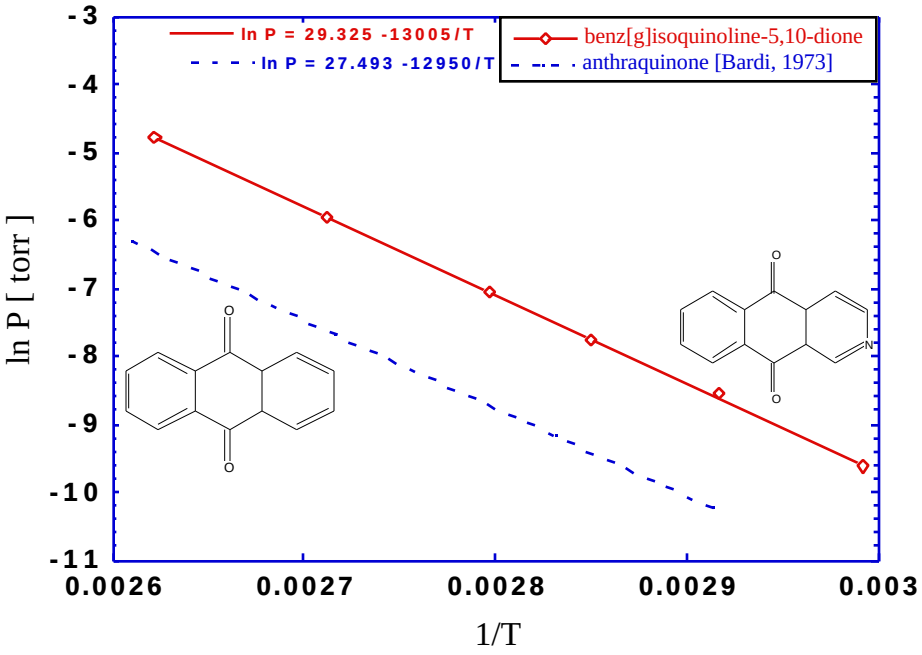

Figure C.12. Effusion method applied to benz[g]isoquinoline-5,10-dione. Data for anthraquinone are shown for comparison.

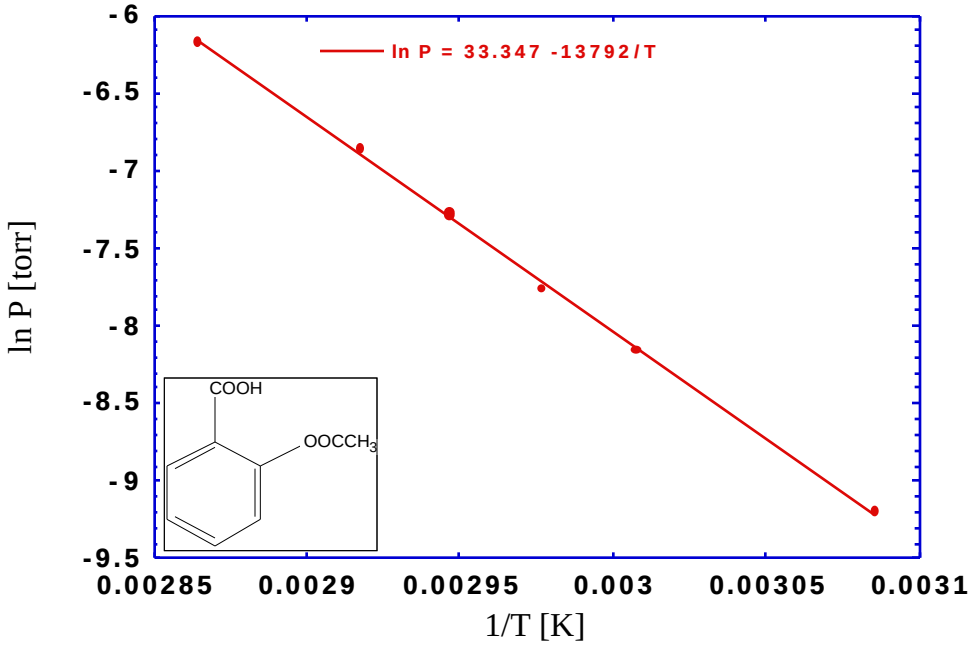

Figure C.13. Effusion method applied to solid Aspirin.
The main salicylic acid acetate component is illustrated.

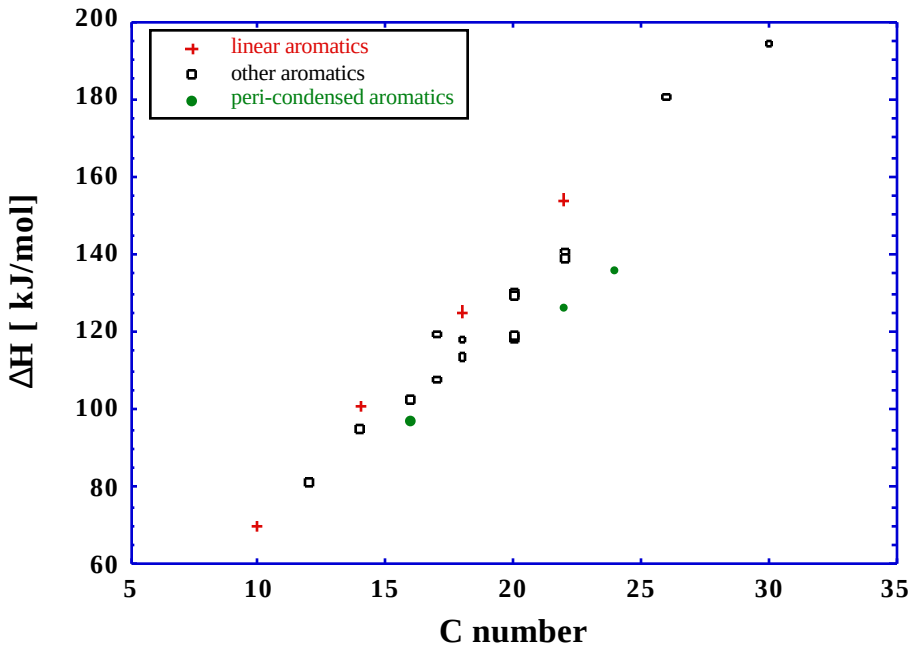

Figure C.14a. Enthalpy of sublimation against carbon number for PAH.

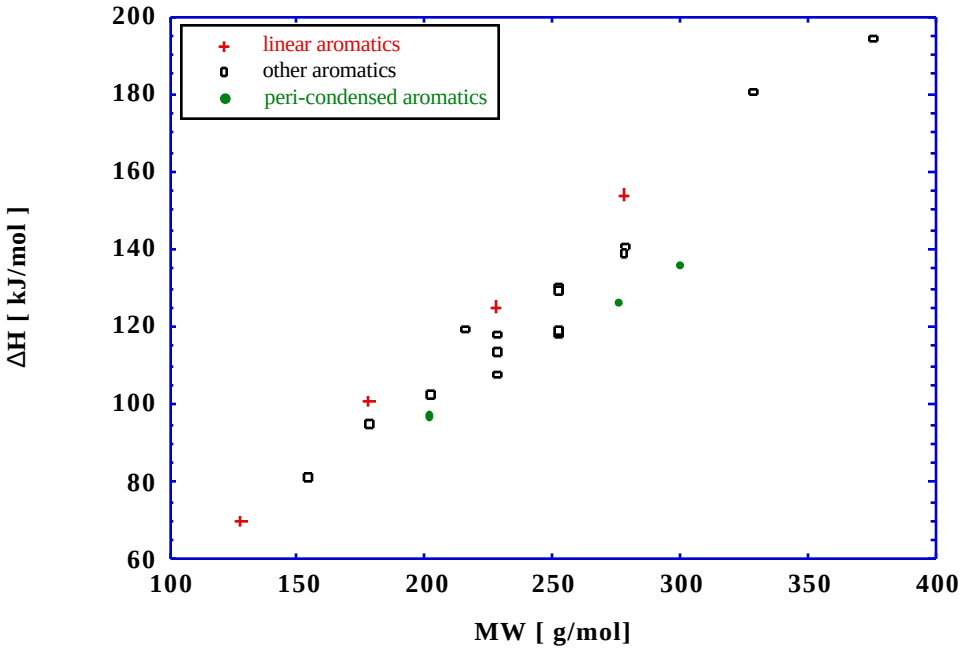

Figure C.14b. Enthalpy of sublimation against molecular weight for PAH.

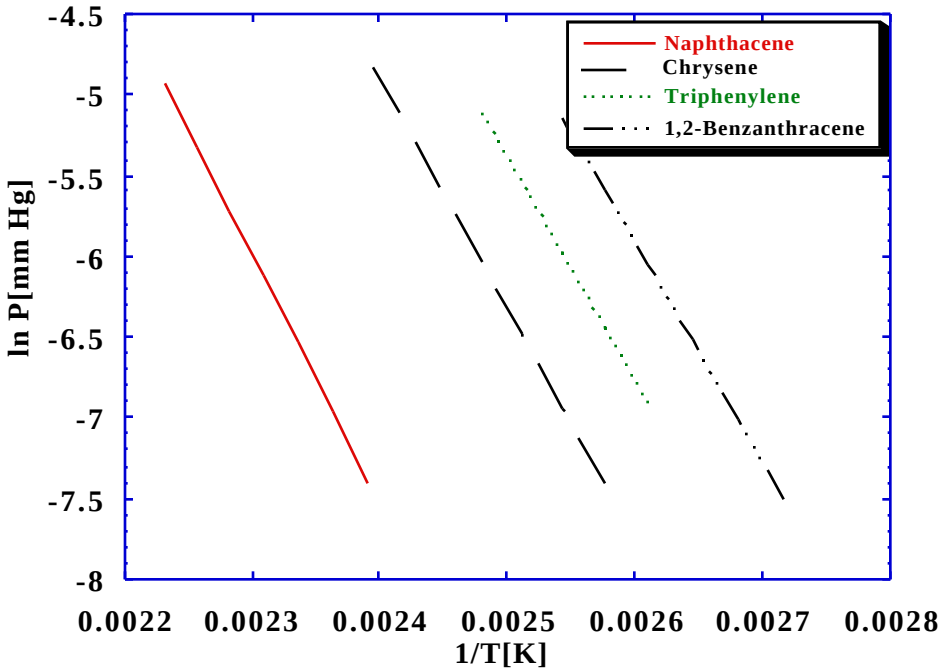

Figure C.15. Comparison of the vapor pressure data on selected aromatic hydrocarbons M(C_{18} H_{12})=228.19

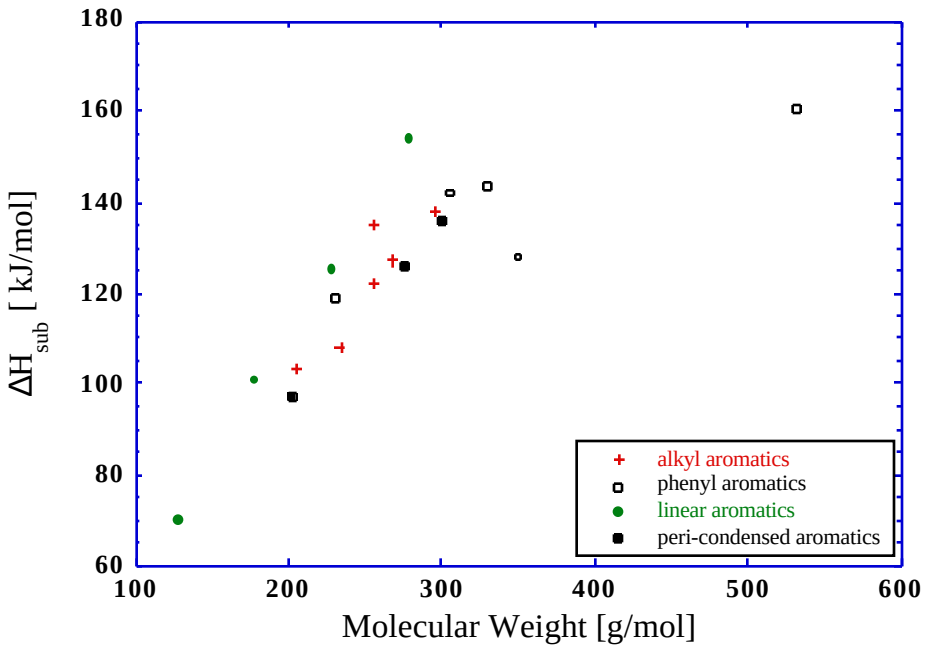

Figure C.16. Enthalpy of sublimation against molecular weight for alkyl and phenyl substituted PAH.

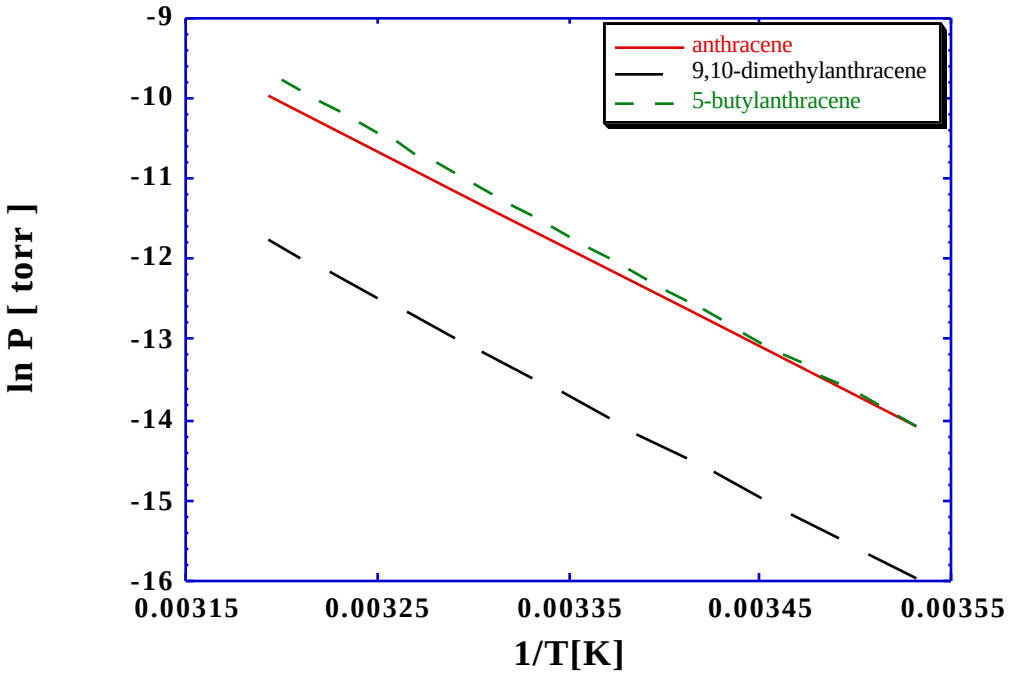

Figure C.17. Comparison of the solid vapor pressure data of anthracene (MW 178), 9,10-dimethylanthracene (MW 206) , and 5- butylanthracene (MW 234). [Data from Stephenson and Malanowski, 1987]

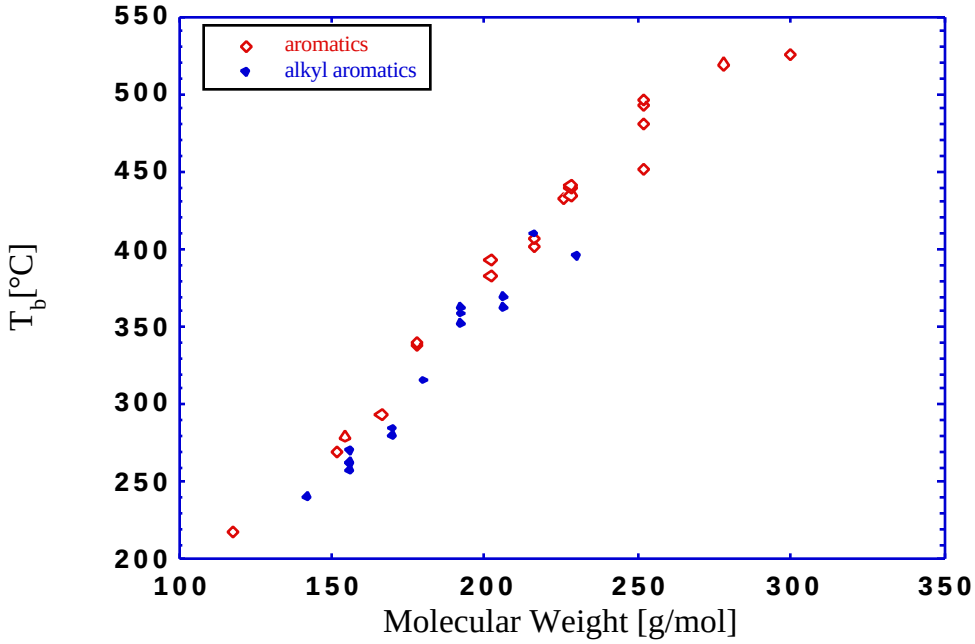

Figure C.18. Normal boiling point against molecular weight for PAH and alkyl substituted PAH. [Data from Bjorseth, 1983]

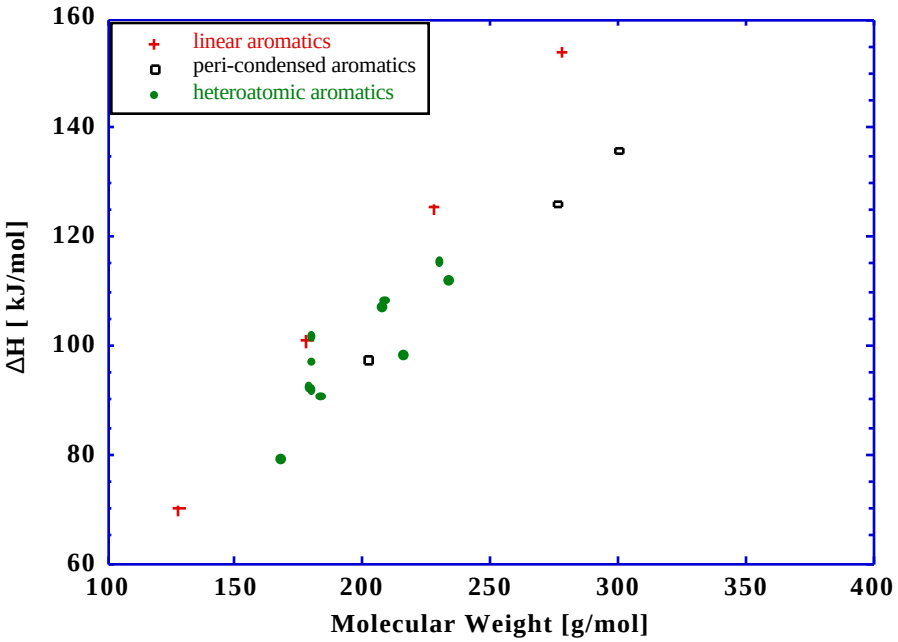

Figure C.19. Enthalpy of sublimation against molecular weight of heteroatom containing PAH. Data for linear and peri-condensed PAH are shown for comparison.

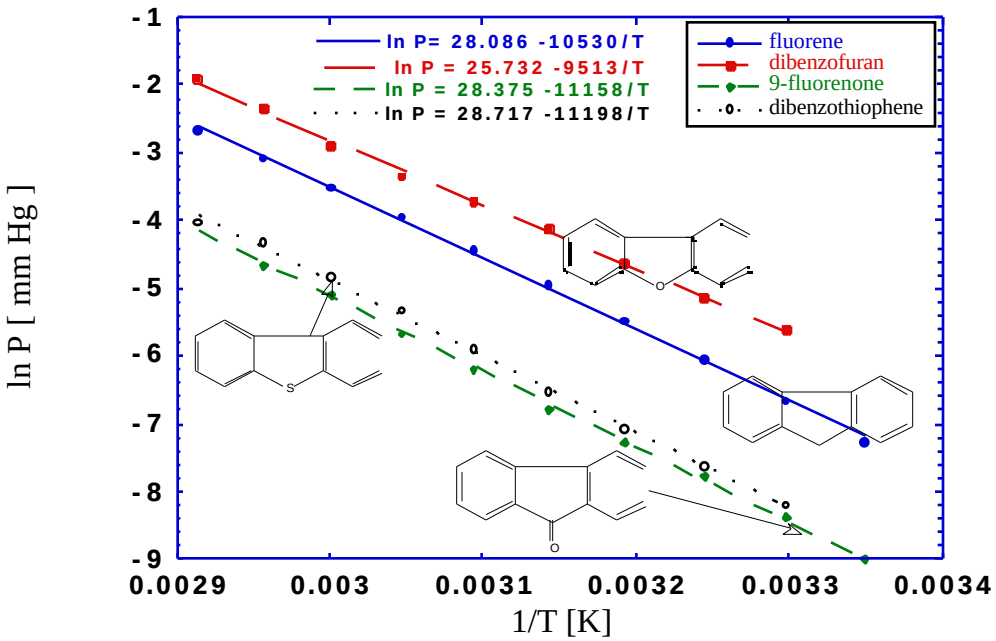

Figure C.20. Comparison of vapor pressures of four aromatic compounds. [fluorene from Sato et al., 1986; dibenzofuran, 9-fluorenone, and dibenzothiophene from Hansen and Eckert, 1986]

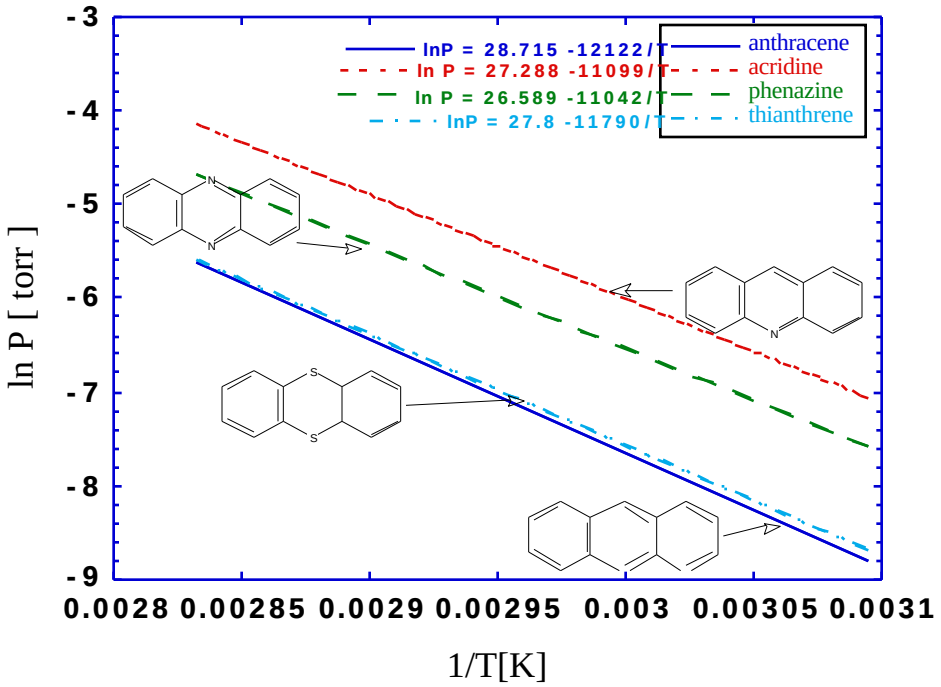

Figure C.21. Comparison of vapor pressures of four aromatic compounds. [data from Stephenson and Malanowski, 1987]

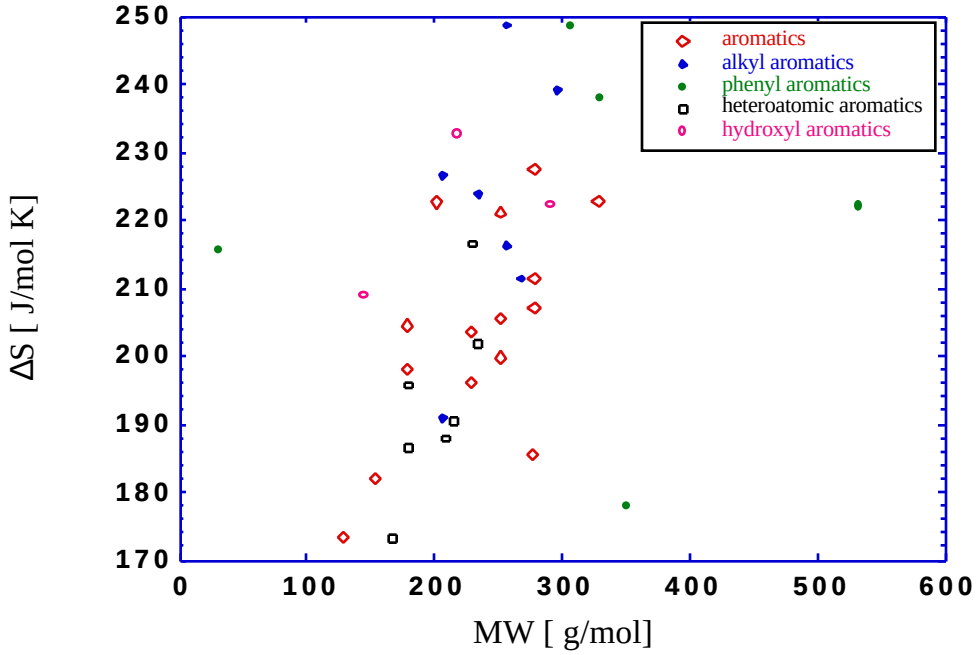

Figure C.22. Entropy of sublimation for various aromatics.

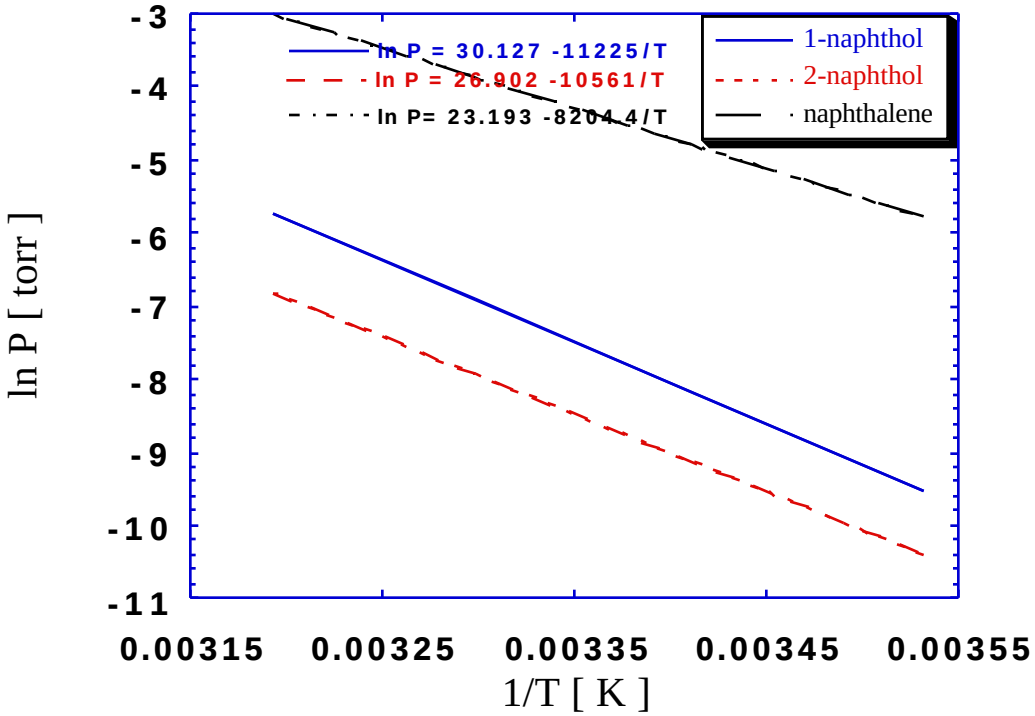

Figure C.23. Comparison of vapor pressures of naphthalene, 1-naphthol and 2-naphthol. [Data from Stephenson and Malanowski, 1987]

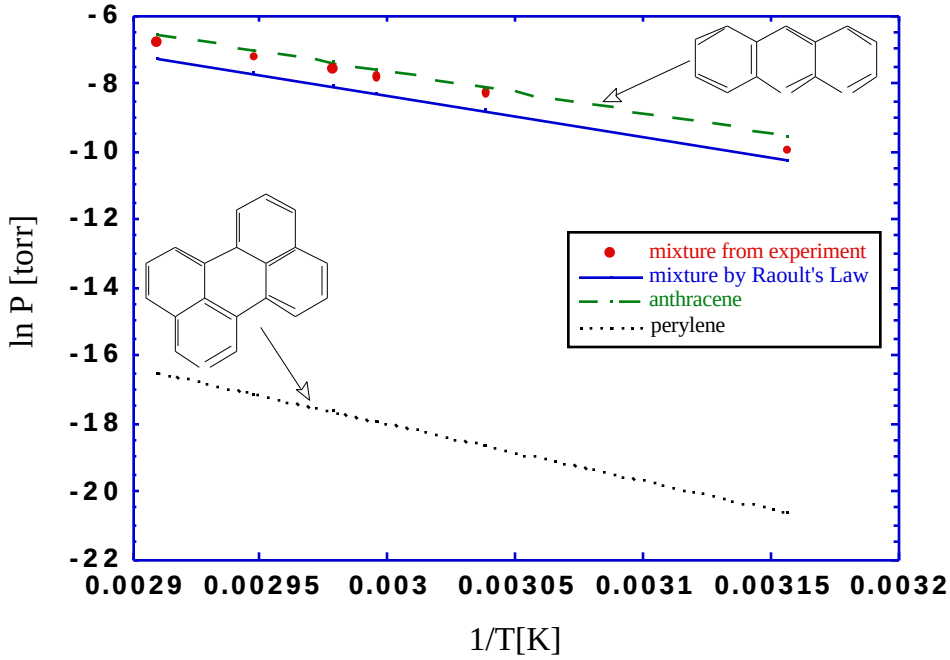

Figure C.24. Effusion method applied to a mixture of anthracene (50%) and perylene (balance). Data for pure components are shown for comparison.

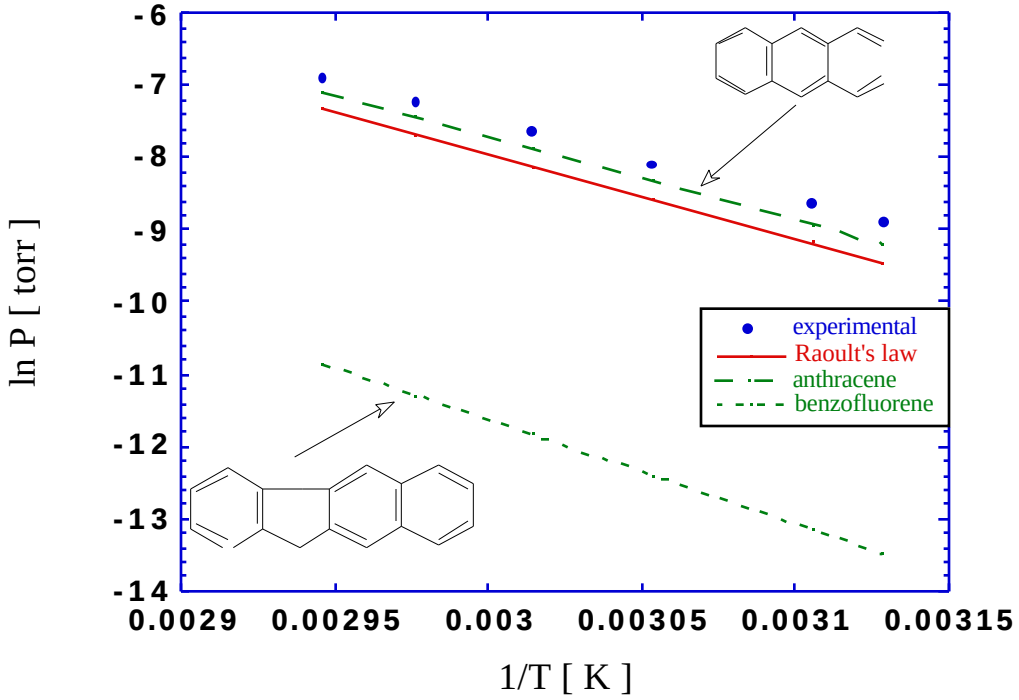

Figure C.25. Effusion method applied to mixture of anthracene 75 % and benzofluorene (balance). Data for pure components are shown for comparison.

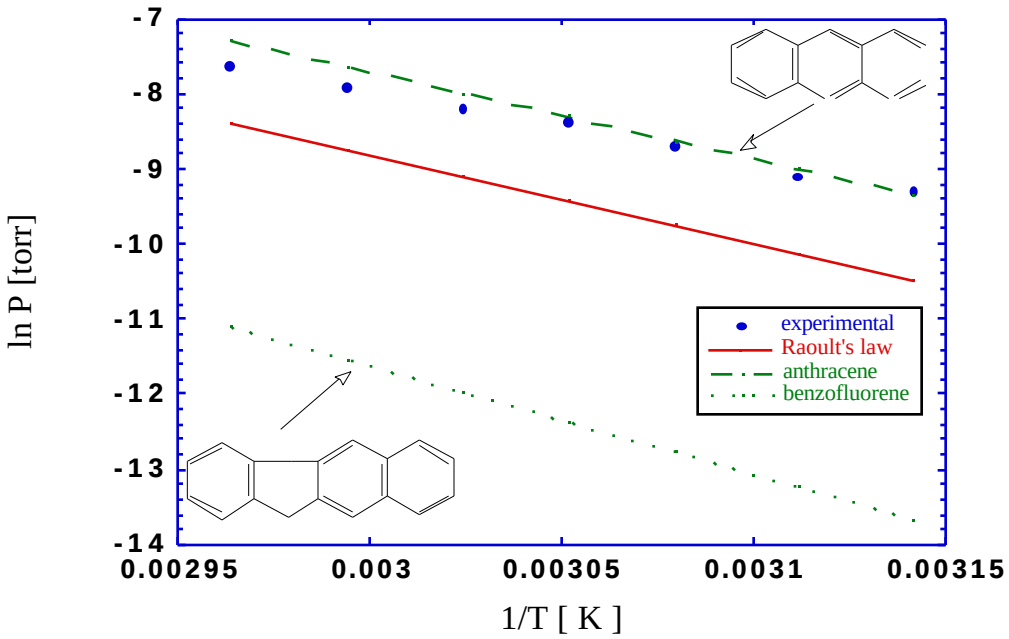

Figure C.26. Effusion method applied to mixture of anthracene (25%) and benzofluorene (balance). Data for pure components are shown for comparison.

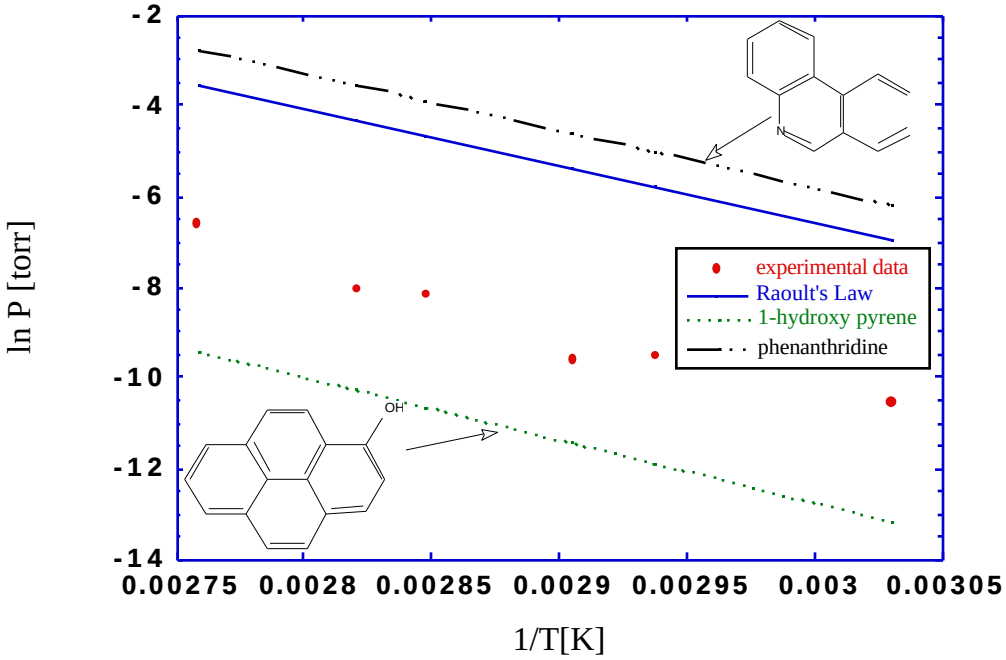

Figure C.27. Effusion method applied to a mixture of 1-hydroxypyrene (54%) and phenanthridine (balance). Data for pure components are shown for comparison.

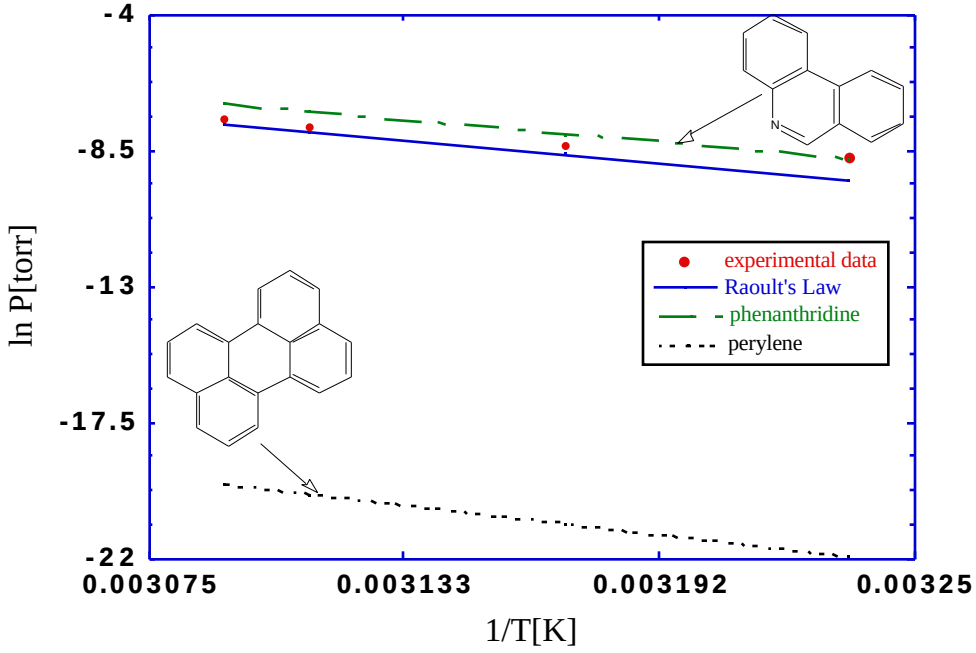

Figure C.28. Effusion method applied to a mixture of phenanthridine (50%) and perylene (balance). Data for pure components are shown for comparison.

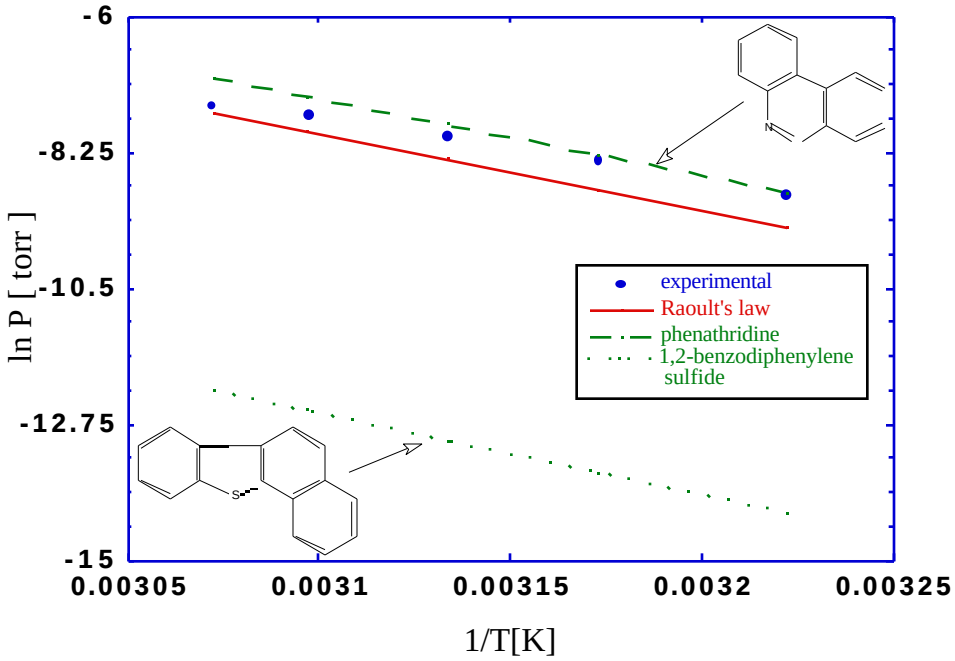

Figure C.29. Effusion method applied to a mixture of phenanthridine (50%) and 1,2-benzodiphenylene sulfide (balance). Data for pure components shown for comparison.

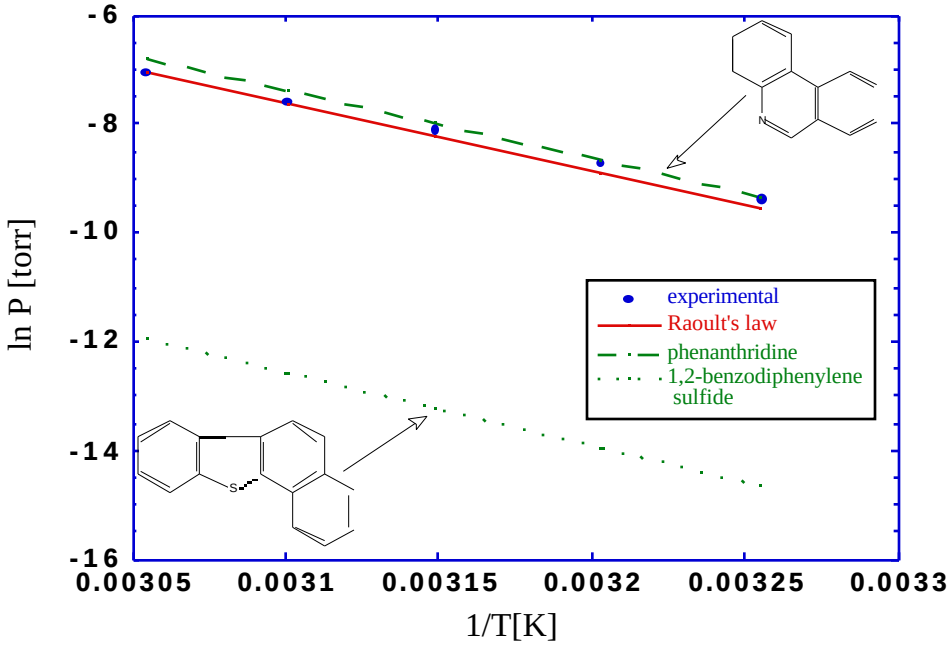

Figure C.30. Effusion method applied to a mixture of phenanthridine (75%) and 1,2-benzodiphenylene sulfide (balance). Data for pure components are shown for comparison.

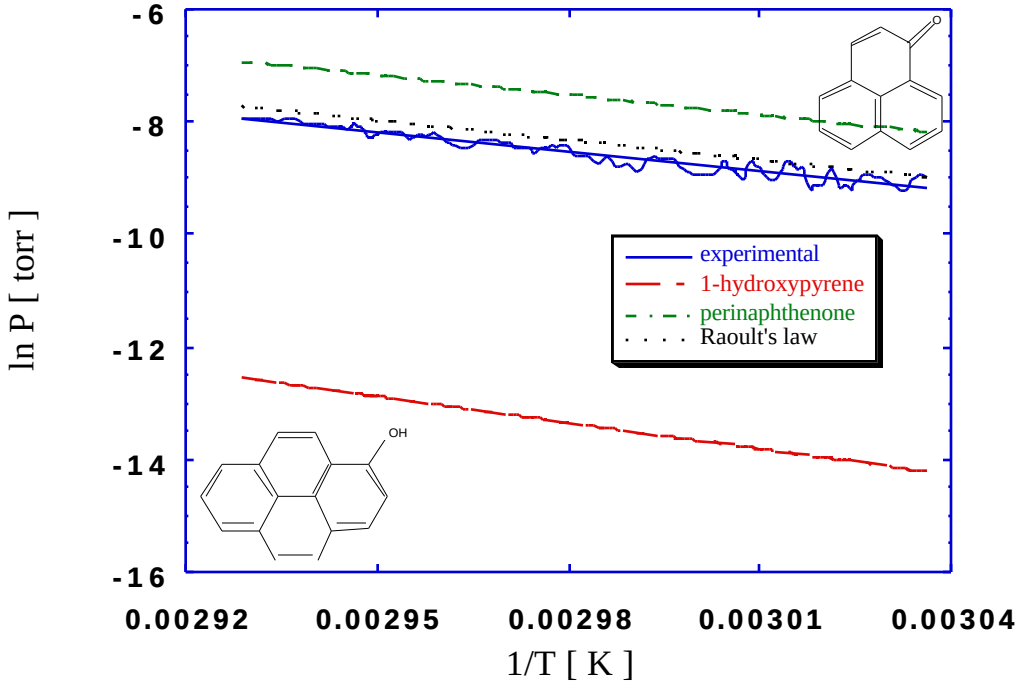

Figure C.31. Non-isothermal effusion method applied to a mixture of 1-hydroxypyrene (mole fraction 0.55) and perinaphthenone (balance).

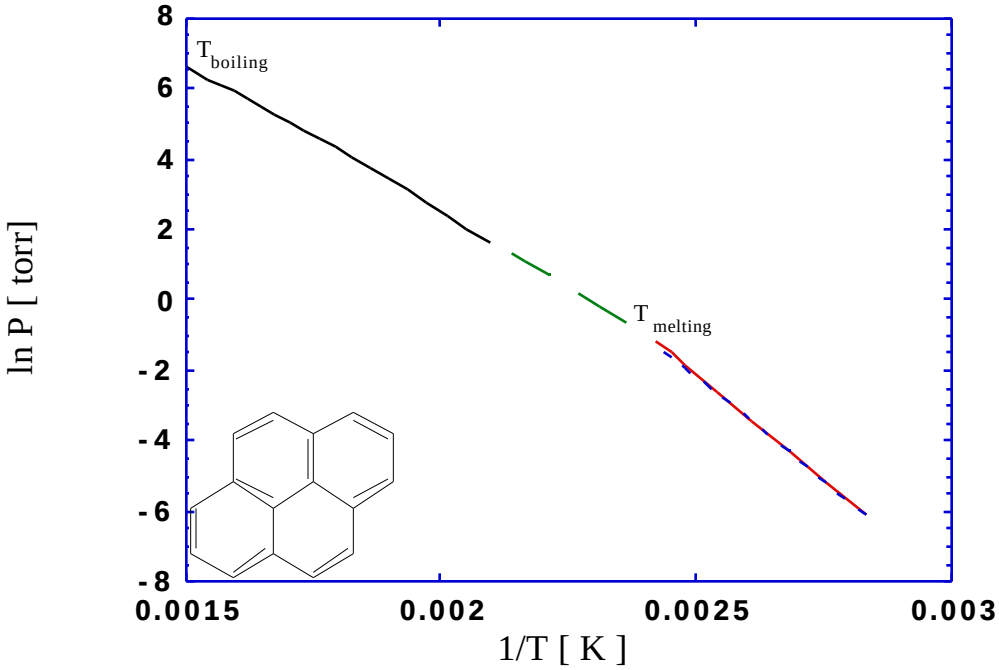

Figure C.32. The vapor pressure curve for pyrene.

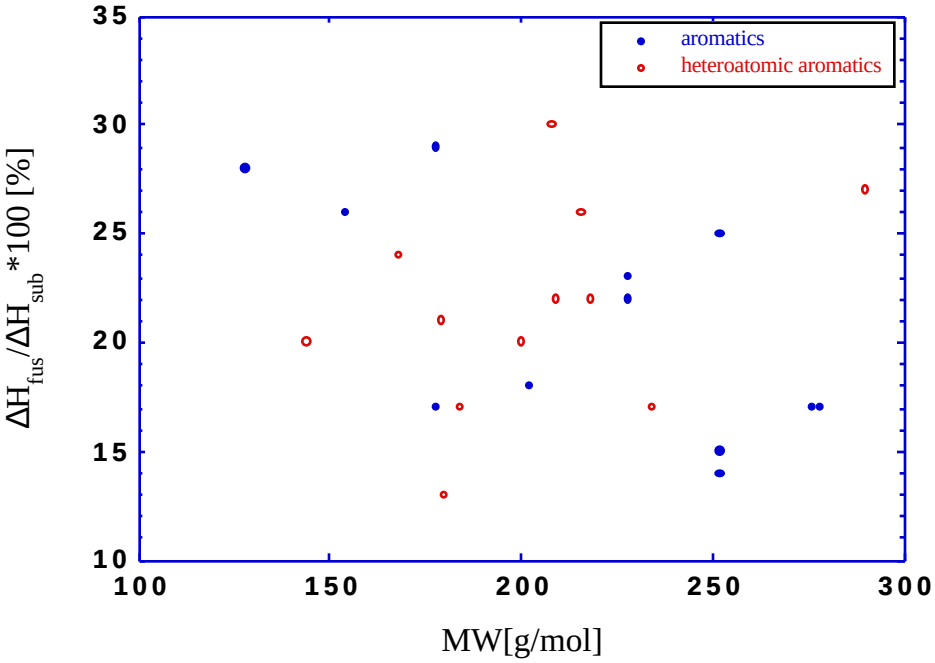

Figure C.33. $\Delta H_{fus}/\Delta H_{sub}$ ratio for aromatic hydrocarbons.

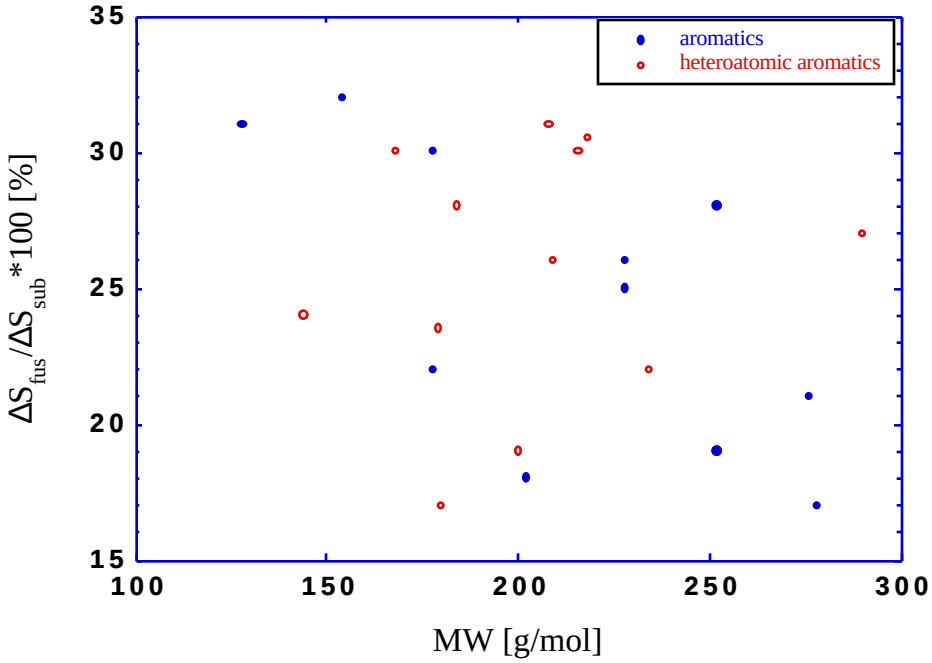

Figure C.34. $\Delta S_{fus}/\Delta S_{sub}$ ratio for aromatic hydrocarbons.

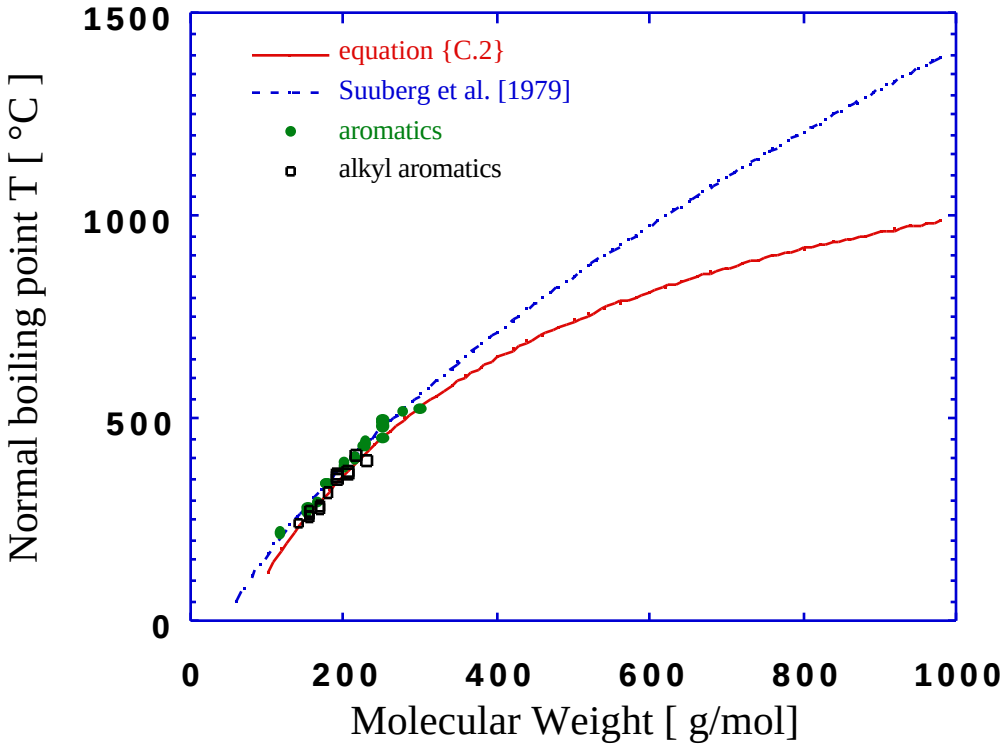

Figure C.35. Comparison of the equation {C.2} and the Unger-Suuberg correlation {A.1} with pure compound boiling point data at a pressure of 760 torr.

Chapter D. Vapor Pressures and Heat of Vaporization of Model Compounds and Primary Cellulose Tar.

In this laboratory, we have for some time been concerned with the behavior of cellulose during pyrolysis. This material is of some interest as a model for "biomass", an often-discussed alternative energy source. It was realized that this material presented both some interesting questions in its own right, as well as some interesting opportunities as another, simpler model for the kinds measurements we perform with coal tar.

There is some evidence that the mass transfer of tar plays a key role in cellulose pyrolysis. Under conditions in which the tar cannot rapidly escape the solid phase it cracks to char. This is similar to what happens during coal pyrolysis. Since the vapor pressure of the tar may be a key factor in determining its escape rate, we decided to extend these studies, using our equipment for vapor pressure measurements to primary cellulose tars. The cellulose tar has a much narrower distribution of molecular weights than does coal tar, and is much more homogenous. Thus it was better to develop the methods to be used for coal tars on this simpler model system first.

D.1. Cellulose Tar Characteristics and Its Volatility.

Cellulose releases copious amounts of tar during pyrolysis. One difference between cellulose and coal is the molecular weight of the tar species involved. In coal pyrolysis, the tar exhibits molecular weight distributions up to order of a thousand daltons [Suuberg, 1985; Solomon *et al., 1992*]. The cellulose tar species in contrast have number average molecular weights around 200 daltons and a narrower molecular weight distribution than coal tars.

Another important difference between coal and cellulose pyrolysis is the temperature range of tar evolution. Typical cellulose pyrolysis results obtained from the TGA apparatus

are illustrated in Figure D.1, which compares the rates of mass loss from a standard open TGA pan, and from a DSC pan which was used to contain the sample in the TGA. Figure D.1 shows that the tar evolution (which represents most of the mass loss) at 6°C/min heating rate occurs in a narrow range of temperatures between 310 and 370°C. At comparable heating rates coal pyrolysis occurs over a much broader range of temperatures, not reaching completion until over 500°C [Solomon *et.al.*, 1992]. This means that higher molecular weight (and thus less volatile) tars can evaporate during coal pyrolysis because of the higher temperatures that are involved.

To begin to address the cellulose tar volatility issue, experiments were performed in which tar from cellulose pyrolysis experiments was collected and recoated onto a wire mesh, which was then heated from room temperature in the heated wire mesh reactor. The results are shown in Figure D.2. The experiments were performed at a heating rate of 60 °C/min, in inert gas. Each datum shows the result of a single experiment in which a few milligrams of tar was heated to the indicated temperature at 60 °C/min, and then held for one minute before being permitted to cool at a rate of several hundred degrees per second. These experiments define a pseudo-distillation curve for the tar. Bubble formation in the tarry mass was noted at around 260°C, suggesting boiling. More precise measurements of vapor pressure will be shown below. The results of Figure D.2 indicate that most tar evaporation occurs below the temperature range associated with active pyrolysis. Thus in the absence of mass transport limitations, tars should immediately evaporate, as commonly assumed [e.g., Ponder *et al.*, 1992]. The results of Figure D.2 however emphasize that there are finite kinetics associated with evaporative loss of tar, even from a heated wire mesh. These will be considered further below.

A second notable feature in Figure D.2 is that the tar cannot all be vaporized. The fraction of tar vaporized reaches an asymptote of around 76% at 320-350°C, which is the range of temperature at which the pyrolytic pathways are active in cellulose itself. Since all of the tar on the mesh had earlier vaporized (and had been soluble), its inability to

completely re-evaporate is associated with pyrolytic reactions driving some of the tar to a non-volatile char. Alternatively, during reheating the tar might be undergoing reactions involving pathways not available, or suppressed, during the original cellulose pyrolysis.

The heat of vaporization of cellulose tars has not been reported and direct calorimetric measurements of this latent heat proved to be impossible, because the cellulose tar was observed to thermally degrade in such experiments. The Clapeyron equation {A.2} relates the heat of vaporization to the temperature derivative of the vapor pressure. Thus, the enthalpy of sublimation of the tar can be estimated from the Clausius-Clapeyron equation, using suitable vapor pressure data obtained under very low temperature conditions, at which the tars do not degrade.

According to the literature [Haplern and Patai, 1969; Shafizadeh and Fu, 1973; Halpern et al., 1973; Shafizadeh et al., 1979; Shafizadeh, 1975] the pyrolysis of the cellulose under vacuum and atmospheric pressure gives a tar containing various amounts of 1,6-anhydro-β-D-glycopyranose (known as levoglucosan), 1,6-anhydro-β-D-glycofuranose, α− and β-D-glucose, disaccharides (cellobiose) and their further condensation products, consisting of various oligo- and polysaccharides (polymeric materials, that are similar to condensation products of levoglucosan), and some dehydration products (3-deoxy-D-hexosulose and its isomer, levoglucosenone). It has shown also that the pyrolytic reaction may produce a variety of products through concurrent and consecutive reactions. Vacuum or atmospheric pyrolysis of cellulose provides a tar fraction containing mainly 1,6-anhydro-β-D-glucopyranose and its condensation products (20 to 60 % of tars). The fraction of levoglucosan in this mixture varies and depends upon conditions.

Because cellulose tar vapor pressures have not been previously determined, we set about to do so. In order to validate the work performed with the tars, we have first obtained results with model compounds.

D.2. Vapor Pressure of the Cellulose Tar Related Compounds.

In this study we have examined the vapor pressures of levoglucosan (of 99% purity, from Adrich Chemical company, Inc.) between 71 and 140°C; D-(+)−glucose (of 99.5% purity from the Sigma Chemical Company) between 122 and 133 °C; D-xylose or wood sugar (of 99% purity, from Adrich Chemical company, Inc.) between 97 and 122 °C; and cellobiose (of 99% purity, from Adrich Chemical company, Inc.) between 201 and 215 °C. The enthalpies of sublimation have been estimated from the vapor pressure data. Vapor pressures and heats of sublimation of these solid compounds have not previously been reported. Only one study of liquid levoglucosan has been found in the literature [Enstein, 1964].

The chemicals were used as supplied. As these materials are hygroscopic, 5% of each sample's mass was evaporated as a precaution before beginning actual vapor pressure data collection. The presumption was that any water present in the samples would be evaporated in this initial 5% mass loss. Since these compounds are quite thermally labile, the differential scanning calorimeter was used to study the thermal behavior of the compounds in the temperature region of interest. The DSC would reveal where any thermally significant reaction events took place, so that the temperatures of measurement could be kept below such temperatures. The latent heats of fusion of the samples have been also estimated from the DSC results. This latent heat is important, to the extent that any of the measured vapor pressure results would be extrapolated to higher temperatures, at which the materials of interest would be liquids as opposed to solids.

The vapor pressure data have been obtained using the isothermal method in both the "forward" direction (the temperature was raised stepwise during data collection) and in the "backward" direction (the temperature was decreased stepwise after achieving the highest temperature of the experiment).

D.2.1. Vapor Pressure of Levoglucosan.

Levoglucosan or 1,6-anhydro-β-D-glycopyranose is known to be the major component of cellulose tars [Ponder et al., 1992; Shafizadeh et al., 1979; Mok and Antal, 1983; Arseneau, 1971]. Figure D.3 shows our Differential Scanning Calorimetry (DSC) experiments for levoglucosan. Two well-established reversible phase transitions are apparent from this plot at 113 °C and at 183°C. It has been suggested by Shafizadeh [1971] that there is a plastic crystalline phase transition around 113°C and that melting occurs around 180°C. Similar solid state transition behavior has also been shown for the stereo isomers of the levoglucosan and for the 2-deoxy derivative, but not for the other closely related compounds [Shafizadeh, 1971]. From our DSC experiments the heat of phase transitions can be estimated 24.5 kJ/mol and 3.2 kJ/mol respectively. The second feature visible on Figure D.3 is a levoglucosan decomposition event above 250°C. This is thought to occur before boiling and therefore it is not possible to clearly determine the boiling point from the DSC data.

The vapor pressure results before and after the first so called "solid state phase transition" are shown in Figure D.4. If the assumption is made that the heat of sublimation is not a function of temperature, then the integration of the Clausius-Clapeyron equation gives $\Delta H_{sub(I)}$=125.1 kJ/mol before the first phase transition and $\Delta H_{sub(II)}$=100.3 kJ/mol after the first phase transition. This gives 23.3 kJ/mol for the phase change, which is quite consistent with our DSC data. Taking into account the enthalpy of the phase change of 3.2 kJ/mol at 183°C we may predict the normal boiling point for levoglucosan to be about 350°C. Our prediction is higher than an earlier estimate of the boiling point for levoglucosan at 260°C [Mok *et.al.* 1983]. The earlier estimate appears to be more likely associated with the decomposition of levoglucosan. The extrapolation is shown on Figure D.5 together with other reported experimental data on liquid levoglucosan [Enstein et al., 1964]. Those results also imply a boiling point of about 315°C. Enstein et al. measured liquid levoglucosan vapor pressure at three different temperatures from 195 °C to 255°C

using the static method. These data give a heat of vaporization 92.3 kJ/mol, while our data suggest 97 kJ/mol. Additional liquid levoglucosan data are given by Stephenson and Malanowski [1987] in the "Handbook of the Thermodynamics of Organic Compounds". However, there is reason to suspect based on a comparison of the cited temperature range with that of Enstein et al. that they show erroneous data obtained from that study.

D.2.2. Vapor Pressures of Sugar Compounds.

Since "tars" are complicated mixture of many products we have studied the vapor pressures of additional saccharides (D-xylose, D-(+)-glucose and cellobiose) that allow comparisons to be drawn. Figure D.6 shows a comparison between the results of four cellulose tar model compounds in the solid phase. The vapor pressure of levoglucosan appears to be greater and its latent heat of sublimation appears to be lower than the same quantities for the other similar molecular weight compounds, D-xylose and D-glucose. It is important to note that a correlation based on molecular weight alone would show an uncertainty of at least an order of magnitude about a mean. The intermolecular forces that play important role in sugar-like compounds are van der Waals, polar attraction, and hydrogen bonding. Our data imply the important role of hydrogen bonding interactions in these materials, since the vapor pressure at any temperature decreases as OH content increases. Likewise, the heat of sublimation and the entropy of sublimation both increase with increase in OH content. Table D.1 summarizes the vapor pressure experimental results for solid sugar like compounds:

Table D.1. Enthalpy and entropy of sublimation for sugar like compounds.

substance	number of (-OH)	MW [g/mol]	temperature range [°C]	A	B	ΔH [kJ/mol]	ΔS [J/mol K]
levoglucosan	3	162.4	71…112	15085	34.175	125.5	234.4
D-xylose	4	150.1	97…122	19006	41.359	157.9	303.5
D-β-glucose	5	180.2	122…133	24142	50.565	194.5	360.6
Cellobiose	8	342.3	201…215	36260	65.397	301.3	503.1

Figure D.6a shows the variation of ΔH_{sub} and Figure D.6b shows the variation of ΔS_{sub} with hydroxyl content. There are not many points upon which to draw very general conclusions, but a correlation is certainly implied.

The thermal behaviors for D-xylose, D-(+)-glucose and cellobiose are shown in Figures D.7, D.8 and D.9 respectively. All of these compounds show signs of decomposition shortly after melting. The heat of fusion and melting point values for the compounds of interest are presented in Table D.2.

Table D.2. Measured melting points and heats of fusion for sugar-like compounds.

compound	nr OH	MW	T_m [°C]	ΔH_f [kJ/mol]
levoglucosan	3	162.4	113	24.5
D-xylose	4	150.1	152	30.5
D-β-glucose	5	180.2	172	34.5
Cellobiose	8	342.3	247	

The increases in both the melting point and the heat of fusion are evident as the number of hydroxyl groups increases.

In closing, it should be noted that these materials are characterized by extremely low vapor pressures, considering their low molecular weights. This was anticipated, since sugars are practically non-volatile at near ambient temperatures. The low vapor pressures are attributable to the important role of hydrogen bonding interactions in these materials. For example, consider the predicted 25°C vapor pressure of glucose ($6.2*10^{-14}$ torr) with that of a similar molecular weight alkane (hexadecane: MW 226, $1.26*10^{-3}$ torr [Bell and

Groszek, 1962]). The vapor pressures decrease monotonically with the number of hydroxyl groups that the sugars carry.

D.3. The Vapor Pressure of Primary Cellulose Tar.

D.3.1. Production of the Cellulose Tar.

In this chapter we are interested in the vapor pressures of primary cellulose pyrolysis tars. A flash pyrolysis apparatus, the so-called wire mesh reactor, was used to prepare the cellulose tars. This apparatus permits rapid electrical heating of the cellulose within the folds of a wire mesh. The fact that only a thin wire mesh that contains the particles becomes hot minimizes the cracking of tars in the reaction vessel. The tars may therefore be considered "primary" pyrolysis tars. The tars were prepared from two different cellulose samples. One was Whatman fibrous cellulose powder (CF11). This cellulose powder contains less than 0.009% ash. Some of the tars were prepared from Munktell's Filter paper, with an average ash content 0.007%. The cellulose samples were not dried prior to pyrolysis. The tars were felt to be similar from both sources, since earlier studies of pyrolysis had indicated that their pyrolysis behaviors were similar. Thus the samples were pyrolyzed together, as described below.

The cellulose samples consisted of two thin sheets of filter paper with a layer of cellulose powder folded between them. This was necessary to prevent loss of the fine cellulose powder through the holes of the wire mesh. Operating conditions were chosen based upon the literature on cellulose pyrolysis. It was shown that the tar yield increases with temperature to a maximum at 700 °C, and at these temperatures pyrolysis is completed in 5 to 10 seconds.

Material that collected on the cold walls of the pyrolysis reactor is called condensed material. The condensed material was collected at room temperature by supplying a flow of cooling water to the jacketed walls of the reactor. Some condensed material was also collected on a glass wool filter at the exit of the reactor. These materials were collected after reaction by washing the primary collection surfaces with-high purity methanol and in one

case with a mixture of THF and methanol. This procedure left a small amount of solvent insoluble residue in the reactor walls.

Condensed material includes tar, water, organic acids, and various low molecular weight hydrocarbons. The subsequent handling of this material was intended to prepare a tar sample by evaporation of water and light hydrocarbons. Solvent was evaporated from the condensed material solution by drying in a vacuum oven at room temperature for 12 hours followed by additional vacuum drying at 55 °C for another 24 hours. It was previously shown in this laboratory that vacuum drying at a temperature of 55°C will result in the loss of some light material. All components with a vapor pressure equal to or greater than that of naphthalene are lost, while there is better than 95% retention of materials with vapor pressure of anthracene. For comparison it may be noted that the vapor pressure of anthracene is of the order of 10^{-4} torr at the maximum temperature of drying, but levoglucosan, which is assumed to be the major component of the tar, has a vapor pressure of 10^{-6} torr at this temperature.

The cellulose tar was not fractionated prior to vapor pressure measurements. Characterization work in this laboratory gave a fairly narrow molecular weight distribution centered below 200 daltons.

D.3.2. Characterization of the Cellulose Tar.

The molecular weight distribution of the our samples has been examined using gel permeation chromatography (GPC). The analyses were performed on a Water μ-Styragel column using pyridine as the mobile phase. The detailed description of this technique is given in the section B.3.2. Products eluting from the column were analyzedsimultaneously by ultraviolet detector and refractive index detector. Analysis of the tar products of

pyrolysis by GPC are shown as absorbance as a function of time in Figure D.10 using the ultraviolet detector and in Figure D.11 using the refractive index detector. The UV detector did not reveal high concentrations of UV-active compounds, which implies the absence of high aromatics content in tar. Comparison of Figures D.10 and D.11 together with the observation of a high content of UV-inactive low molecular weight material near an elution time of 2700 seconds implies, that the broad UV-active peak represents small amounts of secondary decomposition products. Attempts were made to make the analysis more quantitative by using coal tar as a calibration material for aromatics. We estimated the aromatic contents from the UV detector response curve. This gave 0.02 mg of aromatic compounds in 0.75 mg cellulose tar or roughly 3.5 wt%. From refractive index detection, as shown in Figure D.11, comparison of the peak elution times of the tar (2688 sec), cellobiose (2080 sec), levoglucosan (2664 sec), D-xylose (2672 sec) and, D-(+)-glucose (2720 sec), it appeared that the cellulose tar consists manly of 6-carbon sugar residues (note the shorter elution time for the tars, as compared with cellobiose, the glucose dimer). Thus the cellulose tars are much lighter and have narrower molecular weight distribution than coal tars.

The number of average molecular weight of the three different tars were determined to be around 180 daltons (between 172 and 184 daltons) using vapor-phase osmometry. This value is in good agreement with literature values and shows again that the tar is in a molecular weight range consistent with single 6-carbon sugar residues. The vapor phase osmometer was calibrated using β-D-glucose at 0.04, 0.07 and 0.1 M solutions in methanol at 45 °C (See chapter B). The VPO and elemental analysis results for the tars are shown in Table D.3. Corresponding values for levoglucosan, assumed to be the main compound of tar, are shown for comparison. The values for glucose, also shown in Table D.3, are not seen to be in as good agreement.

Table D.3. Elemental analysis results for cellulose tars.

material	solvent	MW	C%	H%	O%	H/C
levoglucosan		162	44.4	6.2	49.2	1.8
glucose		180	40.0	6.6	53.3	2.0
tar nr. 1	methanol	179	46.8	7.03	46.2	1.8
tar nr. 2	methanol	172	46.1	6.9	47.0	1.8
tar nr. 3	methanol/THF	184	46.5	7.3	46.2	1.9

This supports the previous hypothesis that levoglucosan could be a major component of flash pyrolysis cellulose tar. The data on aged cellulose tars, seen in Figures D.10 and D.11, will be discussed in the next section.

D.3.3. Vapor Pressure Measurements of Cellulose Tar.

Both the "isothermal step" and "non-isothermal" Knudsen effusion techniques were applied to cellulose tars. The results for all three tars of Table D.3 are shown in Figure D.12. The isothermal step Knudsen effusion technique was used to measure the vapor pressures of tar 1 and tar 2. The vapor pressure of tar 3 was measured by a "non-isothermal" technique with heating and cooling rates of 0.8 °C/min. The comparison of the three experimental runs shows that the new "non-isothermal" Knudsen effusion technique results are in good agreement with the traditional "isothermal" technique results. The second conclusion from Figure D.12. is that the vapor pressure curves are reproducible if the tar is produced under similar conditions.

It was seen in performing the vapor pressure measurements with cellulose tars that vapor pressures could be significantly lowered by prolonged heating of the sample at temperatures in excess of 100°C. This is the reason for the distinction between "fresh" and "aged" tars in Figure D.12. In one case, the sample was deliberately heated to 155°C. Figure D.13 presents the same data, emphasizing separation between the fresh tar and the

"aged" tar based on the data for cellulose tars 1 and 2 and a sample of pure levoglucosan. The non-isothermal results of Figure D.12 can be understood in light of this behavior. As temperatures approach 100°C, the non-isothermal results which initially follow the fresh tar, low temperature isothermal results, begin to curve off towards lower vapor pressures. There is a dramatic curvature at around 110°C, when the vapor pressure takes a steep drop, and thereafter follows "aged" tar behavior.

Differential Scanning Calorimeter (DSC) studies of fresh tars were performed. These experiments, the results of which are given in Figure D.14, showed several irreversible processes occurred above 100°C, under slow heating conditions (5 °C/min). These processes were not studied in any detail, but it is believed that both evaporative loss from the DSC pan and reaction processes were involved.

The sharp endothermic peak at just above 110°C occurs at the temperature of the dramatic decrease in vapor pressure. The peak was seen to be irreversible and is therefore distinct from reversible plastic phase transition in levoglucosan. It is very sharp, just like the levoglucosan phase change. Why one peak would be reversible and the other irreversible is not presently understood. It may, however have to do with a reaction that accompanies the phase change. If not heated above 100°C, a tar sample showed no shift in its vapor pressure-temperature curve, over the course of an entire day's measurements, involving a loss of almost 50 wt% of the tar. The narrowness of the molecular weight distribution for the fresh tar appeared to be supported by the constancy of its vapor pressure in these experiments. The correlation derived from the data in Figure D.13 for the fresh cellulose tars is of the form:

$$\ln P\,[\text{torr}] = A - B / T\,[\text{K}] \qquad \{D.1\}$$

where A= 40.289 and B=16948 for fresh cellulose tars.

A downward shift of vapor pressure might be expected as a result of driving off lighter components. The residue from an experiment in which about 44% of the mass of sample had been driven off (at temperatures up to 155°C, over several days) was remeasured for

molecular weight, and yielded a value of 270 daltons. Such a shift could indeed indicate evaporation of lower molecular weight fragments, but it is unreasonably large. The number average molecular weight of the components that would have had to be driven off is approximately 115 daltons, which is somewhat low, given how the samples were prepared in the drying step. Thus we believe that the shift is instead related to formation of higher molecular weight condensation products. It has been observed that reheated cellulose tars become much more difficult to solubilize, suggesting formation of higher molecular weight species. Some of the tar was insoluble in both methanol and in methanol/THF mixture. Also, it should be recalled that Figure D.12 showed that a non-volatile residue was formed from the tars upon heating. Analysis of the "aged" tar by GPC is shown in Figure D.10 using the ultraviolet detector and in Figure D.11 using the refractive index detector. Figure D.10 indicates formation of some large molecules with aromatic nature and molecular weight of several thousand daltons eluting at the elution limit of the GPC column. The data of Figure D.11 show that part of the non-UV active materials also shift upward in molecular weight. The fact that not all material shifts is important, in that this means that there is still a significant fraction of low molecular weight material even after "aging". The order of magnitude drop in vapor pressure that accompanies "aging" requires that even though much of the material remains low molecular weight, that its properties change drastically. This can be easily explained if there were, for example, one extra OH group created per residue upon "aging".

The effusion data for the “aged” tars are seen to be more scattered, in part because the shifting of molecular weight during the experiment occurs more rapidly at the higher temperatures. The slope of the aged tar curve is however generally consistent with that from the fresh tar, even if vapor pressures are lower. Assuming formation of high molecular weight, non-volatile materials in the sample, and ideal solution behavior, Raoult’s Law would predict the observed result provided that the concentration of the volatile species were to decrease by an order of magnitude. As noted above, it is not clear

from Figure D.11 that this is realistic. Thus it remains unestablished whether the shift of the vapor pressure curve is attributable to reacting away most of the higher vapor pressure material, or whether the shift is more attributable to reacting away some fraction, and merely reducing its concentration. We favor the former explanation by inference, from the data of Figure D.11 as well as the implausibly of a reproducible 90% extent of reaction irrespective of heating history. It may be noted that levoglucosan itself showed no thermal instability up to 230°C. Cellulose tar contains a much broader range of materials, so it is unclear which components, if not levoglucosan, itself contribute to its thermal instability. It is also known that introduction of additives produce discernible modifications of the levoglucosan thermogram [Shafizadeh and Lai, 1971], so reaction of levoglucosan itself cannot be ruled out.

An important feature of Figures D.12 and D.13 is that the vapor pressures of the cellulose tars are quite low (fractions of a torr, at the temperatures studied). The tar would be quite non-volatile at 150°C (P=1.2 torr), but would have a vapor pressure of 86 torr at 200°C. This is consistent with the results shown in Figure D.12. Using the correlation derived from the data of Figure D.13, the cellulose tar is predicted to boil at around 504 K (=231 °C). We have not taken account the temperature dependence of ΔH_{vap}, so the actual boiling point could be a bit higher. This is in fair agreement with the limited observations of Figure D.12, which qualitatively indicated boiling at near 260°C. It is difficult to verify this boiling point by DSC, because the tar appears to decompose at a lower temperature.

Using the Clausius-Clapeyron equation, $d [\ln P]/ d[1/T] = -\Delta H_{vap}/R$, the enthalpy of vaporization of the levoglucosan was 120 kJ/mol. The enthalpy of vaporization of the fresh cellulose tar was 141 kJ/mol in the two experiments with fresh tar shown in Figure D.13. In both experiments, there was a tendency for ΔH_{vap} to decrease with time if the tar was heated to only around 100°C (because of chemical changes in the tar).

The value of 141 kJ/mol can be compared with the curve in Figure D.2, by assuming an activated zero- or first-order mass loss process in which the rate of transport is proportional

to the vapor pressure, and thus, in which it is assumed that $E=\Delta H_{vap}$. The rate of mass loss may be therefore represented by:

$$d(m/m_0)/dt = - (k_0/m_0) \bullet \exp(-E/RT) (m)_n \qquad \{D.2\}$$

where m is the mass, m_0 is the ultimate mass loss, t is time, and n the order. The value of k_0 is $3 \bullet 10^{13}$ min^{-1} for n=1, and $k_0/m_0 = 2 \bullet 10^{13}$ min^{-1} for n=0. For a transport process, the zero-order form should be more realistic. It is seen that a reasonable, though not outstanding, approximation to the curve is obtained with either model. If one were to take into account a decrease in the value of ΔH_{vap} due to tar "aging" reactions, a better fit could be obtained. It may be noted that the value of k_0 obtained here is higher than that observed for actual cellulose pyrolysis (for which $k_0=4.07 \bullet 10^{11}$ min^{-1}, [Milosavljevic and Suuberg 1995]), but this is to be expected, since the physical situations are quite different in the two experiments.

The value of heat of vaporization for the cellulose tar gives some explanation for the reported kinetics of the cellulose pyrolysis processes, and this is discussed in the following section.

C.3.4. Heat of Vaporization - Contribution to the Heat of Pyrolysis.

It is quite plausible that the measured "heat of pyrolysis" of cellulose is actually a composite of several different contributions. The role of exothermic char formation is counterbalanced by an endothermic heat of volatile release [Milosavljevic and Suuberg, 1995]. In this latter case there may be enthalpy effects associated with actual decomposition reactions, and there is also a latent heat of evaporation of many primary decomposition products (especially tars and oils). Milosavljevic et al. [1996] suggest that the yield of char is the main factor determining whether the overall pyrolysis process is endo- or exothermic. Also an experimental estimate of the enthalpy of volatiles release is available from this work. The extrapolation of the results to zero char yield provides an estimate of the

enthalpy of pyrolysis, where there is no char formation at all. This yields an estimate of about 538 J/g volatiles. Thus it would be expected that if char formation could be experimentally suppressed, the actual heat of pyrolysis would be close to the extrapolated value of 538 J/g. Comparing this value with the tar's enthalpy of vaporization of 735 J/g shows that the major enthalpy sink during pyrolysis involves the enthalpy of vaporization of the tars. This is explored in detail in Appendix C.

D.3.5. Cellulose Tar Evolution - Controlled Kinetics.

The global decomposition kinetics of cellulose appear to be heating rate dependent. At heating rates below about 10°C/min, the pseudo-first order activation energy for pyrolytic mass loss is 218 kJ/mol. At higher heating rates, there appears to be a cluster of data in the literature implying an activation energy of around 140 kJ/mol [Milosavljevic and Suuberg, 1994]. The similarity of the enthalpy of vaporization for the fresh cellulose tar (141 kJ/mol) and the activation energy for the global mass loss kinetics in the high temperature regime (140 kJ/mol) is intriguing, particularly in light of the evidence that mass transport limitations may be playing a role within quite small particles and external to the samples. The tar evolution rate could be proportional to its vapor pressure if the tar escapes by either diffusional processes or convective flow. The latent heat of vaporization of the tars (approximately 141 kJ/mol) is suggested to be the origin of the temperature dependence of mass loss kinetics at high heating rates. This is explored in detail in Appendix D.

D.4. Conclusions.

The vapor pressures of the fresh cellulose tars have been measured, and reveal a material of limited volatility. The volatility of the tar is similar to that of a widely accepted major component of the tar, levoglucosan. The cellulose tar exhibits the same magnitude of vapor pressure as levoglucosan. The molecular weight of levoglucosan is 162 daltons, which is near the average molecular weight of the actual fresh cellulose tar samples, which ranged from 170 to 178 daltons. Also the heat of vaporization of real cellulose tars is close that obtained for levoglucosan, 126 kJ/mol for levoglucosan and 141 kJ/mol for tar. It is seen that the levoglucosan could be a reasonable model for the fresh tars, because the thermophysical properties of tar are unknown.

The results prove that the approach used here give satisfactory results working with simple system such as cellulose tar. The importance of thermal alteration of tars, and the difficulties that this can cause, has also been explored. In the next chapter the work is extended to coal tar.

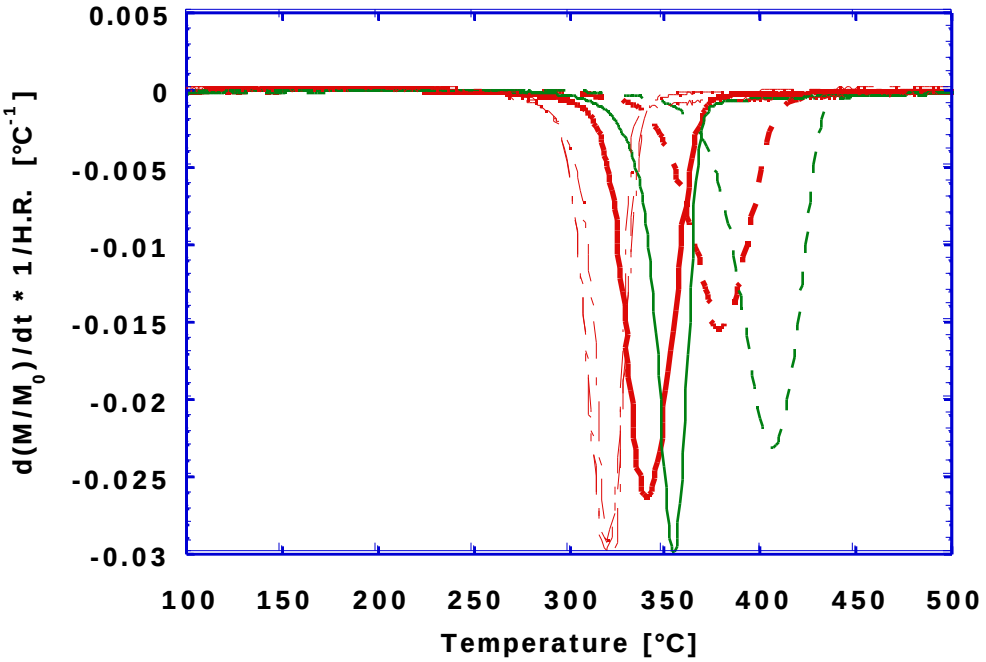

Figure D.1. Mass loss rates during cellulose powder pyrolysis at different heating rates in the TGA. The notation H.R. refers to heating rate, in °C/min. Heavy curves-open TGA pans; thin curves-DSC pans (with mass transport limitations). Dashed curves-60°C/min; solid curves-6°C/min; dashed/dotted curves-1°C/min.

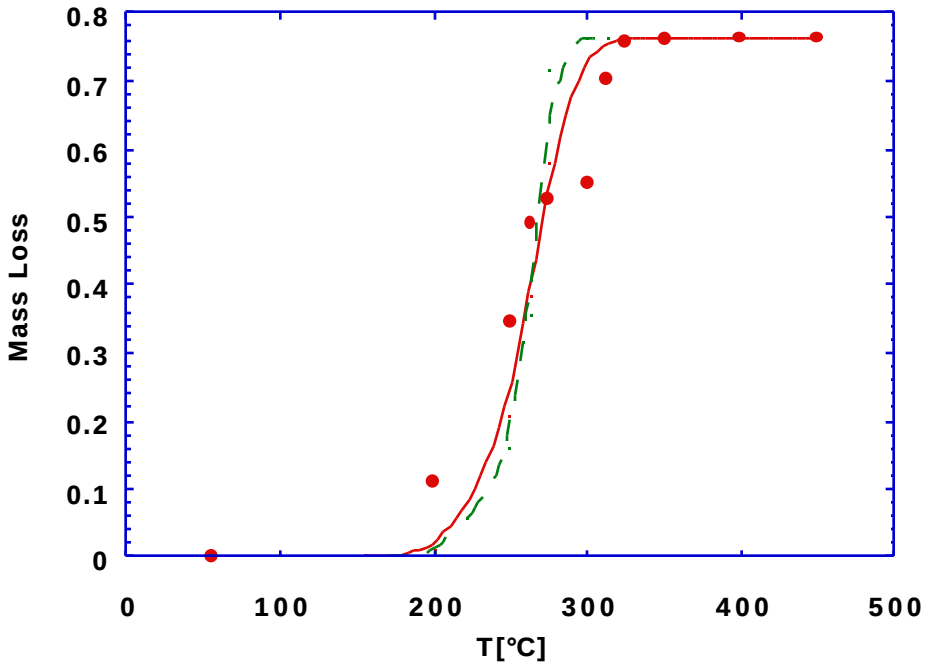

Figure D.2. Mass loss from reheating cellulose tar at 60°C/min, in the heated wire mesh reactor. Dashed curve - zero order mass loss model; Solid curve - first order mass loss model (see text).

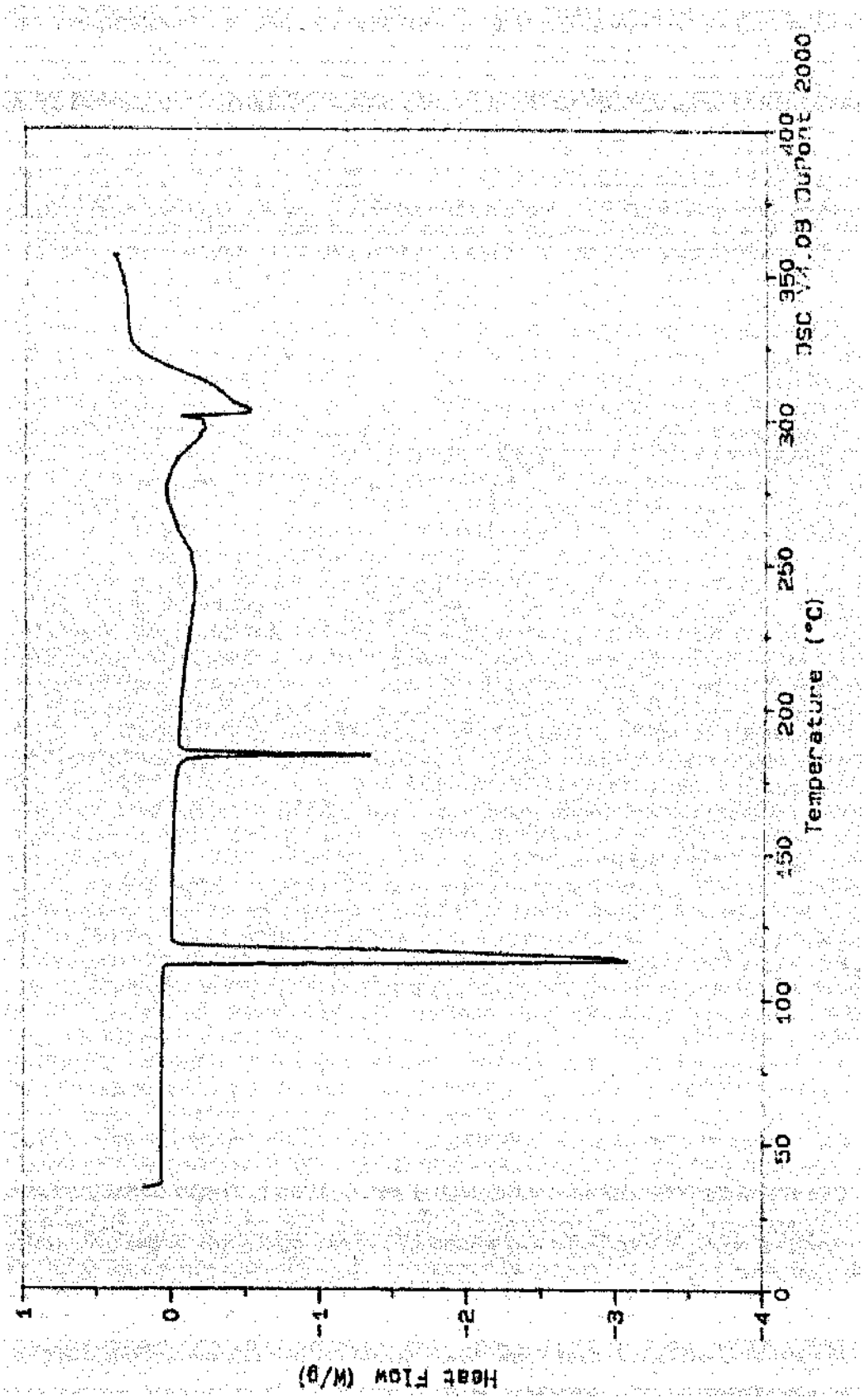

Figure D.3. DSC applied to levoglucosan. Heating rate 5 K/min. .

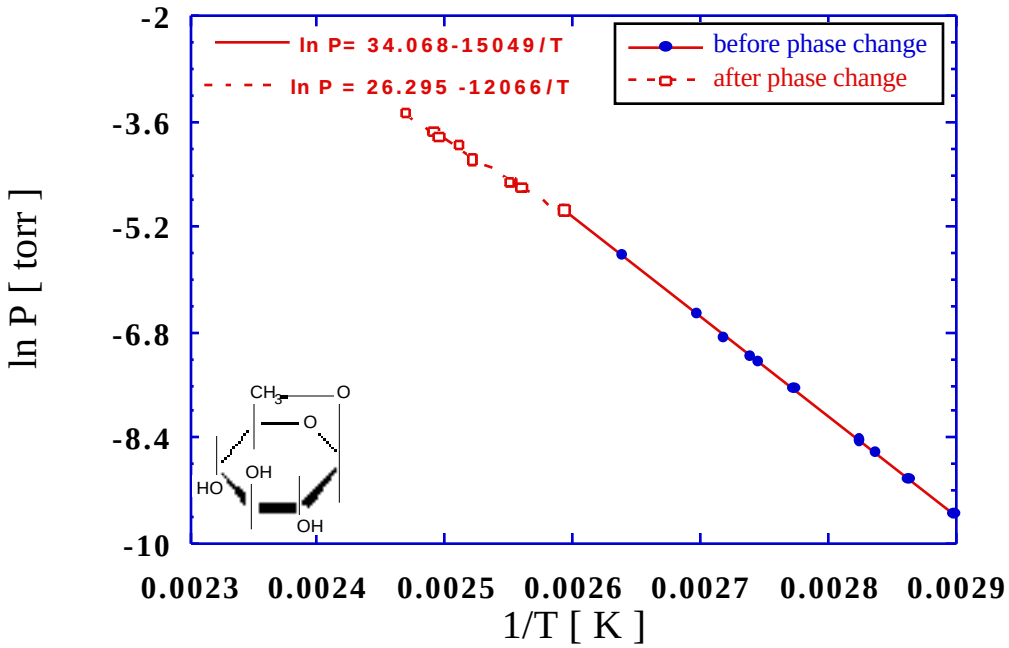

Figure D.4. Effusion method applied to levoglucosan.
Solid points - before phase transition; open points - after phase transition.

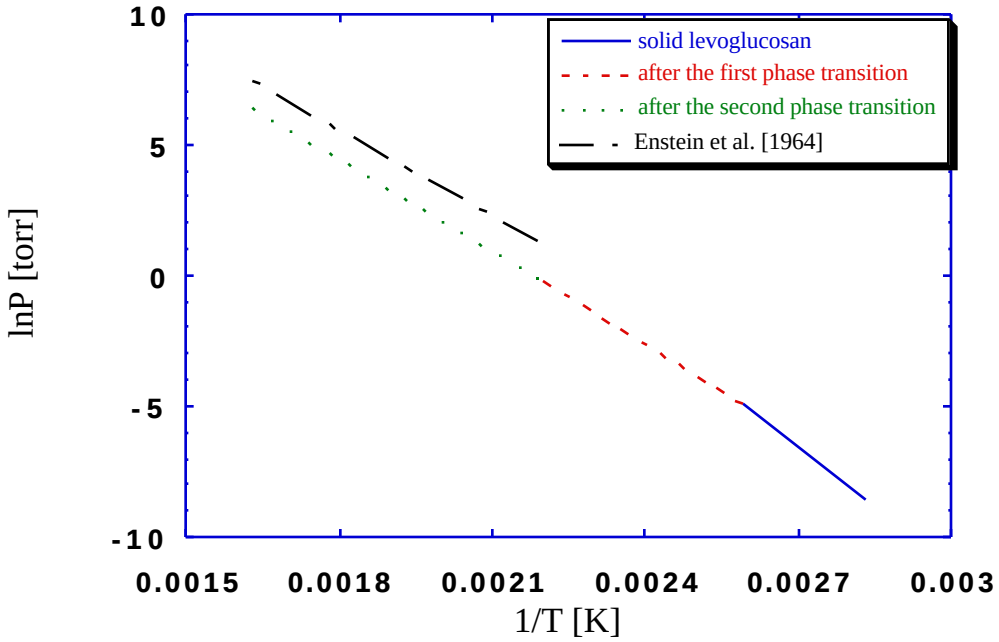

Figure D.5. The extrapolation of levoglucosan data up to the boiling point at 760 torr. Other reported experimental results for liquid levoglucosan [Enstein et al., 1964] are shown for comparison.

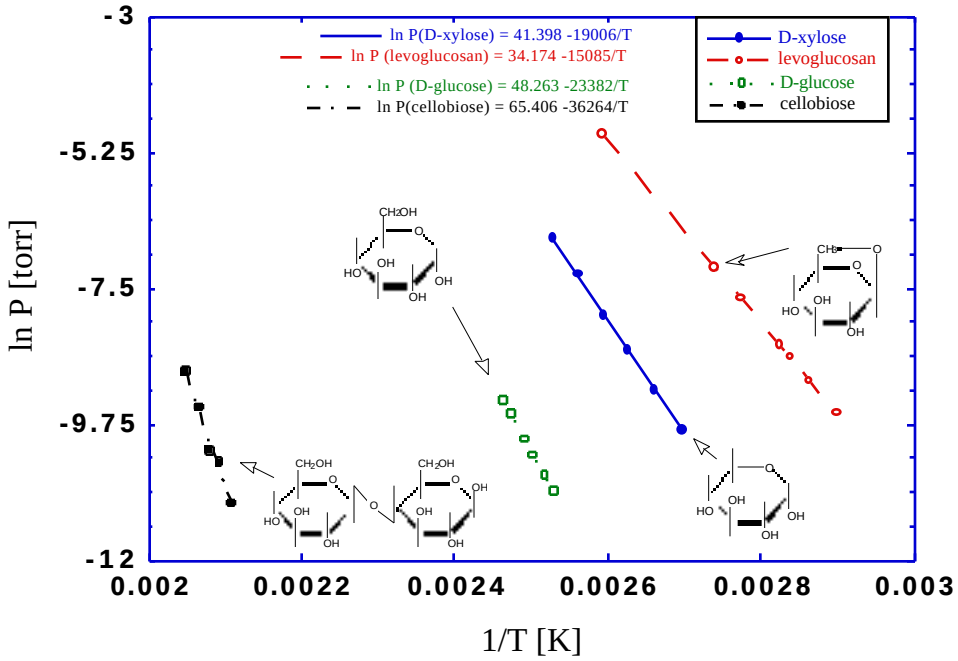

Figure D.6. Effusion method applied to solid D-xylose, levoglucosan, D-glucose and cellobiose.

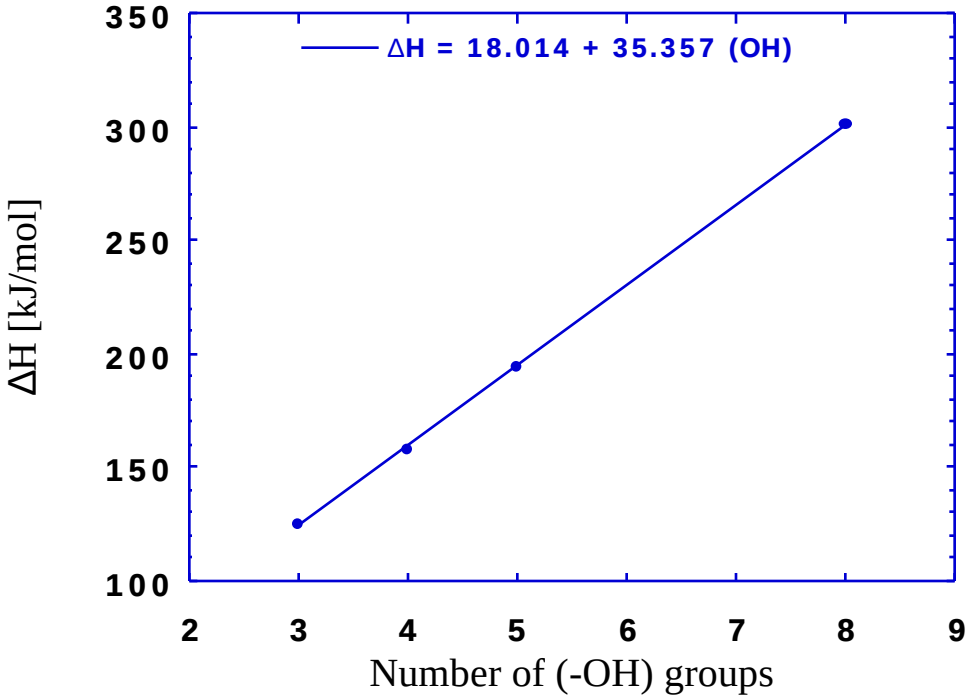

Figure D.6a. Variation of sublimation enthalpy with hydroxyl group content.

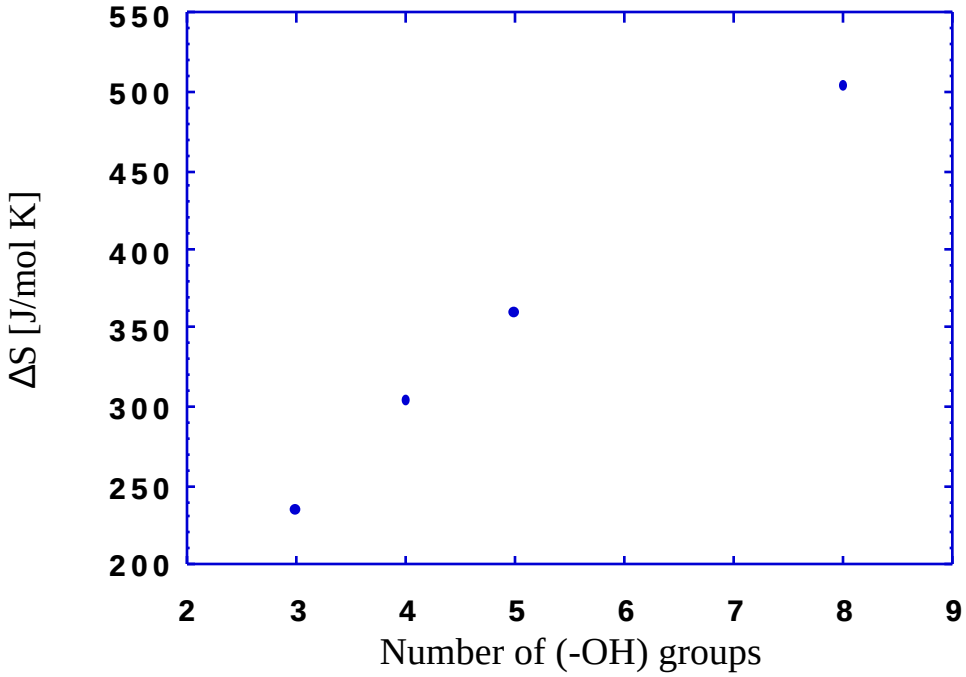

Figure D.6b. Variation of sublimation entropy with hydroxyl group content.

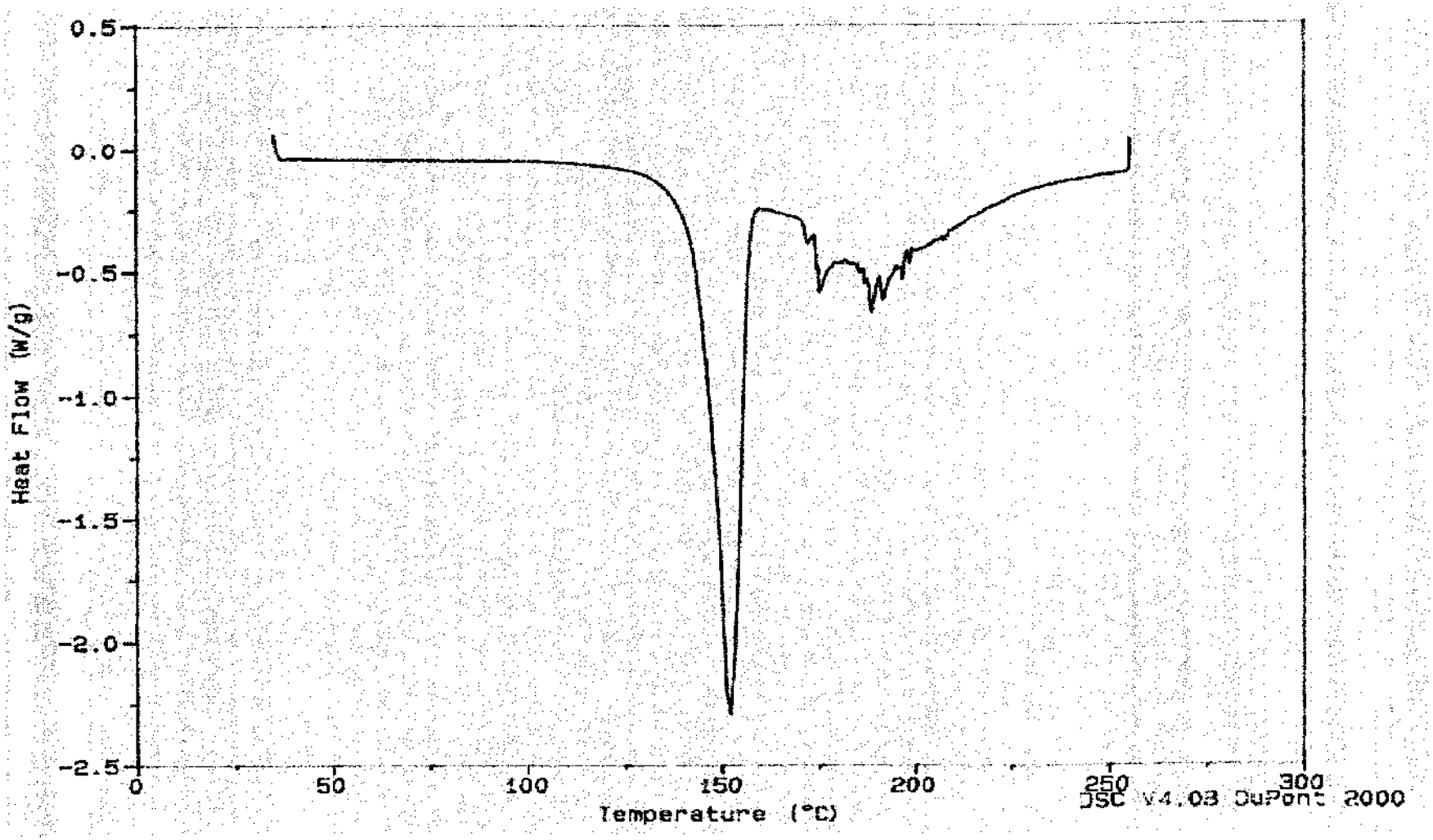

Figure D.7. DSC applied to D-xylose. Heating rate 5 K/min.

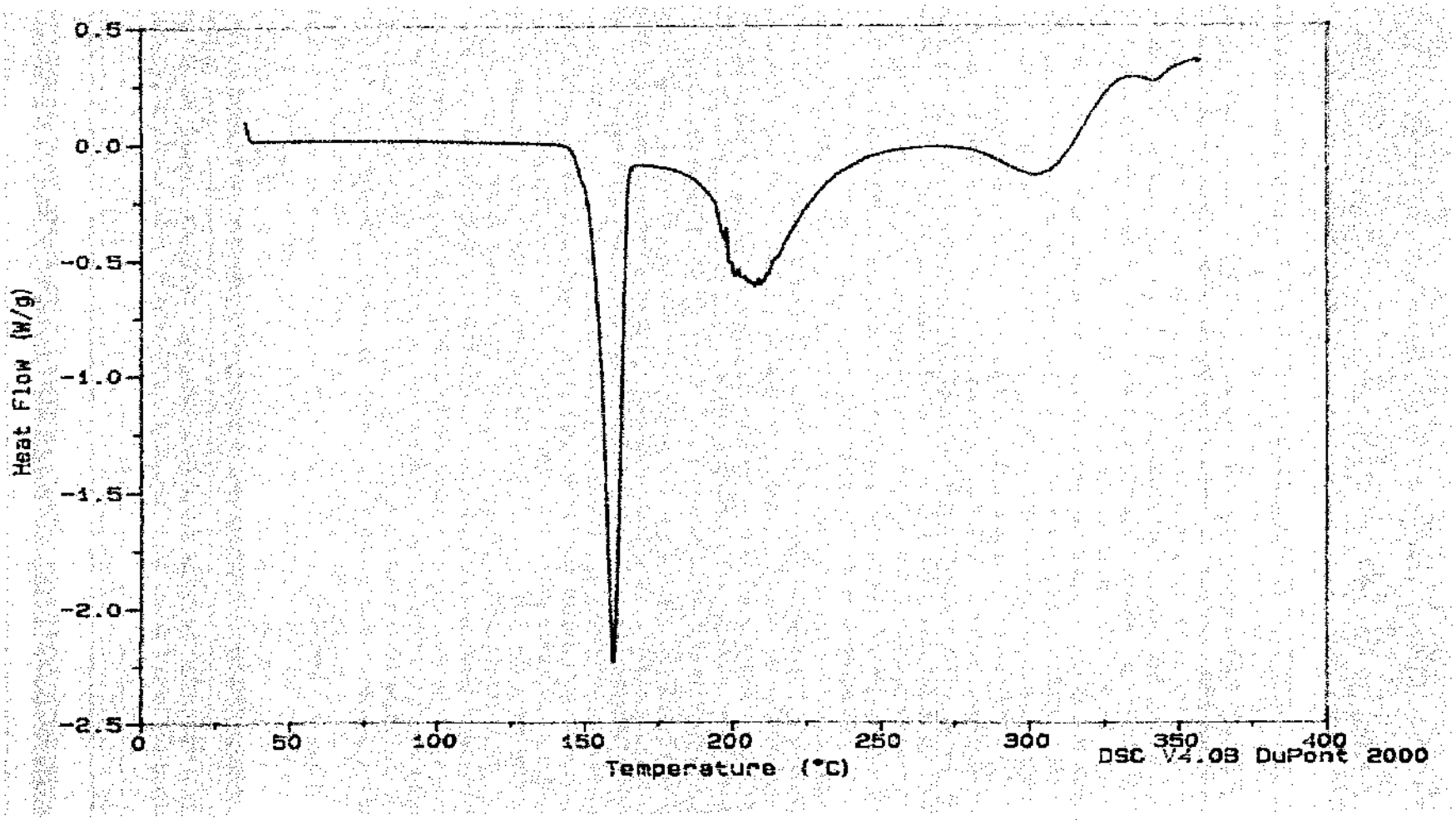

Figure D.8. DSC applied to D-(+)-Glucose. Heating rate 5 K/min.

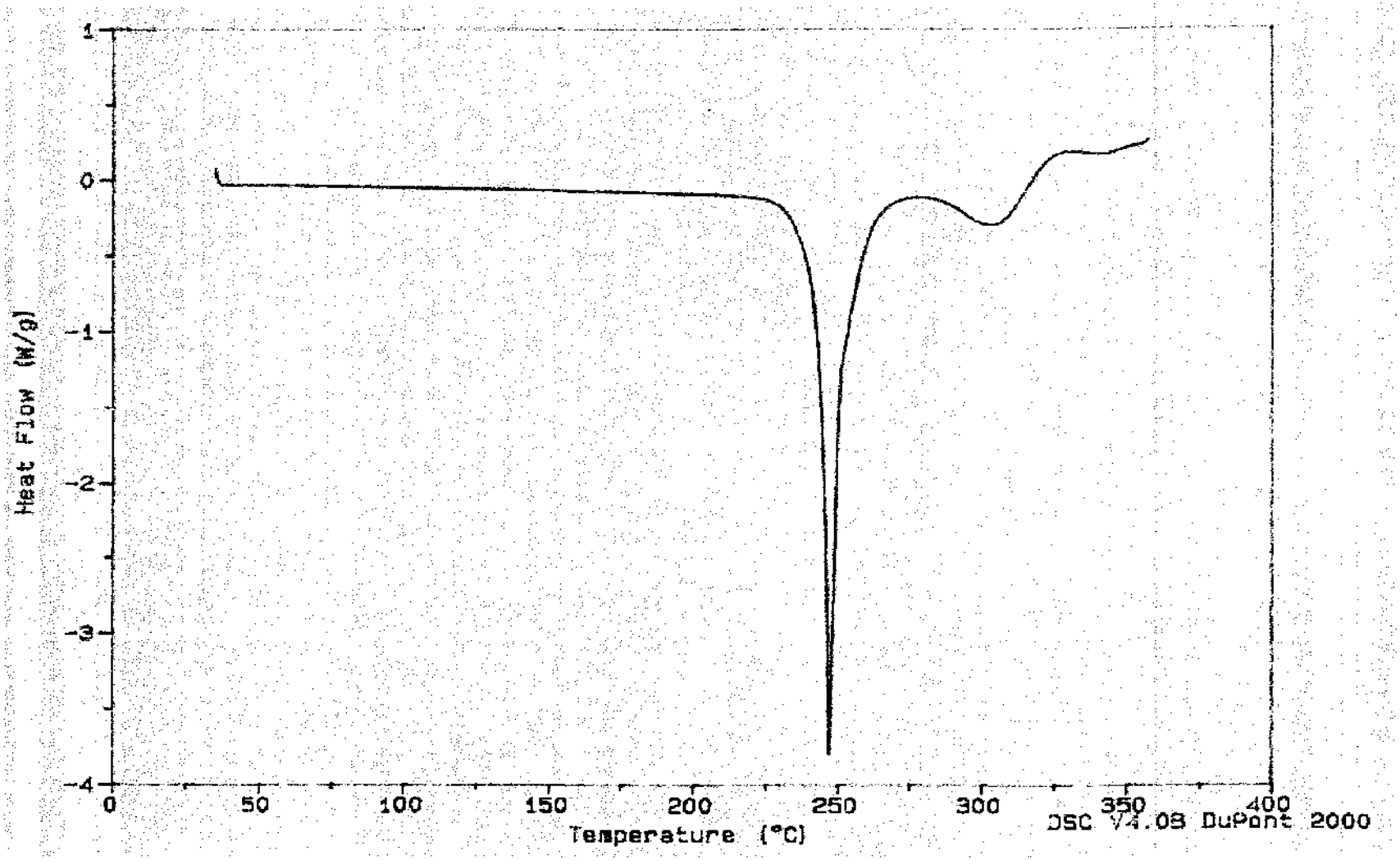

Figure D.9. DSC applied to cellobiose. Heating rate 5 K/min.

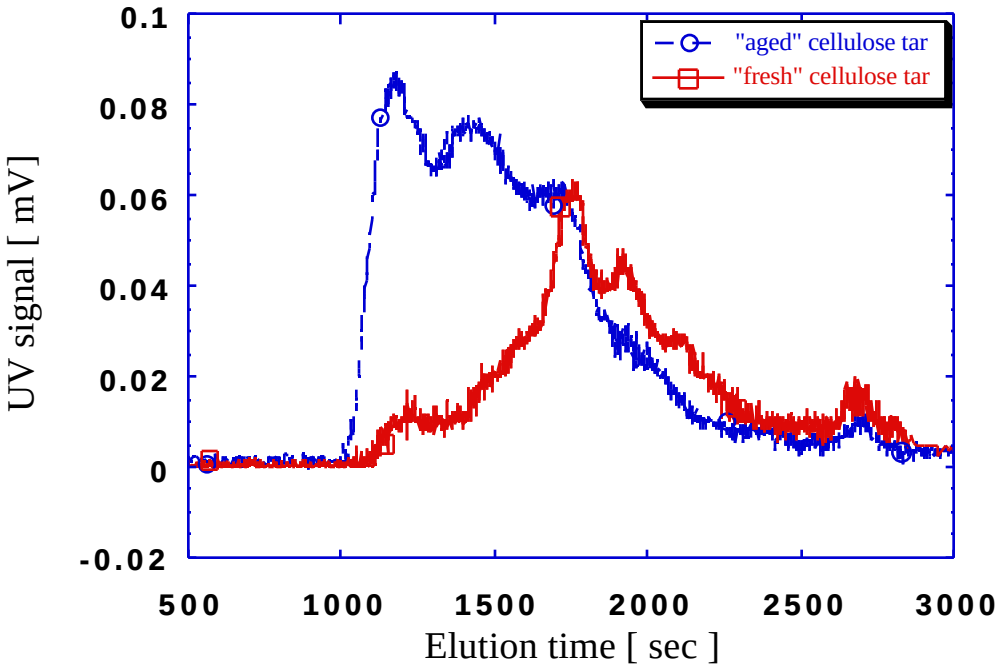

Figure D.10. GPC chromatograms (UV spectra at 305 nm) for cellulose tars. 30 mg of cellulose tar in 1 ml of pyridine have been used in each case.

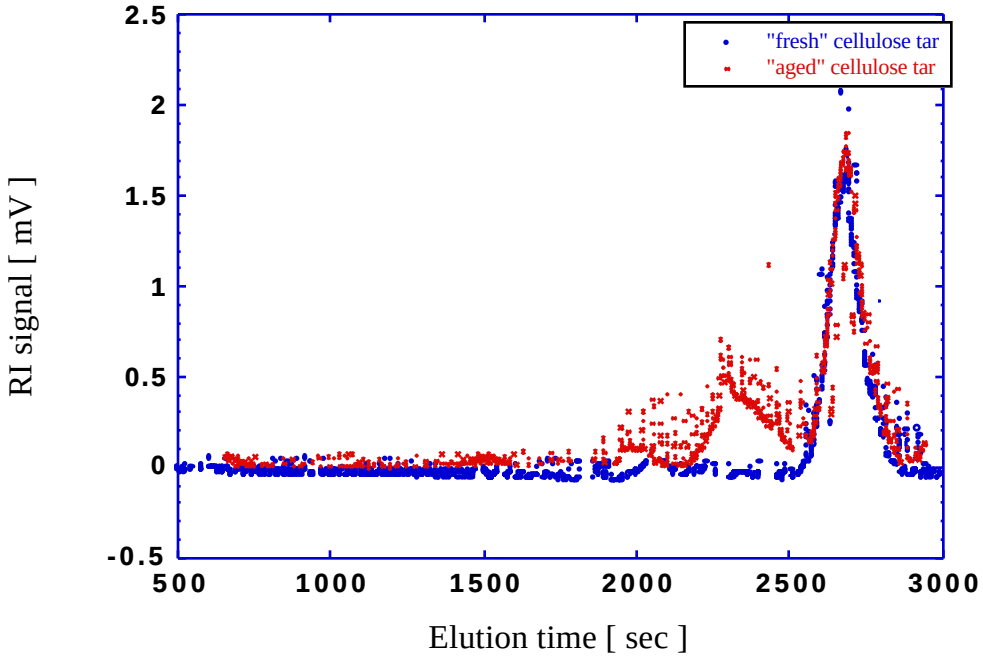

Figure D.11. GPC chromatograms (refractive index detector) for cellulose tars. 30 mg of cellulose tar in 1 ml of pyridine have been used in each case.

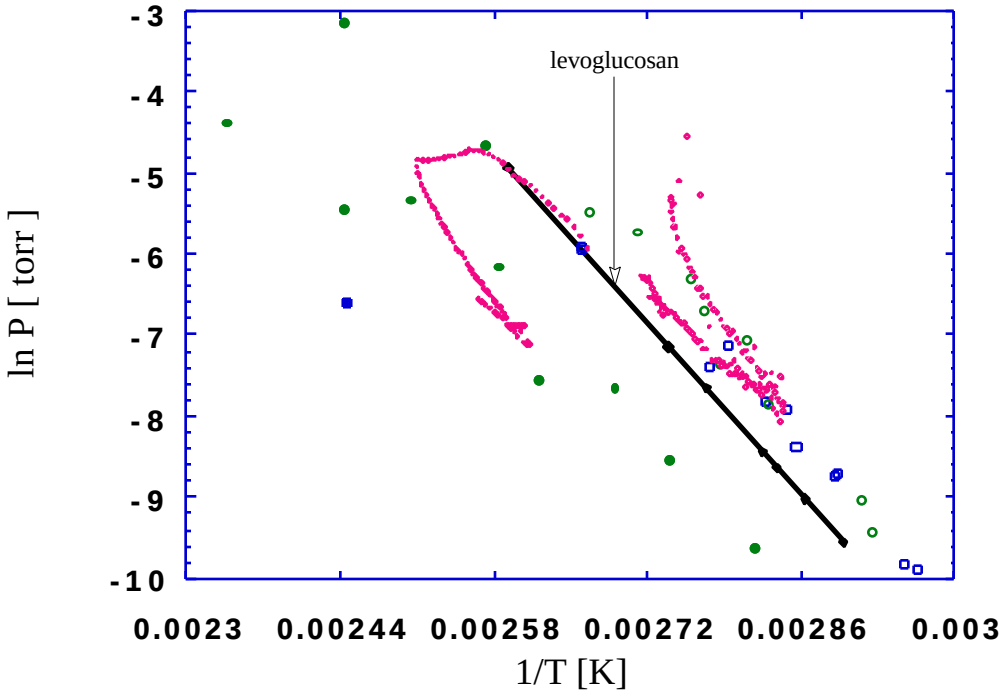

Figure D.12. Effusion data for cellulose tars and levoglucosan.
The isothermal effusion method was used for tars 1 (squares) and 2 (circles).
The non-isothermal method was used for tar 3 (small data points).
Open points for "fresh" tars, solid points for "aged" tars, which have been exposed to temperatures above 100°C.

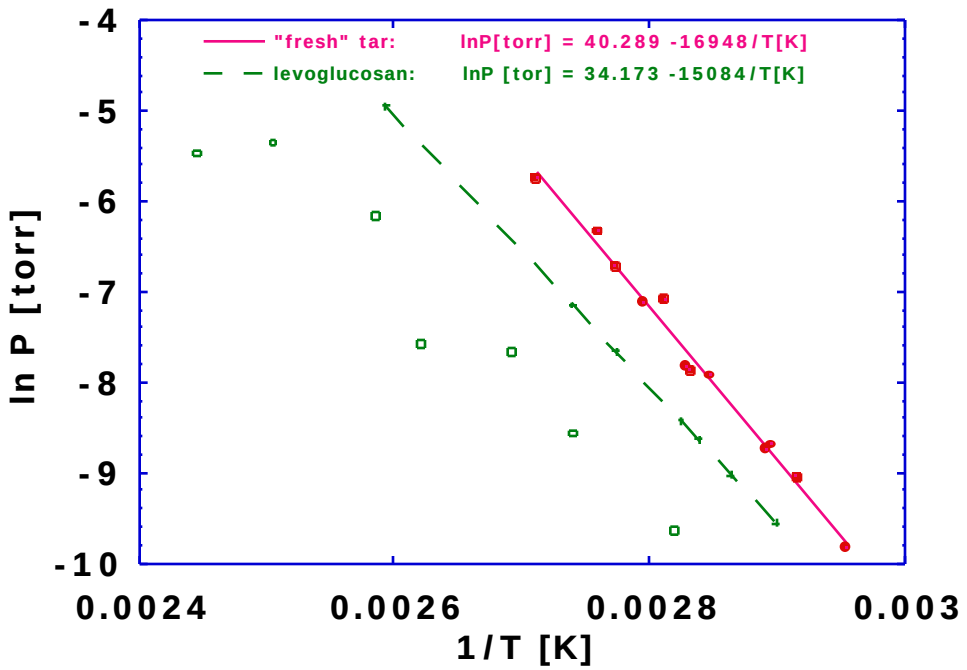

Figure D.13. Vapor pressure of "fresh" cellulose tar and levoglucosan as a function of temperature. Solid points-fresh cellulose tar; open points-cellulose after exposure to 155°C; crosses-levoglucosan.

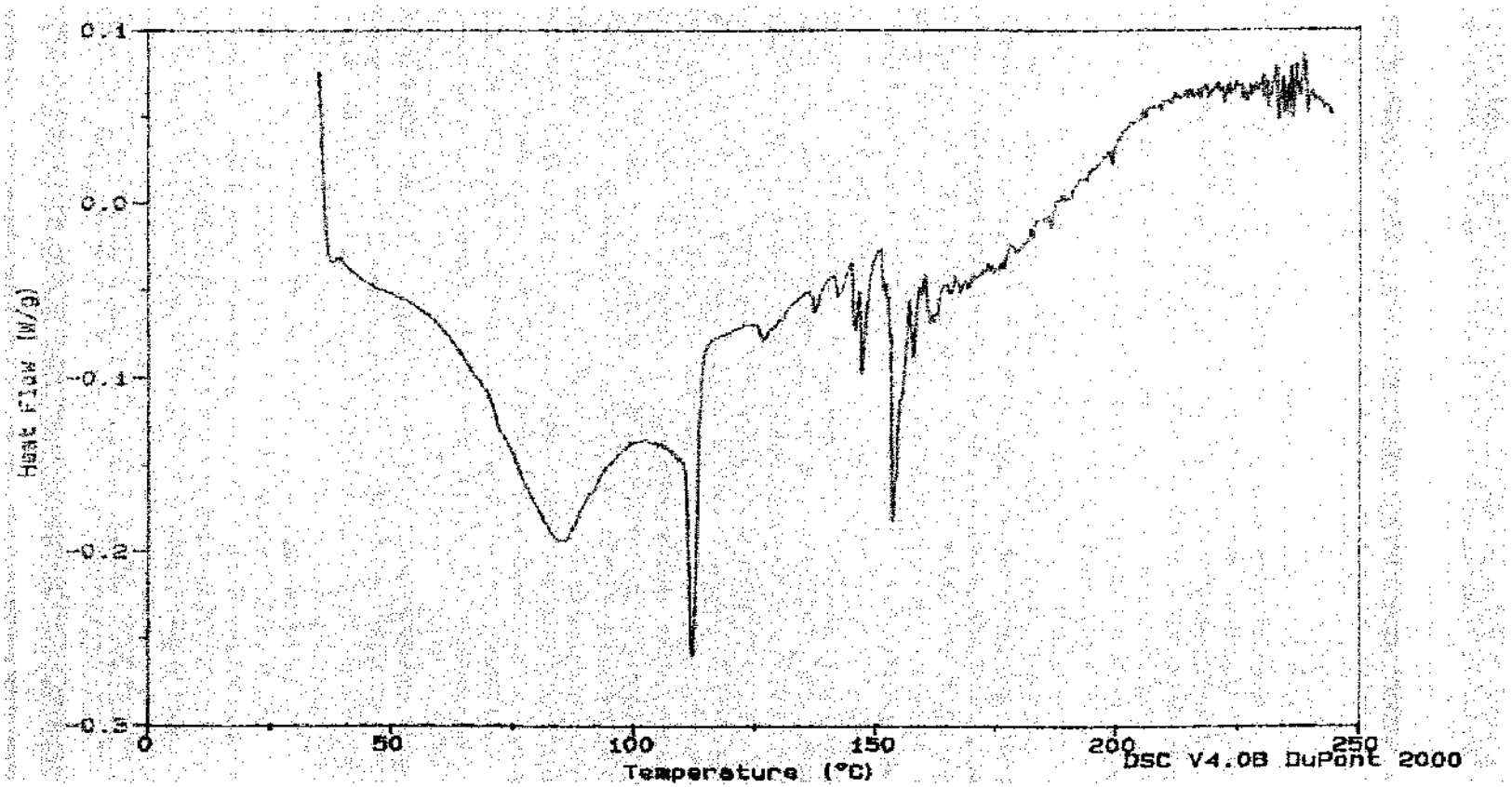

Figure D.14. DSC applied to "fresh" cellulose tar. Heating rate 5 K/min.

Chapter E. Coal Tar - Experimental Results and Discussion.

Tars were prepared from various coal samples. Four coals from the Argonne Premium Coal Set [Vorres, 1990] - the Illinois No. 6, the Pittsburgh No. 8, the Pennsylvania Upper-Freeport and the Wyodak - were selected for this study because of their specific chemical and physical properties. They were used as received. These coals have been well characterized with respect to bulk chemical and physical properties, and were mined, stored, and processed in an inert atmosphere to prevent oxidation and/or chemical alteration of the original coal samples. The samples studied were fairly fine powders of <100 mesh size. Detailed petrographic, chemical, and physical analysis data on the coals can be found elsewhere [Vorres, 1990]. The reported elemental compositions are given in Table E.1 together with that of another Pittsburgh No.8 sample, the so-called Bruceton standard coal [Suuberg et al., 1985], which was examined here in preliminary work.

Table E.1. Ultimate analyses dry (wt %) of coals studied.

Seam	Rank	C	H	O	N	S	Ash
Upper-Freeport	Low. Vol. Bit.	74.4	4.1	6.5*	1.3	0.7	13
Illinois No. 6	High Vol. Bit.	66	4.2	11.5*	1.2	2.1	15
Pittsburgh No. 8	High Vol. Bit.	75.7	4.9	8*	1.5	0.8	9
Wyodak	Subbituminous	68.3	4.9	16.4*	1	0.4	9
Bruceton	High Vol. Bit.	80.4	5.3	6.7	1.6	1.0	4.6

*by difference.

The actual pyrolysis methods used to produce the tars were described in section B.2.2. Attention is turned here to characterization of the tars.

E.1. Characterization of Coal Tars by GPC in the "Analytical Mode".

Since the rate of escape of tar from pyrolyzing coal particles depends upon the vapor pressure of the tar, and this property is assumed to depend upon the molecular weight of the tar, efforts were made to measure of tar molecular weight distributions. There is no single absolute method available for measuring molecular weight distributions of coal tars. The classical gel permeation chromatography (GPC) technique is one which has been widely applied for this purpose.

The initial strategy was one of relating measured elution times of coal tars from the analytical GPC column to their molecular weights. This strategy has often been followed in other studies, in this laboratory and elsewhere [Unger and Suuberg, 1984; Oh et al., 1986]. The separation of asphaltenes, bituminous resins, coal liquids and coal tars by size exclusive chromatography using poly(divinylbenzene) or Styragel columns and solvents such as THF, toluene and CH_2Cl_2 has been reported by several investigators [Unger and Suuberg, 1984; Philip and Anthony, 1982; Strachan and Johns, 1985; Evans et al., 1985; Bartle et al., 1986; Lafleur and Wornat, 1988; Lafleur et al., 1993]. The initial strategy proved difficult to implement for the intended purpose, however.

A major problem was encountered in calibration of the GPC for coal tars. Several factors preclude the direct determination of molecular mass distributions of coal tars by GPC. The first problem is encountered in obtaining suitable calibration standards. Pure, suitable model compounds are available in a limited molecular weight range and are also limited structurally and functionally. This has earlier been addressed by use of fractionated tars themselves. A more difficult problem in calibration is caused by the non size-exclusion behavior of heterogeneous mixtures of moderate molecular weight compounds. The separation is much more complex than that based upon the molecular size, as it is in

the case of single polymers. Besides molecular size, chemical characteristics such as polarity can play an important role in separation. It has, for example, been observed that neutral molecules elute much later than compounds which are known to form H-bonded complexes with THF or pyridine, and appear to exhibit greater than expected linear molecular size. Philip and Anthony [1982] observed that when THF is used as the mobile liquid phase, certain molecules can form hydrogen bonds with the THF, thus lowering their retention times, but when non-polar solvents such as toluene were used, the retention times were more like those expected. Even in the case of aromatic hydrocarbons, the separation depends upon more than molecular weight and there is difficulty in predicting elution behavior. The pericondensed PAH show a reversal of the classical GPC separation process and exhibit different behavior from the catacondensed PAH [Strachan and Johns, 1985; Lafleur et al., 1993; Evans et al., 1985]. This is attributable to an adsorption effect. For this reason, it is not feasible to calibrate a GPC column with coal tar model compounds.

In fact, a separation according to functionality allows lumping of similar components into distinct groups and can be used for characterizing complex mixtures [Philip and Anthony, 1982; Lafleur et al., 1993]. For example as shown in Figure E.1, Philip and Anthony [1982] separated coal liquids using 100Å μ-Styragel columns and THF as mobile phase into four fractions containing heavy nonvolatiles (polymers and colloidal carbons), long chain alkanes and asphaltenes, phenols and aromatics. However, these fractions may still strongly overlap. Evans et al. [1985] showed that the greatest deviation from the molecular weight based calibration line constructed with PAH in THF is in the elution of phenols. Molecules with more than one hydroxyl group elute very early. They used this effect to separate coal tar into two fractions, which were examined by GC-MS, NMR spectroscopy, infrared spectroscopy and elemental analysis. The earliest eluting fraction (MW 285 by VPO in pyridine) contained high concentrations of phenols (by direct oxygen analyses, and from the strong peak at ~ 3300 cm-1 in the infrared spectra) and long chain

paraffins. Its oxygen content was 11.2 wt. %, nitrogen content 1.3 wt. %, sulfur 0.4 wt. % and the H/C ratio 1.03 by elemental analyses. Based on this characterization, it can be shown that an average molecule in this fraction would contain about 2 oxygen atoms, therefore possibly 2 hydroxyl groups. The later fraction (MW 220) was composed predominantly of polynuclear aromatics (N-heterocyclic, S-heterocyclic and O-heterocyclic compounds), aliphatic carbon was present as side chains on aromatic rings. The OH band was absent in the infrared spectrum of this fraction. Its oxygen content was 3.2 wt. %, nitrogen content 1.2 wt. %, sulfur 0.8 wt. % and H/C ratio 0.8.

Similar conclusions may be drawn from Figures E.2 and E.3, constructed using the experimental data on pure compounds obtained by Strachan and Johns [1985] and Rodgers et al. [1987]. The columns used were 1000Å, 500Å and 100Å μ-Styragel columns, with THF as the solvent. It is noted that our preparative GPC column should show similar separation behavior, because a 100Å and 500Å μ-Styragel packing with THF solvent was also used by us. It should be noted that the general order of elution is aliphatic, substituted aromatics, heteroatomic aromatics, and pure aromatics.

E.1.1. GPC Chromatogram Characterization.

In this study, the analytical GPC column had Phenogel packing and pyridine was used as the mobile phase. Figure E.4 shows some of the pure compound data obtained using this analytical GPC column . Molecular weights and elution times are shown in Table E.2.

Table E.2. GPC elution data for compounds used as standards.

Nr.	compound	formula	MW	retention time [sec]
1	phenanthrene	$C_{14}H_{10}$	178	2310
2	pyrene	$C_{16}H_{10}$	202	2368
3	perylene	$C_{20}H_{12}$	252	2320
4	coronene	$C_{24}H_{12}$	300	2408
5	decacyclene	$C_{36}H_{18}$	450	2160
6.	rubrene	$C_{42}H_{28}$	533	1936
7	2-butylbenzofuran	$C_{12}H_{14}O$	174	2224
8	2-methyl naphthalene	$C_{11}H_{10}$	142	2336
9	vitamin K_1	$C_{31}H_{46}O_2$	451	1864
10	quinoline	C_9H_7N	129	2304
11	phenanthridine	$C_{13}H_9N$	179	2250
12	benzodiphenylene sulfide	$C_{16}H_{12}S$	234	2288
13	benz[g]isoquinoline-5,10-dione	$C_{13}H_7NO_2$	209	2104
14	naphthol	$C_{10}H_7O$	144	2032
15	hydroxypyrene	$C_{16}H_{10}O$	218	2040
16	hydroxyphenalenone	$C_{13}H_8O_2$	196	2024
17	dihydroxynaphthalene	C10 H8 O2	160	1856
18	dihydroxynaphthadione	$C_{18}H_{10}O_4$	290	1920
19	myricetin (contains 6 OH groups)	$C_{15}H_{10}O_8$	318	1776
20	tetraphenyl cyclopentadione	$C_{29}H_{20}O$	384	1904

It is apparent that there is no unique correlation of molecular weight with retention time. In an ideal separation, it should be recalled that the compounds elute in reverse order of molecular weight, *i.e.*, higher molecular weight compounds should elute first. Note that in fact the pure aromatic hydrocarbons elute last and the pericondensed PAH show an elution behavior reversed from the expected separation process. The lower molecular weight hydroxyl group-containing aromatics (*e.g.*, 14) elute considerably earlier than the much higher molecular weight PAH. This may be attributable to both the polar interactions that the hydroxyls and pyridine could be involved in, as well as adsorption of the PAH.

This means that calibration of a GPC column must be performed with compounds of a similar chemical nature to those of interest. This, in turn, requires that the column be calibrated with narrow tar fractions of known molecular weight, because there are no other obvious choices of good model compounds. Unfortunately, even this strategy is deficient, due to the separation based upon chemical characteristics.

Figure E.5 shows the analytical GPC chromatograms for the first five fractions (in terms of elution from the preparative GPC column) derived from Bruceton bituminous coal tar. Figure E.6 shows the chromatograms of the last four fractions, as well as the whole coal tar. The earliest eluting fractions, presumably those containing high molecular weight components, are generally characterized as broad peaks with a well-defined maximum (see Figure B.4). The higher the fraction number, the more bimodal the peak becomes - this is particularly evident in Figure E.6. The whole tar is seen to comprise all of these different features.

Figure E.7 shows that it is possible to curve fit the whole tar with the fractions by calculating the total absorbance at any elution time using the following equation:

$$A_j = \sum_i x_i a_{ij} \qquad \{E.1\}$$

where A_j is the total absorbance at j elution time, x_i is the mass fraction of tar in fraction i in the whole tar and a_{ij} is absorbance of fraction i at j elution time. The values of x_i were determined by evaporation of the fractions collected from the preparative column and the values of the a_{ij} were obtained assuming a constant response factor for each fraction, and from that, calculating each contribution to the whole tar. The values of x_i for the different fractions are shown in Table E.3 together with the number average molecular weight of these fractions, as determined by VPO.

Table E.3. Relative amounts of different fractions from Bruceton coal tar.

fraction	0	1	2	3	4	5	6	7	8
MWi	820	520	395	320	310	275	250	275	290
mass %	1.2	8.1	16.6	23.6	22.9	15.4	7.5	2.8	1.9

From the values of x_i, the number average molecular weight of the whole tar ($\overline{MW}$) could be calculated from the measured molecular weights of the individual fractions, MW_i.

$$\overline{MW} = \sum_i y_i MW_i \qquad \{E.2\}$$

where y_i is the mole fraction of the tar in fraction i. Note that $y_i \neq x_i$, in general.

$$y_i = \frac{\left(\frac{x_i}{MW_i}\right)}{\sum_i \left(\frac{x_i}{MW_i}\right)} \qquad \{E.3\}$$

hence

$$\overline{MW} = \sum_i \frac{x_i}{\sum_i \left(\frac{x_i}{MW_i}\right)} \qquad \{E.4\}$$

The number average molecular weight of whole tar measured by VPO (MW 341) is similar to the value (MW 323) calculated from {E.4}, using measured fraction molecular weights. Thus the separation is seen to be reliable, as far as accounting for all material is concerned.

The separations in the two GPC systems (preparative and analytical) cannot be simply compared. Clearly materials with similar elution times in THF can sometimes have very different elution times in pyridine. This is particularly the case for the lower molecular weight materials (or at least those with the longest elution times). The results for the final three preparative scale fractions of Figure E.6 show very little shift in the analytical column elution times of either of the two peaks that comprise the fractions. In the case of these materials, there was obviously a significant difference in retention times when the tars were dissolved in THF. When they were redissolved in pyridine, however, these fractions behaved as though they were made up of differing proportions of the same two components, whose sizes and chemical nature were comparable in all of these fractions. Examined more closely, the peak positions of the later eluting peaks of these last three fractions do slightly shift towards longer elution times, with increasing fraction number. Considering the results of Figure E.4, it appears possible that the later eluting peaks in the last three fractions might contain mainly aromatic hydrocarbons of progressively lower molecular weight as fraction number increases, whereas the earlier eluting peaks contain more polar fractions. It is also clear from Table E.3 that these later fractions also contain most of the lower molecular weight material. Still, since as yet undefined polar interactions appear to play a major role in determining the elution times of some components of these fractions, there appears to be little hope of defining a reliable calibration curve based purely on molecular weight vs. elution volume in this range of molecular weight.

It is immediately apparent that since many of the elution curves for different preparative scale GPC fractions are composed of at least three peaks, no single calibration curve could be drawn to relate molecular weight to elution volume. It is noted, however, that there appear to be three general clusters of peaks - the first occurs at times less than 1820 seconds, the second between 1820 and 2050, and the third above 2050. For example, the third, fourth and fifth fractions of Figure E.5 both show two merged peaks, which are then more fully developed in later fractions (see Figure E.6). The whole coal tar GPC curve also clearly indicates all three of the peaks. Figures E.8 to E.11 show the GPC chromatograms for Pittsburgh No.8, Illinois No.6, Wyodak and Upper-Freeport coal tars and their fractions. All show multiple peaks.

The relative position of the first peak, occurring at time less than 1820 sec, suggests that it could contain long molecules. From our own work, we cannot say what these might be. Our results from Figure E.4 suggest that at least some of the peak may be attributable to poly-hydroxylated aromatics. Other compounds, not studied here, are more likely, however. The effect of long alkyl substitutents in minimizing retention times of PAH has been observed in several studies using THF as solvent [Strachan and Johns, 1985; Rodgers et al. 1987; Philip and Anthony 1982; Lafleur and Wornat, 1988]. It has been also noted by Calkins [1984] that the concentration of polymethylene (series of n-olefins-paraffin pairs from C_{14} to C_{26} and higher) in pyrolysis tars increases with decreasing rank from about 4% for high volatile bituminous coals compared to about 8% for lignites. The alkyl nature of the peak in questions is supported by fact that more than 50% of this fraction is volatile below 300°C, even though these fractions have number average molecular weight between 300 and 700 daltons. Our elemental analysis show that fractions of all tars with elution time below 1800 sec have a hydrogen/carbon (H/C) ratio above 1.2. For comparison, the polynuclear aromatic hydrocarbons have H/C ratio around 0.5 and long chain alkanes tend towards 2. Two of our choices for GPC calibration compounds giving the correct elution times, #17 and #19 in Figure E.4, cannot be correct

models, since their H/C ratios are 0.8 and 0.7, respectively. Thus with molecules more like #9, but with higher molecular weight, a more reasonable calibration could have been obtained.

The second peak occurs between 1820 and 2050 sec. Comparison with the pure compounds of Figure E.4 shows that these could be strong hydrogen bond forming compounds (e.g., containing hydroxyl groups) with number average molecular weights between 200 and 400 daltons, such as #17 or #18. As can be seen in Figure E.4, the hydroxyl groups shift retention times to shorter times (compare #14 naphthol with #17 dihydroxy-naphthol, or #15 hydroxypyrene to #2 pyrene). The elemental analyses of this peak still show a quite high H/C ratio between 1 and 1.2, and also high oxygen content. This suggests hydroxyl group containing aromatics with several alkyl side groups, in order to achieve the high H/C ratios.

The third peak occurs above 2050 sec. It is apparent from the fact that the molecular weight of the later fractions increases with retention time above 2200 seconds, there could actually be two superimposed peaks. The elemental analysis indicates increased nitrogen content and lowering H/C when peak size increased. VPO results show the number average molecular weight of this fraction between 200 and 300 daltons. Comparison with the pure compounds of Figure E.4 also shows that here is no simple unique interpretation of the general retention times with chemical characteristics. These late peaks will contain unsubstituted aromatics, and aromatics which contain not particularly polar heteroatoms (those not involved in strong hydrogen bonding), and alkyl aromatics with short sidechains.

In summary, it may be said that there can be no simple conclusions drawn based upon the GPC spectra. Separation occurs as a result of size and chemical functionality. Still, GPC with pyridine as the mobile phase permits multimode separation of the tars into three general fractions and therefore can be applied to the characterization of tars even if it does not allow characterization by molecular weight. It can be crudely hypothesized that the first

peak consists of large molecules with significant polymethylene substitutents, the second is enriched in hydroxyl groups, and the third contains PAH.

E.1.2. Absorbance

Another problem in use of GPC for quantitative analysis of the tars is encountered in the dependence of absorbance on UV detector wavelength. The pure aromatic compounds present absorb more strongly at progressively longer wavelengths with increasing molecular weight, as the detector wavelength is changed from 230 to 350 nm [Bartle et al., 1986]. This shift is significant in the case of pure compounds, but its importance in coal tars, which are extremely complex and may contain several thousands of compounds is unclear. Unger and Suuberg [1984] considered carefully the fact that different fractions of the Bruceton coal tar might have different absorption characteristics and concluded that there was linearity of the actual detector response with sample concentration over the entire elution range studied.

This can be also supported by Figure E.12, which shows data of Figure B.4, replotted by rescaling each peak to overlap near 1000 sec retention time. The maximum signal was obtained using the UV detector at a wavelength of 305 nm (UV cutoff was found to be slightly below 305 nm). Comparison of the normalized peaks at the six different wavelengths in Figure E.12 shows that the absorbance increases uniformly over the entire spectral range studied, up to 305 nm. This indicates that the *relative* amounts of UV light absorbing species are accurately reflected, irrespective of choice of wavelength. This is presumably because the main UV-absorbing species have polycyclic aromatic character, and that there is no dependence of this character on elution time. The variation in intensity with time reflects a variation in amount of the chromophoric species eluting with time. This can be explained by assuming that the polynuclear aromatics making up the tar are all of comparable ring cluster size. Substitutents have a small effect on the absorptivity of a

PAH chromophore and therefore the molar absorbance of most UV-absorbing species of similar cluster size is nearly the same at any wavelength [Lafleur et al., 1993]. Thus, it is unnecessary to concern oneself about the choice of the UV wavelength. The choice is guided by detector response, which was highest at 305 nm (see Figure B.4).

The average molar absorbance is different for each tar from each different coal. The following average molar absorbances were found for tars investigated:

Table E.4. Average molar absorbances of tars.

tar	absorbance before effusion [area/mmol]	absorbance after effusion [area/mmol]
Bruceton, HVB	$339 * 10^6$	$552 * 10^6$
Illinois No. 6, HVB	$308 * 10^6$	$767 * 10^6$
Pittsburgh No. 8, HVB	$377 * 10^6$	$1082 * 10^6$
Upper-Freeport, MVB	$487 * 10^6$	$746 * 10^6$
Wyodak, Subbituminous	$236 * 10^6$	$547 * 10^6$

Although a wavelength of 305 nm gave similar average molar absorbances for Bruceton, Illinois No.6 and Pittsburgh No.8 coal tars, it was notably higher for Upper-Freeport coal tar and lower for Wyodak coal tar. This could be explained in terms of the pyrolysis products of these tars having different basic aromatic cluster sizes. There is some evidence to support this from Solum et al.[1989]; aromatic cluster size in the parent coal increases only slightly with rank. But it is also likely that a greater mole fraction of the tars from the higher rank coals contain the highly UV-absorbing aromatic chromophores because higher rank tars are more aromatic. Purely aliphatic materials would not absorb at all. Moreover, observed increases in absorbance ranging from 35 to 65%, after effusional evaporation of the tars suggest an enrichment of the UV absorbing fraction in the residue. There can be evaporation of non-aromatic and smaller aromatic compounds, both of which can result in increased molar absorbance in the residue. Larger aromatic cluster compounds tend to be more absorbing on a molar bases [Bartle et al., 1986]. We favor an explanation which emphasizes a shift in remaining aromatic cluster size (due to differential evaporation), because as will be shown later, the shape of the GPC

spectrum shows only minor evidence of differential evaporation, based on functional character (see Figure E.22 and E.23). No one peak of the GPC is lost before all others.

E.2. Thermal Behavior and Stability of Tar.

E.2.1. DSC Results.

The thermal behavior of tar samples and their fractions was observed by DSC using two different heating rates. Figures E.13 and E.14 present results for Pittsburgh No. 8 tar with heating rates of 5°C/min and 0.5°C/min respectively. It is impossible to determine the latent heat of fusion from these DSC results. Our vacuum sublimation experiments show "melting" between 100 and 150°C for the tars and tar fractions examined. This can be explained by the fact that tar is complex mixture of many compounds with very different melting behaviors, and which are soluble in each other. There is no unique, pure component melting point.

"Melting" and sublimation behaviors have been also determined by Freihaut et al. [1993] for the following tars:

Table E.5. Sublimation behavior for some tars.

tar	Sublimation [°C]	initial softening [°C]	complete melting [°C]
Lignite , Lower Wilcox , TX	NA	68-70	76-78
Pittsburgh No. 8, HVA	91-95	110-115	140-150
Pocahontas No. 3, MVB	85-90	90-95	135-140

Additional key data here are those for sublimation, which suggest a rather volatile material. Moreover, the tars are in a softened state under temperature conditions such as we use for vapor pressure measurement.

Since the actual DSC spectra show little information about tar thermal behavior, other thermal experiments were performed. These experiments are discussed below.

E.2.2. Thermal Treatment of Tar and its Effect on Molecular Weight.

From the difference in the two DSC plots, it seems that there could be some slow physical and chemical changes that occur during long term heating below 300°C. To address this issue, experiments were performed in which glass capillaries were filled with coal tar under an inert gas environment, closed hermetically and heated at desired temperatures.

It should be noted that there was an increase in number average molecular weight of Illinois No.6 coal tar of about 20% by VPO (from 310 to 380 daltons) after heating Illinois tar about 2 hr at 200°C and there were also slight changes in the GPC spectra, as can be seen in Figure E.15. Figure E.15 suggests that there are changes in the second (OH rich) peak producing species eluting before 1700 sec. There is only a small increase in the average molar absorbance, by 5%, after heating, but this is well within the experimental error. This supports the hypothesis that the earlier cited change of between 35 and 65% in average molar absorbance during an effusion experiment is a result of preferential vaporization of the species smaller aromatic cluster size as opposed to formation of PAH by reaction.

Figures E.16 and E.17 present GPC spectra for similar experiments carried out for Wyodak and Upper-Freeport coal tars, respectively, using heating at 280°C two hours. These data suggest that copious amount of what is believed to be very high molecular weight compounds have formed during heating. The elution time suggests large polymer type molecules with molecular weights several thousands daltons eluting near the elution limit of the GPC column. The number average molecular weight change was from 350 to 620 for Wyodak coal tar and 320 to 440 for Upper-Freeport coal tar, confirming that the shift is at least in large part a true molecular weight shift.

It is well known that the primary tar changes in its properties during storage periods. Figures E.18 and E.19 show comparison of GPC chromatograms between fresh and old

Illinois and Pittsburgh tars respectively. The "old tar" is in this study defined as a tar, which has been kept five months in dark amber bottles under nitrogen at room temperature. There is an increase in the number average molecular weight of about 15% and also some slight changes in the GPC spectra.

There is a concern about condensation-type reactions in primary tars. The GPC elution time around 800 seconds strongly suggests the formation of materials of very large molecular mass up to 10,000 daltons, the nominal column exclusion limit. This is consistent with the results of Pindoria et al. [1997]. They showed that residue tars from a coal gasification plant showed significant mass spectra up to 20,000 to 30,000 daltons. Additionally, several percent of our tar became insoluble in THF or pyridine after reheating at 200°C for several hours.

The data of Figures E.15 to E.19 are significant from the point of view of tar thermal stability, and show that some changes in tar composition can occur even at very low temperatures. This supports the original premise that the tars had to be analyzed for vapor pressure at as low temperatures as possible.

E.3. Tar Volatility and Stability.

The majority of the collected pyrolysis tar presumably escaped the pyrolyzing coal particles by evaporation. Then the presumption is that reevaporation is also possible. Crude characterization of volatility has been made by revaporizing tars.

Freihaut et al. [1993] studied the tar volatility by revaporizing lignite and bituminous coal tars in the wire mesh reactor. Figure E.20 shows their results and displays the mass fraction of samples of primary lignite and bituminous coal tars that can be revaporized in the heated grid apparatus. All tar could not be revaporized. The fraction of tar vaporized reaches an asymptote of around 60 to 90% at 500°C, which is below the temperature range associated with active pyrolysis. The fraction of tar vaporized is higher for lignite (Lower Wilcox, TX) 90% and vacuum HVA bituminous coal tar (Pittsburgh No.8) 80%, and around 65% for HVA bituminous (Pittsburgh No. 8) and MVB bituminous (Pocahontas No. 3).

Such experimental results have important implications for our vapor pressure measurements, showing that in no case could all tar be re-evaporated. This is presumably mostly because of the thermal instability of tar, as was noted in the previous section of this report. Again, the importance of keeping experimental temperatures low is reinforced. There is the possibility, discussed by Suuberg et al. (1985) that physical entertainment contributes to tar production. This material may have been non-volatile to start. Thus it would be unrealistic to expect 100% volatility. The results of Figure E.20 confirm that most is evaporable, however.

E.3.1. Vacuum Sublimation Experiments.

The tar volatility issue was addressed here in vacuum sublimation experiments that involved tar separation based upon volatility. The preliminary vacuum sublimation experiments were performed using a standard vacuum sublimator. Two isothermal steps and a vacuum $5*10^{-2}$ torr were used to produce volatilized fractions, which were investigated by GPC and VPO. The original tar was generally dark brown and was like a paste or a very viscous liquid. The earlier and later GPC fractions were usually harder and the middle fractions more like a viscous liquid. The fractions prepared by sublimation were light brown. Each fraction evaporated at higher temperature was progressively darker, and the residue left after evaporation was almost black. Thus sublimation may favor loss of smaller, and thus less colored aromatic clusters, consistent with what was proposed above.

Results are shown in Figure E.21 for Bruceton coal tar. There are several features of the data of Figure E.21 that need consideration. All three main GPC peaks are apparent in the evaporated fractions. This shows that all of the different fractions, containing different functional groups, can be revaporized. This also shows that the vaporized fractions have character similar to the parent coal tar and indicates again that the separation is by structure in the GPC column. The shift in peak retention times to lower values and increase in average molar absorbance of higher temperature fractions suggests the tars evaporate in a "distillation-like" fashion with earlier fractions both lower in molecular weight and in aromatic cluster size or aromatic content. The average molar absorbances were $199*10^6$, $329*10^6$ and $991*10^6$ respectively for fractions vaporized at 140°C, 280°C and the residue left in the sublimator, respectively. The lower molecular weight portions of all three main peaks evaporate first. Their lower molar absorbances suggest either a lower content of aromatics, or a lower content of larger aromatic clusters. We cannot at present distinguish between these possibilities, though we believe it is the latter.

The second conclusion from Figure E.21 is that there is reaction producing a new, early peak. A simple mole balance in the form $N_{initial} = N_{left} + N_{evaporated}$ shows that the molecular weight of fraction that was left after heating at 280°C should be 486, instead of the measured 628 daltons, unless a reaction took place. Additionally in support of occurrence of a reaction was the fact that the fraction left in the sublimator was hardly soluble in THF.

All of these features are consistent with the results of the experiments of Figures E.15 to E.20 and show the occurrence of some slow reactions during long term heating, leading to formation of high molecular weight compounds. This will be analyzed in more detail below.

Based on the preliminary sublimation data and the thermal treatment experimental results, there developed a concern about condensation-type reactions influencing the results of the vapor pressure measurements, even at the modest temperatures of interest below 250°C. Indirect evidence of a problem did come from the decreasing solubility of the tar, and in the changes in the GPC spectra and number average molecular weight after heating to higher temperatures. Figure E.21 suggested the formation of non-volatile residue. Thus, if a non-volatile residue were to form during the vapor pressure measurement, then the volume fraction of volatile species would be decreased, and assuming that ideal solution behavior is maintained, the vapor pressure would decrease in proportion to the fraction of non-volatile residue (accounting, of course, for the loss of more volatile material by reaction).

E.3.1.1. Vacuum Sublimation/Knudsen Effusion Experiments.

The question of coal tar mixture behavior was pursued further, using the vacuum sublimation/Knudsen effusion device under vapor pressure measurement conditions.

Figure E.22 presents GPC spectra for Wyodak coal tar, its four evaporated fractions and the fraction left in the effusion cell following sublimation. Figure E.23 shows similar results for Upper-Freeport coal tar. Again the absorbance increases in going from the higher volatile fractions to the residue fraction. It was noted earlier that molecules with larger aromatic clusters have higher absorbance factors. Comparison of the H/C ratios of Wyodak coal tar sublimation fractions gives 1.15 at 150°C and 1.25 at 250°C. The increase in H/C ratio is needed to compensate for a higher molecular weight and large aromatic content in the higher temperature factions. It should be also noted that the GPC spectra of fractions obtained at the higher temperatures are more like the GPC spectra of whole tar. Unfortunately GPC with a constant wavelength UV detector cannot be used for quantitative evaluation of the changes resulting from condensation type reactions.

Equation {E.1} has been used to curve fit the whole tar GPC spectra from the absorbances of the evaporated and residue fractions at any elution time. Results are shown in Figures E.24 and E.25 for Wyodak and Upper-Freeport coal tars respectively. The notable feature from these plots is that the sum of the evaporated fractions (as well as the fractions themselves) have the characteristics of the parent tar, but the characteristics of the residue left after sublimation are different. The residue formed might well be less-volatile under the vapor pressure experimental conditions. Again, the changes in the second (OH rich) peak suggest the origin of the nonvolatile residue, in condensation type reactions. The fact that less shift occurs in the case of the Upper-Freeport coal tar is probably consistent with its lower hydroxyl content. Therefore, it would be concluded that most of the tar could have been evaporated if reactions would have not occurred. A firm conclusion in this regard requires a variety of further experiments, however.

E.3.1.2. Molecular Weight Determination for Evaporated Fractions.

The vacuum sublimation experiments were also important in determining the number average molecular weights of fractions evaporated at certain temperatures. The number average molecular weights of tar fractions were measured by VPO. The same data have been also used in order to determine the vapor pressures from the effusion data by formula {B.11}. The results are shown in Figures E.26 and E.27, and presented in Table E.6 for Pittsburgh No.8, Wyodak and Upper-Freeport coal tars. The molecular weight dependence on effusion temperature has been constructed and is shown in Figure E.26 for Wyodak, Upper-Freeport and Pittsburgh No.8 coal tars. This plot is based upon the data of Table E.6.

Table E.6. Molecular weights and amount of evaporated fractions.

	Wyodak		Upper-Freeport		Pittsburgh No.8	
fractions	MW	mass %	MW	mass %	MW	mass%
evaporated at 100°C	230	1.6	200	3.3	225	2
evaporated at 125°C	250	11.2	225	7.5	240	6
evaporated at 150°C	270	14.2	250	10	265	8
evaporated at 175°C	320	11.7	275	11.5	272	9.5
evaporated at 200°C	375	11.6	290	12.7	290	10.5
evaporated at 225°C	405	11.5	300	14	311	9
evaporated at 250°C	430	11.3	310	14.3	318	7
residue	935	26.9	575	26.7	990	48
original tar	340		276		320	
calculated from fractions	392		318		426	
calculated from evaporated fractions	323		273		279	

As noted above, each evaporated fraction has the characteristics of its parent coal tar. Thus, compounds of very different molecular weight and chemical structure can be present

in each fraction. The molecular weights and amounts of fractions evaporated in the same temperature intervals are different for different tars, reflecting differences in the starting materials. The number average molecular weights of tars calculated from the evaporated fractions and residue are higher than the measured molecular weights of the fresh tars indicating once again that condensation reactions took place. On the other hand, the molecular weights calculated from the evaporated fractions alone are lower, as expected due to differential evaporation.

It may thus be seen that there is some shift in molecular weight during the effusion experiments up to 250 °C. This confirms the results of Figure E.22 and E.23, which both indicate a shift, in the residue, towards quite high molecular weights. It should, however, be noted that very large species do not contribute as heavily to a number average molecular weights as do smaller species. For example, if the residue molecular weight in the Upper-Freeport coal tar case were 1000 rather than 575, the number average calculated from all factions would shift only up to 341 daltons. Thus what appears to the eye to be a major shift in the GPC behavior will not necessarily be highlighted in a number average characterization, as shown in Table E.6.

Raoult's law is of course based upon mole fractions, and the actual molecular weights of the residue will influence the mole fractions of the more volatile compounds rather little. For example, using the measured 575 daltons for the Upper-Freeport coal tar residue, the mole fraction of the fraction evaporating at 100°C is 5.2%. If the molecular weight of the residue were instead 1000 daltons, the 100°C fraction would represent above 6% of the mixture. In fact, it may be more reasonable to work with mixture rules based upon volume fractions in this case. These would perhaps scale better with mass fractions. Regardless of which way calculated, the largest, least volatile residue fraction may shift in molecular weight but not influence the evaporative process very much, all else being equal.

E.3.1.3. Comparison with Pure Compounds.

Table E.7. presents data concerning volatility of pure aromatic compounds under sublimation conditions, assuming that compounds with a vapor pressure of 10^{-3} torr can be fully evaporated.

Table E.7. The temperature of volatility of pure aromatic compounds.

volatility at T [°C]	compound	Molecular weight	number of aromatic rings
65	anthracene	178	3
75	pyrene	202	4
155	perylene	252	5
170	1,12-benzoperylene	276	6
200	coronene	300	7
315	ovalene	398	10

Comparing the volatility data in Tables E.6 and E.7 suggest that 7 ring aromatic compounds (e.g. coronene) could be present in the coal tar in large amounts. This is not to claim that they are, since this is not consistent with the literature data. Fletcher et al. [1993] have shown the presence of 1, 2 and 3 ring aromatic compounds in Illinois No. 6 coal and Zap lignite tars based on ^{1}H NMR analysis. Nelson et al. [1988] showed that the predominant components of Millmerran coal tar above 800°C were unsubstituted polycyclic aromatic hydrocarbons with up to five rings. Hayashi et al. [1995] showed the presence of up to 6 aromatic rings per molecule and that the two - to four-ring compounds predominate in Wandoan coal tars. They also showed that secondary reactions hardly changed the ring-size distribution. Essentially, the coal tars are not pure aromatic hydrocarbons and are known to have heteroatomic and aliphatic character (see Appendix A).

Thus the low volatility of the coal tars has more to do with how many aromatic clusters there are per molecule, and even more importantly, how many and what types of sidegroups the clusters carry. Literature data presented in Figure C.17 suggested that alkyl

substitutents did not lower the volatility relative to the base aromatic compound. Consider tetramethyl-pyrene, which has molecular weight 262 daltons and an H/C ratio of 1.1. Tetramethyl-pyrene could be expected to evaporate below 100°C as does pyrene. Clearly, this is not the correct model for coal tar, as seen in Table E.6, where almost all tar evaporated above 100°C. This strongly suggests the important role of polar substitutents, particularly hydroxyl groups in lowering vapor pressure. Adding even small amounts of hydroxyl substitutent to 3 or 4 ring aromatics enormously decreases their vapor pressure (see Figures C.9 and C.11 for example). Also the interactions between nitrogen bases and hydroxyl groups could be important (see Figure C.27). This fact is significant from the point of view of developing the vapor pressure correlations for coal tars.

E.3.2. The Effusion Experiments on Coal Tars.

The results of the experiments to measure the vapor pressures of Bruceton coal tar are shown in Figure E.28. The vapor pressures of this and other primary coal tars and their GPC fractions were examined using the non-isothermal Knudsen Effusion method, modified for application to mixtures containing components with a wide range of volatilities. The technique was described in detail in section B.4.2. The technique was applied to a fresh unfractionated coal tar in this case. The tar was produced by the pyrolysis of the Bruceton “standard” Pittsburgh No. 8 high volatile bituminous coal, in a fluidized bed at approximately 550°C. The tar was collected in THF, and carefully dried prior to measurement. The detailed procedure was described in section B.2.

In the vapor pressure experiments, the temperature of the tar sample was continually raised from an initial value of 60 °C to a final temperature of 220 °C, at a rate of 0.5 °C/min. Because the tar changes in composition during evaporative loss of its components, the ability to relatively quickly scan the whole temperature space of interest is of great importance. The results of Figure E.28 show again that the tars evaporate in a "distillation-

like" fashion. This is consistent with the results of the experiments shown in Figure E.21. More volatile species are lost earlier in the process, leaving behind a progressively less volatile residue. It can be noted that the vapor pressure remains in the range from about 7 x 10^{-5} to 7 x 10^{-3} torr as the temperature of the sample is raised from 60°C to 225°C, as a result of the loss of progressively less volatile components.

The experiments of Figure E.28 involved tracking the vapor pressure during both heatup and cooldown cycles. It can be seen that the trace of each heatup cycle (at a progressively higher total level of mass loss) tracks well the immediately preceding cooldown curve. This is not surprising, because during cooldown, the rates of mass loss fall quite low, and until the temperature is again raised to considerably higher values, little further mass loss occurs. Thus there should be little change in vapor pressure attributable to composition change due to mass loss during the cooldown and early part of the next heatup cycle.

It is unlikely that residue formation, as discussed above, can influence the results to the extent shown by the shift of vapor pressure curves in Figure E.28. At any given temperature, the shift of vapor pressure with cycling involves many orders of magnitude of pressure. For the development of a non-volatile residue to influence the pressures this much would mean that its concentration would likewise have to vary by orders of magnitude from the beginning to the end of the experiment. No such variation is seen, so the shifts are mainly attributable to the loss of progressively less volatile materials from the tar. If the condensation type reactions take place, formation of some high molecular weight residue does not affect the vapor pressure measurements very much. Thus, the main influence of the condensation type reactions on the vapor pressure measurement can be expected by virtue of removing some volatile material itself but not by forming non-volatile residue. It was noted in section D that cellulose tar showed similarly dramatic shifts of the vapor pressure curve, without the loss of all of the low molecular weight

fraction. It is, therefore important to know whether a similar sort of reaction might not be taking place here. The answer comes from the data of Table E.6, which showed that regardless of how long the tar was kept at a particular temperature, there was upper limit to mass loss. In contrast with this, if not heated over 100°C, the cellulose tar could almost all be evaporated at the lower temperatures.

Keeping in mind our earlier self-imposed temperature limit of 250°C for these experiments, we now see that it is possible to examine at least half of the tar under such conditions.

E.4. Tar Characterization.

E.4.1. Tar Composition.

The elemental compositions of tars and fractions investigated are given in Appendix B. In addition, the comparison of the H/C and N/C ratios for the parent coal and tar are presented in Table E.8.

Table E.8. Elemental analysis results for coals and tars studied.

coal tar	MW	H/C coal	H/C tar	N/C coal	N/C tar
Upper-Freeport	290	0.66	1.07	0.016	0.012
Pittsburgh No.8	320	0.77	1.09	0.017	0.015
Bruceton	347	0.79	1.13	0.017	0.013
Illinois No.6	273	0.773	1.15	0.015	0.014
Wyodak	324	0.85	1.21	0.013	0.011

These data show that the primary tar has a higher H/C ratio than its parent coal. The H/C ratios are comparable to the results of the other investigators as given in Appendix A. The exception is the low volatile bituminous Upper-Freeport coal tar which differs from earlier results. These results above also show comparable nitrogen heteroatom content in the tar and the parent coal.

Figure E.29 shows GPC chromatograms for the tars studied. As stated in a previous section, GPC with a pyridine mobile phase separates tar into three fractions according to chemical character, upon which is superimposed a separation based upon size. This allows one to characterize tars in terms of compound classes by drawing lines designating the regions of elution between large molecules with number average molecular weight over 400 daltons, hydroxyl-substituted aromatics, and aromatics without hydroxyl functionalities. The actual assignments are still tentative. We cannot firmly assign them on the basis of the limited data in hand.

Again, the GPC elution times below 1850 sec suggest large molecules. A GPC fraction showing higher molar absorbance suggest bigger aromatic clusters or characterization higher molar aromaticy. Thus the Upper-Freeport tar is most aromatic, but is lighter than the other tars, and exhibits only a broad shoulder below 1820 seconds. Taking into account the number average molecular weight of these early-eluting fractions (between 400 and 700 daltons), such volatility strongly suggests a large amount of alkyl character. This is consistent with the H/C ratio being higher than 1.2. These fractions may even involve some amounts of polymethylene compounds or polymethylene substituted aromatics [Calkins, 1984]. The elemental analysis also shows the presence of several oxygen atoms and therefore possibly several hydroxyl functionalities per average molecule.

The GPC elution time of the second peak (between 1820 and 2050 seconds) and the fact that the H/C ratios are all around 1 for fractions showing a significant contribution of this peak (see Appendix B) suggests that this peak contains mainly hydroxyl group-containing alkyl substituted aromatics. It may also contain alkyl substituted big aromatic molecules which contain oxygen in the ring structure.

The third peak elutes above 2050 seconds and as noted before cannot be easily assigned. The fact that the third peak is relatively speaking the largest in the Upper-Freeport coal suggests that it may involve structures that would be most characteristic of that coal and least characteristic of low rank coal. This supports the notion that the size of the aromatic clusters determines the size of the peak, as discussed above. Its height, in Upper-Freeport coal tar, relative to the second peak, could indicate the relatively greater importance of non-OH -containing clusters in the Upper-Freeport, compared with the other coal tars. Thus this peak could be associated with alkyl aromatics in which long alkyl chains play only a small role (the chains would not be polymethylene in character). This is consistent with what is known about Upper-Freeport's structure.

A separation based upon crudely defined chemical characteristics allows one to characterize tars using the areas under the three peaks. The hypothetical split into three classes is shown in Table E.9.

Table E.9. Separation of tars by compound classes.

tar	MW	relative absorbance	peak 1 wt%	peak 2 wt%	peak 3 wt%
Upper - Freeport	267	2.1	5%	60%	35%
Pittsburgh	320	1.6	10%	70%	30%
Bruceton	347	1.4	20%	60%	20%
Illinois	273	1.3	20%	60%	20%
Wyodak	324	1	60%	30%	10%

The values under the peaks are given in mass percents and the calculation is based on fractions separated by preparative GPC. This characterization suggests a large amount of hydroxyl substituted aromatics in all the tars. It also suggests the increase in aromatic cluster size or aromaticity with rank, as noted above (see relative absorbance). A relatively greater role of less substituted aromatics, with increasing rank, is also suggested by the data on peak 3, which include most of these species.

The elemental analyses suggest that an average molecule of Pittsburgh No.8, Illinois No.6 and Wyodak tar would contain about 2 oxygen atoms, therefore possibly 2 hydroxyl groups. This is in good agreement with the elemental analyses performed by other investigators (see Appendix A). It has also been noted that infra-red analysis of bituminous coal tars shows a large amount of phenolic (-OH) character in spectra at 3400 cm^{-1} [Fynes et al, 1984; Evans et al., 1985; Pindoria et al., 1997]. Fynes et al. [1984] identified that 4.7 to 6.1 wt. % of Linby HVB (811) coal tars could contain ionizable protons in the form of OH (the oxygen atom content of these tars was measured to be between 7.5 and 8.1 wt.%). The values assigned to peak 2 above suggest even higher percentages.

E.4.2. Is the Tar an Ideal Mixture?

All tars show heteroatomic content comparable to the parent coals (see N/C ratio in Table E.8), and likely contain a large amount of hydroxyl functionality. This means that they could exhibit very strong electron donor-acceptor interactions. This may have an important influence on the vapor pressure behavior of the tars, and suggests significant departures could be observed from Raoult's Law. Here, we explored this issue further by studying the vapor pressure of two artificially made mixtures consisting of a hetero-atom rich pure compound and Illinois No. 6 coal tar fraction 4. Note that fraction 4 (MW = 270 by VPO) occupies 42% of the mass of the total tar, and that the GPC spectrum is dominated by the second (probably OH rich) peak. Elemental analysis predicts that an average molecule could contain about two hydroxyl groups and that every fifth molecule contains N.

The first model mixture contained 50 mass percent of hydroxypyrene ($C_{16}H_{10}O$, MW = 218) in tar and the second mixture 40 mass percent of phenanthridine ($C_{13}H_9N$, MW = 179) in tar. Each model mixture was prepared by dissolving the tar and the pure component in THF, and then evaporating the solvent in a vacuum oven. The vapor pressure was measured by the non-isothermal Knudsen effusion technique. Figure E.30 shows that the mixture with hydroxypyrene exhibited vapor pressures quite close to those "predicted" from Raoult's law. The prediction was based on assuming the tar to be a single pseudo-component of a binary mixture.

Figure E.31 presents the results for the mixture with phenanthridine and shows lower vapor pressure than would be expected from Raoult's law. This is similar to the result presented in Figure C.27. It is known that the formation of hydrogen bonds between pyridinic or pyrrolic nitrogen (as exists in the coal) and hydroxyl groups is favorable. The fact that the nitrogen compound lowers the vapor pressure is consistent with the results shown in Table E.8, where it is seen that the tars have a slightly lower N/C ratio than the

parent coals. It is also worth noting that the difference in the results with hydroxypyrene and phenanthridine would be expected. There is an excess of the phenolic hydroxyl in the tar, compared to nitrogen. It would not be expected that addition of further phenolic hydroxyl would result in many new specific donor-acceptor interactions. On the other hand, addition of nitrogen species would be expected to help involve more of the hydroxyls in specific strong interactions. The numbers of these interactions would be larger than in the tar itself.

The above result suggests that assuming ideal mixture behavior could be acceptable for rough pyrolysis modeling work despite the possibility of strong specific interactions between certain functional groups.

E.5. Results of the Vapor Pressure Measurements.

Typical vapor pressure effusion results for coal tars are shown in Figure E.28 and were discussed in section E.3.2. The experiment used to obtain the data in Figure E.28 involved the evaporation of tar in a "distillation-like" fashion, tracking the vapor pressure during both the heat-up and the cool-down cycles. More volatile species are lost earlier in the process, leaving behind a progressively less volatile residue. This experiment tracked the vapor pressures of the tar as the lighter volatile fractions evaporated, starting at several percent of mass loss.

The analysis of the effusion data, shown in Figure E.28, allows determination of a vapor pressure curve as a function of mass loss, based on heat-up and cool-down cycle data using equation {B.11}. It can be seen that the trace of each heatup cycle tracks well the immediately preceding cooldown curve.

The curves diverge at high pressures, when mass loss rates become significant. In order to better analyze the effusion data on mixtures, a theoretical vapor pressure experiment was simulated based on experimental pure compound effusion rates and assuming ideal mixture behavior. The idea was to study the effusion behavior of an idealized mixture and to avoid the complications due to the experiment itself (e.g. heat transfer, noise). The simulated results for a five component mixture are shown in Figure E.32. The vapor pressure curves determined for mixtures left after the each cool-down are in good agreement with the heat-up and cool-down cycle data. Several features are worth noting in Figure E.32. First, the shape of the curves is quite similar to what is obtained in an actual tar experiment (see Figure E.28). the curvature noted at the high temperature end of each heat-up cycle reflects the fact that the vapor pressure is decreasing as volatile species are being lost. Actually, this is observed as in increase in the temperature required to maintain a particular pressure. As temperature is decreased (towards points 1 and 2), the

rate of mass loss decreases to such an extent that composition no longer is changing very much with time. This is why both the cool-down curve, and the subsequent heat-up curve, both approach the constant composition vapor pressure lines drawn through points 1 and 2.

Figure E.32 also shows that the extent of curvature observed depends very much on the maximum temperature of a cycle. The lower the maximum temperature, the less the change in composition, and the less curvature is observed. Thus the most reliable points for drawing vapor pressure curves are points 1 and 2. Bisection of the cooling and subsequent heating curves gives a realistic estimate of the vapor pressure at a well-defined composition point.

As is evident from formula {B.11}, it is necessary to know the molecular weight of the vapor in order to determine vapor pressure by the effusion method. As a coal tar vapor is composed of hundreds of gaseous species, it was assumed that each evaporated fraction can be considered as a single pseudo component, described by an average molecular weight. The molecular weights of the evaporated coal tar fractions were determined from vacuum sublimation experiments as described in section E.3.1 and were shown in Figures E.21 to E.23. The results shown in Figures E.21 to E.23 suggest that vacuum sublimation/effusion does not provide separation purely by molecular weight, size or composition. There are several features of the data of Figures E.21 to E.23 that need consideration. It is evident that each evaporated fraction has the characteristics of the parent tar, and that each fraction can contain species with a wide range of molecular weight and chemical structure; this is apparent from the GPC chromatograms. It is critical to consider this when developing new vapor pressure correlations using the vapor pressure data available. It is also interesting to note that the volatility increases from peaks 1, 2 to 3. This may be seen in the relative growth of the peaks from lower to higher temperatures. Our hypothetical structure-based characterization of the coal tars according to GPC peaks

is explained in section E.4. The most volatile peak (the third, at around 2200 seconds) is that attributed to the lowest molecular weight, most hydrocarbon-like components. The other peaks contain higher amounts of hydroxyl-containing tars.

The correlations used in pyrolysis models are based on the molecular weights of vaporizable fractions. The calculations of whole tar vapor pressure is related to the vapor pressure of fractions. Using the assumption of ideal mixture behavior of the tar, as was suggested in section E.4, i.e., Raoult's law, the following relation applies:

$$P = \sum_{i=1}^{\infty} x_i P_i \qquad \{E.5\}$$

where x_i is the mole fraction of fraction i in the condensed phase and the measured total pressure P is the weighted sum of the vapor pressures P_i of the fractions. In order to use equation {E.5} the mole fraction for each fraction i must be estimated from mass loss results obtained from the effusion experiments, and molecular weight (MW) is obtained from the vacuum sublimation results discussed earlier. It should be noted that the fractions defined here are neither the fractions obtained by preparative GPC, nor the fractions defined by the analytical GPC. These fractions are defined based upon the vaporization experiments.

E.5.1. High Volatile Bituminous Coal Tars.

Two coal tars - Pittsburgh No.8 and Bruceton - are discussed together because of the similarities in their vapor pressure behaviors. The GPC chromatograms of the high volatile bituminous coal tars show all three of the usual peaks but the largest concentration is under peak 2, believed to be associated with phenolic compounds. Elemental analysis predicts that an average molecule of Pittsburgh No.8 and Bruceton coal tars would contain up to two hydroxyl groups and every fourth molecule contains N.

Figure E.33 shows the constructed vapor pressure curves for Bruceton coal tar left after the cool-down cycles, superimposed on the non-isothermal effusion data shown in Figure E.28. Figure E.34 shows the analogous data for Pittsburgh No.8 coal wire mesh tar, and Figure E.35 shows the same for Pittsburgh No.8 coal tubular reactor tar. The vapor pressure curves could thus be obtained as a function of mass loss. To convert to a molecular weight basis, the curves of Figure E.26 were used, together with the temperature range of the experiment.

From these data the vapor pressure curves were constructed for evaporated fractions (which, again are not the same as GPC fractions). Extrapolations of the correlations were examined up to 800°C. It has been shown by Suuberg et al. [1985] that the yield of tar from Bruceton coal is essentially complete with peak temperatures > 750°C at 164 kPa, and in fact even by around 650°C, in the atmospheric pressure experiments. The vapor pressure curves for evaporated fractions extrapolated up to 800°C together with the estimates of the molecular weights in each interval are shown for Pittsburgh No.8 coal wire mesh tar in Figure E.36, for Pittsburgh No.8 coal tubular reactor tar in Figure E.37 and for Bruceton coal fluidized bed tar in Figure E.38. In each case, the actual temperature range over which data were obtained has been indicated. The fitted curves obviously pertain to only limited portion of the raw data curves.

It is notable from Figures E.36 to E.38 that the slopes and intercepts for any given molecular weight have quite similar values for the different tars studied which means that they likely contain similar components. This suggests that tar volatility does not seem to be a very sensitive function of tar preparation conditions.

Figure E.39 supports this view. This figure displays the vaporization enthalpy as a function of molecular weight. A good linear correlation is seen, with data from all these tar samples falling quite close to the same correlation line. The linear dependence of enthalpy with molecular weight is not consistent with many earlier tar vapor pressure correlations in which there was a fractional exponent on molecular weight.

Figure E.40 shows the data for the pre-exponential (A) from correlating vapor pressure with temperature, by using an expression of form:

$$\ln P[\text{torr}] = A - \frac{\Delta H_{vap}}{RT} \qquad \{E.6\}$$

The correlation of A with molecular weight is much more scattered than that of enthalpy with molecular weight, and strongly suggests systematic differences between samples. Combining the results of these correlations, it is possible to see that

$$\ln P[\text{torr}] = 28.72 + 0.04\ MW - \frac{77\ MW}{T}$$

For a typical temperature of interest of T = 873 K, the correlation would be:

$\ln P[\text{torr, } 873\text{ K}] = 28.72 - 0.048 \bullet MW$

Under similar conditions, the Unger-Suuberg correlation predicts:

$\ln P[\text{torr, } 8773\text{ K}] = 15.3 - 0.292 \bullet MW^{0.586}$

For a typical tar of molecular weight 300, the two correlations give ln P = 14.32 and ln P=7.04, respectively. It is apparent that the new results give much higher vapor pressures than provided by the old correlation, which had been derived for pure aromatics, for the most part.

Comparison with the pure compound vapor pressure curves in Figures C.2 to C.13 shows that the tar fractions have higher enthalpy and entropy of vaporization values than the pure compounds chosen as models. This can be explained by the larger molecules and existence of hydroxyl groups in the tars. It should of course be remembered that each evaporated fraction contains a large number of compounds with very different chemical character and molecular weight. The above cited results seem to strongly suggest that the vapor pressure curve is heavily influenced by the hydrogen-bond forming compounds. This suggests different volatility behavior than exhibited by alkyl-substituted aromatic compounds or hydrogenated coal liquids, because of the more limited hydrogen bonding opportunities in those model systems. The higher the enthalpy of vaporization the greater the increase of vapor pressure with temperature.

E.5.1.1. Pittsburgh No.8 Coal Tar GPC Fractions.

Attempts were made to study the influence of chemical character on vapor pressure. The idea was to separate the tar into fractions in the preparative GPC column and compare the vapor pressure curves of these GPC fractions. These fractions have been shown to contain differing proportions of different types of compounds. The comparison was based on the general chemical character obtained from elemental analysis and analytical GPC spectra. The characterizations of selected fractions are shown Table E.10, and also in Appendix B (Tables BA.1a and BA.1b). These tars were produced in the tubular reactor.

Table E.10. Chemical characterization of the Pittsburgh No.8 coal tar and its preparative GPC fractions.

	wt% of tar	MW	H/C	N/C	main peak number in GPC	N/ molecule	OH max/ molecule*	relative wt% of O*
tar		320	1.03	0.012	1	0.3	2	1.1
fraction 1	2.7	540			1			
fraction 2	14.6	410	1.2	0.01	1	0.3	2.2	1
fraction 3	29	340	1.02	0.01	1 &2	0.25	2.1	1.1
fraction 4	33	310	1.09	0.012	2	0.25	2.2	1.25

* maximum number OH per average molecule was estimated from elemental analysis data given in Tables DA.1a and DA.1b assuming that all O is present as OH. Amount of S is considered not to be significant based on Table E.1.

The raw data on fraction vapor pressures are shown in Figures E.41 to E.44. the whole tar data were previously shown in Figure E.35. The extrapolated vapor pressure curves are shown for these fractions in Figures E.45 to E.48 up to 800°C. The comparable whole tar curve was given in Figure E.37. It can be seen that there is an increase in the magnitude of both entropy and enthalpy terms with molecular weight. Again, enthalpy is related to the slope of the ln P vs. 1/T curve, and entropy to the intercept value. At the same time there is also a decrease of molecular weight from fraction 1 to 4. Comparison of the whole tar values with the GPC fraction values indicate that no

one fraction is fully representative of the tar, though some fractions clearly come closer. This will be further considered below.

The estimation of the number average molecular weights for GPC fractions was based on the correlation in Figure E.26 for Pittsburgh No.8 coal tar and correcting it by a factor φ:

$$MW = 1.613 * T[K] * \varphi \qquad \{E.7\}$$

This relationship was obtained by tracking the extent of the molecular weight changes in the tar fractions during vaporization using the effusion data and a simple mole balance. The tracking was accomplished by using a suitable φ to obtain the same molecular weight of the residue as that measured by VPO after the effusion experiment. The factor φ was found to be close to the relative difference between the GPC fractions and whole tar molecular weights ($\varphi \approx MW_{GPC\ fraction}/MW_{tar}$). The results are shown in the Table E.11.

Table E.11. Comparison of the correction factor φ with the ratio $MW_{GPC\ fract}$ to MW_{tar}

	initial MW by VPO	final MW by VPO	mass loss %	φ	$MW_{fraction}/MW_{tar}$
tar	320				
GPC fraction 2	410	873	58	0.87	1.281
GPC fraction 3	340	415	49	1.06	1.063
GPC fraction 4	310	410	49.4	0.97	0.969

The value 0.87 for fraction 2 suggests the formation of high a molecular weight residue caused by condensation type reactions. This is supported by comparison of the GPC chromatograms of fraction 2 and evaporated fraction 2 in Figure E.49a. Thus, the increase in MW with temperature is faster than predicted and the value 1.28 has been used for estimation of effusing species molecular weight. It is apparent that since φ is nearly unity for GPC fractions 3 and 4 that the model derived for the whole tar applies equally well in this case. The GPC chromatograms in Figures E.49b and E.49c show no clear signs of the condensation type reactions after effusion.

Figure E.49 shows the variation of the enthalpy of vaporization with molecular weight, for the different fractions of the tar, superimposed on the data of Figure E.39.

Figure E.50 is the analogous figure for the pre-exponential (A). It is clear that there is an enormous variability of behavior from one fraction to another. Given the shape of the distribution indicated by the preparative GPC chromatogram, fractions 3 and 4 comprise more than half of the tar. Thus their behavior is seen to be reflective of the mean behavior of the whole tar. Fractions 1 and 2 are, however, notably different. Fraction 1 behaves much more like many of the model compounds studied earlier. Its enthalpy of vaporization is much lower, and a linear correlation with molecular weight might not be appropriate, though there are not nearly enough data to conclude this. The fact that these higher molecular weight species were even volatile at the same range of temperatures as the much lower molecular weight materials of the other fractions strongly suggests that they are not strongly hydrogen bonded species. The conclusion is that these may be larger aromatics, but with enough alkyl substitutents to prevent their delayed elution from the analytical GPC column due to the strong adsorption. They may or may not have hydroxyl content (the oxygen content was not determined), but if they do, these hydroxyls cannot be participating in strong hydrogen bonding.

Fraction 2 shows behavior that is intermediate between the main fractions (and the mean) and fraction 1. The suggestion is that hydrogen bonding is again not playing as strong a role as in fractions 3 and 4, despite a similar level of oxygen and nitrogen in all three fractions. The slightly higher H/C and lower O/C ratio of fraction 2 compared to fraction 3 and 4 implies, again, a more hydrocarbon like character (larger molecules with many aliphatic substitutents).

In order to compare the vapor pressure results of the GPC fractions the following modified correlation with the simplest vapor pressure correlations of the form {C.2} has been constructed:

$$P_i = \alpha \exp(\delta\, MW_i) \exp\left(-\frac{\beta\, MW_i^{\gamma}}{T}\right) \qquad \{E.8\}$$

where T is temperature in K, P_i is pressure in torr, MW_i is pseudo-molecular weight of fractions in daltons, and α, β, γ and δ are adjustable parameters.

The enthalpy and pre-exponential variations with molecular weight were determined by the linear fit to the data of Figure E.50 and E.51. The parameters obtained are shown in Table E.12.

Table E.12. Vapor pressure correlations for Pittsburgh No.8 coal tar and its GPC fractions.

	α	δ	β	γ
whole tar	$2.98*10^{12}$	0.04	76.9	1
fraction 1	$5.726*10^{5}$	0.031	33.8	1
fraction 2	$5.657*10^{14}$	0.009	54.9	1
fraction 3	$2.212*10^{12}$	0.043	71.7	1
fraction 4	$3.776*10^{11}$	0.067	83.2	1

The values in table E.12 show the expected increase in both enthalpy of vaporization and pre-exponential with molecular weight. As these data and Figure E.50 and E.51 show, the main fractions (3 and 4) have a higher enthalpy of vaporization and pre-exponential than do fractions 1 and 2, for any given molecular weight. The increase in these quantities with molecular weight is also greater. This would be expected if the fractions 3 and 4 are more polar, and that the number of polar interactions increases with molecular weight. It might be anticipated with increasing value of molecular weight, van der Waals-type interactions will become more important than polar interactions, because of the numbers of van der Waals interactions is roughly linear in molecular weight, while polar interactions are not. This is, however, not observed here.

Comparison with some of the existing vapor pressure correlations are shown in Figure E.52a at 500°C and at 600°C in Figure E.52b. There are several features that apparently need consideration. The data of Figures E.52a and E.52b are useful for recognizing the complexity of the tar vaporization process during pyrolysis. The overall vapor pressure, and therefore the tar evaporation process is determined by the chemical character of tar. The above cited results seem to suggest that there are three very different vapor pressure behaviors. The first is for the compounds with high molecular weight with

significant aliphatic content, the second for compounds with significant hydroxyl group content and medium molecular weight, and the third for medium molecular weight compounds without hydroxyl groups, including pure PAH. This is a bit different from what may be seen in coal liquids which do not necessarily contain as large a variety of constituents after a high degree of hydrogenation. Figures E.52a and E.52b imply that the commonly employed correlations may easily be quite far off from the true behavior, in critical ranges of molecular weight. This will be further discussed below, in the context of data from a larger number of tars.

E.5.2. Upper-Freeport Medium Volatile Bituminous Coal Tar.

Upper-Freeport (medium volatile bituminous) coal gives a tar number average molecular weight of 280 and an H/C ratio of 1.05. Elemental analyses predict that every second molecule would contain one hydroxyl group and that every fifth molecule contains N. The GPC shows few compounds with polymethylene character (peak 1) and the chromatogram is dominated by the second and third peaks. The higher average molar absorbance of this tar suggests a larger aromatic content than that in the other tars investigated (see Table E.9). The experimental and extrapolated vapor pressure curves are shown for Upper-Freeport wire mesh tar up to 800°C in Figure E.53. The raw data and the curve fits for tar left after the cool-down cycles are shown in Figure E.54. The Upper-Freeport coal tar generally has higher vapor pressure and a lower heat of vaporization for any particular molecular weight than does than Pittsburgh No.8 coal tar (compare Figures E.36 and E.53). This is consistent with the hypothesis of the influence of hydrogen bonding, especially involving hydroxyl groups. Figure E.55 shows a comparison of the $\Delta H_{vap}/R$ of the Upper-Freeport coal tar with the fractions of the Pittsburgh No.8 coal tar. This comparison suggest Upper-Freeport coal tar is similar to the Pittsburgh No.8 coal tar fraction 2 or 3. Figure E.56 shows that the pre-exponential for the Upper-Freeport coal tar

extrapolates to that for the Pittsburgh No.8 coal tar fraction 2. It is apparent that the behavior of the Upper-Freeport coal tar, on this basis, is somewhat similar to that of fraction 2. The implication is that the Upper-Freeport coal tar is somewhat more hydrocarbon-like in character than is most of the Pittsburgh No.8 coal tar in which fraction 2 is a small contributor. Still, the implication is that hydrogen bonding (through hydroxyl groups) could be having some influence an behavior, because the results track Pittsburgh fraction 2 not fraction 1. The latter was above judged to be most hydrocarbon like.

E.5.3. Wyodak Subbituminous Coal Tar.

The Wyodak subbituminous coal tar studied here has a number average molecular weight of 350 and an H/C ratio of 1.2. Elemental analysis predicts that an average molecule could contain about two hydroxyl groups and that every fifth molecule contains N. The GPC shows a higher concentration of molecules enriched in polymethylene substitutents and the lowest average molar absorbance implying the smallest aromatic cluster sizes or aromatic content. This suggests more aliphatic character in the tar. The experimental and extrapolated vapor pressure curves, up to 800°C, are shown for Wyodak coal wire mesh tar in Figure E.57. The raw data and the curve fits for tar remaining after the cool-down cycles are shown in Figure E.58. The enthalpy of vaporization and pre-exponential are comparable to those seen in Pittsburgh No. 8 coal tar. Figure E.59 compares the variation in ΔH_{vap} of the Wyodak coal tar with the Pittsburgh No.8 coal tar fractions. In this case, the whole Wyodak coal tar appears quite similar to fraction 3 of the Pittsburgh No.8 coal tar. Since fraction 3 is the fraction that best characterizes the whole Pittsburgh No.8 coal tar, the surprising result emerges that the enthalpies of the two tars show a very similar molecular weight dependence. Figure E.60 shows that the correspondence also carries over to the pre-exponential (A).

The experimental and extrapolated vapor pressure curves up to 800°C are shown also for Wyodak coal tar fraction 1 in Figure E.61. It may be noted in Figures E.59 and E.60 that this fraction is quite similar to fraction 1 of the Pittsburgh No.8 coal tar, and therefore quite different from the rest of the tar. The curve fits and raw data are shown in Figure E.62. Fraction 1 has been shown to contain up to 50 % of the mass of the Wyodak coal tar (see Appendix BA.5b) and elutes below 1820 sec from analytical GPC column. Comparison with the results in Figure E.57 strongly suggests that the measured vapor pressure behavior of this fraction is quite different than that of the fractions eluting above 1820 second (see Appendix BA.5b and Figure E.10). The whole tar and fraction one are very different because the latter is presumably dominated by large hydrocarbons, whereas the former shows a significant effect of polar functionality as well.

E.5.4. Comparison of Boiling Point Correlations at 760 Torr.

Figure E.63 presents the comparison of the atmospheric boiling point data of tars with the Unger-Suuberg [1985], Fletcher-Grant-Pugmire (FGP) [1992], Oh et al. [1989], Niksa-Kerstein [1991] correlations. These correlations were selected for comparison because they are widely used in coal pyrolysis models.

All atmospheric boiling points are lower than predicted from the Unger-Suuberg correlation. Unger and Suuberg [1985] developed this vapor pressure correlation based on the boiling points of six aromatic hydrocarbons with molecular weights between 198 and 342 at a total pressure of 0.5 torr. The Unger-Suuberg correlation has been limited in its application to typical coal pyrolysis condition. For example, Oh and coworkers [Oh et al., 1989] found that the Unger-Suuberg correlation is consistent with high-temperature pyrolysis data (T > 600°C) but not with low temperature data (T < 600°C). Solomon and co-workers [Solomon et al., 1988] have used this correlation multiplied by a factor of 10

in order to fit tar and total volatiles yields. Thus, the general opinion was that the Unger-Suuberg correlation over-predicts boiling point, or under-predicts vapor pressure.

As shown, there is fair agreement between the Oh et al. correlation and Wyodak coal tar fraction 1 and Pittsburgh No.8 coal tar fraction 1 data. The correlation is especially good for the low fraction numbers. It may be recalled that these fractions eluted below 1820 second from the GPC column and contain large molecules with highly alkylated character. As hypothesized earlier, this may reduce the influence of hydrogen bonding in this fraction. This agreement is not surprising, since Oh et al. again emphasized aromatic hydrocarbons in developing their correlation..

The parameters in the vapor pressure correlation used by Niksa and Kerstein were used as fitting parameters to achieve agreement with the measured molecular weight distribution of the pyrolysis tars. This equation is used in the FLASHCHAIN pyrolysis model. It is seen here to underpredict the estimated boiling points of all fractions.

The Upper-Freeport coal tar shows good agreement with the FGP correlation. The FGP correlation was based on vapor pressure data of 12 narrow boiling point fractions distilled from coal liquids produced from SRC-II processing of Pittsburgh seam bituminous coal [Gray et al., 1983, 1985]. The FGP correlation agrees with the measured vapor pressures of coal liquids and boiling points of pure compounds over a wide range of pressures [Fletcher and Kerstein, 1992]. The Upper-Freeport coal tar elemental analyses show comparable oxygen content to SRC-II coal liquids. Additionally, the coal liquids are considered to be made up primarily of two- to five condensed ring compounds [Tsonopoulos et al., 1986]. Thus the coal liquids are likely closest to Upper-Freeport coal tar in terms of composition. They are the least polar. This could be reason why the FGP correlation appears to apply best to Upper-Freeport coal tar.

Pure Pittsburgh No. 8 coal tar, its fractions 3 and 4, and Wyodak coal tar show a rapid increase in boiling point with increasing temperature. In these tars, the phenolic compounds, probably the major type of oxygen-containing compounds present, are

believed to be responsible for this behavior. The role of hydroxyl group content and molecular size has again been demonstrated. Therefore, there is unquestionably an important effect of chemical character on coal tar vapor pressure behavior. The construction of a new, more general vapor pressure correlation is discussed below.

E.5.5. New Tar Vapor Pressure Correlations.

A summary of existing vapor pressure correlations for coal tars has been given in the Chapter A . The heterogeneous nature and the complexity of coal tar has made it unrealistic to apply detailed vapor pressure correlations which take into account the variation in the chemical structure. Since the vapor pressure correlations in the form of the Unger and Suuberg correlation {A.1} are the used in pyrolysis models, the following vapor pressure correlation will be developed:

$$P_i = \alpha \exp(\delta M_i) \exp\left(-\frac{\beta M_i}{T}\right) \qquad \{E.9\}$$

The enthalpy and entropy dependencies with the molecular weight were determined by linear fit to the data. The obtained parameters are shown in table E.13 for Pittsburgh No. 8, Upper-Freeport and Wyodak coal tars. The parameters for Wyodak coal tar fraction 1 have also been developed to describe the vapor pressure behavior of compounds eluting below 1820 seconds in the analytical GPC column.

Table E.13. Vapor pressure correlations for tars studied.

coal tar	α	β	δ
Pittsburgh No. 8	$2.98*10^{12}$	76.9	0.04
Upper-Freeport	$3.6*10^{7}$	61	0.05
Wyodak	$5.03*10^{13}$	66.7	0.028
Wyodak fraction 1	$2.86*10^{7}$	34.7	0.027

The comparison with FGP, Unger-Suuberg and Niksa-Kerstein correlations are shown at 300°C, 500°C and 700°C in Figures E.64 to E.66 respectively. The middle non-striped area indicates the actual molecular weight region where the measurements were performed. It is apparent that the new results validate the predictions of the vapor pressures in this molecular weight range provided by the older correlations, but the new correlations also show relatively weaker dependence on temperature. Again, the correlation based on Wyodak coal tar fraction 1 data shows better agreement with the Niksa-Kerstein correlation. The correlation based on Upper-Freeport tar data agrees better with the FGP correlation as expected. The correlations based on Wyodak and Pittsburgh No. 8 coal tars data are significantly different from the previous correlations; the vapor pressures initially have very high values and then drop quickly with molecular weight. It was suggested above that such vapor pressure behavior could be expected from polar medium size molecules with molecular weight below 400 daltons. As molecular weight increases, these vapor pressure correlations should change from being dominated by species characteristic of Pittsburgh or Upper-Freeport coal tar to being dominated by behavior such as that of Wyodak fraction 1.

The correlations indicate again the important effect of chemical character on coal tar vapor pressure behavior. Again, the results suggest that there are three very different vapor pressure behaviors (see section E.5.1.): first the compounds with high molecular weight (Wyodak coal tar fraction 1), second the compounds of high hydroxyl group content with medium molecular weight (Pittsburgh No.8 coal tar and Wyodak coal tar) and third the medium molecular weight compounds without significant hydrogen bonding character (Upper-Freeport coal tar).

In summary, vapor pressure correlations for the Pittsburgh No.8, the Wyodak and the Upper-Freeport coal tars have been developed for use in pyrolysis models. It may be seen that tar volatility is in no sense "simple" and is considerably more complicated than had been believed. The volatility is quite different for different coal tars. It does not depend on

molecule size only. Based upon the work performed here, however, there is generally a good possibility of developing a general vapor pressure correlation based on the molecular weight and some certain specific chemical character. There is a notable dependence of coal tar vapor pressure on hydroxyl group content .

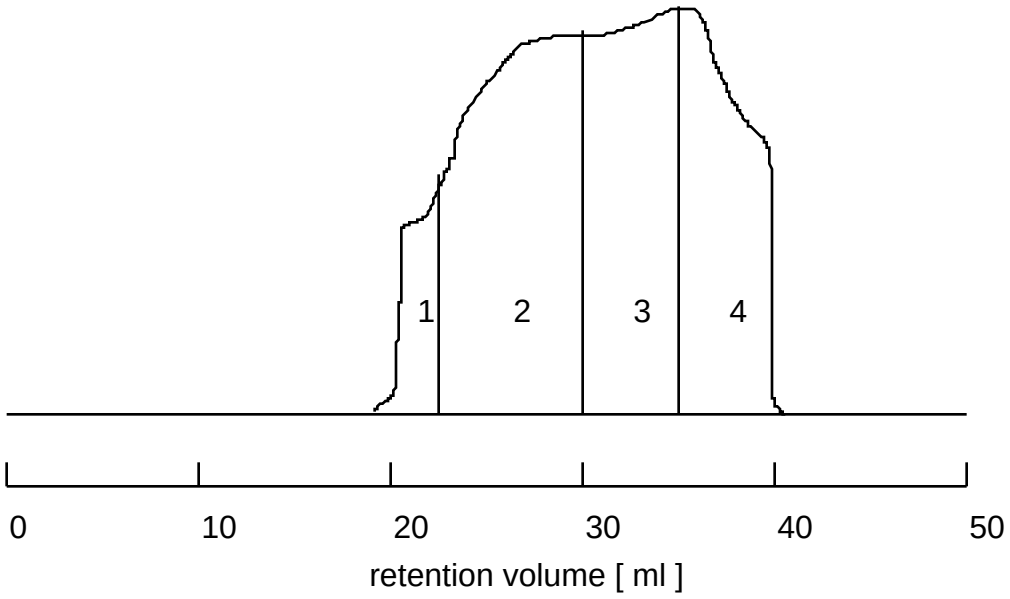

Figure E1. Separation of coal-derived liquids by GPC based upon Philip and Anthony [1982]. Column μStyragel, THF flowrate 1ml/min.
1- polymers +colloidal carbons; 2 - alkanes(C14...C44) + asphaltenes;
3 - phenols; 4 - aromatics

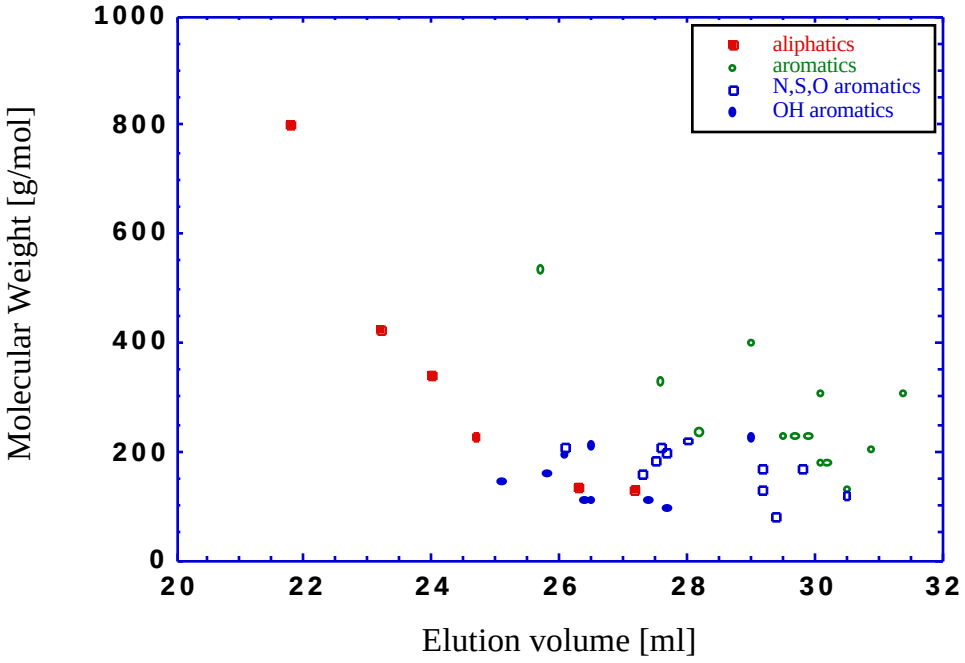

Figure E.2. GPC elution data for standard compounds (Strachan and Johns, 1985). Conditions: Columns, 100Å and 500Å µStyragel; solvent THF.

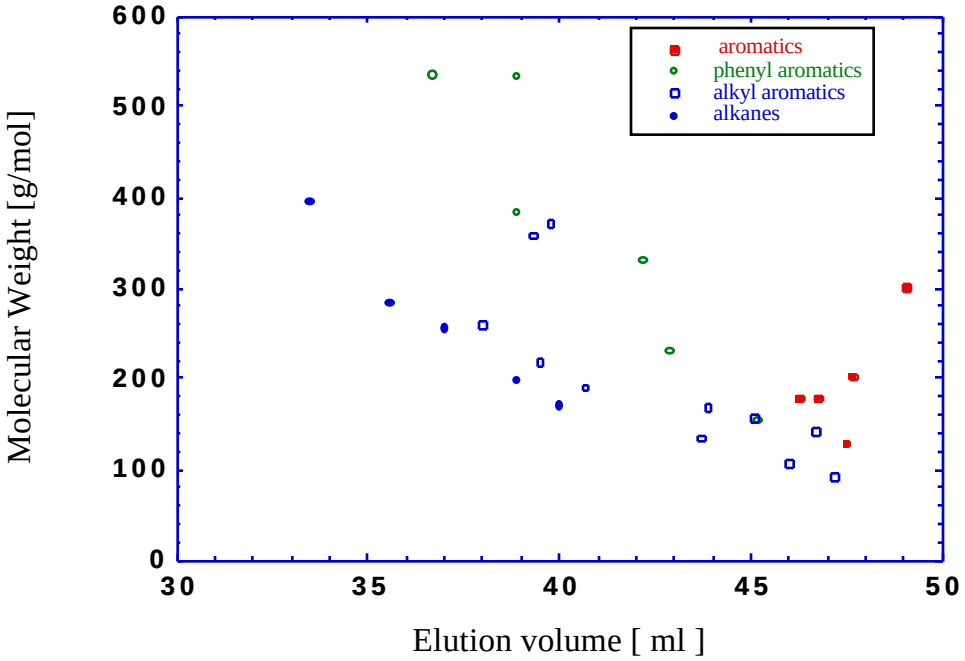

Figure E.3. GPC elution data for standard compounds (Rodgers et al.,1987). Conditions: Columns, 1000Å, 500Å and 100Å µStyragel; solvent THF

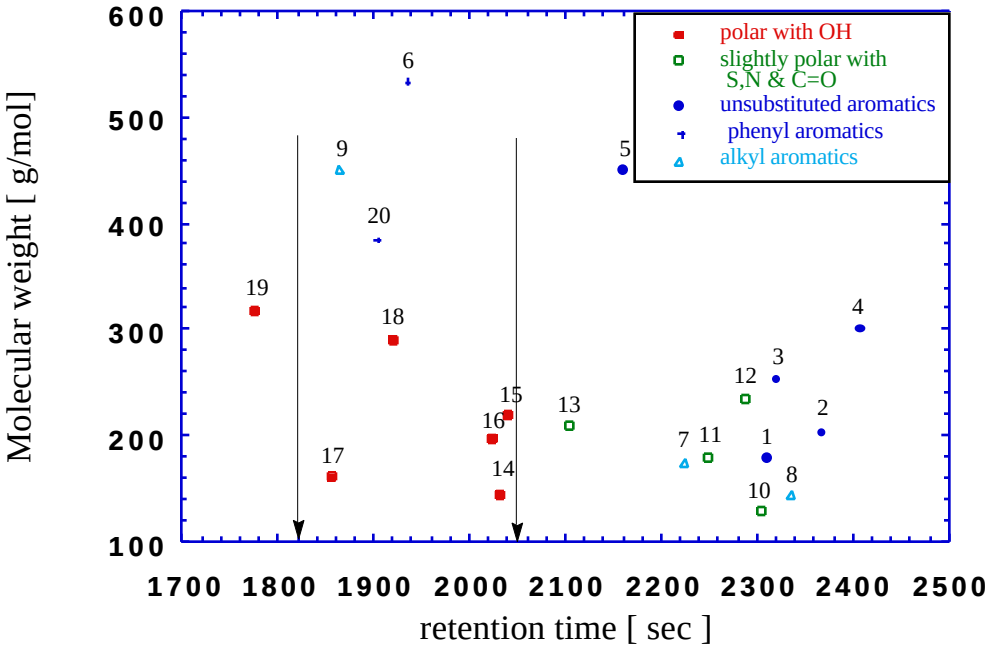

Figure E.4. GPC elution data for standard compounds.
Solvent: pyridine, flowrate 0.3 ml/min;
Column: packing - 10...100Å Phenogel, temperature: 30°C.

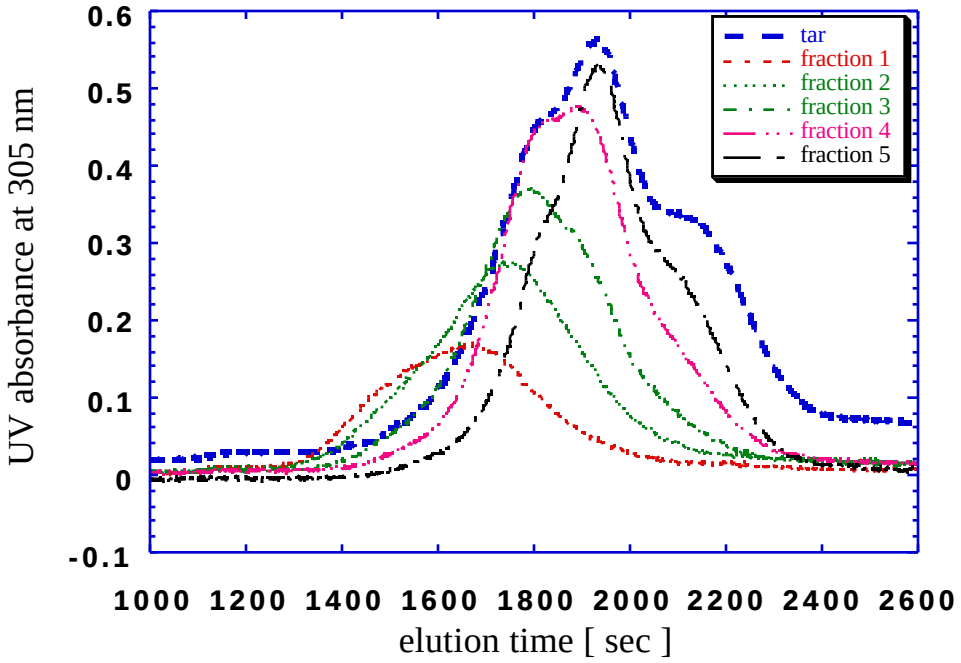

Figure E.5. GPC chromatograms for Bruceton coal tar and the first 5 fractions, collected from the preparative GPC column.

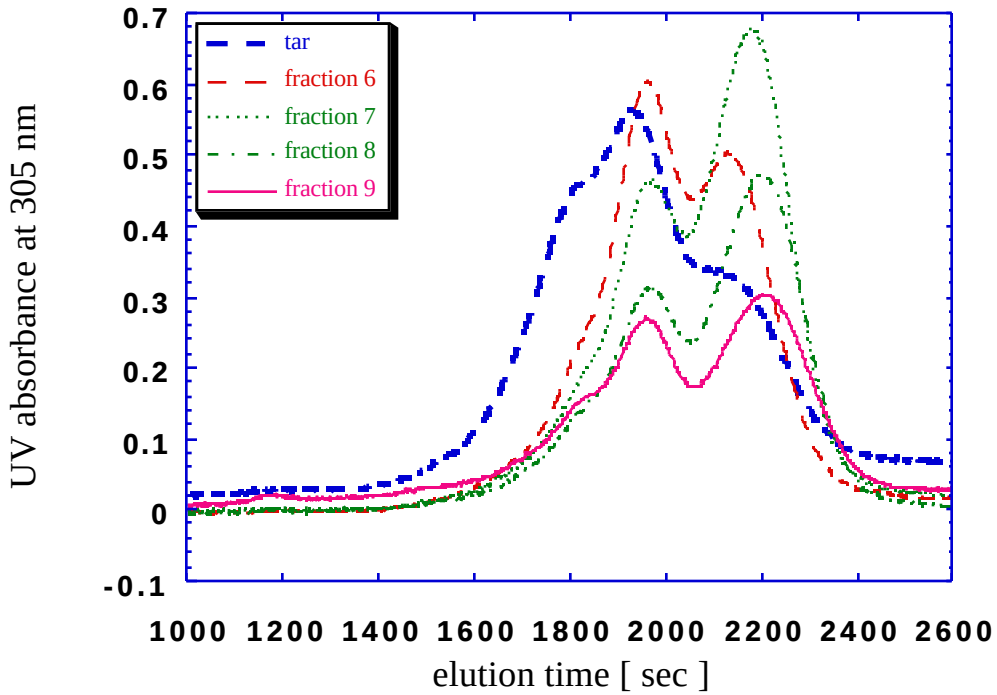

Figure E.6. GPC chromatograms for whole Bruceton coal tar and the last 4 fractions collected from the preparative GPC column.

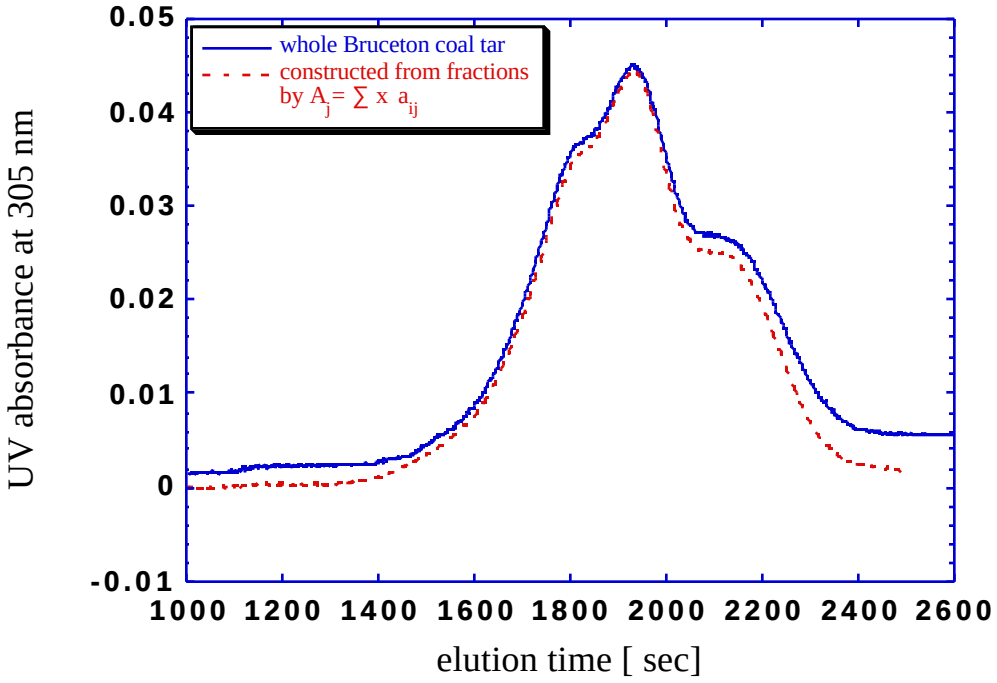

Figure E.7. Reconstruction of the curve for whole Bruceton coal tar by summing the contributions of tar fractions, where A_j is total absorbance at j elution time, x_i is the mass fraction of fraction i and a_{ij} is the absorbance of fraction i at j elution time.

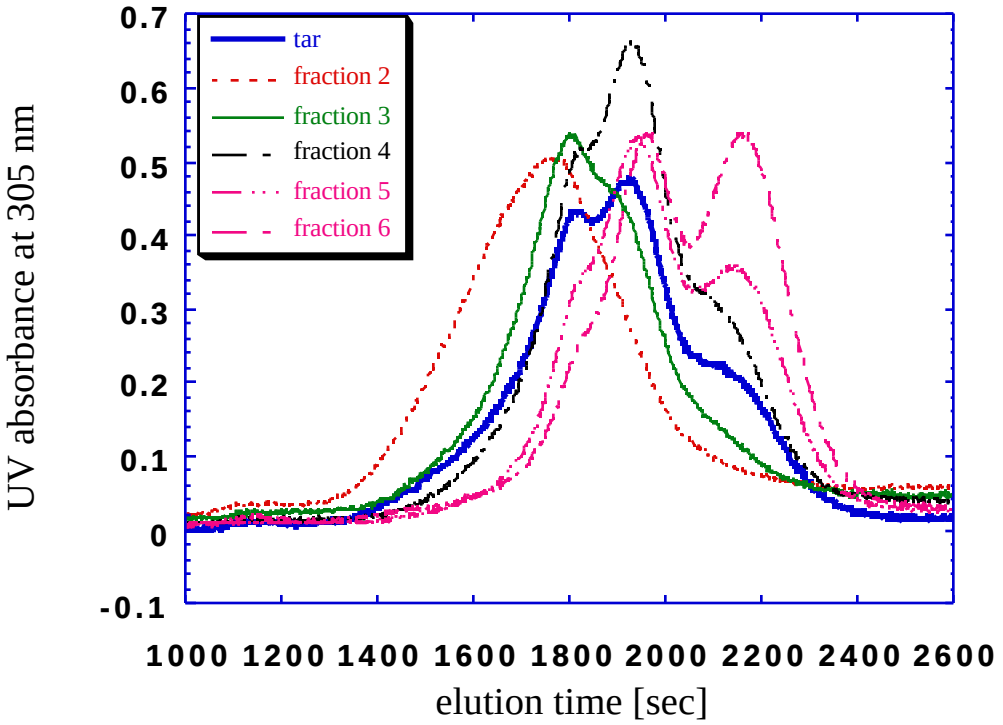

Figure E.8. Analytical GPC chromatograms for Pittsburgh No.8 coal tar and its fractions, separated by preparative GPC.

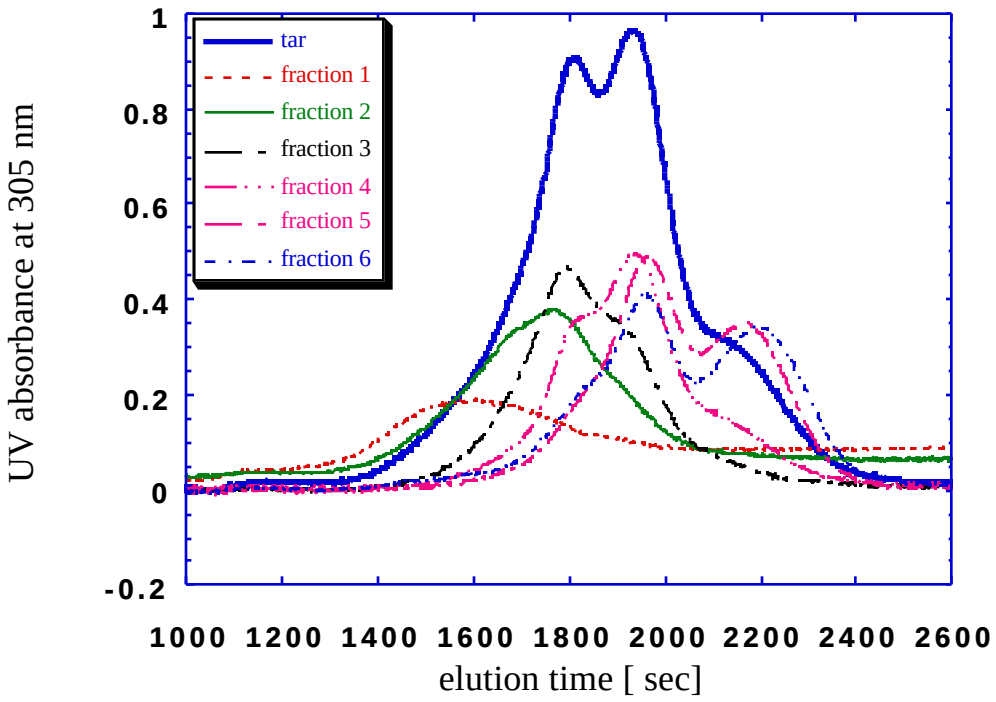

Figure E.9. Analytical GPC chromatograms for Illinois No.6 coal tar and its fractions, separated by preparative GPC.

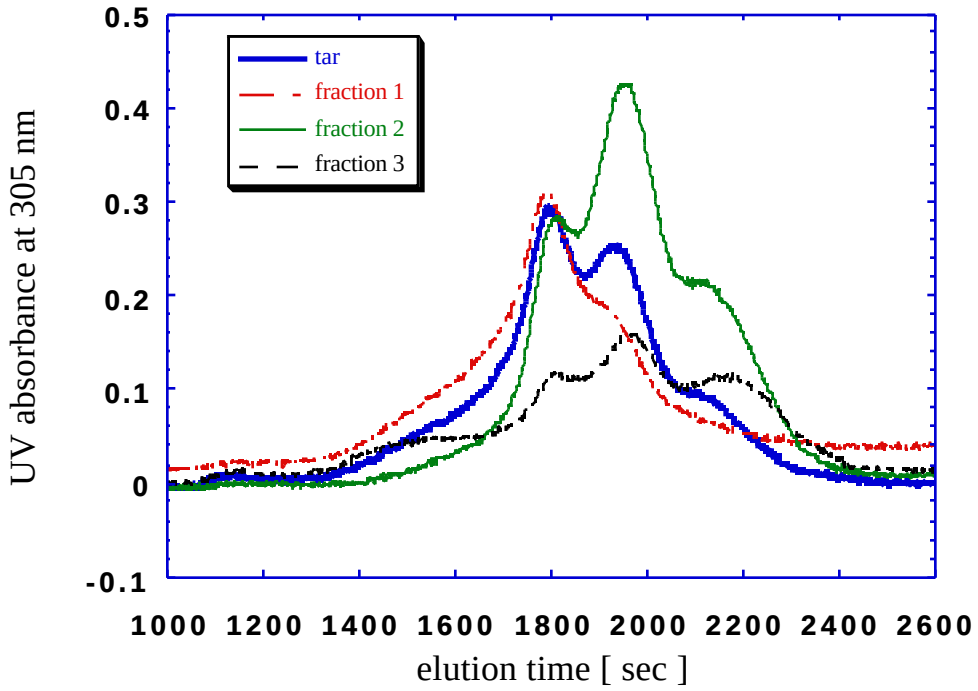

Figure E.10. Analytical GPC chromatograms for Wyodak coal tar and its fractions, separated by preparative GPC.

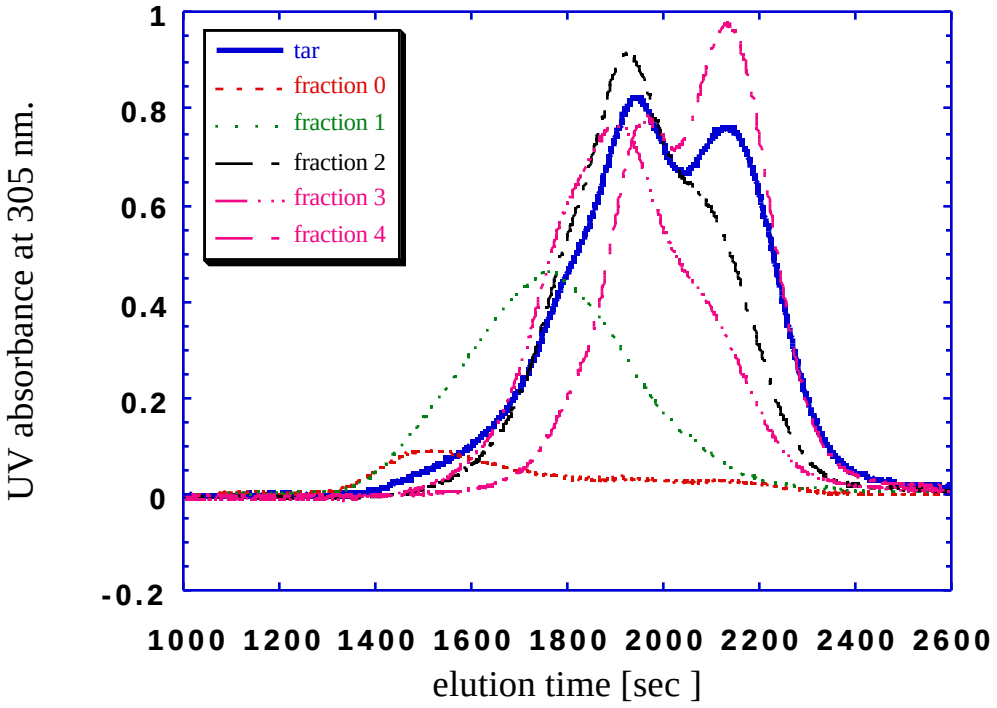

Figure E.11. Analytical GPC chromatograms for Upper Freeport coal tar and its fractions, separated by preparative GPC.

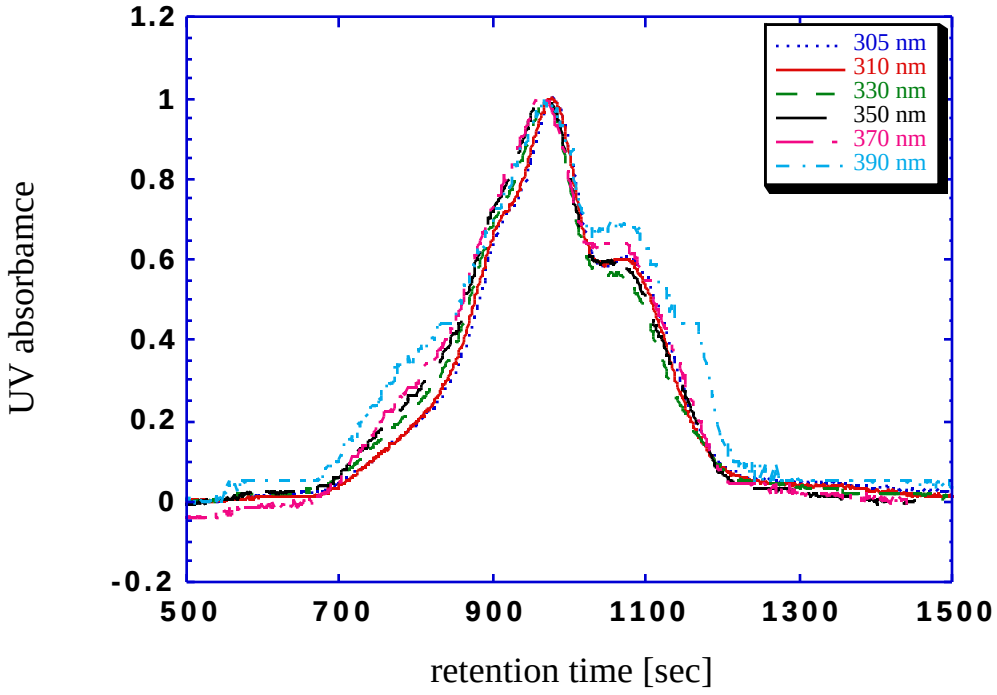

Figure E.12. Normalized absorbance for whole Bruceton coal tar at different UV wavelengths.

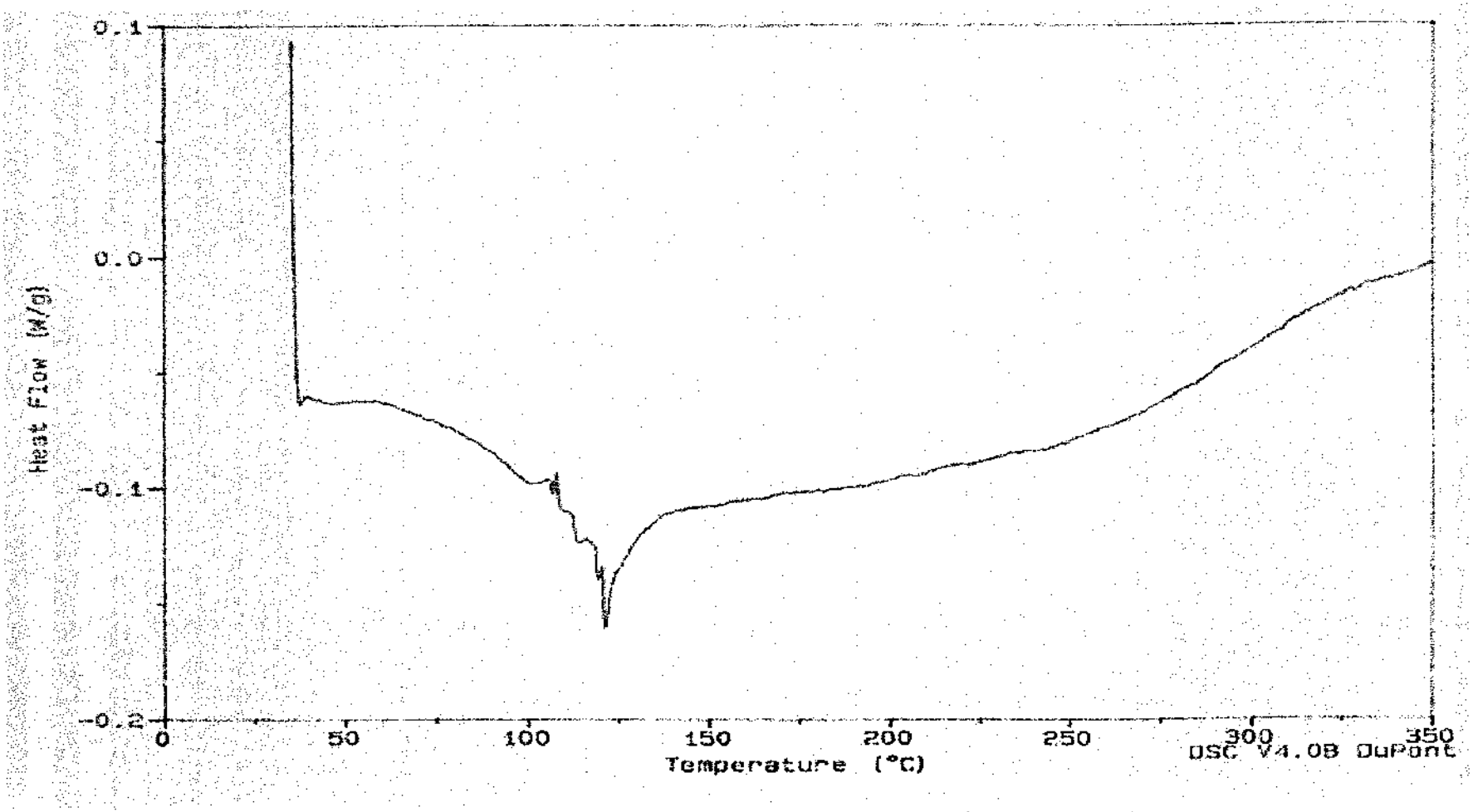

Figure E.13. DSC applied to Pittsburgh No. 8 coal tar. Heating rate 5 K/min.

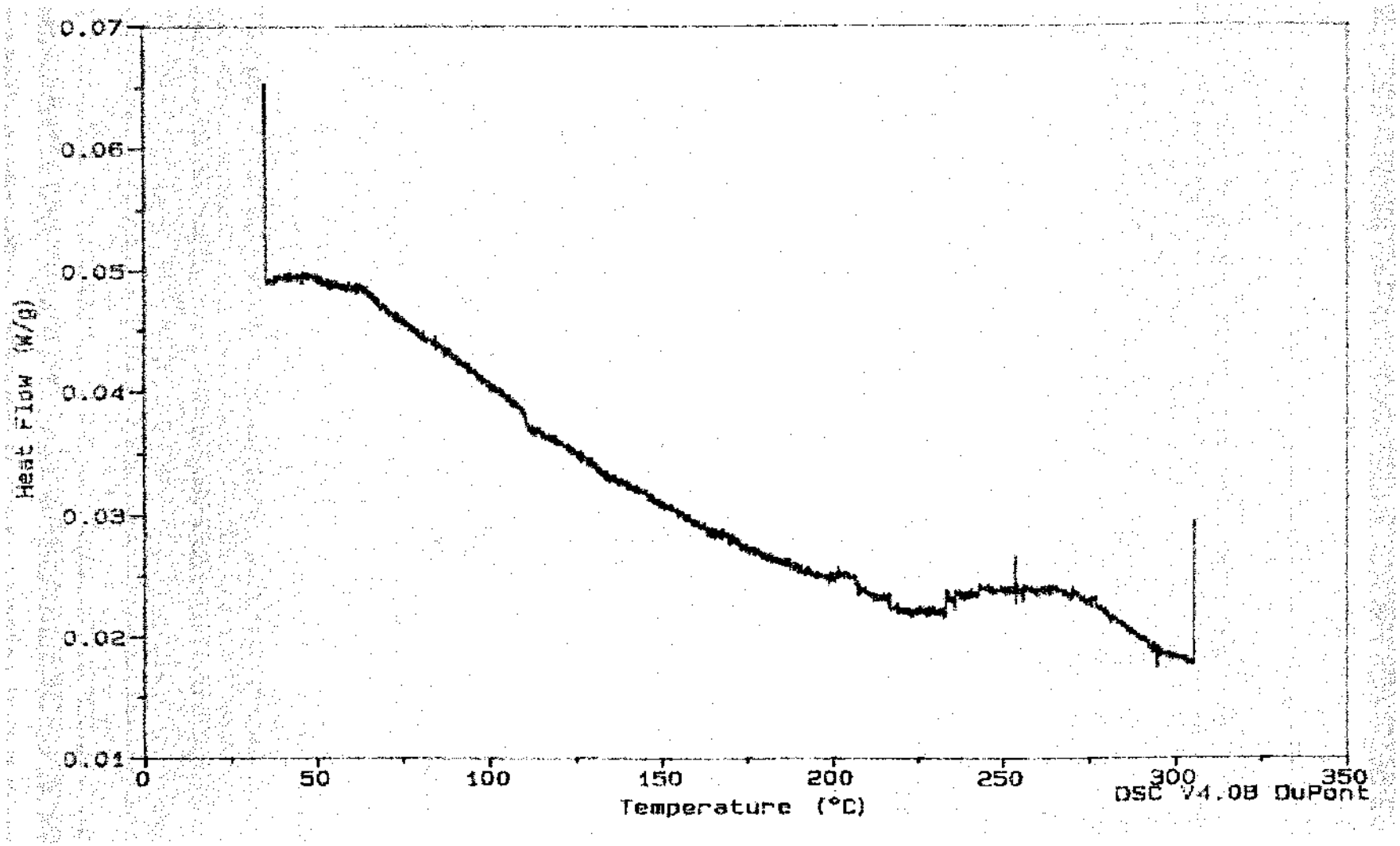

Figure E.14. DSC applied to Pittsburgh No. 8 coal tar. Heating rate 0.5 K/min.

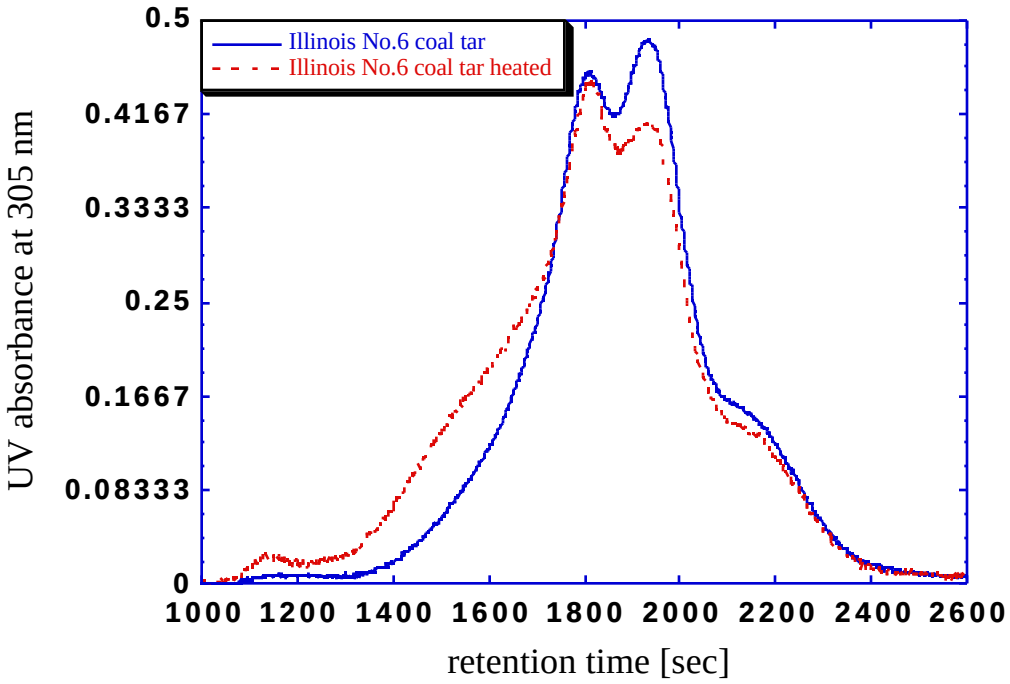

Figure E.15. Comparison of Illinois No.6 coal tar GPC chromatograms before and after heating at 200°C for 2 hours. Comparison is based on 0.2 mg of each material injected into the GPC column.

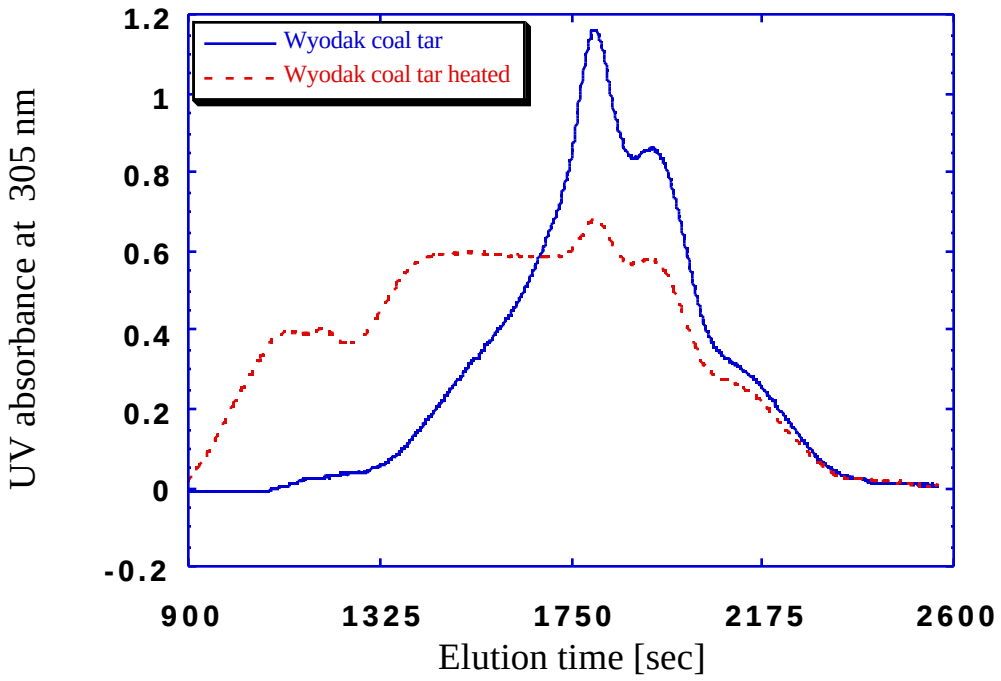

Figure E.16. Comparison of Wyodak coal tar GPC chromatograms before and after heating at 280°C for 2 hours. Comparison is based 0.5 mg of each material injected into the GPC column.

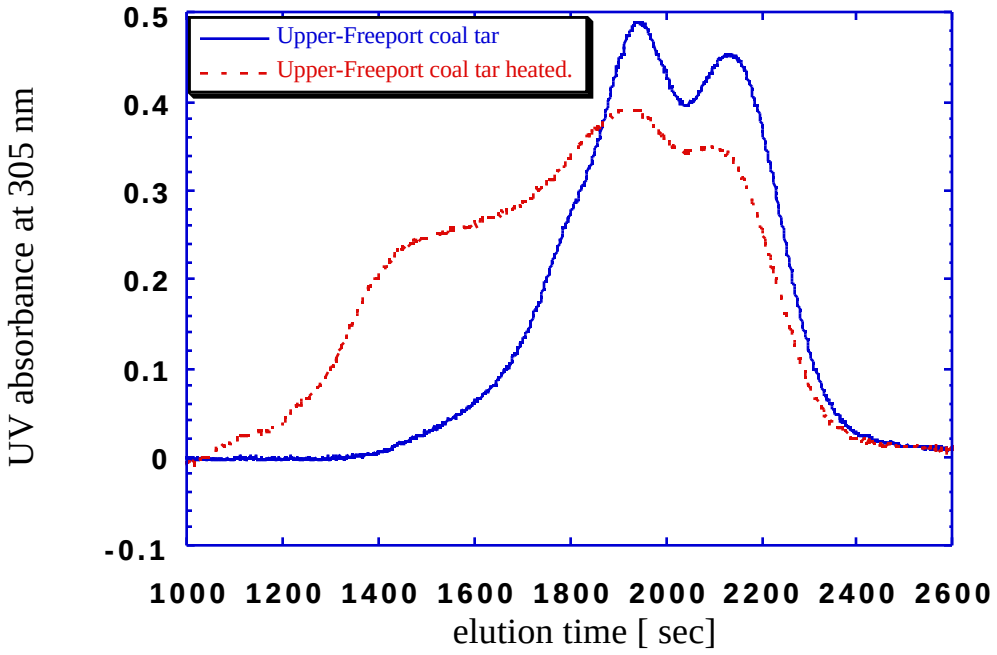

Figure E.17. Comparison of Upper-Freeport coal tar GPC chromatograms before and after heating at 280°C for 2 hours. Comparison is based on 0.2 mg each material injected into the GPC column.

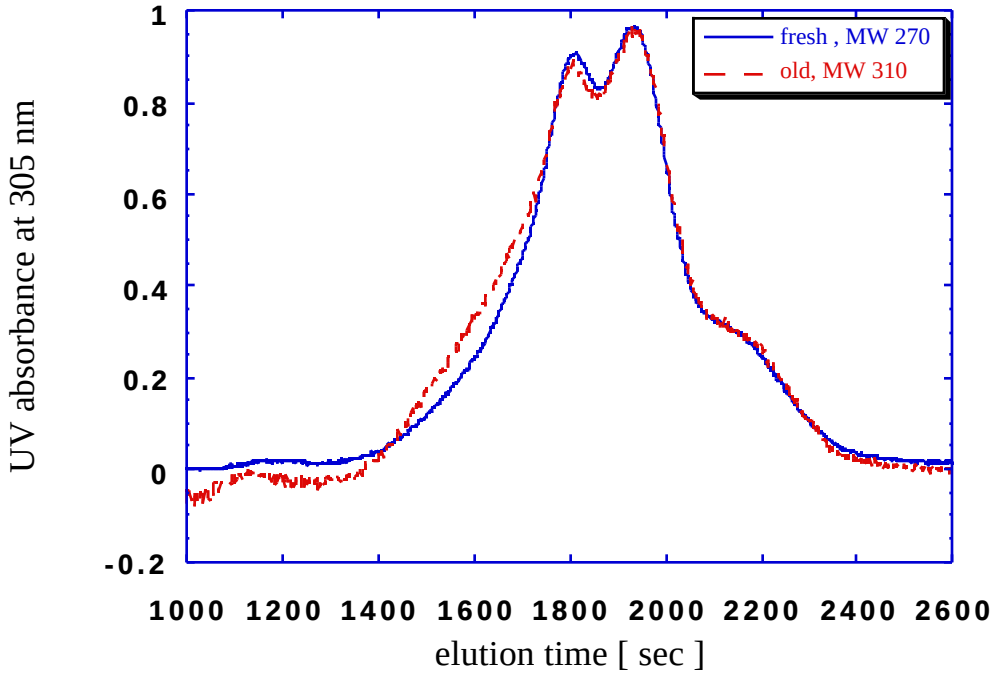

Figure E.18. Comparison of the old and fresh Illinois No.6 coal tars, GPC spectra.

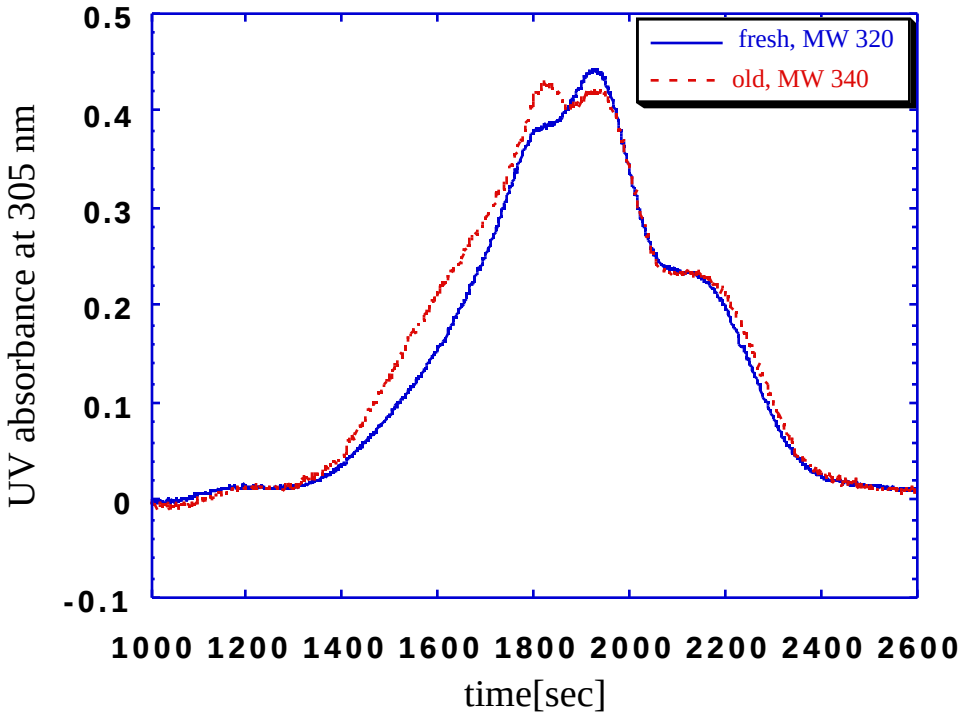

Figure E.19. Comparison of the fresh and old Pittsburgh No.8 coal tars, GPC spectra.

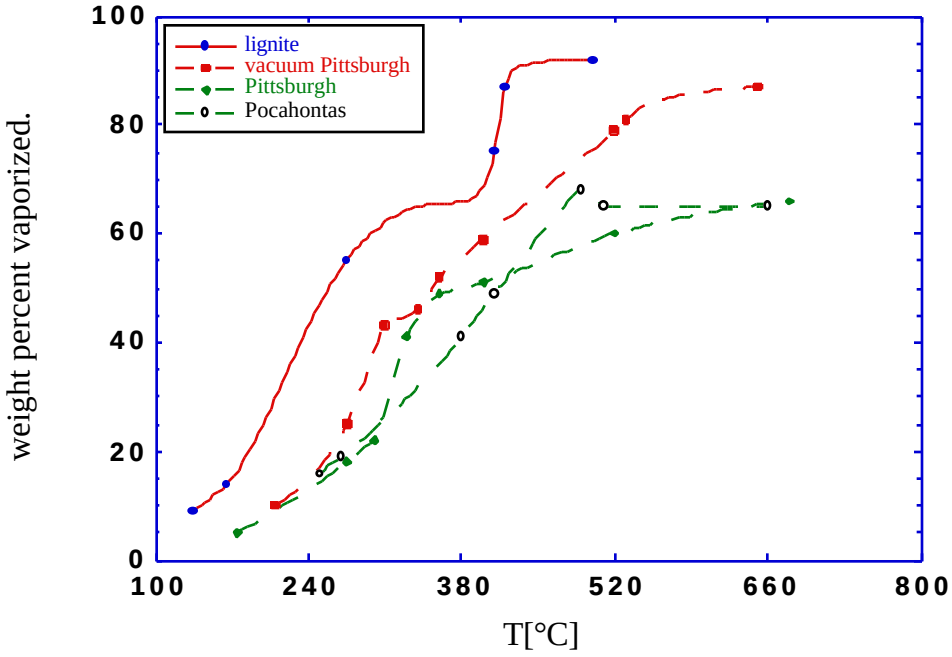

Figure E.20. Relative volatility of lignite and bituminous coal tars as a function of heated grid temperature [Freihaut et al., 1993].

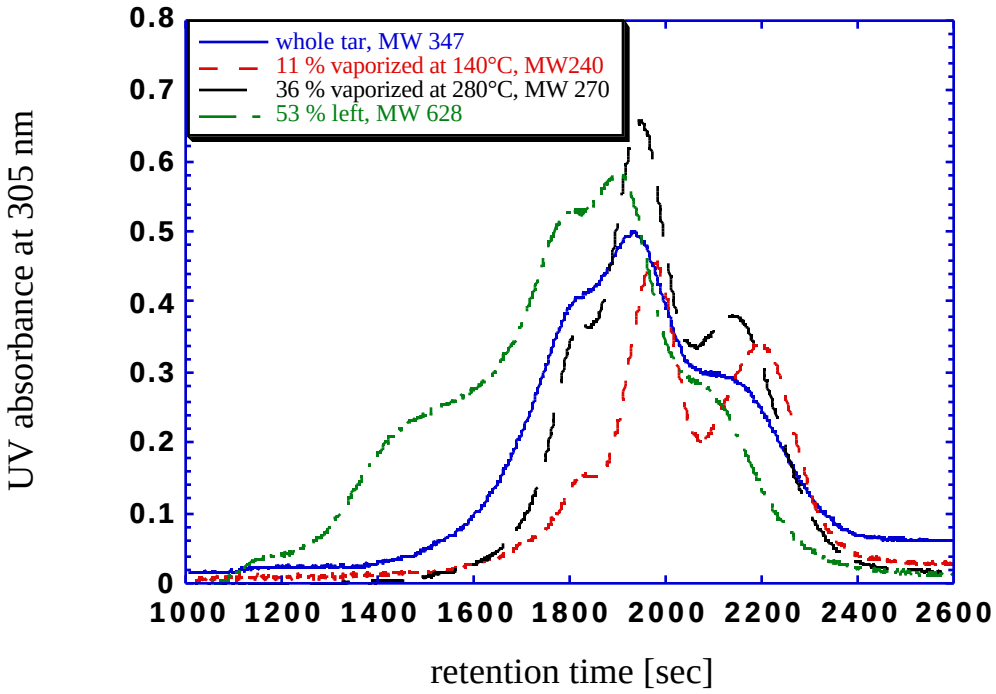

Figure E.21. GPC chromatograms for Bruceton coal tar and its fractions separated by vacuum sublimation. Comparison is made based on 0.2 mg of each material injected into the GPC column.

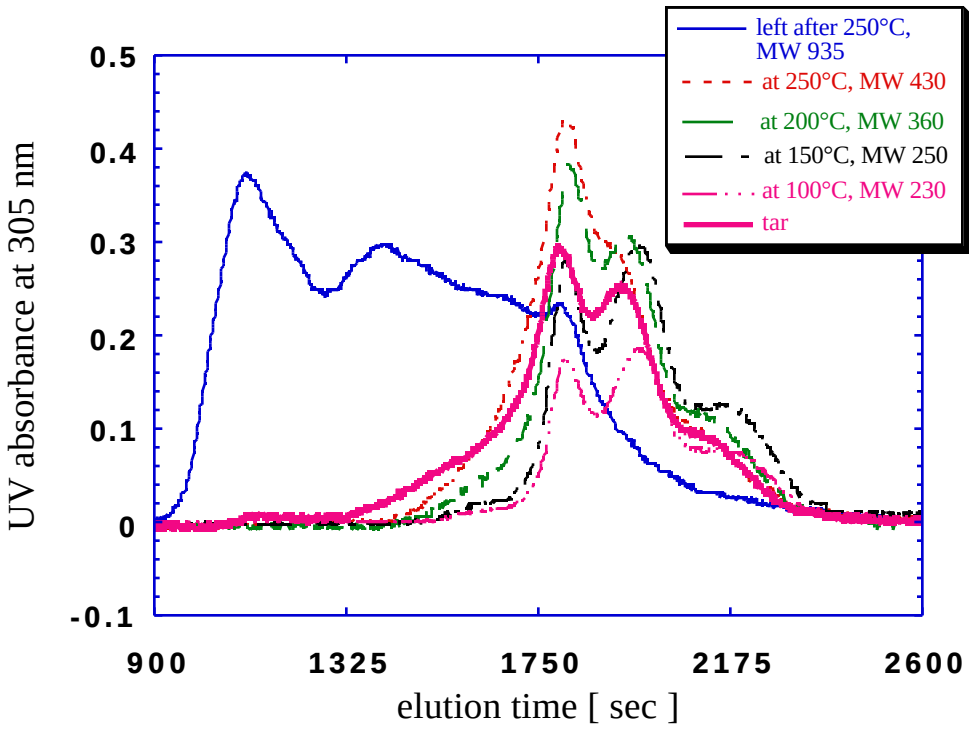

Figure E.22. GPC chromatograms for Wyodak coal tar and its fractions separated by vacuum sublimation. Comparison is made based on 0.2 mg of each material injected into the GPC column.

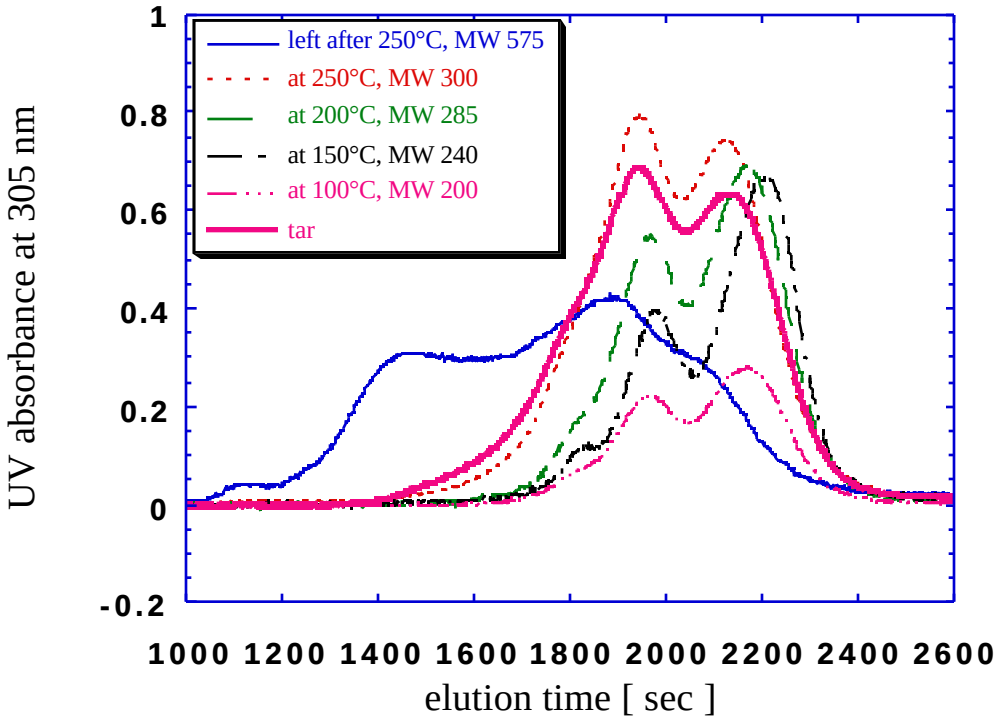

Figure E.23. GPC chromatograms for Upper-Freeport coal tar and its fractions separated by vacuum sublimation. Comparison is made based on 0.2 mg of each material injected into the GPC column.

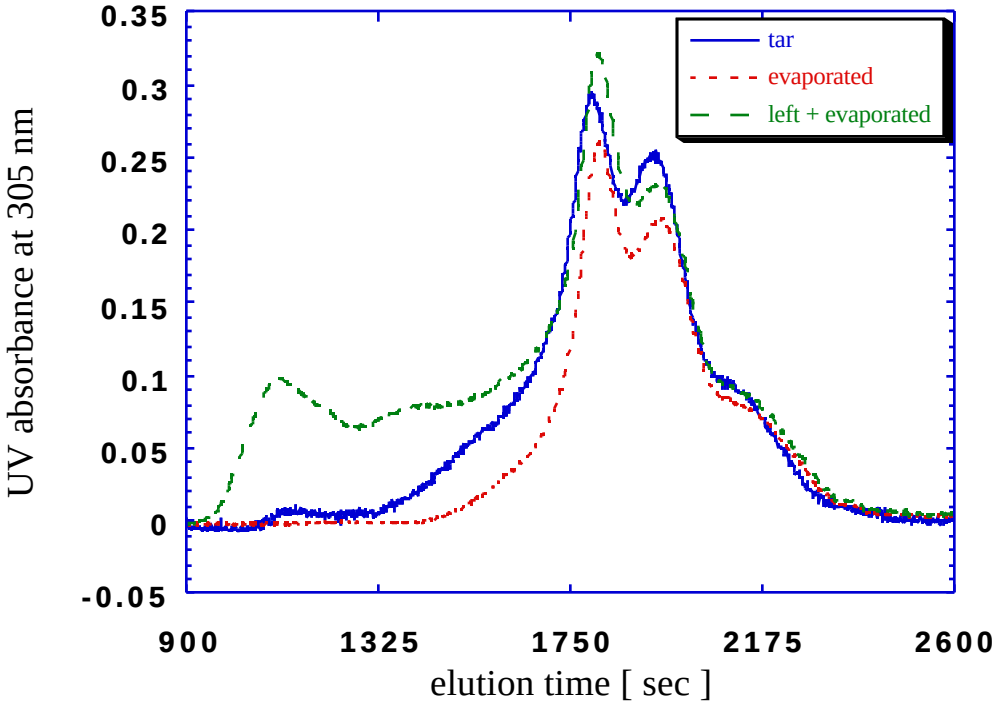

Figure E.24. Reconstruction of the GPC spectra for Wyodak coal tar by summing the contributions of tar vacuum sublimation fractions.

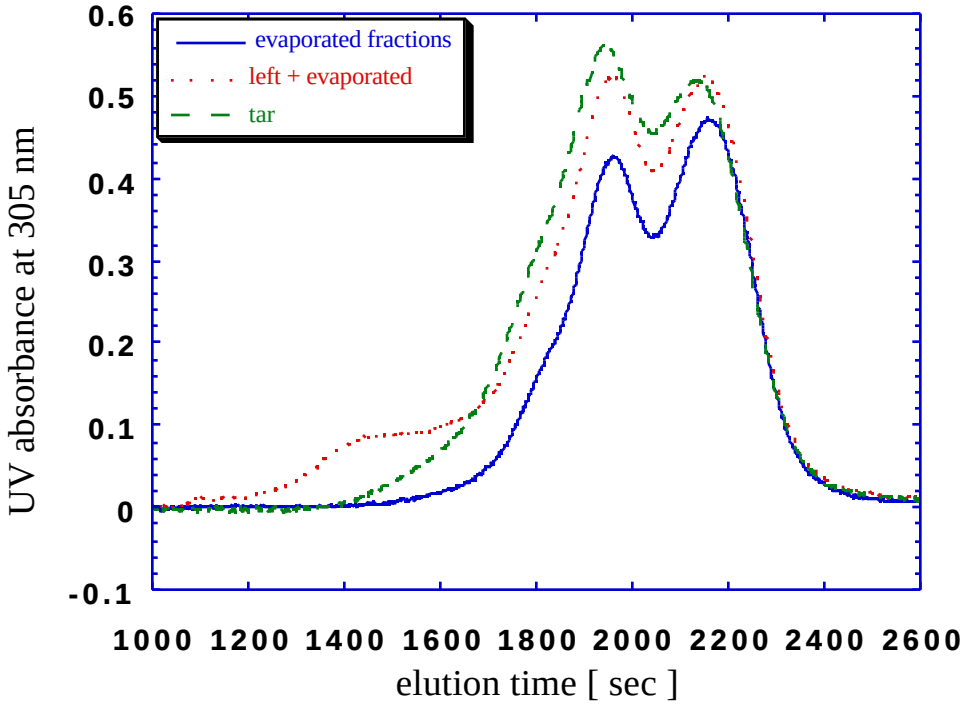

Figure E.25. Reconstruction of the GPC spectra for Upper-Freeport coal tar by summing the contributions of tar vacuum sublimation fractions.

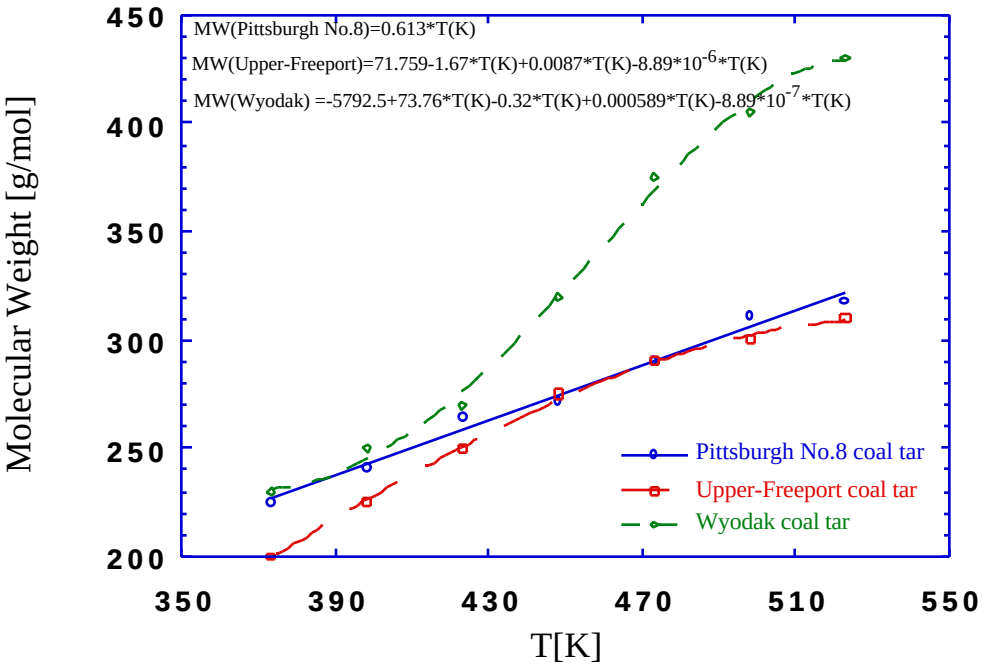

Figure E.26. Vapor phase molecular weight dependence on effusion temperature.

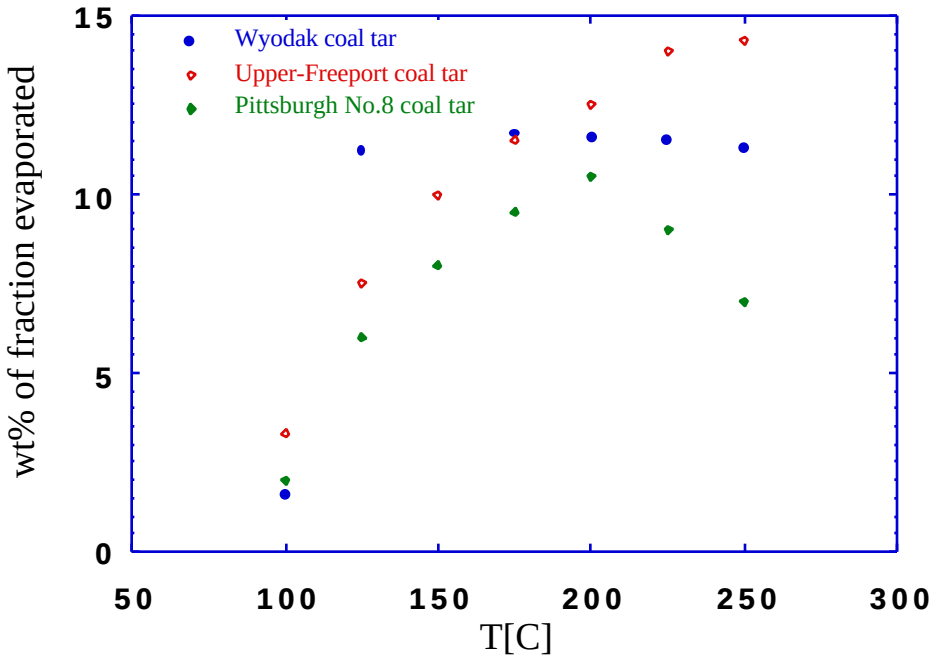

Figure E.27. Mass percents of evaporated fractions as a function of evaporation temperature.

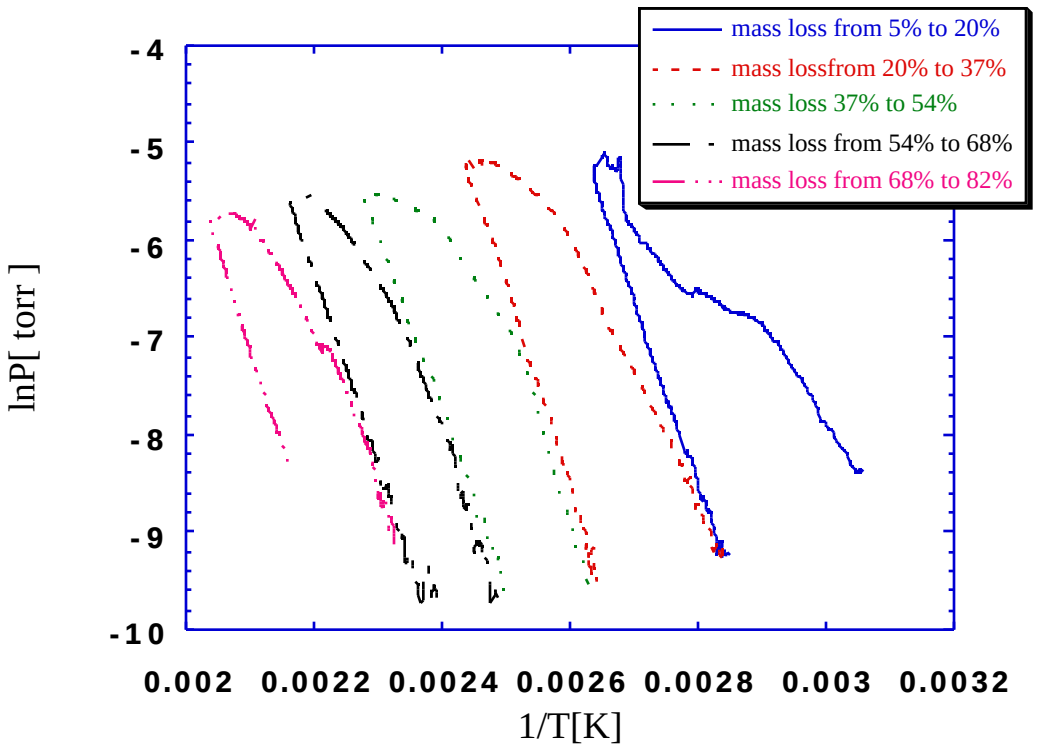

Figure E.28. The non-isothermal Knudsen effusion method applied to whole Bruceton coal tar.

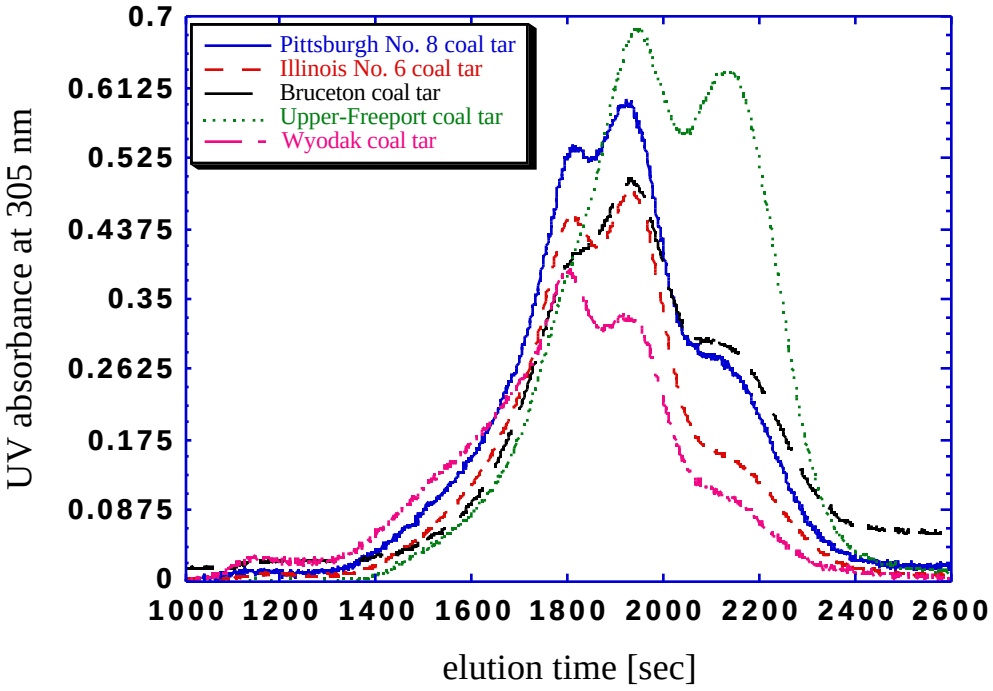

Figure E.29. GPC chromatograms for various coal tars studied. Comparison is based on 0.2 mg of each material injected into the GPC column.

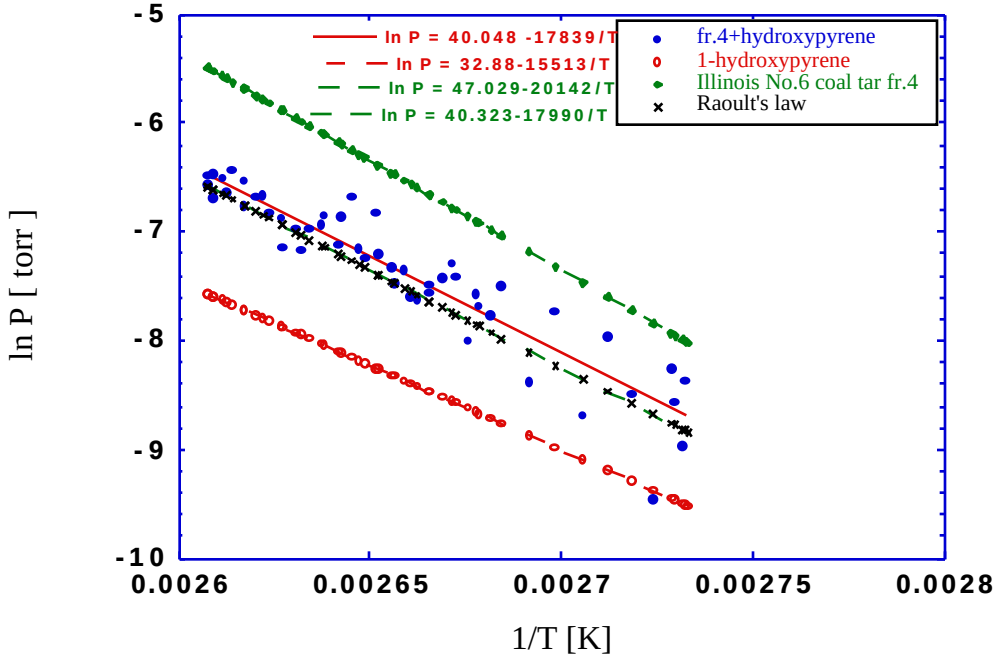

Figure E.30. Effusion method applied to a mixture of Illinois No.6 coal tar GPC fraction 4 (50%) and 1-hydroxypyrene (balance).

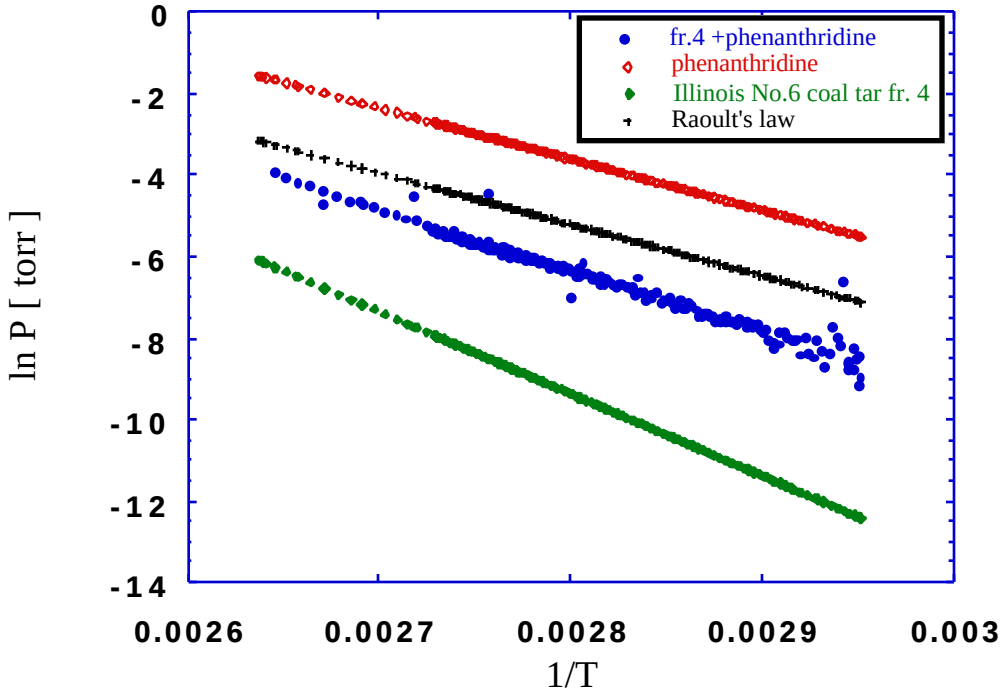

Figure E.31. Effusion method applied to a mixture of Illinois No.6 coal tar GPC fraction 4 (65%) and phenanthridine (balance).

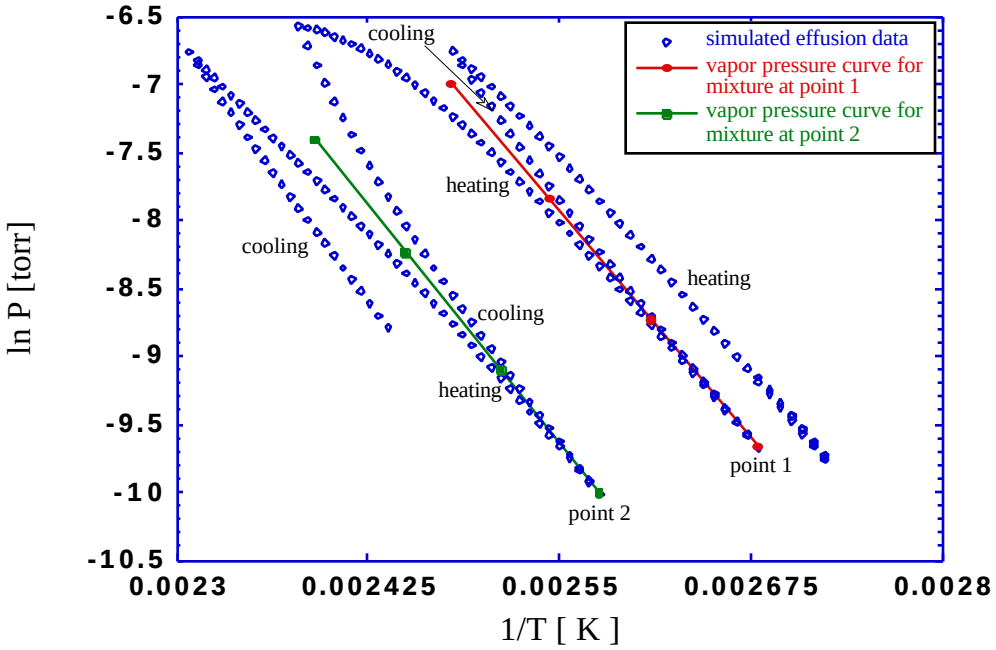

Figure E.32. Simulated vapor pressure experiment. Open points are simulated effusion data. Solid points show the vapor pressure curve for mixture left after each cool-down cycle.

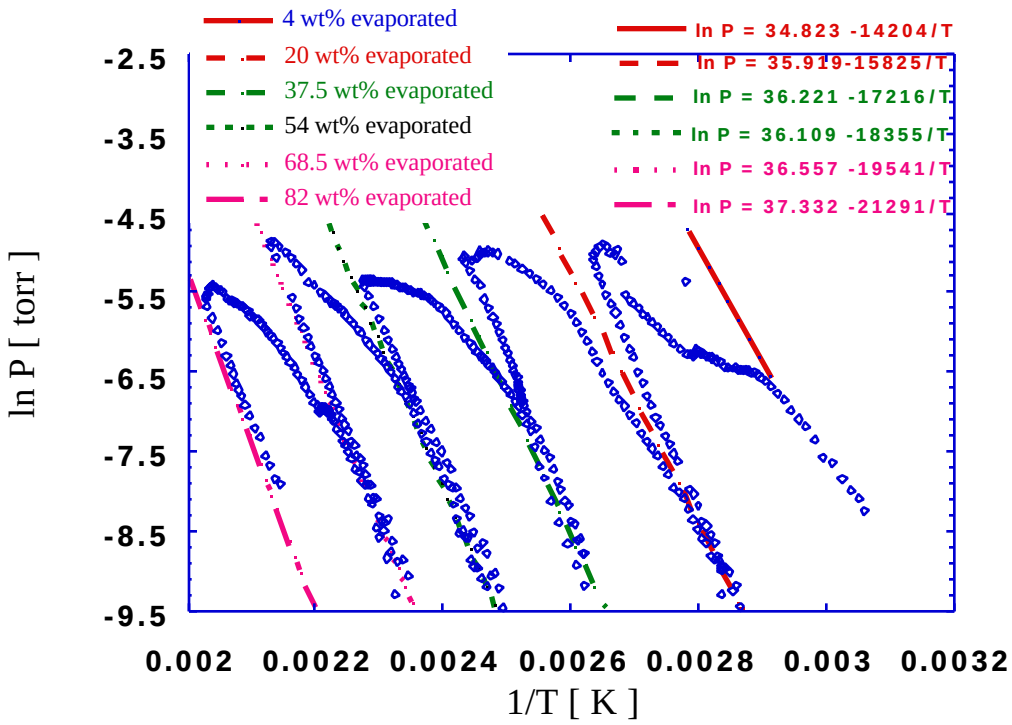

Figure E.33. Raw vapor pressure data for Bruceton coal tar produced in the fluidized bed reactor.

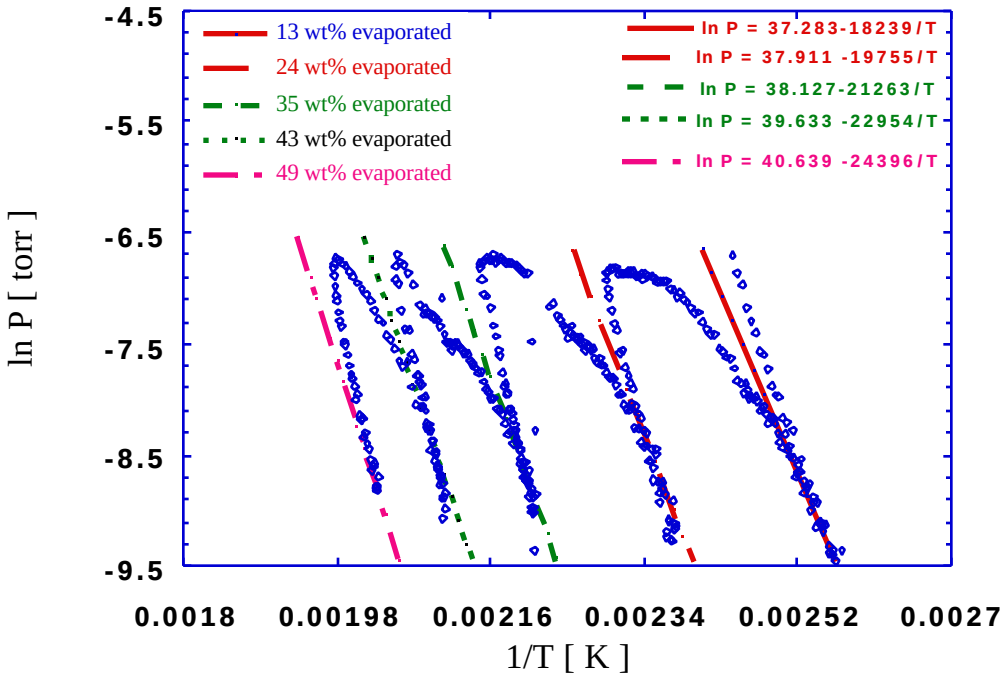

Figure E.34. Raw vapor pressure data for Pittsburgh No.8 coal tar produced in the wire mesh reactor.

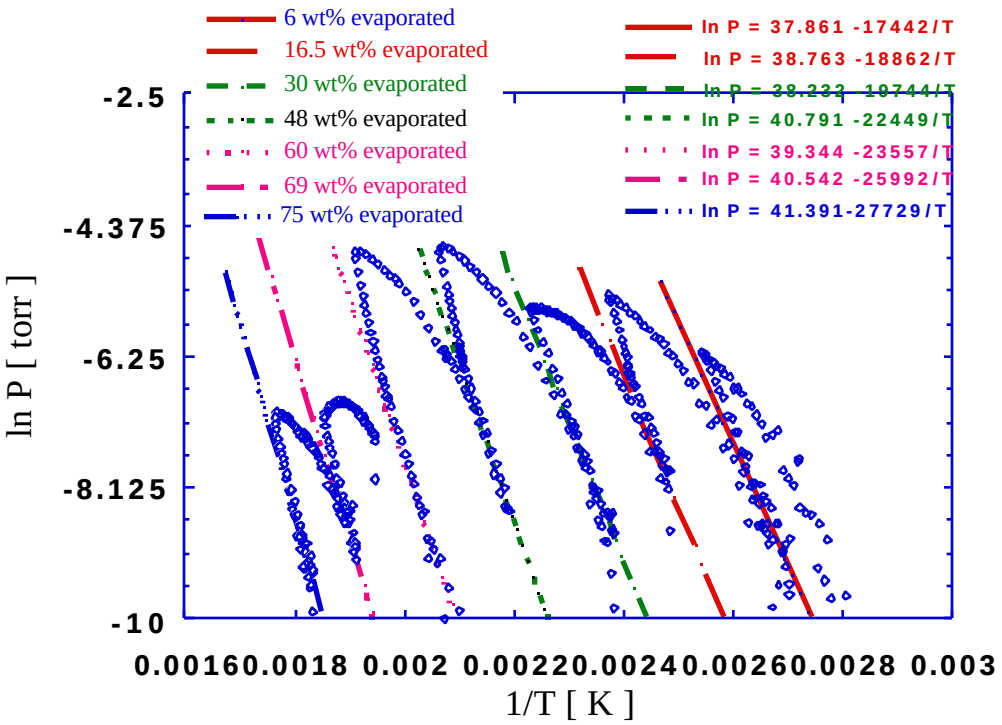

Figure E.35. Raw vapor pressure data for Pittsburgh No.8 coal tar produced in the tubular reactor.

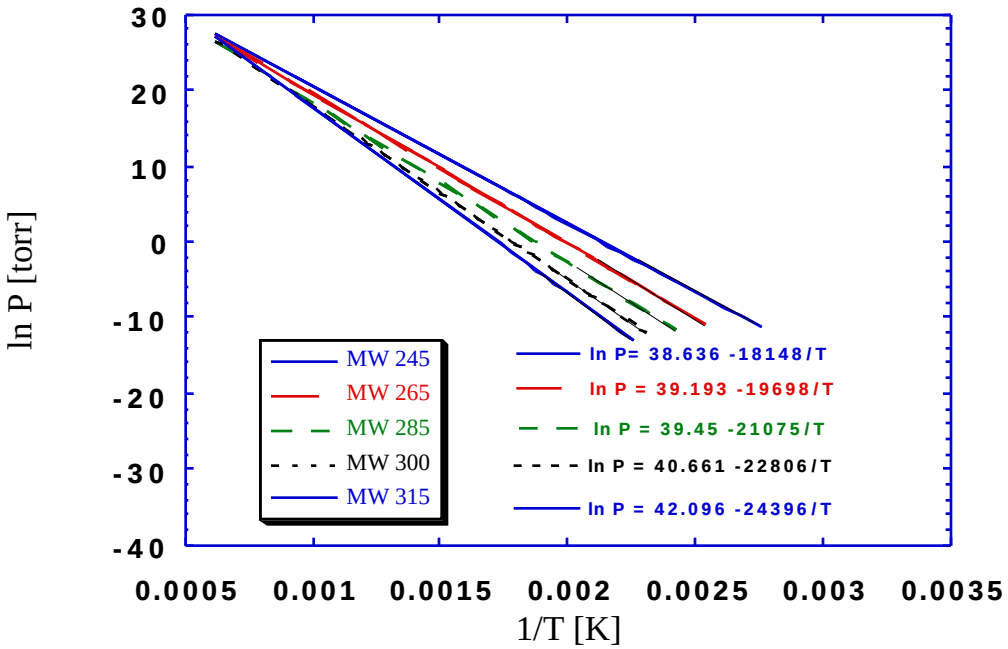

Figure E.36. The vapor pressure curves for Pittsburgh No.8 wire mesh coal tar. The heavier portion of the curves indicates the actual range of temperatures over which the data were obtained.

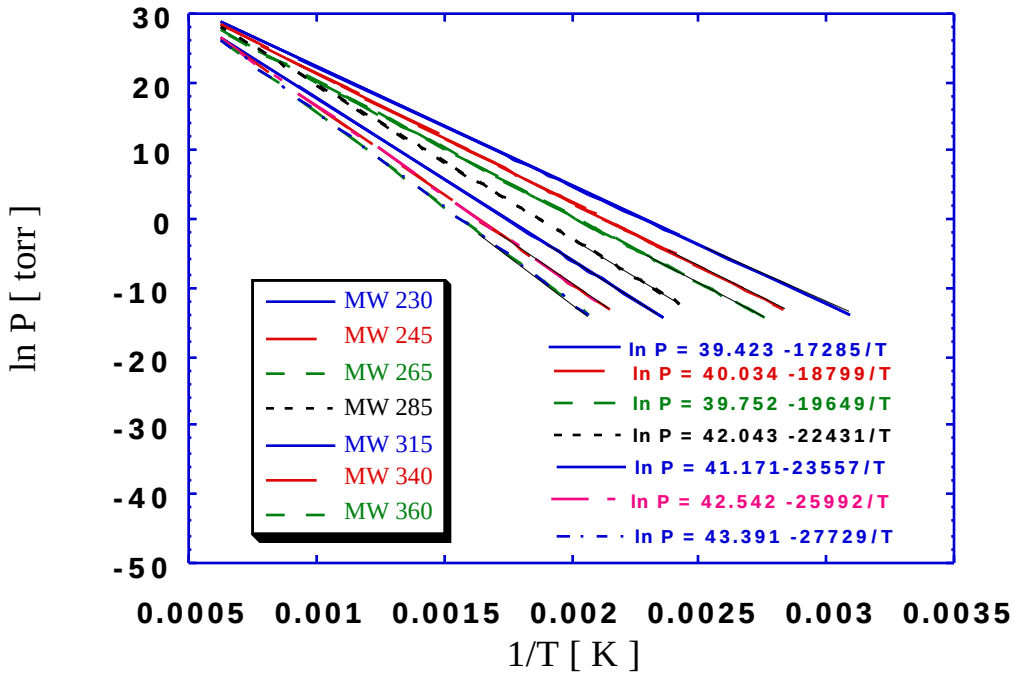

Figure E.37. The vapor pressure curves for Pittsburgh No.8 tubular reactor coal tar. The heavier portion of the curves indicates the actual range of temperatures over which the data were obtained.

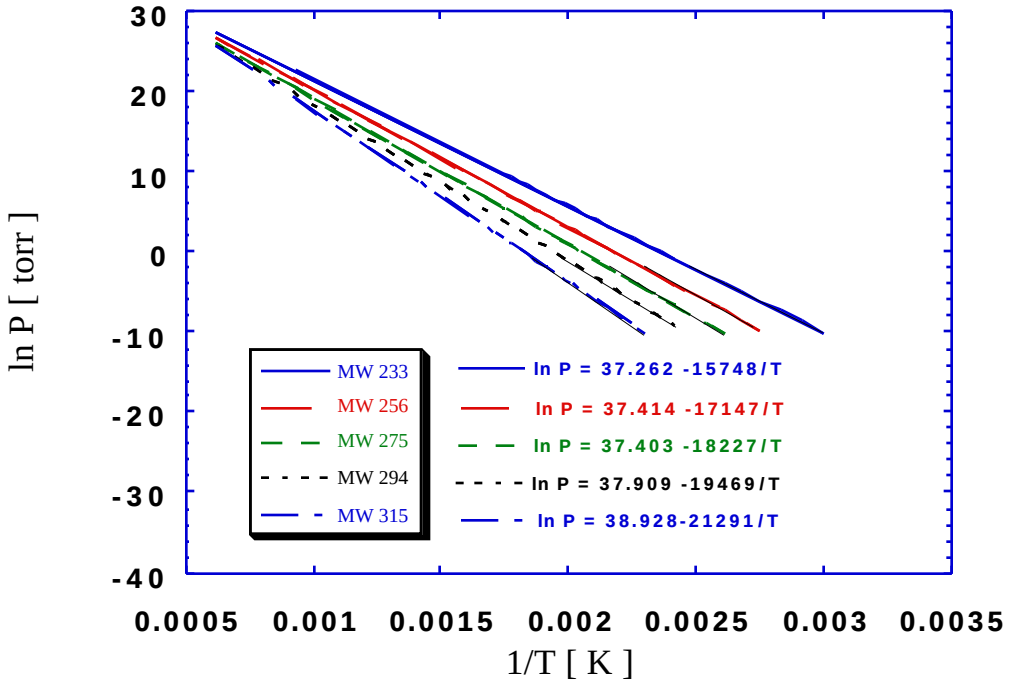

Figure E.38. The vapor pressure curves for Bruceton coal tar. The heavier portion of the curves indicates the actual range of the temperatures over which the data were obtained.

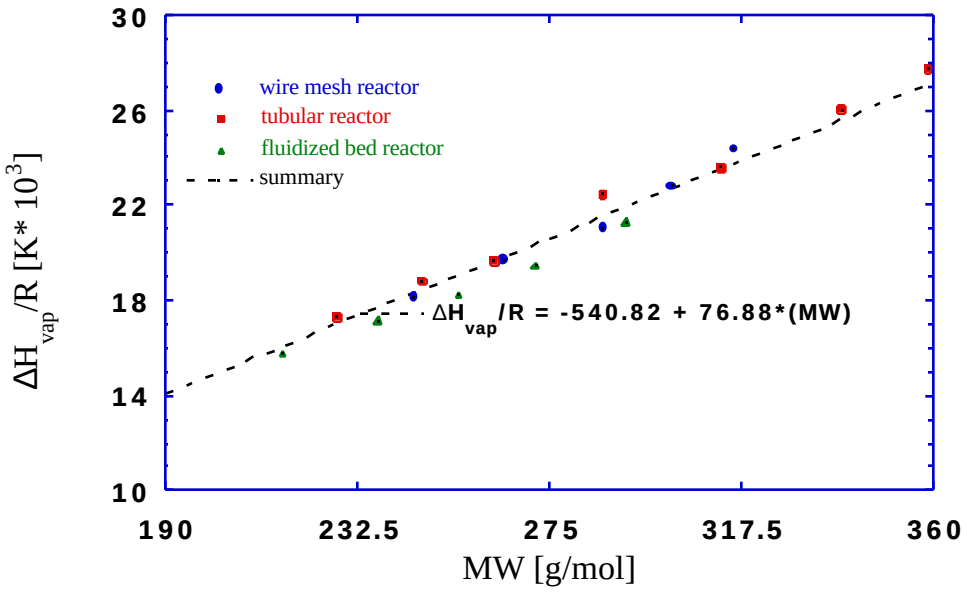

Figure E.39. Vaporization enthalpy as a function of molecular weight for Pittsburgh Seam coal tars.

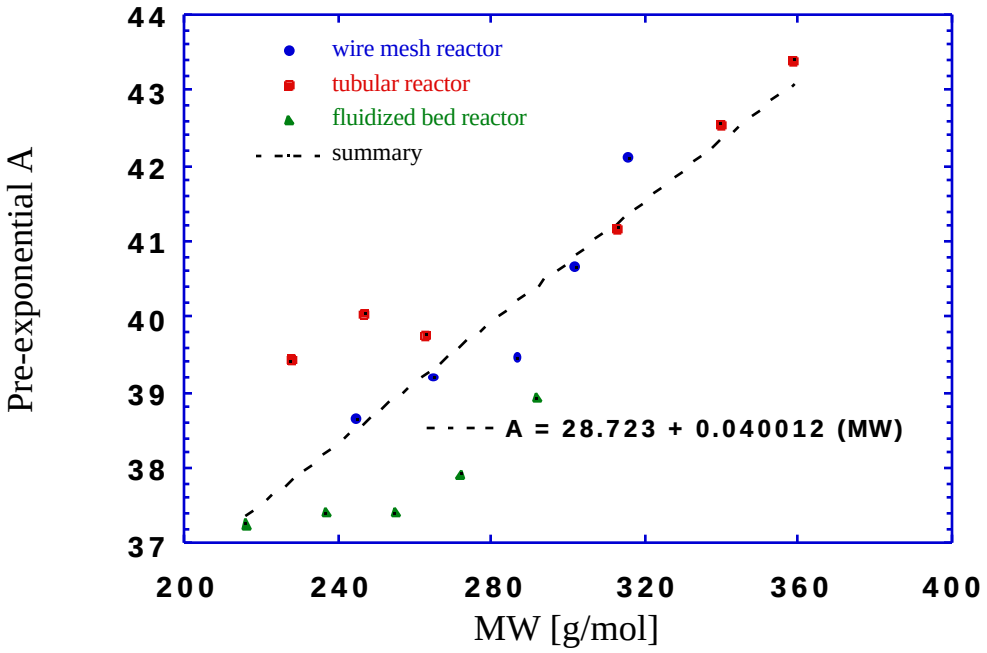

Figure E.40. The pre-exponential (A) as a function of molecular weight for Pittsburgh Seam coal tars.

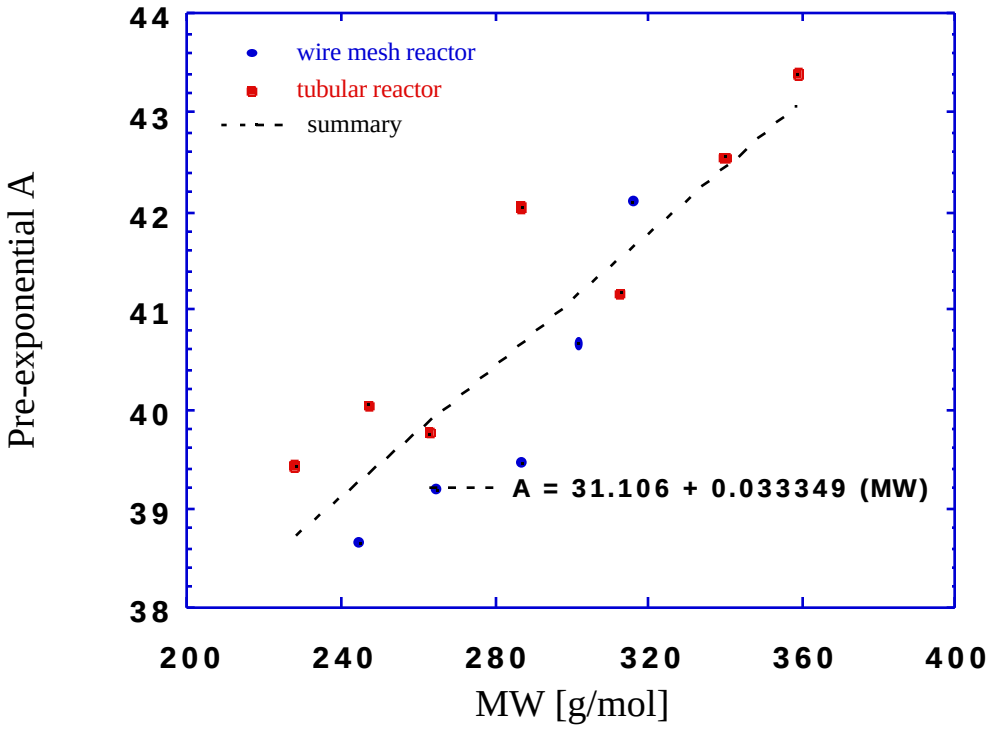

Figure E.40a. The pre-exponential (A) as a function of molecular weight for Pittsburgh No.8 coal tars, excluding fluidized bed data.

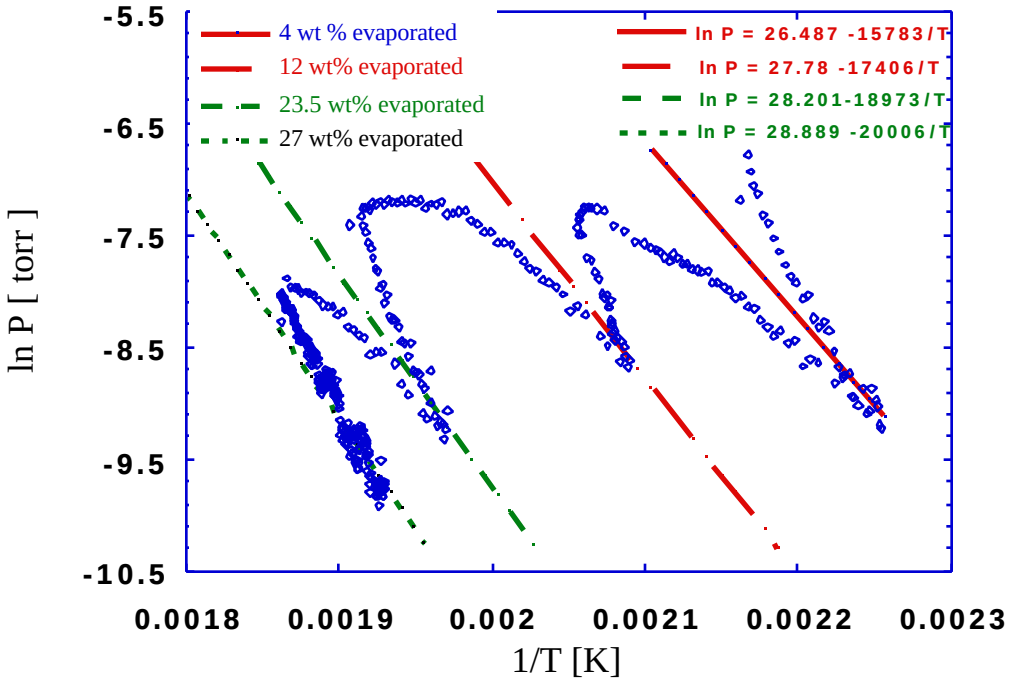

Figure E.41. Raw data for Pittsburgh No.8 coal tar fraction 1 separated by preparative GPC.

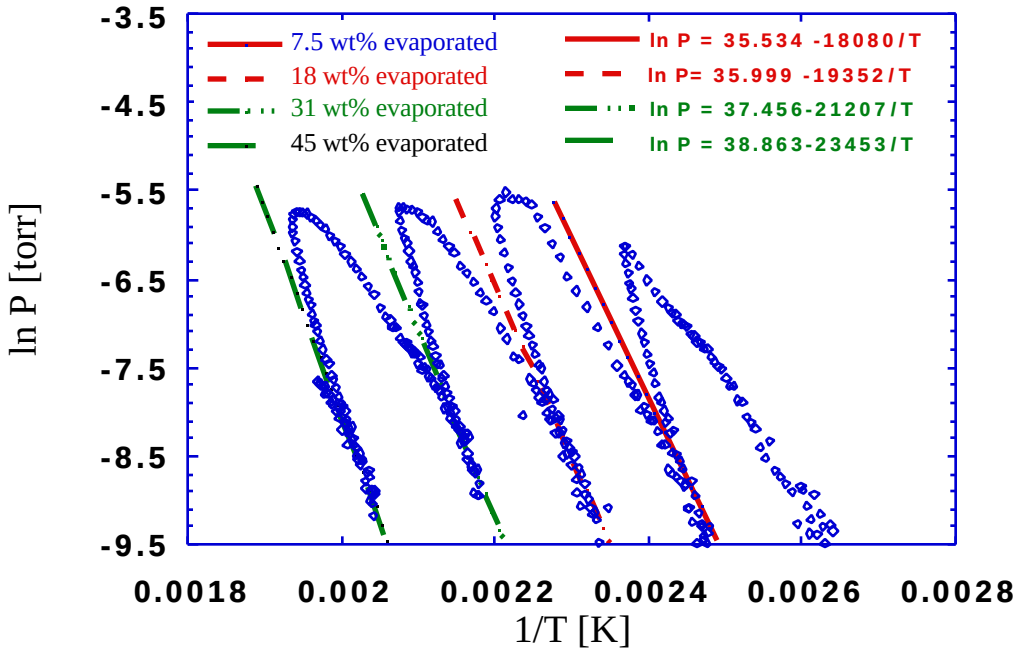

Figure E.42. Raw data for Pittsburgh No.8 coal tar fraction 2 separated by preparative GPC.

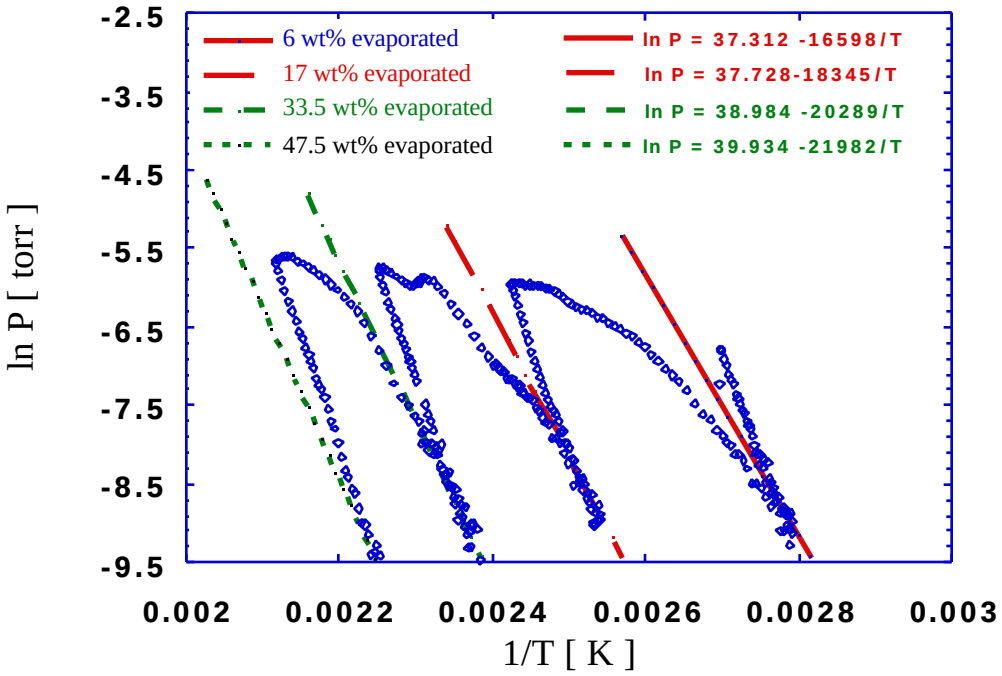

Figure E.43. Raw data for Pittsburgh No.8 coal tar fraction 3 separated by preparative GPC.

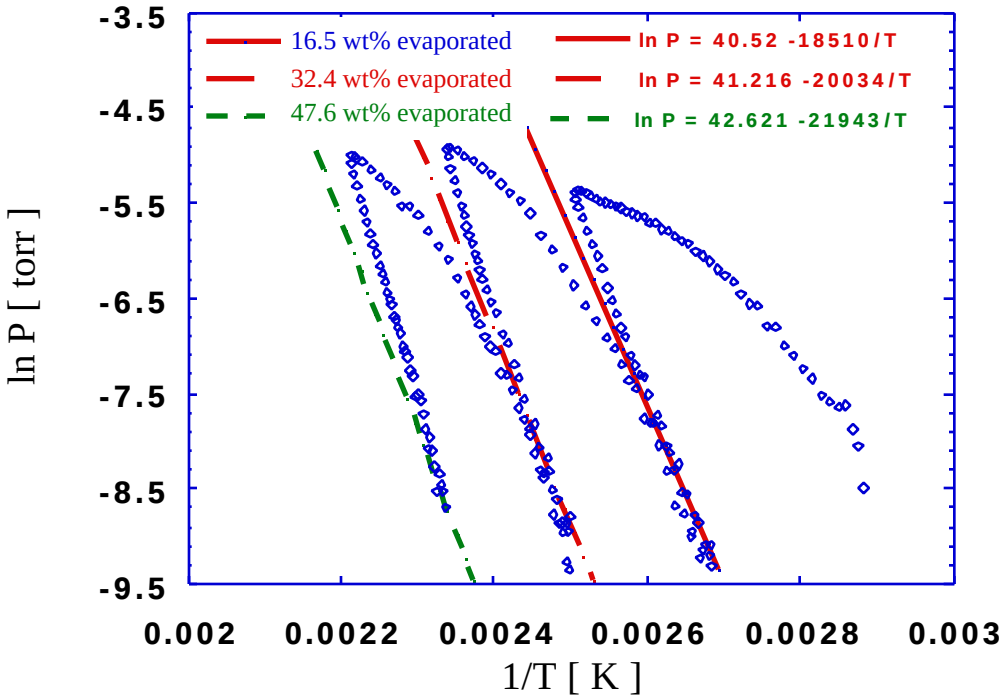

Figure E.44. Raw data for Pittsburgh No.8 coal tar fraction 4 separated by preparative GPC.

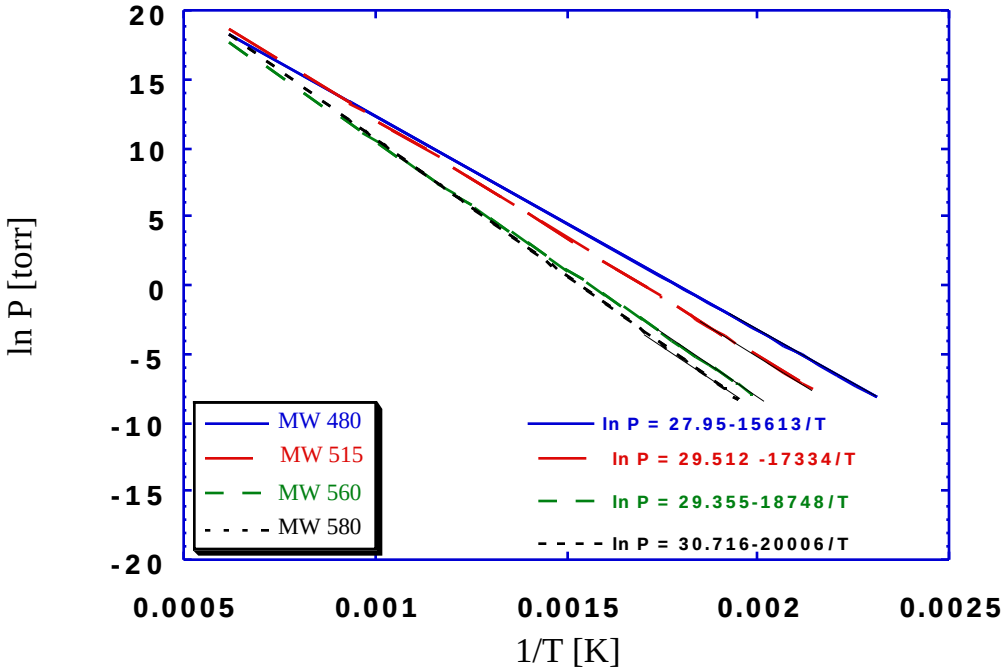

Figure E.45. The vapor pressure curves for Pittsburgh No.8 coal tar fraction 1 separated by preparative GPC. The heavier portions of the curves indicate the actual range of temperatures over which the data were obtained.

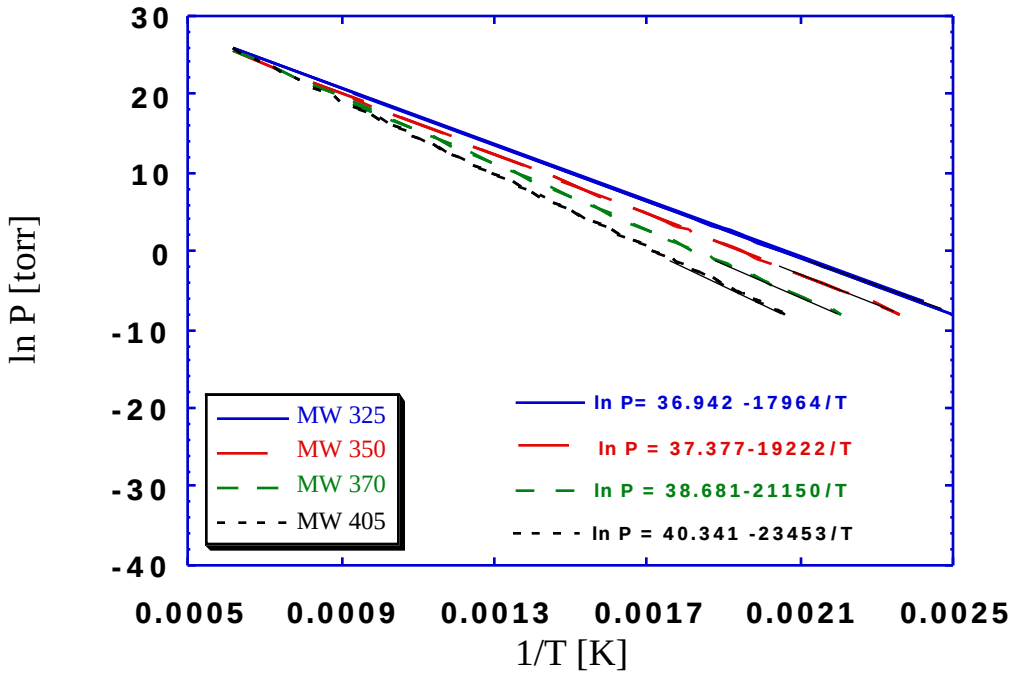

Figure E.46. The vapor pressure curves for Pittsburgh No.8 coal tar fraction 2 separated by preparative GPC. The heavier portions of the curves indicate the actual range of temperatures over which the data were obtained.

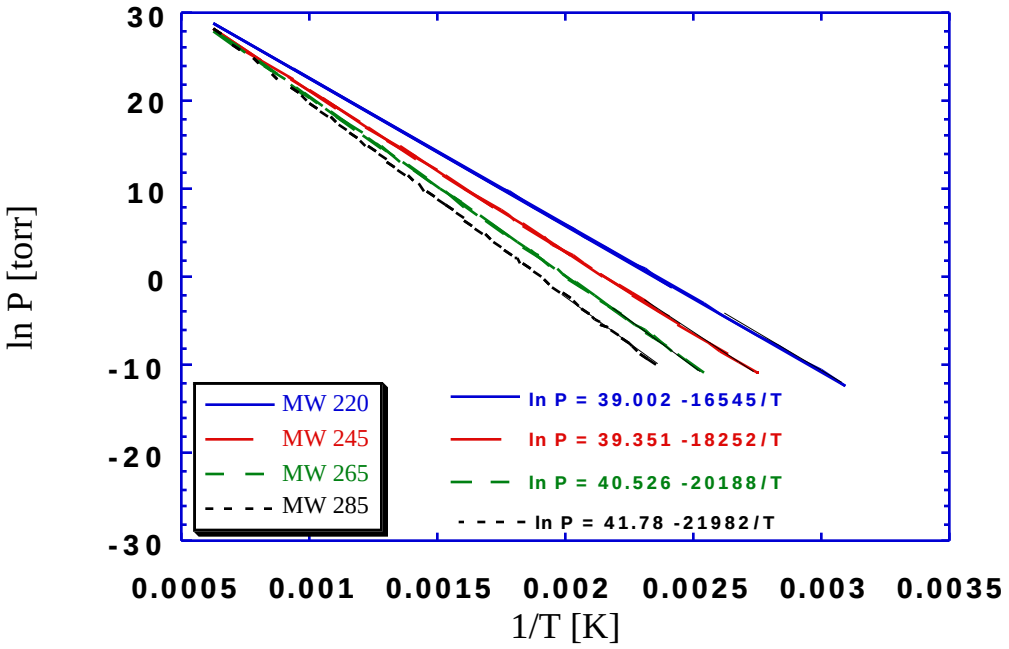

Figure E.47. The vapor pressure curves for Pittsburgh No.8 coal tar fraction 3 separated by GPC. The heavier portions of the curves indicate the actual range of temperatures over which the data were obtained.

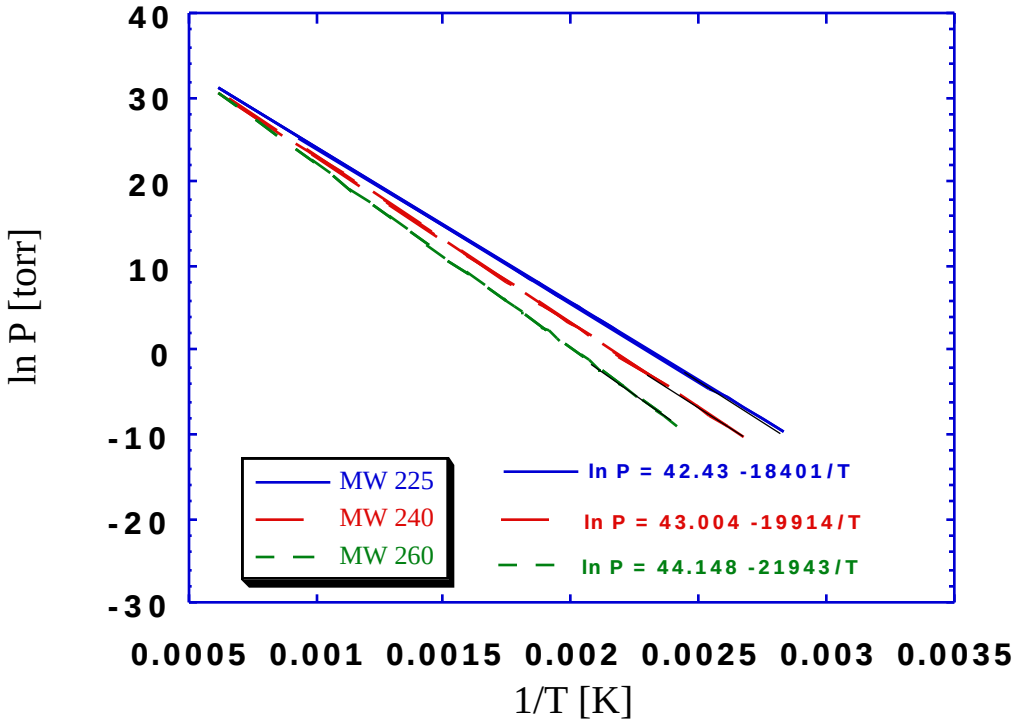

Figure E.48. The vapor pressure curves for Pittsburgh No.8 coal tar fraction 4 separated by GPC. The heavier portions of the curves indicate the actual range of temperatures over which the data were obtained.

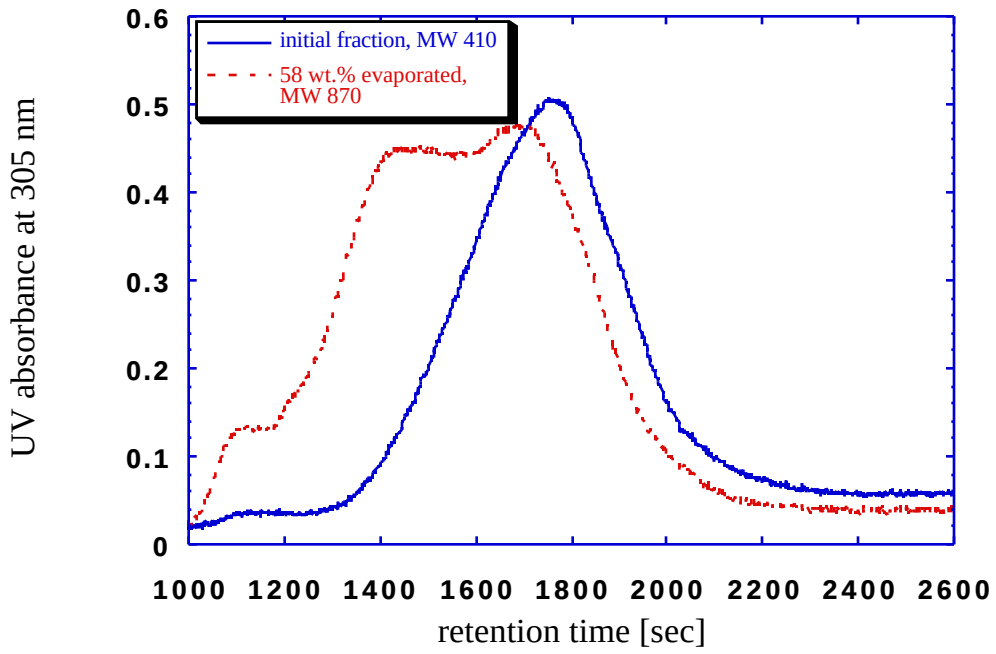

Figure E.49a. Comparison of Pittsburgh No.8 coal tar fraction 2 GPC chromatograms before and after effusion. Comparison is based on the same signal height.

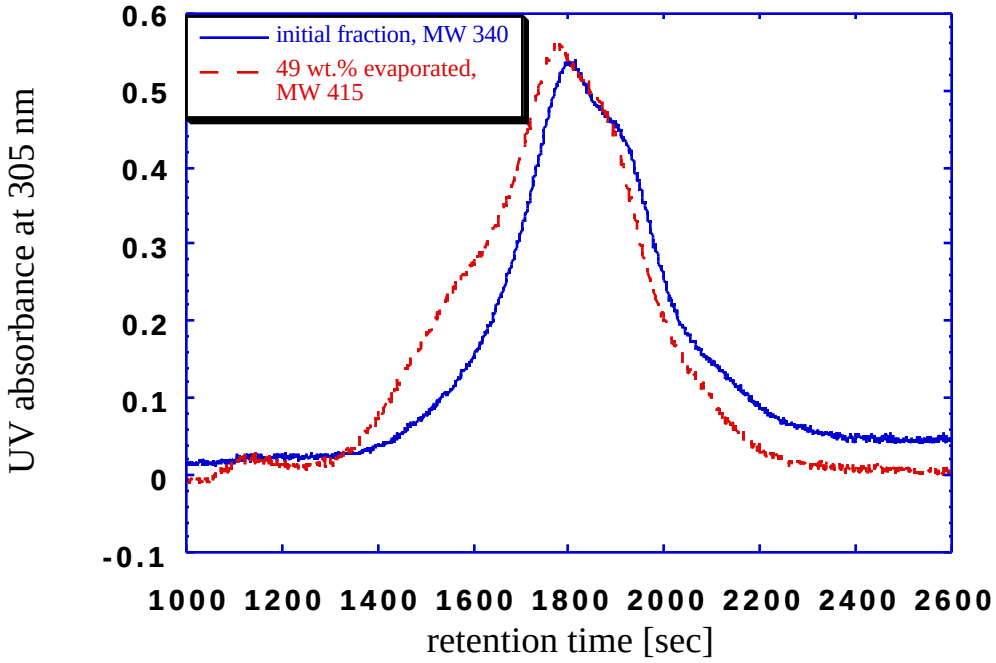

Figure E.49b. Comparison of Pittsburgh No.8 coal tar fraction 3 GPC chromatograms before and after effusion. Comparison is based on the same signal height.

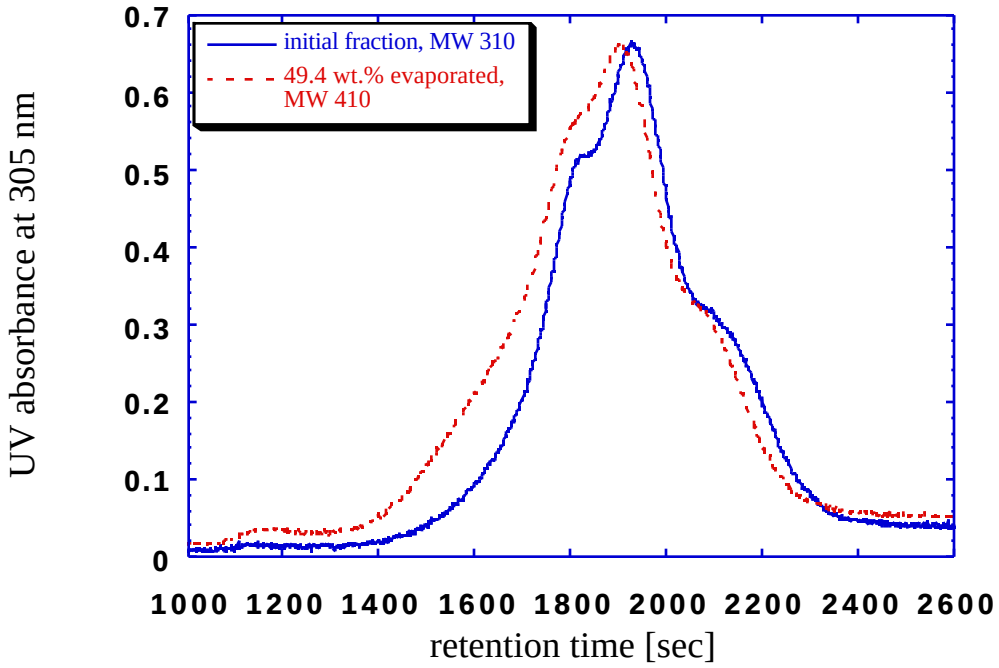

Figure E.49c. Comparison of Pittsburgh No.8 coal tar fraction 4 GPC chromatograms before and after effusion. Comparison is based on the same signal height.

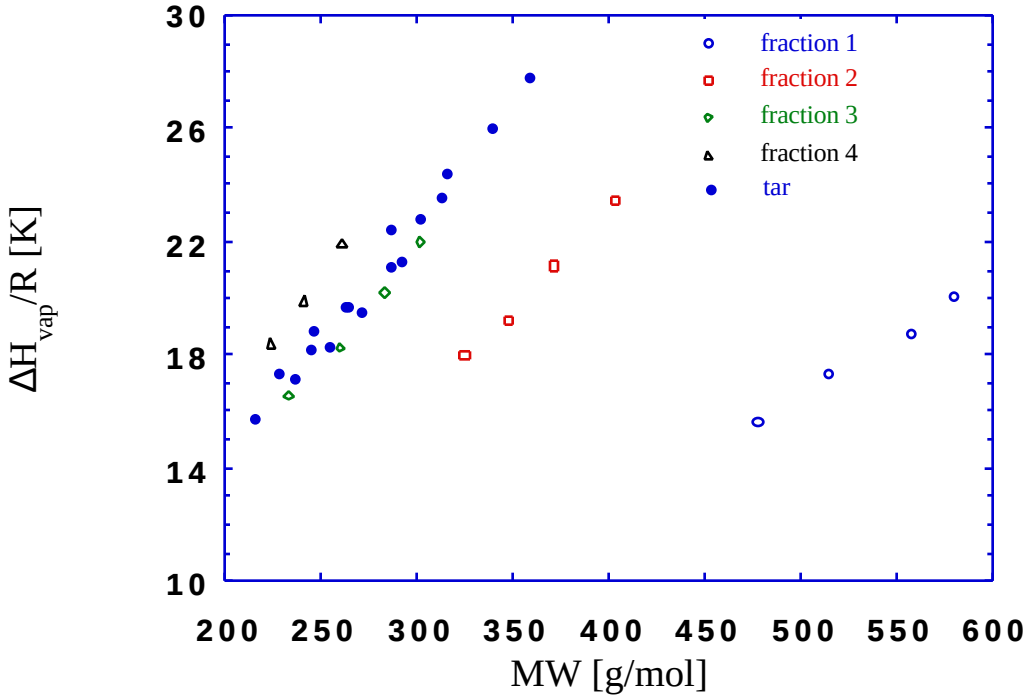

Figure E.50. Vaporization enthalpy as a function of molecular weight for Pittsburgh No.8 coal tar GPC fractions.

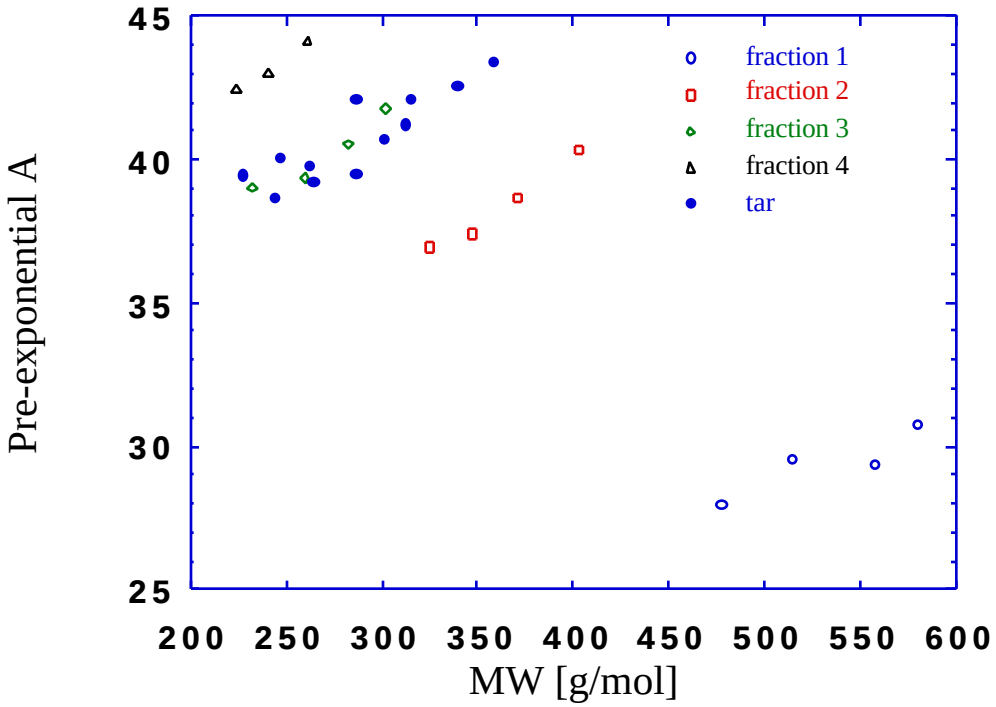

Figure E.51. The pre-exponential as a function of molecular weight for Pittsburgh No.8 coal tar GPC fractions.

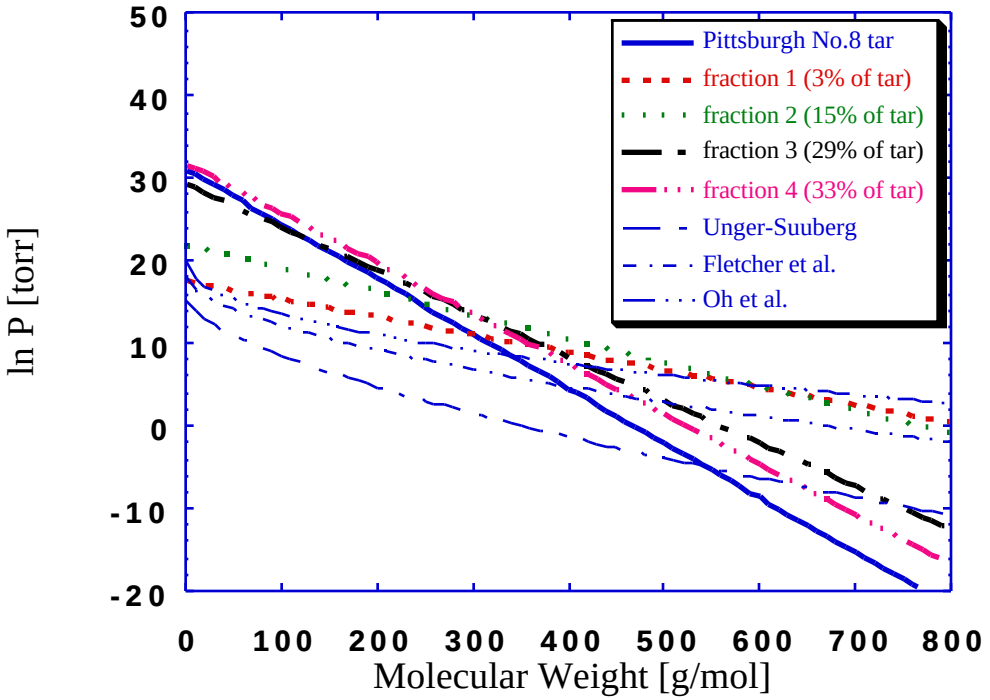

Figure E.52a. The vapor pressure correlation curves for Pittsburgh No.8 coal tar and GPC fractions at 500°C. The Unger-Suuberg [1985], Fletcher et al. [1992] and Oh et al. [1989] correlations are shown for comparison.

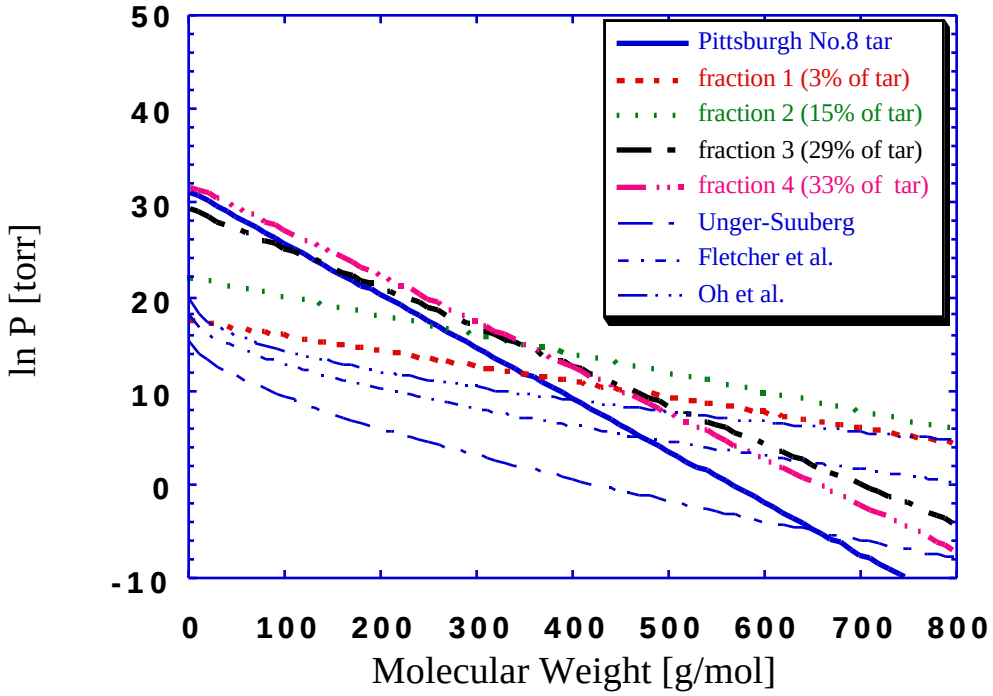

Figure E.52b. The vapor pressure correlation curves for Pittsburgh No.8 coal tar and GPC fractions at 600°C. The Unger-Suuberg [1985], Fletcher et al. [1992] and Oh et al. [1989] correlations are shown for comparison.

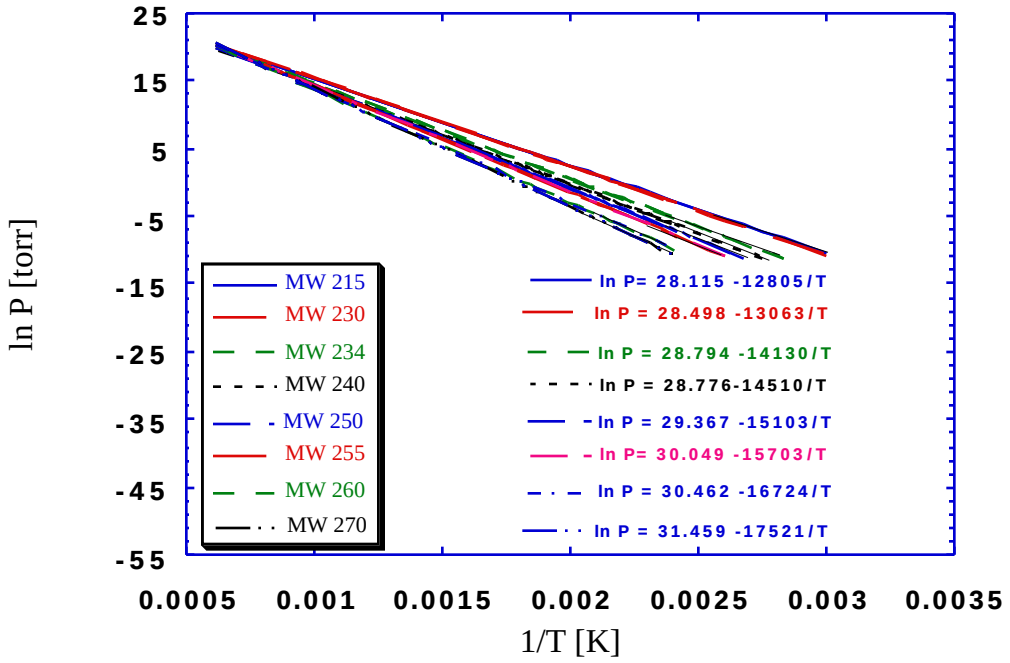

Figure E.53. The vapor pressure curves for Upper-Freeport coal tar produced in the wire mesh reactor. The heavier portions of the curves indicate the actual range of temperatures over which the data were obtained.

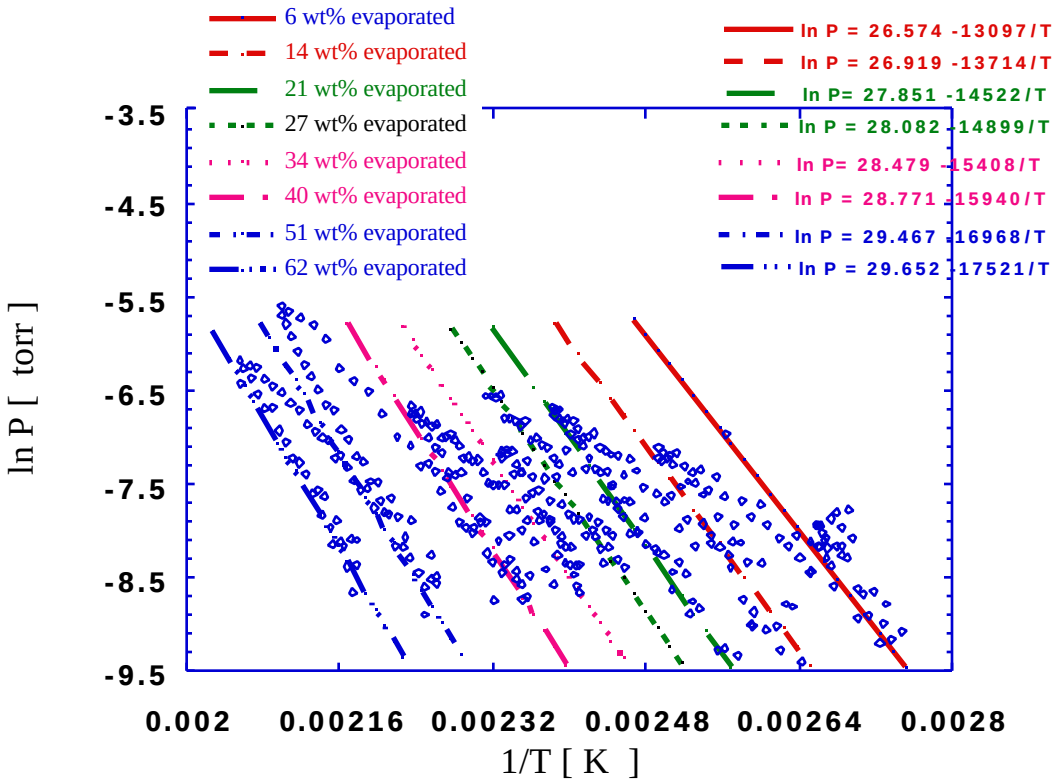

Figure E.54. Raw data for Upper-Freeport coal tar produced in the wire mesh reactor.

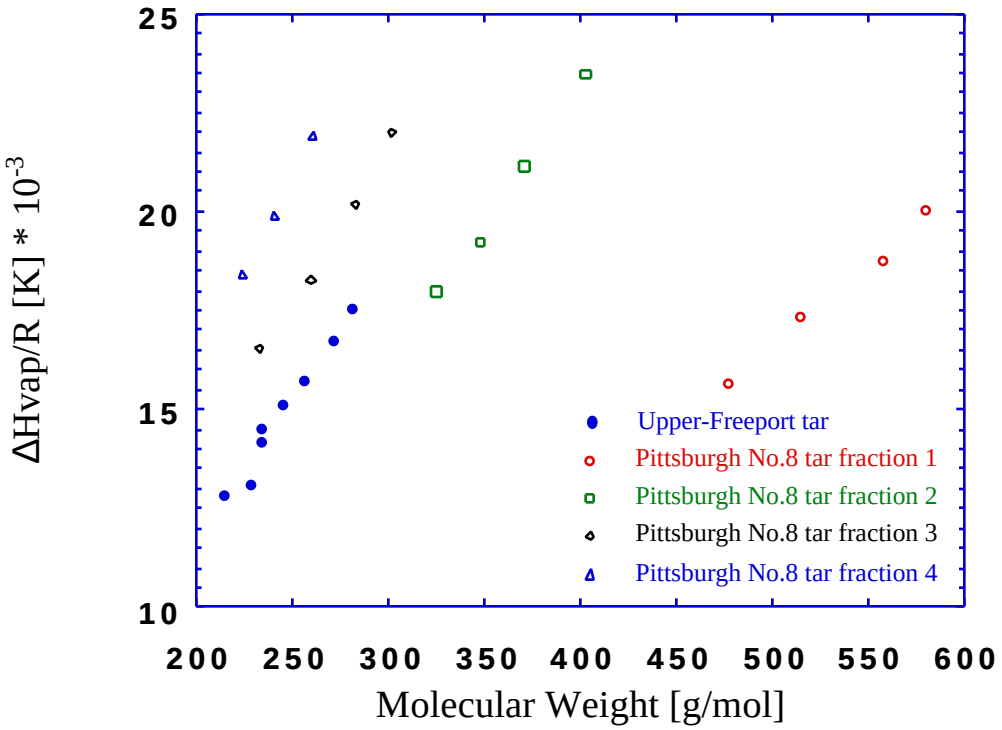

Figure E.55. Vaporization enthalpy as a function of molecular weight for Upper-Freeport coal tar. Pittsburgh No.8 coal tar fractions are shown for comparison.

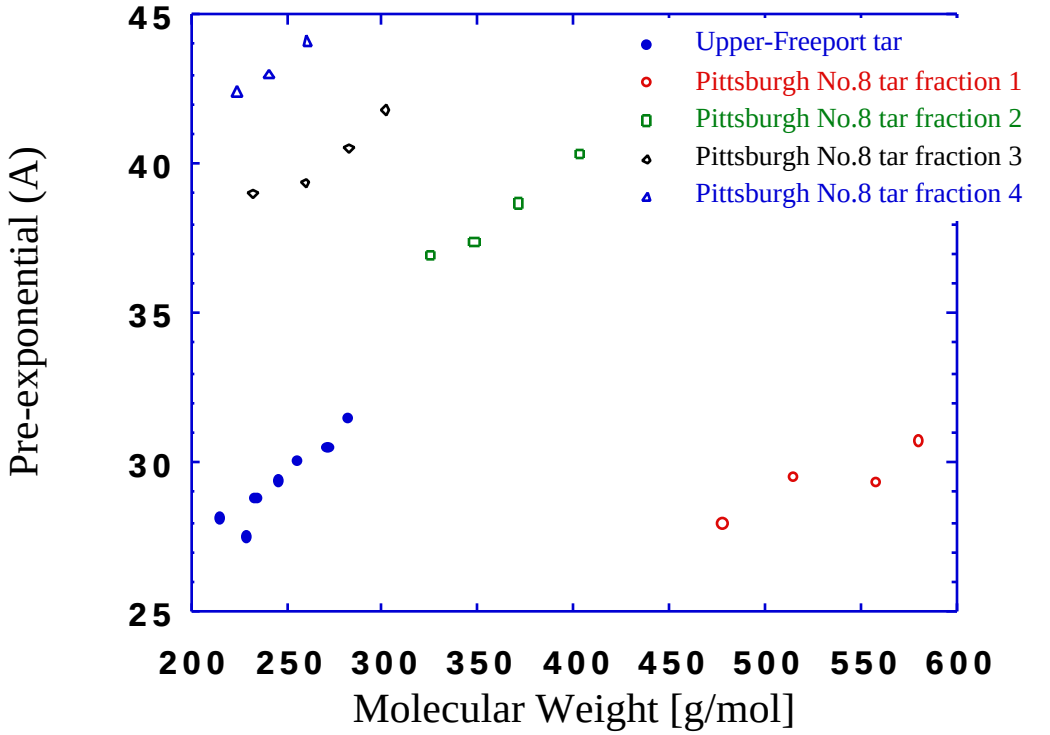

Figure E.56. The pre-exponential (A) as a function of molecular weight for Upper-Freeport coal tar. Pittsburgh No.8 coal tar fractions are shown for comparison.

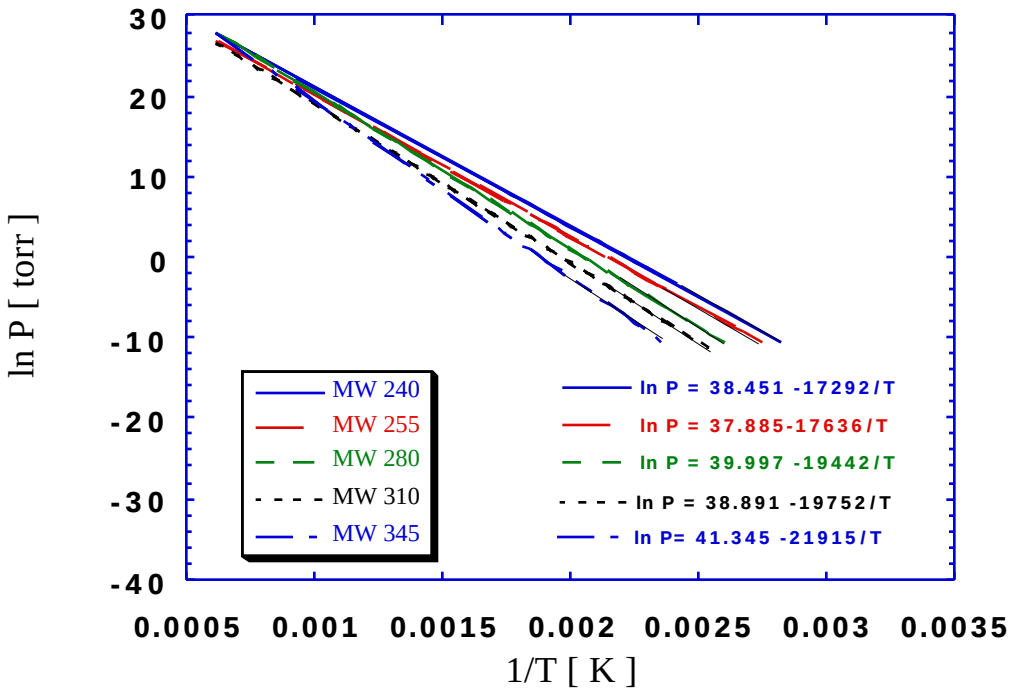

Figure E.57. The vapor pressure curves for Wyodak coal tar. The tar was produced in the wire mesh reactor. The heavier portions of the curves indicate the actual range of temperatures over which the data were obtained.

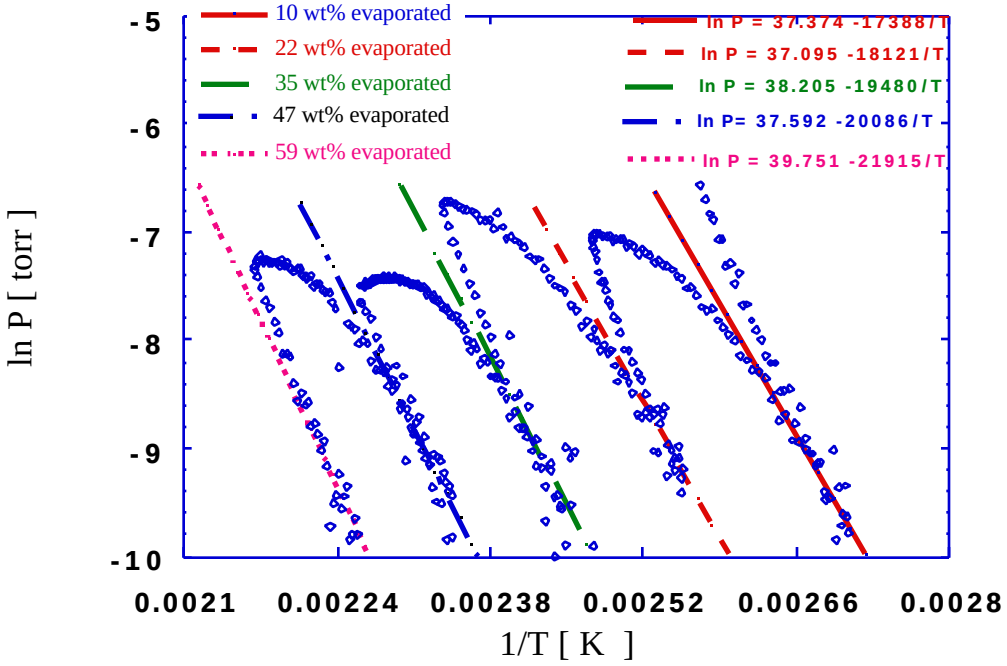

Figure E.58. Raw data for Wyodak coal tar produced in the wire mesh reactor.

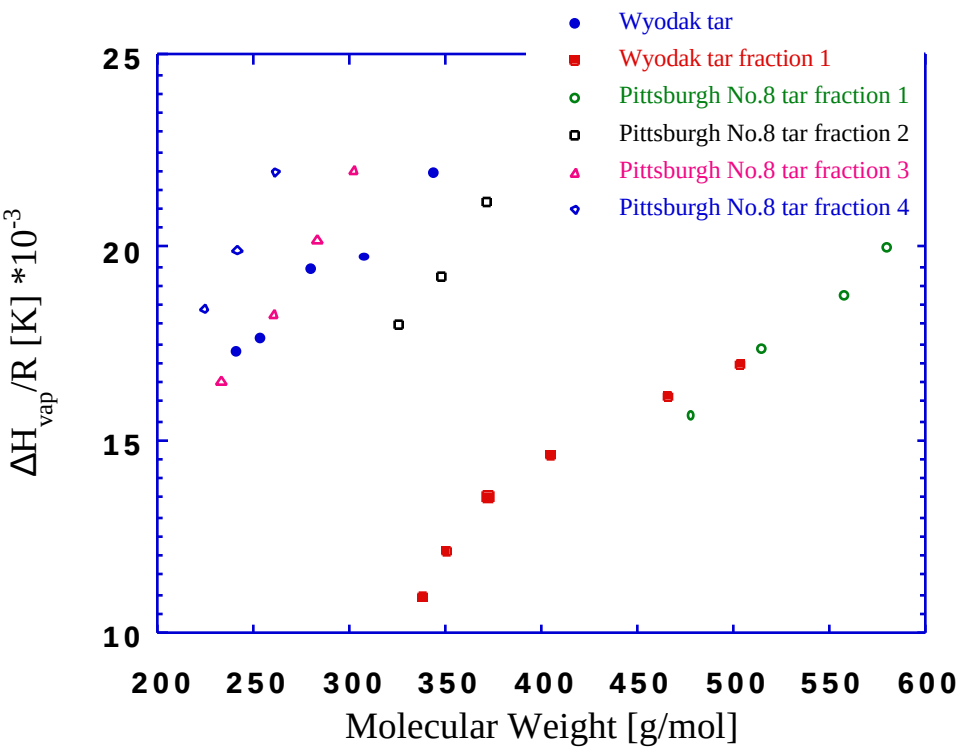

Figure E.59. Vaporization enthalpy as a function of molecular weight for Wyodak coal tar and Wyodak coal tar fraction 1. Pittsburgh No.8 coal tar fractions are shown for comparison.

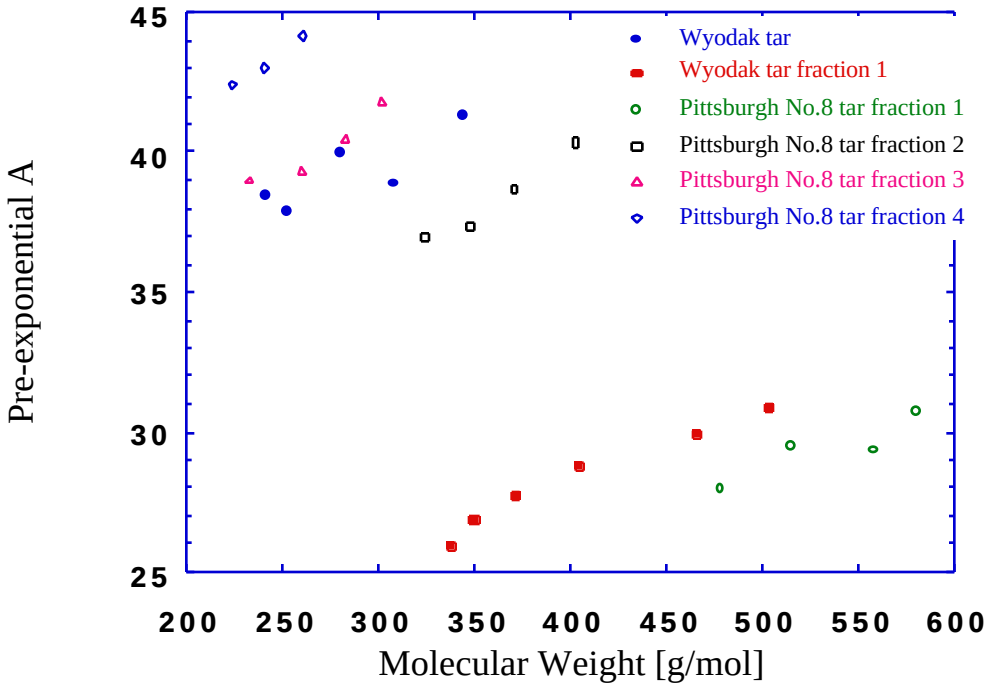

Figure E.60. The pre-exponential factor (A) as a function of molecular weight for Wyodak coal tar and Wyodak coal tar fraction 1. Pittsburgh No.8 coal tar fractions are shown for comparison.

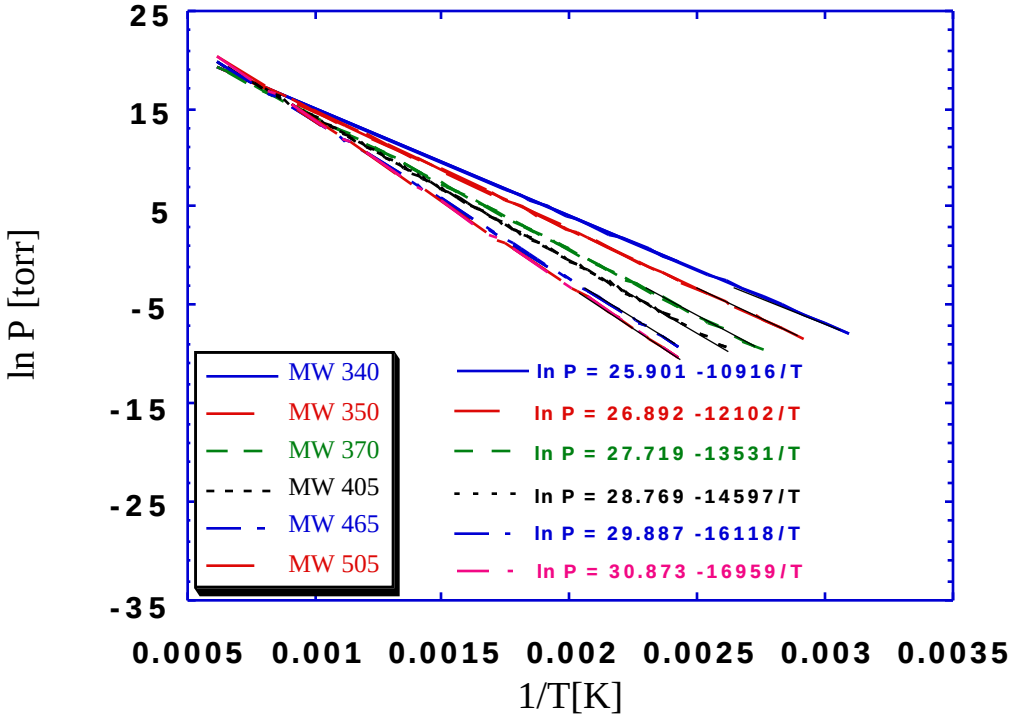

Figure E.61. The vapor pressure curves for Wyodak coal tar fraction 1 separated by GPC. The heavier portions of the curves indicate the actual range of temperatures over which the data were obtained.

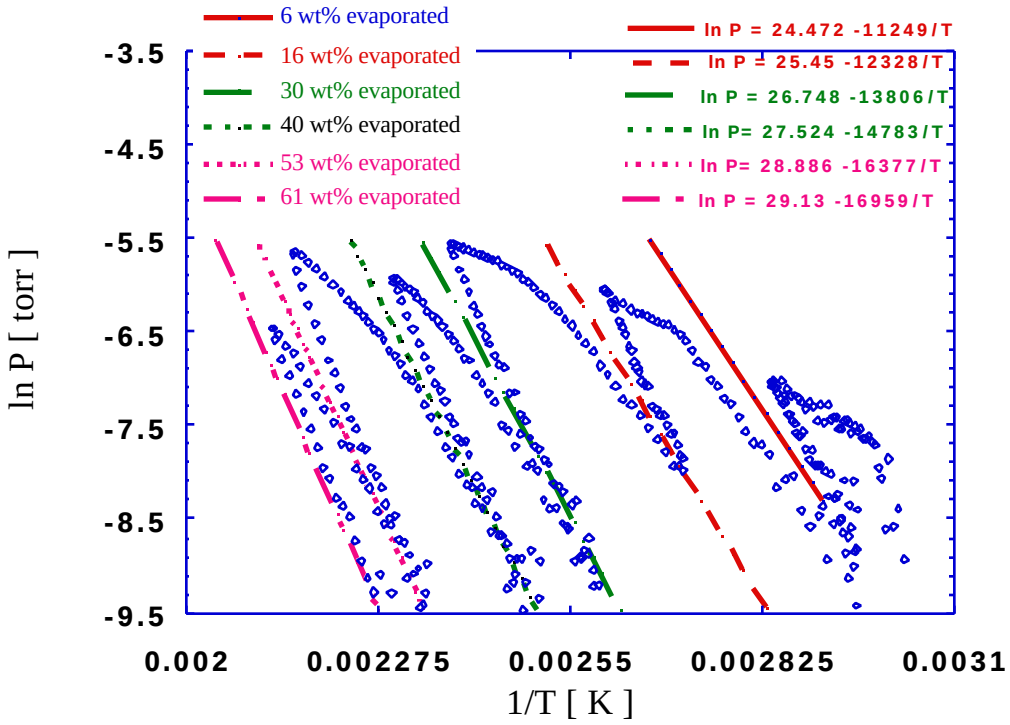

Figure E.62. Raw data for Wyodak coal tar fraction 1.

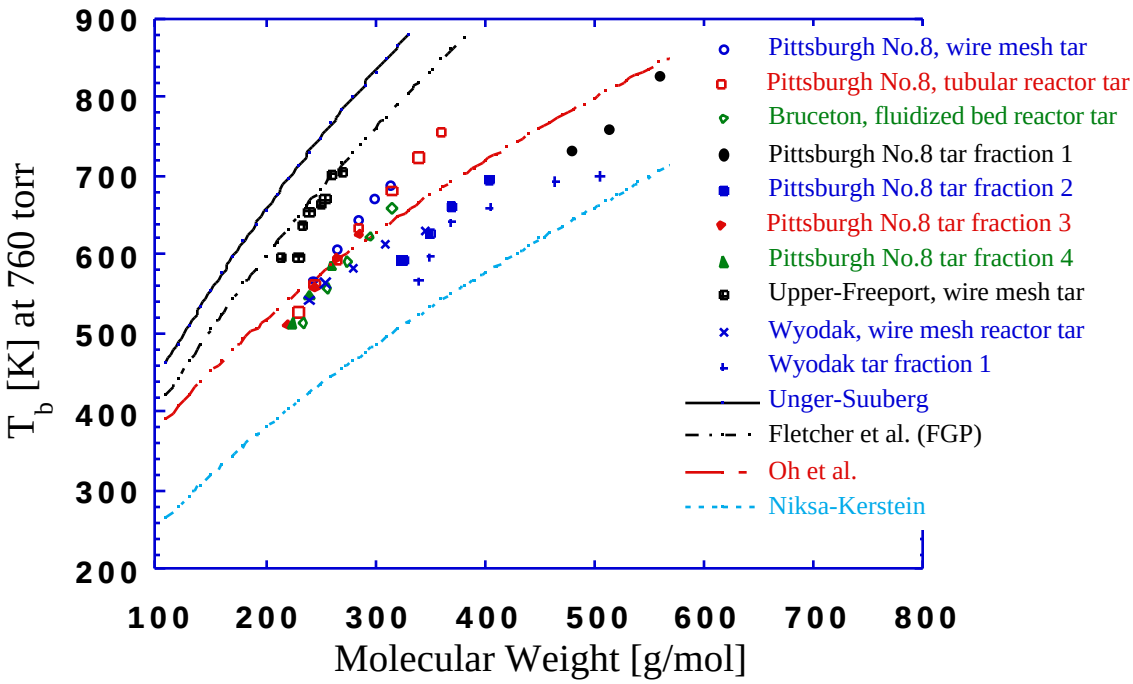

Figure E.63. Comparison of predicted coal tar boiling point at 760 torr with the Unger-Suuberg [1985], Fletcher et al. [1992], Oh et al. [1989] and Niksa-Kerstein [1991] correlations.

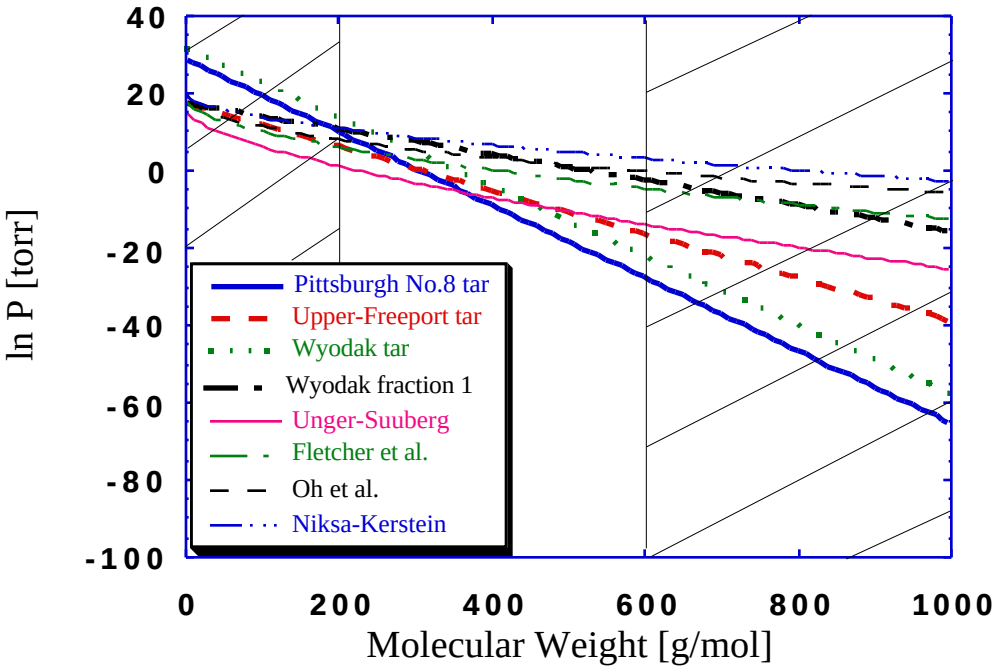

Figure E.64. Comparison of the different vapor pressure correlations at 300°C (573 K).

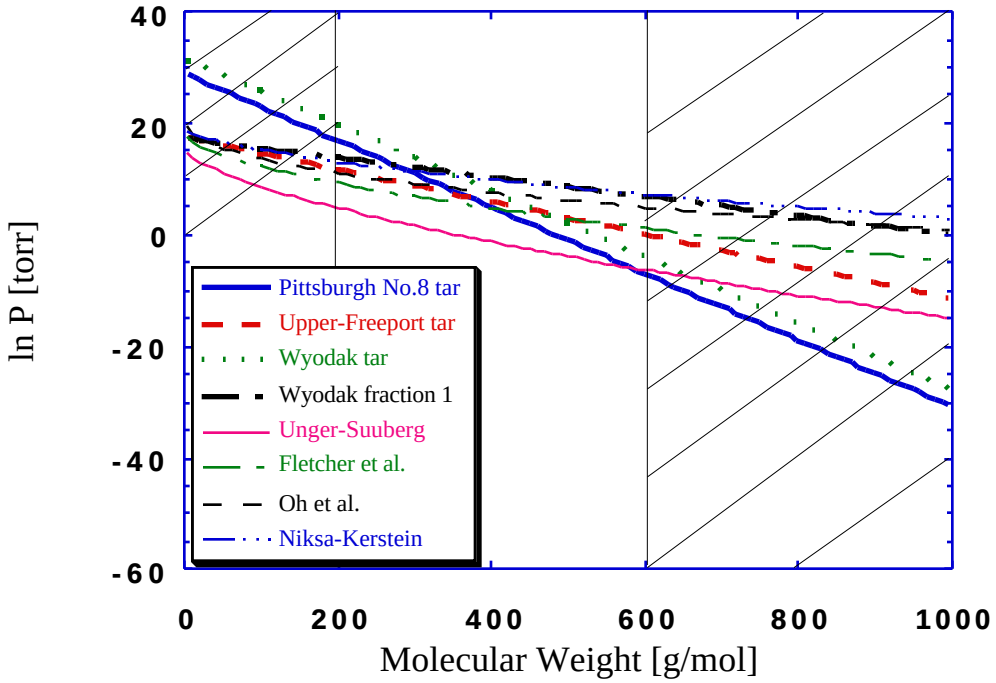

Figure E.65. Comparison of the different vapor pressure correlations at 500°C (773.15 K).

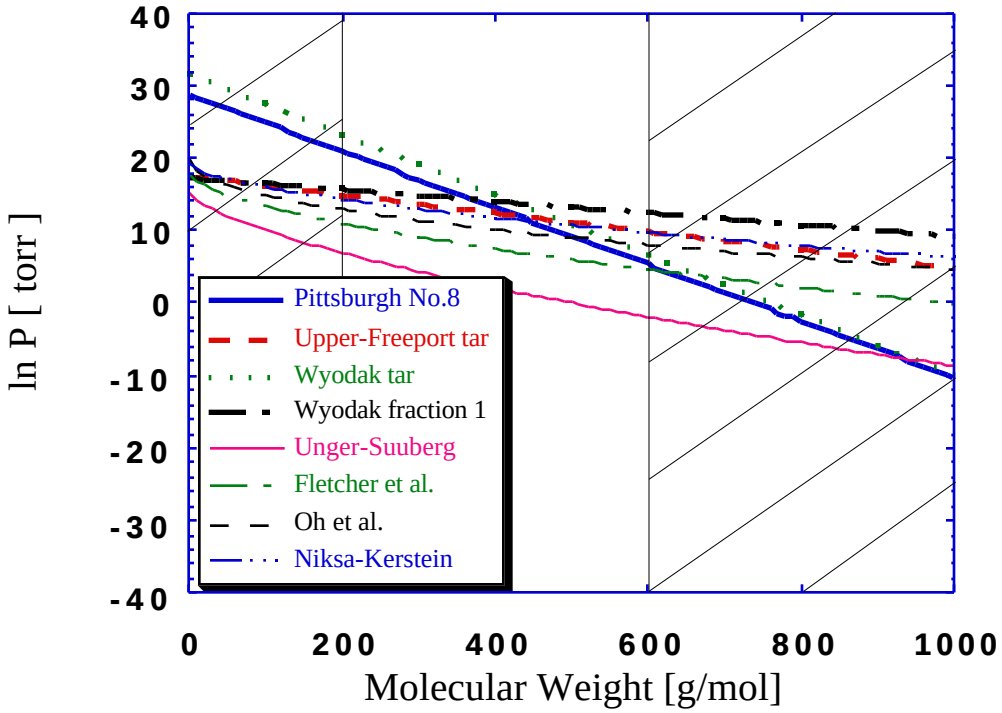

Figure E.66. Comparison of the different vapor pressure correlations at 600°C (873.15 K).

Chapter F. Concluding Remarks

As a consequence of the modular organization of this report, conclusions have been offered on various subtopics throughout the report. Chapter A reviewed the general nature of coal tars and offered a rationale for conducting this study. It was shown that the heterogeneous nature and the complexity of coal tars have made it unrealistic to apply detailed vapor pressure correlations developed for simpler organics. Nevertheless there has been a strong driving force to develop simple correlations, since these are critical in "advanced" pyrolysis models. There has always been the concern that since all such correlations have been developed for "model" compounds, they may fail in application to coal tars.

Chapter B summarized the main experimental approaches for coal tar preparation and characterization, as well as the vapor pressure measurement device designs. A significant aspect was the development of the new "non-isothermal" Knudsen effusion technique to measure the vapor pressures of complicated mixtures. It is difficult to apply the traditional method to complex mixtures of compounds, since the long time-scales required in the usual measurement permit significant change in composition while waiting for pseudo-steady-state. The new technique has been applied to polycyclic aromatics and pyrolysis tars.

Chapter C was concerned with the selection of the model compounds for coal pyrolysis tars and reviews the data available to us on the vapor pressures of high boiling point aromatic compounds. This chapter also dealt with the question of identifying factors that govern the vapor pressures of coal tar model materials and their mixtures. The measurements of vapor pressures for various large polycyclic aromatic hydrocarbons (PAH), including those containing heteroatoms, and some mixtures of these compounds were presented. We believe that our results might be among the first available on some of these materials.

Chapter D covered the vapor pressures and heats of vaporization of primary cellulose tars. Cellulose tar has a much narrower distribution of molecular weights than does coal tar, and is much more homogenous. Thus it was better to develop the methods to be used for coal tars on this simpler model system first. New vapor pressure data for sugar-compounds (levoglucosan, D-xylose, D-glucose and cellobiose) and for cellulose tar were presented. Again, we believe that some of these may be the first on some of the materials of interest. The volatility of cellulose tar was seen to be similar to that of a widely accepted major component of the tar, levoglucosan.

This work has also resulted in a hypothesis regarding the role of tar evaporation in the global kinetics of cellulose pyrolysis. This study of the cellulose tar vapor pressure and heat of vaporization has been the first in the field of biomass pyrolysis. Therefore, future research could be directed at measuring the vapor pressures for the other biomass pyrolysis tars and at developing the pyrolysis models which take into account the heats of vaporization.

Chapter E presented the results of the main focus of this study. Coal tars were prepared from various coal samples. Four coals from the Argonne Premium Coal set - the Illinois No.6, the Pittsburgh No.8, the Pennsylvania Upper-Freeport and the Wyodak - were selected for this study. Also another Pittsburgh No.8 sample, Bruceton standard coal, was also examined. Characterization of tars was obtained via elemental analysis and gel permeation chromatography (GPC). This characterization showed the heteroatomic content of all tars to be comparable to the parent coal, and that tars likely contain a large amount of hydroxyl functionality. The coal tar separation by GPC, using a Phenogel column and pyridine as mobile phase, was a failure as far as separation of tar by molecular weight, but allowed characterization of tars in terms of compound classes. This technique could serve as a simple basis for characterizing complex mixtures such as coal tars. This needs further verification by detailed chemical analysis.

The significant product of this study is a much improved understanding of the volatility and thermal behavior of coal tars. The volatility was studied by vacuum sublimation and Knudsen effusion experiments. The volatility behavior is considerably more complicated than had been earlier believed. The tars evaporate in a "distillation-like" fashion. More volatile species are lost earlier in the process, leaving behind a progressively less volatile residue. The results suggest that there are three very different classes of compounds, and therefore, at least three different vapor pressure behaviors exhibited by each tar. The first class consists of compounds of high molecular weight and significant alkyl character, the second to compounds with significant hydroxyl group content and medium molecular weight, and the third to medium molecular weight aromatic compounds without hydroxyl groups. Hydrogen bonding plays a major role in the determining the tar volatility. Specific correlations of vapor pressure with temperature and molecular weight are given in Chapter E for both the whole tars and their GPC fractions.

There has been concern in pyrolysis modeling about how closely Raoult's law is followed in coal tar. It appears from our results that the assumption of ideal mixture behavior could be acceptable for rough models of pyrolysis despite the possibility of strong specific interactions between certain functional groups.

The results from the current work show that measuring the vapor pressures of complicated and thermally unstable mixtures is possible at low temperatures. There had been some concern about condensation-type reactions influencing the results of vapor pressure measurements, even at modest temperatures, below 250°C. It was shown to be unlikely that such residue formation could affect the vapor pressure results very much, though the thermal instability of the tars was clearly demonstrated. The major reactions promote formation of some kinds of non-volatile residue.

In summary, this work has provided an improved understanding of the volatility of coal and cellulose pyrolysis tars. It has resulted in new experimentally verified vapor pressure correlations for use in pyrolysis models. Further research on this topic should aim at

developing general vapor pressure correlations for all coal tars, based on their molecular weight together with certain specific chemical characteristics *i.e.* hydroxyl group content.

References

Abrams, D.S., Massaldi, H.A., and Prausnitz, J.M., *Ind. Eng. Chem. Fundam.* **1974**, *13,* 259.

Acree, W.E., *Thermochimica Acta* **1991**, *189,* 37.

Aihara, A., *J. Chem. Soc. Japan* **1959**, *32,* 1242.

Ambrose, D., and Davies, R.H., *J. Chem. Thermodynamics* **1980**, *12*, 871.

Ambrose, D., and Patel, N.C., *J. Chem. Thermodyn* **1984**, *16,* 459.

Ambrose, D., and Walton, J., *Pure Appl. Chem.* **1989**, *61*, 1395.

Ambrose, D., Counsell, J.F., and Davenport, A.J., *J. Chem. Thermodyn.* **1970**, *2*, 283.

Ambrose, D., *J. Chem. Thermodynamics* **1978**, *10*, 765.

Ambrose, D., *J. Chem. Thermodynamics* **1986**, *18,* 45.

Ambrose, D.", Vapor Pressures," Butterworth, University College, London, **1975**.

Angus, S.", Guide to the Preparation of Thermodynamic Tables and Correlation of Fluid State," **1983**, COTATA Bull., No. 51.

Antoine, C., *Compt. Rend. Acad. Sci.* **1988**, *Paris 107,* 681, 836, 1143.

Arseneau, D.F., *Can. J. Chem.* **1971**, *49*, 632.

Balson, E.W., *J. Phys. Chem.* **1961**, *65*, 115.

Bardi, G., Gigli, R., Malaspina, L., and Piacente, V., *J. Chem. Eng. Data* **1973**, *18*, 126.

Bardley, R.S., *J. Chem. Soc. London* **1953**, *2*, 1690.

Bartle, K.D., Derek, G.M., Mulligan, M.J., Amaechina, I.O., Taylor, N., *Anal. Chem.* **1986**, *58*, 2403.

Bell, H.G., and Grozek, A.J., *J. Inst. Petrol.* **1962**, 48.

Bidleman, T.F. *Anal. Chem.* **1984**, *56*, 2490.

Bjorseth, A.", Handbook of Polycyclic Aromatic Hydrocarbons," Marcel Dekker, New York, **1983**.

Blair, D.W., Wendt, J.D.L., and Bartok, W., *16h Symp.(Intern.) on Comb.*, The Combustion Institute **1976**, 475.

Boehncke, A., Martin, K., Müller, M.G., and Cammenga, H.K., *J. Chem. Eng. Data* **1996**, *41*, 543.

Borwitzky, H., and Schomburg, G., *J. Chromatogr.* **1979**, *170*, 99**.**

Boublik, T., Fried, V., and Hala, E.", The Vapor Pressures of Pure Substances," 2nd ed., Elsevier, Amsterdam, **1987**.

Bouwstra, J.A., Leeuw, V.V., and Van Miltenburg, J.C., *J. Chem. Thermodyn.* **1985**, *17*, 685.

Bouwstra, J.A., Oonk, H.A.J., Blok, J.G., and DeKruif, C.G., *J. Chem. Thermodyn.* **1984**, *16*, 403.

Brown, J.K., Dryden, I.G.C., Dunevein, D.H., Joy, W.K., and Pankhurst, K.S., *J. Inst. Fuel.* **1958**, *31*, 259.

Brule, M.R., Lin, C.T., Lee, L.L., and Starling, K.E., *AIChE J.* **1982**, *28*, 616.

Burkhard, L.P., *Ind. Eng. Chem. Fundam.* **1985**, *24*, 119.

Calkins, W.H., and Tyler, R.J., *Fuel* **1984**, *63*, 1119.

Calkins, W.H., *Fuel* **1984**, *63*, 1125.

Calkins, W.H., Hagaman, E., and Zeldes, H., *Fuel* **1984**, *63*, 1113.

Carlson, K.D., Gilles, P.W., and Thorn, R.J., *J. Chem. Phys* **1963**, *38*, 2064.

Carrier, B., Rogalski, M., and Peneloux, A., *Ind. Eng. Chem. Res.* **1988**, *27*, 1714.

Carter, E.D., Chapter 2A, Rapp. R.A., ed.", Physico-Chemical Measurements in Metal Research," Vol. IV, part 1, New-York, John Wiley & Sons, **1970**.

Cerny, J., *Energy Fuels* **1991**, *5*, 781.

Chandar, S.C.R., and Singh, R.P., *Fluid Phase Equilibria* **1985**, 24, 177.

Chase, J.D., *Ind. Eng. Chem. Res.* **1987**, *26*, 107.

Chung, K.E., Anderson, L.L., and Wiser, W.H., *Fuel* **1979**, *58*, 847.

Clausing, P., *Ann. Physik.* **1932**, *12*, 961.

Collin, P.J., Tyler, R.J., and Wilson, M.A., *Fuel* **1980**, *59*, 483.

Colomina, M., Jimenez, P., and Turrion, C., *J. Chem. Thermod.* **1982**, *14*, 779.

Colomina, M., Jimenez, P., Perez-Ossorio, R., Roux, M.V., and Turrion, C., *J. Chem. Thermod.* **1988**, *20*, 575.

Cox, E.R., *Ind. Eng. Chem.* **1923**, *15*, 592.

De Kruif, C.G., *J. Chem. Thermodyn.* **1980**, *12*, 243.

DeKruif, C.G., Kuipers, T., Van Miltenburg, J.C., Schaake, R.C.F., and Stevens, G., *J. Chem. Therodyn.* **1981**, *13*, 1081.

DeKruif, C.G., Van Genderen, C.G., Bink, J.C.W., and Oonk, H.A.J., *J. Chem. Thermodyn.* **1981b**, *13*, 457.

DePablo, R.S., *J. Chem. Eng.* **1976**, *21*, 141.

Dushman, S.", Scientific Foundations of Vacuum Technique," New-York, John Wiley & Sons, 2nd edition, **1962**.

Edwards, D., and Prausnitz, J.M., *Ind. Eng. Chem. Fundam.* **1981**, *20(3)*, 281.

Edwards, D., Van de Rostyne, C.G., Winnick, J., and Prausnitz, J.M., *Ind. Eng. Chem. Process Des. Dev.* **1981**, *20(1)*, 139.

Edwards, D.R., and Prausnitz, J.M., *J. Chem. Eng. Data* **1981**, *26,* 121.

Edwards, J.G., and Franzen, H.F., *J. Phys. Chem.* **1995**, *99*, 4779.

Eggersten, V.T, Seibert, E.E., and Stross, F.H., *Anal. Chem.* **1969**, *41*, 1175.

Enstein, J.V., Duronina, L.I., and Pashinkin, A.S., *Zh. Prikl. Khim.* **1964**, *37 (11)*, 2543.

Evans, N., Terry, M.H., Mulligan, M.J., and Thomas, K.M., *Fuel* **1985**, *65*, 694**.**

Fletcher, T.H., Bai, S., Pugmire, R.J.,Solum, M.S., Wood, S., and Grant, D.M., *Energy Fuels* **1993**, *7,* 734**.**

Fletcher, T.H., Kerstein, A.R., Pugmire, R.J., and Grant, D.M., *Energy Fuels* **1990**, *3,* 54**.**

Fletcher, T.H., Kerstein, A.R., Pugmire, R.J., Solum, M.S., and Grant, D.M., *Energy Fuels* **1992**, *6,* 414**.**

Fredenslund, A., and Rasmussen, P., *AIChE J.* **1979**, *25,* 203.

Fredenslund, A., Jones, R.L., and Prausnitz, J. M., *AIChE J.* **1975**, *21*, 1086.

Fredenslund, A.,Gmehling, J., and Rasmussen, P.", Vapor-Liquid Equilibria Using UNIFAC," Elsevier, Amsterdam, **1977**.

Freihaut, J.D., Proscia, W.M., and Mackie, J.C., *Combust. Sci. Tech.* **1993**, *93*, 323.

Freihaut, J.D., Proscia, W.M., and Seery, D.J., *Energy Fuels* **1989**, *3* , 692**.**

Frenklach, M, Clary, D.W., Gardiner, W.C, and Stein, S.E., *20th Symp. (Int.) on Combustion*, The Combustion Institute, Pittsburgh, **1984**, 887.

Frost, A.A., and Kalkwarf, D.R., *J. Chem. Phys.* **1953**, *21*, 264.

Fynes, G., James, R.G., Ladner., W.R., and Newman, J.O.H., *Fuel* **1984**, *63*, 896**.**

Gomez-Nieto, M., and Thodos, G., *Ind. Eng. Chem. Fundam.* **1977**, *16,* 254.

Gomez-Nieto, M., and Thodos, G., *Ind. Eng. Chem. Fundam.* **1978**, *17,* 45.

Grant, D.M., Pugmire, R.J., Fletcher, T.H., and Kerstein, A.R., *Energy Fuels* **1989**, *3,* 175.

Gray, J.A., Brady, C.J., Cunningham, J.R., Freedman, J.R., Wilson, G.M., *Ind. Eng. Chem. Process Des. Dev.* **1983**, 22, 410.

Gray, J.A., Holder, G.E., Brady, C.J., Cunningham, J.R., Freeman,J.R., and Wilson, G.M., *Ind. Eng. Chem. Process Des. Dev.* **1985**, *24,* 97.

Hajaligol, M., Horward, J.B., Longwell, J.P., and Peters, E.A., *Ind. Eng. Chem. Proc. Des. Dev.* **1982**, *21*, 457.

Halpern, Y., Riffer, R., and Broido, A., *J. Org. Chem.* **1973**, *38*, 204.

Hansen, P.C., and Eckert, C.A., *J. Chem. Eng. Data* **1986**, *31*, 1.

Haplern, Y., and Patai, S., *Israel J. Chem.* **1969**, *7*, 673.

Herod, A.A., Stokes, B.J., and Schulten,H., *Fuel* **1993b**, *72,* 31**.**

Herod, A.A., Stokes, B.J., Tye, E.R., Gaines, A.F., Li, C., and Kandiyoti, R., *Fuel* **1993a**, *7 (9),* 1321**.**

Hinckley, D.A., Bidleman, T.F., Foreman, W.T., and Tuschall, J.R., *J. Chem. Eng. Data,* **1990**, *35,* 232.

Hollahan, J., *J. Chem. Educ.* **1962**, *39,* 23.

Homann, K.H, *20th Symp. (Int.) on Combustion,* The Combustion Institute, Pittsburgh, **1984**, 857.

Hortounian, H., and allen, D.T., *Fuel* **1989**, *68,* 481.

Hoshino, D., Zhu, X.-R., Nagahama, K., and Hirata, M., *Ind. Eng. Chem. Fundam.* **1985**, *24,* 115.

Hoyer, H., *Electrochem.* **1958**, *62,* 61.

Inokuchi, H., Shiba, S., Handa, T., and Akamatu, H., *J. Chem. Soc. Japan* **1952,** *25(5),* 299.

Ivanov, G.A., Guglua, V.G., and Zhukhovitskii, A.A., *Zavod. Lab.* **1973**, *39,* 15.

Jensen, T., Fredenslund, A., and Rasmussen, P., *Ind. Eng. Chem. Fundam.* **1981**, *20* 239.

Kelley, J.D, and Rice, F.O., *J. Phys. Chem.* **1964**, *68(12),* 3795.

Kennard, E.H.", Kinetic Theory of Gases," New-York, McGraw-Hill, **1938**.

Kesler, M.G., and Lee, B.I., *Hydroc. Proc.* **1980**, July, 167.

King, M.B., and Al-Najjar, H., *Chem. Eng. Sci.* **1974**, *29,* 1003.

Knudsen, M., *Ann. Physik* .**1909a**, *28,* 999.

Knudsen, M., *Ann. Physik.* **1909b**, *29,* 179.

Kolkert, W.J., *J. Crystal Growth* **1975**, *30,* 213.

Kroto, H.W., and Mckay, K., *Nature* **1988**, *331,* 328.

Lafleur, A.L., and Wornat, M.J., *Anal. Chem.* **1988**, *60,* 1096.

Lafleur, A.L., Sarofim, A.F., and Wornat, M.J., *Energy Fuels* **1993**, *7,* 357.

Langmuir, I., *Phys. Rev.* **1913**, *2,* 329.

Lee, B.I., and Kesler, M.G., *AIChE J.* **1975**, *21,* 510.

Lee, C., and Diehl, J.R., *Comb. Flame* **1981**, *42,* 123.

Lee, C., Chaiken, R.F., and Singer, J.M., *16th Symp. (Int.) on Combustion* , The Combustion Institute, Pittsburgh, **1976**, 1459.

Lee., M.L., and Wright, B.W., *J. Chromatogr. Sci.* **1980**, *18,* 345**.**

Letcher, T.M., and Bricknell, B.C., *J. Chem. Eng. Data* **1996**, *41,* 639.

Li, C-Z., Bartle, K.D., and Kandiyoti, R., *Fuel* **1993**, *72,* 3.

Li, C-Z., Wu, F., Cai, H-Y., and Kandiyoti, R., *Energy Fuels* **1994**, *8,* 1039.

Löffler, S., and Homann, K.H., *23rd Symp. (Int.) on Combustion*, The Combustion Institute, Pittsburgh, **1990**, 355.

Mackay, D., Bobra, A., Chan, D.W., and Shlu, W.Y., *Environ. Sci. Technol.* **1982**, *16(10)*, 645.

Macknick, A.B., and Prausnitz, J.M., *Ind. Eng. Chem. Fundam.* **1979**, *18(4)*, 349.

Macknick, A.B., and Prausnitz, J.M., *J. Chem. Eng. Data* **1979**, *24*, 176.

Macknick, A.B., Winnick, J., and Prausnitz, J.M., *AIChE Journal* **1978**, *24(4)*, 731.

Majer, V., Svoboda, V., and Pick, J.", Heats of Vaporization of Fluids," Elsevier, 1989.

Malanowski, S., and Anderko, A.", Modelling Phase Equilibria," John Wiley & Sons, 1992.

Malaspina, L., Bardi, G., and Gigli, R., *J. Chem. Thermodyn.* **1974**, *6*, 1053.

Margrave, J.L.", The Characterization of High-Temperature Vapors," New-York, John Wiley & Sons, **1967**.

Mato, F.A., and Carrier, B., *Cem. Eng. Science* **1991**, *46(10)*, 2445.

Maxwell, J.B., and Bonnell, L.S., *Ind. Eng. Chem.* **1957**, *49(7)*, 1189.

McEachen, D.M., *J. Chem. Educ.* **1973**, *50*, 190.

McEachern, D.M., Inigues, J.C., and Ornelas, H.C., *J. Chem. Eng. Data* **1975**, *20*, 3.

McGarry, J., *Ind. Eng. Chem. Process Des. Dev.* **1983**, *22*, 313.

Milosavljevic, I., and Suuberg, E.M., *Ind. Eng. Chem. Res.* **1995**, *34*, 1081.

Milosavljevic, I., Oja, V., and Suuberg, E.M., *Ind. Eng. Chem. Res.* **1996**, *35*, 653.

Mishra, D.S., and Yalkowsky, S.H., *Ind. Eng. Chem. Res.* **1991**, *30*, 1609.

Moelwyn-Hughes, E.A.", Physical Chemistry," 2nd ed., Pergamon Press, New York, **1961**.

Mok, W.S.-L., and Antal, M.J., *Thermohimica Acta* **1983**, *68*, 165.

Morecroft, D.W., *J. Chem. Eng. Data* **1964**, *9*, 488.

Morgan, D.L., and Kobayashi, R., *Fluid Phase Equilibria* **1994**, *94*, 51.

Mortzfeldt, K., *J.Phys. Chem.* **1955**, *59*, 139.

Murray, J.J., and Pottie, R.F., *Can. J. Chem.* **1974**, *52*, 557.

Myers, H.S., and Fenske, M.R., *Ind. Eng. Chem.* **1955**, *47*, 1652.

Nelson, P.F., Smith, I.W., Tyler, R.J., and Mackie, J.C., *Energy Fuel* **1988**, *2*, 391.

Nesmeyanov, A.N.", Vapor Pressure of the Chemical Elements, " Elsevier, **1963**.

Niksa, S., and Kerstein, A., *Energy Fuels* **1987**, *66*, 1389.

Niksa, S., and Kerstein, A., *Energy Fuels* **1991**, *5*, 647.

Niksa, S., *Energy Fuels* **1991a**, *5*, 665.

Niksa, S., *Energy Fuels* **1991b**, *5*, 673.

Niksa., S., *AIChE J.* **1988**, *34*, 790.

Oh, S.M., Peters, A.W., and Howard, J.B., *AIChE Journal* **1989**,*35 (5),* 775**.**

Ohe, S.", Computer Aided Data Book of Vapor Pressure," Data Book Publishing Company, Tokyo, **1976**.

Orning, A.A., and Greifar, B., *Fuel* **1956**, *35*, 318.

Parker, J.E., Johnson, C.A.F., John, P., Smith, G.P., Herod, A.A., Stokes, B.J., and Kandiyoti, R., *Fuel* **1993**, *72 (10)*, 1386.

Philip, C.V. and Anthony, R.G., *Fuel* **1982**, *61*, 375.

Piacente, V., Pompili, T., Scardala, P., and Ferro, D., *J. Chem. Thermodyn.* **1991**, *23*, 379.

Pitzer, K.S., *J. Am. Chem. Soc.* **1955**, *77*, 3427.

Plank, R., and Reidel, L., *Ing. Arch.* **1948**, *16*, 225.

Ponder, G.R., Richards, G.N., Stevenson, T.T., *J. Anal. Appl. Pyro.* **1992**, *22*, 217.

Pribilova, J., and Pouchly, J., *Collect. Czech. Chem. Commun.* **1974**, *39*, 1118.

Prigonine, I.", Molecular Theory of Solution," Amsterdam, North-Holland, **1957**.

Rachenko, L.G., and Kitaigorodskii, A.I., *Russian J. Phys. Chem.* **1974**, *48*, 2702.

Reid, R.C., Prausnitz, J.M., and Poling, B.E.", The Properties of Gases and Liquids," 4th ed., McGraw-Hill, New York, **1987**.

Ribeiro Da Silva, M.A.V., and Monte, M.J.S., *Thermochimica Acta* **1990**, *171*, 169.

Rodgers, P.A., Creagh, A.L., Prange, M.M., and Prausnitz, J.M. *Ind. Eng. Chem. Res.* **1987**, *26*, 2312.

Rogalski, M., *Thermochimica Acta* **1985**, *90*, 125.

Ruzicka, K., and Majer,V., *AIChE J.* **1996**, *42(6)*, 1725.

Ruzicka, K., and Majer,V., *Fluid Phase Equilibria* **1986**, *28*, 253.

Ruziska, V., *Ind. Eng. Chem. Fundam.* **1983**, *22(2)*, 267.

Sasse,K, and Merlin, J., *Fluid Phase Equilibrium* **1988**, *42*, 287.

Sato, N., Inomata, H., Arai, K., and Saito, S., *J. Chem. Eng. Japan* **1986**, *19*, 145.

Scott, D.W., and Osborn, A.G., *J. Phys. Chem.* **1979**, *83(21)*, 2715.

Scott, D.W., and Osborn, A.G., J. Phys. Chem. **1979**, *83*, 2714.

Serio, M.A., Hamblen, D.G., Markham, J.R., and Solomon, P.R., *Energy Fuels* **1987**, *1*, 138.

Shafizadeh, F., and Fu, Y.L., *Carbohyd. Res.* **1973**, *29*, 113.

Shafizadeh, F., and Lai, Y.Z., *J. Org. Chem.* **1972**, *37*, 278.

Shafizadeh, F., *Applied Polymer Symp.* **1975**, *28*, 153.

Shafizadeh, F., Furneaux, H.F., Cochran, G.T., Scholl, J.P., and Sakai, Y., *J. Applied Polymer Sci.* **1979**, *23*, 3525.

Shafizadeh, F., *J. Polymer Sci.* **1971**, *36*, 21.

Sinke, G.C., *J. Chem. Thermodyn.* **1974**, *6*, 311.

Sivaraman, A., Kragas, T., and Kobayashi, R., *Fluid Phase Equilibria* **1984**, *16*, 275.

Skjold-Jorgensen, S., *Fluid Phase Equilibria* **1984**, *16*, 317.

Skjold-Jorgensen, S., *Ind. Eng. Chem. Res.* **1988**, *27*, 110.

Smith, G., Winnick, J., Abrams, D.S., and Prausnitz, J.M., *Can. J. Chem. Eng.* **1976**, *54*, 337.

Smith, K.L., Smoot, L.D., Fletcher, T.H., and Pugmire, R.J.",The Structure and Reacttion Processes of Coal," Plenum Press, New York, **1994.**

Smith, N.K., Stewart, R.C., Osborn, A.G., and Scott, D.W., *J. Chem. Thermodyn.* **1980**, *12*, 919.

Solomon, P.R., and Colket, M.B., *17th Symp. (Intern.) on Comb.*, The Combustion Institute **1979**, 131.

Solomon, P.R., and Colket, M.B., *Fuel* **1978**, *57*, 748.

Solomon, P.R., Beer, J.M., and Longwell, J.P., *Energy* **1987**, *12(8-9)*, 837.

Solomon, P.R., *CoalStructure*, Advances in Chemistry Series 192, American Chemical Society, Washington, DC, **1981**, 7.

Solomon, P.R., Hamblen, D.G., Carangelo, R.M., and Krause, J.L., *19h Symp. (Intern.) on Comb.*, The Combustion Institute **1983**, 1139.

Solomon, P.R., Hamblen, D.G., Carangelo, R.M., Serio, M.A., and Despande, G.V., *Energy Fuels* **1988**, *2*, 405.

Solomon, P.R., Serio, M.A., and Suuberg, E.M., *Prog. Energy Combust. Sci.* **1992**, *18*, 133.

Solomon, P.R., Serio, M.A., Despande, G.V., and Kroo, E., *Energy Fuels* **1990a**, *4*, 42.

Solomon, P.R., Serio, M.A., Hamblen, D.G., Yu, Z-Z., and Charpenay, S., *Prepr. Pap.-Am. Chem. Soc., Div. Fuel. Chem.* **1990b**, *35(2)*, 479.

Solomon, P.R., Squire, K.R., and Carangelo, R.M., *Prepr. Pap.- Am. Chem. Soc., Div. Fuel. Chem.* **1984**, *29(1)*, 10.

Solum, S.M., Pugmire, R.J., and Grant, D.M., *Energy Fuels* **1989**, *3*, 187.

Somayajulu, G.R., *J. Chem. Eng. Data* **1989**, *34*, 106.

Sonnefeld, W.J., Zoller, W.H., and May, W.E., *Anal. Chem.* **1983,** *55*, 275.

Squire, K.R., Solomon, P.R., Carangelo, R.M., and DiTaranto, M.B., *Fuel* **1986**, *65*, 833.

Stephenson, M.R., and Malanowski, S.", Handbook of the Thermodynamics of Organic Compounds," Elsevier, New York, **1987**.

Strachan, M.G., and Johns, R.B., *J. Chromatogr.* **1985**, *329*, 65.

Stryer, L.", Biochemistry," 2nd ed., W.H. Freeman and Company, San Francisco, **1981**.

Suuberg, E.M., in *Chemistry of Coal Conversion* **1985**, (R. Schlosberg, ed.), Plenum, 67.

Suuberg, E.M., Peters, W.A., and Howard, J.B., *17th Symp. (Intern.) on Comb.*, The Combustion Institute **1979**, 117.

Suuberg, E.M., Peters, W.A., and Howard, J.B., *Ind. Eng. Chem. Process. Des. Dev.* **1978**, *17*, 37.

Suuberg, E.M., Unger, P.E., and Lilly, W.D., *Fuel* **1985**, *64*, 957**.**

Svoboda, V., and Basarova, P., *Fluid Phase Equilibria* **1994**, *93*, 167.

Svoboda, V., and Smolova, H., *Fluid Phase Equilibria* **1994**, *97*, 1.

Swan, T.H., and Mack, E., *J. Am. Chem. Soc.* **1925**, *47*, 2112.

Takagi, S., Shintani, R., Chihara, H., and Seki, S., *J. Chem. Soc. Japan* **1959**, *32*, 1937.

Tsonopoulos, C., Heidman, J., and Hwang, S.-C.", Thermodynamic and Transport Properties of Coal Liquids," John Wiley & Sons, 1986.

Tu, C.-H., *Fluid Phase Equilibria* **1994**, *99*, 105.

Tyler, R.J., *Fuel* **1979**, *58*, 680.

Tyler, R.J., *Fuel* **1980**, *59*, 218.

Unger, P.E. , and Suuberg, E.M., *Fuel* **1984**, *63*, 606**.**

Vadji, L.E., and Allen, D.T., *Fuel* **1989**, *68*, 1389.

Van De Rostyne, C., and Prausnitz, J.M., *J. Chem. Eng. Data* **1980**, *25*, 1.

Van Ekeren, P.J., Jacobs, M.H.G., Offrina, J.C.A., and DeKruif, C.G., *J. Chem. Thermod.* **1983**, *215*, 409.

Verhoek, F.H., and Marshall, A.L., *J. Am. Chem. Soc*. **1939**, *61*, 2737.

Vorres, K.S., *Energy Fuels* **1990**, *4*, 420, and ", Users Handbook for the Argonne Premium Coal Samples," **1993.**

Wagner, W., *Cryogenics* **1973**, *13*, 470.

Wakayama, N., and Inokuchi, H., *Bull. Chem. Soc. Japan* **1967**, *40*, 2267.

Wang, H., and Frenklach, M., *Comb. Flame* **1994**, *96*, 163.

Ward, J.W., and Fraser, M.V., *J. Chem. Phys.* **1968**, *49*, 3743.

Weast, R.C., Astle, M.J., and Beyer, W.H.", CRC Handbook of Chemistry and Physics," 66th ed., CRC Press, Boca Raton, Florida, **1985**.

Weber, L.A., and Defibaugh, D.R., *J. Chem. Eng. Data* **1996**, *41*, 382.

White, C.M., and Schmidt, C.E., *Fuel* **1987**, *66*, 1030.

White, C.M., *J. Chem. Eng. Data* **1986**, *31*, 198.

Whitman, C.J., *J. Chem. Phys.* **1962**, *37*, 784.

Wiedemann, H.G., *Thermochim. Acta* **1972**, *3*, 355.

Winans, R.E., *J. Anal. Appl. Pyrol.*. **1991**, *20*, 1.

Winans, R.E., McBeth, R.L., Hunt, J.E., and Melnikov, P.E., in "Proceedings of 1991 International Conference on Coal Science", 16-20 September, University of Newcastle-on-Tyne, UK, Oxford, **1991**, p. 44-47.

Winterbottom, W., and Hirt, J., *J. Chem. Phys.* **1962**, *37*, 784.

Wornat, M.J., Sarofim, A.F., and Longwell, J.P., *Energy Fuels* **1987**, *1*, 431.

Yair, O.B., and Fredenslund, A., *Ind. Eng. Chem. Process Des. Dev.* **1983**, *22*, 433.

Zia, T., and Thodos, G., *Can. J. Chem. Eng.* **1974**, *52*, 631.

Zudkevitch, D., Krautheim, P.D., and Gaydos, D., *Fluid Phase Equilibria* **1983**, *14*, 117.

Appendix A - Elemental composition of tars from typical pyrolysis experiments.

coal	rank	reactor	pressure	T[°C]	H/C	C	H	N	S+O
Pittsburgh No.8	HVB	wire mesh	164kP	540	0.96	82.7	6.6	1.3	9.4
Fucik mine (Czechoslovakia)	HVB	tubular flow			1.08	79.6	8.6	0.7	11.1
Dukla mine (Czechoslovakia)	HVB				1.1	79.9	8.8	0.6	10.7
Frantizek mine (Czechoslovakia)	HVB				1.01	79.4	8.0	0.7	11.9
Staric mine (Czechoslovakia)	HVB				0.98	80.5	7.9	0.6	11.0
Linby, 811	HVB		N2 100 kPa	575	1.19	81.8	8.1		8.1
Linby, 811	HVB		N2 5000 kPa	575	1.24	82.5	8.5		7.5
Linby, 811	HVB		N2 30000kPa	575	1.16	83.0	8.0		7.8
PSOC 1451D (Pittsburgh No. 8)	HVB	entrained-flow		569	0.85	84.07	5.94	1.67	8.32
PSOC 1520 (Smith Roland, WY)	sub-bituminous	entrained-flow		507	0.89	83.97	6.22	1.64	8.14
PSOC 1516D (Lower Kittaning)	LVB	entrained-flow		569	0.75	89.38	5.6	1.39	3.61

Appendix B - Elemental compositions and number average molecular weights of tars and their fractions.

Table BA.1a. Pittsburgh No. 8 coal tars.

tar	MW	C	H	N	S+O *	H/C	N/C
wire mesh	311	81.4	7.4	1.4	9.75	1.09	0.015
tubular reactor	320	81.4	7.0	1	10.3	1.03	0.012

Table BA.1b. Pittsburgh No. 8 coal - tubular reactor tar fractions.

fraction	wt %	MW	C	H	N	S+O *	H/C	N/C
fraction 1	2.7%	540						
fraction 2	14.6%	410	81.87	8.2	1.01	8.92	1.2	0.01
fraction 3	29%	340	82.06	7.0	0.99	9.95	1.02	0.01
fraction 4	33%	310	80.37	7.3	1.16	11.17	1.09	0.0123
			82.2	7.5	0.93	9.3	1.09	0.01
fraction 5	17.2%	290	82.73	7.6	1.61	8.1	1.1	0.012
fraction 6	3.6%	240						

* by difference; __ samples were analysed by Huffman Laboratories, Inc.

Table BA.2a. Bruceton coal tar.

tar	MW	C	H	N	S+O *	H/C	N/C
fluidized bed	347	82.08	7.7	1.22	9.0	1.13	0.013

Table BA.2b. Bruceton coal - fluidized bed reactor tar fractions.

fraction	wt %	MW	C	H	N	S+O *	H/C	N/C
fraction 0	1.2	820						
fraction 1	8.1	520	86.7	8.9	2	2.4	1.23	0.02
fraction 2	16.6	395	86.5	8.25	1.34	2.4	1.14	0.013
fraction 3	23.6	320	82.7	8.1	1.04	8.2	1.17	0.011
fraction 4	22.9	310	82.4	7.8	0.82	9	1.13	0.009
fraction 5	15.4	275	82.0	7.9	0.91	9.2	1.16	0.01
fraction 6	7.5	250	83.57	7.3	1.10	7	1.05	0.011
fraction 7	2.8	275	82.5	7.8	1.24	8.4	1.13	0.013
fraction 8	1.8	290						

* by difference; __ samples were analysed by Huffman Laboratories, Inc.

Table BA.3a. Illinois No.6 coal tars.

tar	MW	C	H	N	S+O *	H/C	N/C
wire mesh	281	75.6	6.7	1.08	16.6	1.07	0.012
tubular reactor	273	80.47	7.7	1.34	10.49	1.15	0.014
		79.2	7.2	1.2	12.4	1.09	0.013

Table BA.3b. Illinois No. 6 coal - tubular reactor tar fractions.

fraction	wt %	MW	C	H	N	S+O *	H/C	N/C
fraction 1	2.6%	560						
fraction 2	16.1%	395	78.8	8.3	0.9	12	1.26	0.01
fraction 3	27%	299	79.9	7.6	0.84	11.7	1.14	0.009
fraction 4	42%	270	80.9	7.4	0.92	10.7	1.1	0.01
fraction 5	10.7%	233	80.6	6.6	1.3	11.4	1.0	0.014
fraction 6	1.9%	248						

* by difference; __ samples were analysed by Huffman Laboratories, Inc.

Table BA.4a. Upper-Freeport coal tars.

tar	MW	C	H	N	S+O *	H/C	N/C
wire mesh	290	87.16	7.8	1.3	3.74	1.07	0.013
tubular reactor	276	86.1	8.8	1.26	3.84	1.23	0.012
		88.2	8.3	1.06	4.2	1.13	0.01

Table BA.4b. Upper-Freeport coal - tubular reactor tar fractions.

fraction	wt %	MW	C	H	N	S+O *	H/C	N/C
fraction 0	0.6							
fraction 1	14.1	390	84.5	8.33	1.0	6.1	1.18	0.01
fraction 2	17.9	315	86	8.07	1.6	4.3	1.12	0.016
fraction 3	19.3	295	86.7	8.7.79	1.5	3.9	1.07	0.015
fraction 4	35.4	265	87.3	7.79	1	3.9	1.07	0.01
fraction 5	12.8	230						

* by difference; __ samples were analysed by Huffman Laboratories, Inc.

Table BA.5a. Wyodak coal tars.

tar	MW	C	H	N	S+O *	H/C	N/C
wire mesh	325	78.49	7.9	1.03	12.58	1.208	0.011
tubular reactor	340	79.3	7.9	0.8	12	1.2	0.009

Table BA.5b. Wyodak coal tubular - reactor tar fractions.

fraction	wt %	MW	C	H	N	S+O *	H/C	N/C
fraction 1	53%	505	77.2	7.8	0.45	14.6	1.2	0.005
fraction 2	45.7%	290	78.9	6.7	0.65	13.75	1.0	0.007
fraction 3	1.3%	240						

* by difference; __ samples were analysed by Huffman Laboratories, Inc.